12-6-1978

The Effect of Volatile Fission Products on Fuel Motion in Nuclear Fuel Elements

Paul Sasa

EFFECT OF VOLATILE FISSION PRODUCTS ON FUEL MOTION IN NUCLEAR FUEL ELEMENTS

SASA

Paul Sasa
Candidate

Chemical and Nuclear Engineering
Department

This dissertation is approved, and it is acceptable in quality and form for publication on microfilm:

Approved by the Dissertation Committee:

August Cronenberg, Chairperson

Jay E Boudreau

H. S. Nuttall

Michael

Ronald A Knief

Accepted:

Bernard Spolsky
Dean, Graduate School

December 6, 1978
Date

THE EFFECT OF VOLATILE FISSION PRODUCTS ON FUEL MOTION IN NUCLEAR FUEL ELEMENTS

by

Paul Sasa

B.S., University of Colorado, 1968

M.S., University of New Mexico, 1974

DISSERTATION

Submitted in Partial Fulfillment of the
Requirements for the Degree of
Doctor of Philosophy in Nuclear Engineering
in the Graduate School of
The University of New Mexico
Albuquerque, New Mexico
December 1978

ACKNOWLEDGMENTS

The author wishes to express his grateful appreciation to the many people who have supported as well as encouraged him throughout his studies at the University of New Mexico.

He is particularly indebted to the chairman of his committee, Dr. A. Cronenberg, for sharing his knowledge and experience with him, and having enough faith to fund him throughout his studies.

Thanks also goes to the members of his committee, Dr. R. Knief, Dr. E. Nuttall, and Dr. M. Stevenson, who have given their time and advice.

He is grateful to the Fast Reactor Safety Group at the Los Alamos Scientific Laboratory headed by Dr. M. Stevenson and later by Dr. J. Boudreau, for supporting his Ph.D. Research.

A personal thanks is extended to Ms. Yvonne Martinez for her extra work in preparing and typing this thesis.

Finally, a special thanks goes to his wife, Janet, for just believing in him.

THE EFFECT OF VOLATILE FISSION PRODUCTS ON FUEL MOTION IN NUCLEAR FUEL ELEMENTS

by

Paul Sasa

ABSTRACT OF DISSERTATION

Submitted in Partial Fulfillment of the
Requirements for the Degree of
Doctor of Philosophy in Nuclear Engineering
in the Graduate School of
The University of New Mexico
Albuquerque, New Mexico
December 1978

THE EFFECT OF VOLATILE FISSION PRODUCTS ON FUEL MOTION IN NUCLEAR FUEL ELEMENTS

Paul Sasa, Ph.D.
Department of Chemical and Nuclear Engineering
The University of New Mexico, 1978

Stringent licensing procedures for commercial nuclear reactor operation require an in-depth analysis of the phenomena associated with postulated reactor core overheating accidents. One aspect of nuclear reactor safety assessment is a prediction of fuel behavior associated with such postulated overheating events, which includes an assessment of the role of fission product inventory contained within irradiated fuel elements on fuel relocation potential. In general the gaseous fission product, such as Xenon and Krypton, have been considered the most likely candidates for fuel relocation due to gas dissolution from the fuel matrix and bubble expansion during fuel overheating; thus, such gaseous fission products have received considerable attention in fuel modeling efforts associated with accident code development work. However, the fissioning of UO_2 fuel in both a fast and slow neutron spectrum also results in the generation of a significant quantity of metallic fission products such as Barium, Iron, Molybdenum, and other metallic species. Metallurgical analysis of irradiated fuel indicates

that such metals aggregate into inclusions found throughout the fuel matrix. During normal reactor operation such metallic inclusions are in a solid state, but at the elevated temperatures expected for overheating accident transients, such inclusions may tend to volatilize, contributing to fuel motion. This work involves an assessment of the potential effect of such metallic fission product inclusions to fuel motion for accident analysis and is the first known attempt at such an assessment.

The first portion of this work involves a characterization of the metallic inclusions with respect to species composition, and inclusion size and distribution within fuel pellets under various irradiation conditions. Such characterization was accomplished through an extensive literature review of metallurgical assay of irradiated fuel rods. A typical inclusion composition for $(U_{.8}\ Pu_{.2})\ O_2$ fuel irradiated in a fast neutron spectrum consists of Molybdenum (14.5 wt%), Ruthenium (43.3 wt%), Technetium (20 wt%) Rhodium (17.6 wt%), Palladium (2.1 wt%) and Iron (2.45 wt%); while for UO_2 irradiated in a thermal neutron spectrum inclusions consist of Molybdenum (41 wt%), Ruthenium (18 wt%), Technetium (18 wt%), Rhodium (5 wt%) and in addition Tellurium (2.1 wt%) Strontium (.9 wt%) and Barium (6.75 wt%).

An equation-of-state, based upon inclusion composition, was then developed from standard thermodynamic principles, considering the inclusions to be either homogeneous solutions of the different metals or complete immiscibility of the various metal constituents. A fuel motion model was then developed and the contributions due to metallic that such metallic segregation does occur with inclusions found throughout the fuel matrix. During normal reactor operation such metallic inclusions are in a solid state, but at the elevated temperatures expected for overheating accident conditions, these inclusions may tend to volatilize, contributing to fuel melting. This work involves an assessment of the potential effect of such metallic fission product inclusions on fuel melting for accident analysis and is the first known attempt at such an assessment.

The first portion of this work involved a characterization of the metallic inclusions with respect to species composition, and inclusion size and distribution within fuel pellets under various irradiation conditions. Such characterization was accomplished through an extensive literature review of metallurgical study of irradiated fuel rods. A typical inclusion composition for $(U_{.8}Pu_{.2})O_2$ fuel irradiated in a fast neutron spectrum consists of Molybdenum (24.0 wt%), Ruthenium (40.0 wt%), Technetium (10 wt%) Rhodium (17.0 wt%), Palladium (2.5 wt%) and Iron (2.45 wt%); while for UO_2 irradiated in a thermal neutron spectrum inclusions consist of Molybdenum (41 wt%), Ruthenium (28 wt%), Technetium (10 wt%), Rhodium (5 wt%) and in addition Palladium (2.1 wt%) Strontium (? wt%) and Barium (6.75 wt%).

An equation-of-state, based upon inclusion composition, was then developed from standard thermodynamic principles, considering the inclusions to be either homogeneous solutions of the different metals or complete immiscibility of the various metal constituents. A fuel melting model was then developed and the contributions due to metallic

inclusion volatilization and fission gas bubble expansion were assessed. Predicted results were compared with previously obtained fuel motion data of irradiated fuel rods tested, in-pile, to elevated temperatures. Metallic inclusion volatilization potential was then assessed for both light water and fast reactor fuels, considering both UO_2 and $(Pu, U)O_2$.

The contribution to fuel expansion due to volatilization of the metallic fission product inclusions were calculated for \$15/s transient overpower (TOP) accident, assuming 3 atom percent burnup. It was initially assumed that each individual species within the inclusion volatilized when its vapor pressure exceeded the internal fuel rod pressure, which for typical liquid metal fast breeder reactor (LMFBR) would be about 20 atm while for light water reactor (LWR) would be either 70 atm for boiling water reactor (BWR) or 160 atm for pressurized water reactor (PWR). For LMFBR conditions and $(Pu, U)O_2$ fuel, a maximum nodal (local) volume expansion (i.e. the percent volume increase from the original volume of 20-30% and a total fuel rod volume expansion of 1% was calculated prior to incipient fuel vaporization.

Thermodynamic consideration indicate that the metallic inclusion constituents may be mutually soluble; thus the effect of single-phase volatilization was also assessed. Making use of Raoult's law of partial pressure, the inclusion vapor pressure for a typical LMFBR type inclusions is found to be less than that required to overcome fuel rod internal constraints, such that fuel vaporization is predicted to occur before significant inclusion volatilization.

For the typical inclusion composition found for LWR fuel, the miscible inclusion vapor pressure was assessed to be much greater than that for LMFBR fuel due to the presence of small quantities of Tellurium, Strontium, and Barium not found in fast reactor fuel metallic inclusions. These three elements are more volatile than Palladium, Iron, and Antimony found in fast reactor fuel inclusions and contribute a minimum of 75% of the nodal volume expansion. The high volatility of the constituents for in LWR-type inclusions also causes expansion to occur much earlier in the transient. It thus appears that thermal reactor fuel may swell due to volatilization of metallic inclusions during an overpower transient, if either segregated or homogeneous inclusions are assumed.

Fission gas analysis and experimental results indicate that the expected fission gas driven fuel volume expansion is on the order of 0-40%, depending on steady state and transient irradiation conditions. In addition, fuel volume expansion due to the solid-liquid change of phase is estimated to be 10%.

In summation, it was found that LWR metallic inclusion volatilization can provide a substantial fuel motion driving potential during transient overheating. However, such is not the case for LMFBR fuels, where the metallic inclusions are not expected to play a role in fuel expansion during accident transients.

TABLE OF CONTENTS

TABLE OF CONTENTS (cont)

TABLE OF CONTENTS (cont)

LIST OF FIGURES

LIST OF FIGURES (cont)

LIST OF FIGURES (cont)

LIST OF FIGURES (cont)

LIST OF TABLES

LIST OF TABLES (cont)

LIST OF TABLES (cont)

1. INTRODUCTION

A major concern in the licensing of Liquid Metal Fast Breeder Reactors (LMFBR) is that of postulated Core Disruptive Accidents (CDA's). These accidents occur when an initiating event is coupled with a failure of the plant protection system. If such negative reactivity feedbacks as fuel expansion are insufficient to cause a neutronic shutdown, it can then only be achieved by core dispersal.

Unlike the Light Water Reactors (LWR), the LMFBR core is not in its most reactive configuration. Thus negative and positive reactivity insertion is very dependent on core dimensional changes and material relocation, making core disassembly accidents of concern even if their probability of occurence is extremely low. The analysis of power excursions is generally broken into three phases: accident initiation, reactor disassembly, and containment evaluation. Two general groups of core disruptive accidents are usually described depending on the type of "initiation" phase. These two are: (1) Loss-Of-Flow Initiated Accidents (LOCA) such as pump failure, pipe breaks, etc., and (2) Transient-Overpower Initiated Accidents (TOP) such as control rod failure, fuel relocation to an area of higher reactivity, etc. These two accidents usually follow differing accident sequences. In the LOCA accident, the "initiation" phase progresses from the loss of coolant, to channel voiding, clad melting and resultant fuel slumping with an attendant rapid rise in temperature at the outside surface of the fuel

element. For a TOP type accident, the pin temperature rises perferentially at the fuel center due to the increased power level, thus the "initiation" phase progresses from positive reactivity insertion, to fuel heating and melting, to clad failure. In a LOF type accident, fuel slumping or movement to areas of high reactivity can cause the remaining intact pins to experience a TOP situation, that is, a loss-of-flow (LOF) driven TOP. To assess fuel relocation problems for such accidents, various codes and models have been developed. However, to date the effect of the potentially volatile fission products on such fuel motion has not been assessed.

In this work, the possible contributions of volatile fission products to the accident sequences is considered. Volatile fission product effects may be broken down into several groups:

1. fission product vaporization and release leading to pin pressurization and clad loading;
2. possible fuel axial motion prior to clad failure due to fission product vaporization and fuel foaming;
3. fission product vapor pressure as a driving force for fuel expulsion and dispersal at clad failure.

Such effects may either terminate or lessen the destructive impact of the accident sequence. For example, item 2 would provide a negative reactivity feedback to the core in a TOP which would decrease the driving transient and may or may not stop the core disruptive accident; however, it could provide a longer time sequence allowing lower fuel temperature at clad failure, probably a less energetic accident, and more time to control the reactor before disruption occurs. Some

fission product effects, such as item 1, might increase the energetics or severity of an accident. Fission product vaporization may contribute substantially to a decrease in time-to-clad-failure. At clad failure the fission product vapor could increase an impulse force generated by a FCI by driving more fuel into the coolant channel and in a shorter Δ time.

This report is concerned primarily with item 2 which could provide a safety reactivity feedback loop. Experimental evidence of fuel foaming and axial fuel motion has been reported by ANL in the F2 test,[1] by General Electric in the C3B,[2] C4A,[3] and C5[4] pins. This phenomena has also been mentioned in ANL-7963[5] in the design of inherently safe fuel pins. Annular blankets and reflectors were proposed to accommodate the fuel foaming and the axial movement.

Up to the present, fuel foaming has been attributed totally to fission gases, i.e., those elements in gaseous form at normal operating temperatures. During a transient condition, fission gas bubble nucleation, growth, and coalescence will occur, also contributing to fuel foaming, pin pressurization, and possible axial fuel motion. Models such as GRASS,[6] HOPE,[7] FRAS[8] - PFRAS,[9] VENUSII[10] are used to assess the role of fission gases during an accident situation. Other models such as BEHAVE3,[11] HOTPIM,[12] and TOFFII[13] calculate axial fuel motion. None of these models, however, account for contributions by volatile fission products. This report assesses the potential of

volatile fission products to fuel motion and, the magnitude of this contribution in comparison to that due to fission gases.

Irradiated oxide and mixed oxide fuels contain metallic inclusions, as seen in Fig. 1.1[*] made up of fission products that include elements which can volatilize in pure form at or below fuel temperatures reached in an accident situation. These aggregates are logical structures to investigate due to the concentration of volatile elements. Some key questions, however, must be answered in order to determine if the inclusions can contribute to fuel foaming and pin pressurization. Such questions include:

1. The composition of typical metallic inclusions;
2. The radial distribution and characteristic size of the inclusions within the fuel;
3. The vapor pressures of the inclusion constituents;
4. The phase diagram of the inclusion, i.e., whether the elements are in solid solution or if two or more phases exist;
5. The comparison of the total vapor pressure of the inclusion to the fuel vapor pressure.

---

[*] Photograph courtesy of W. F. Murphy, Argonne National Laboratory.

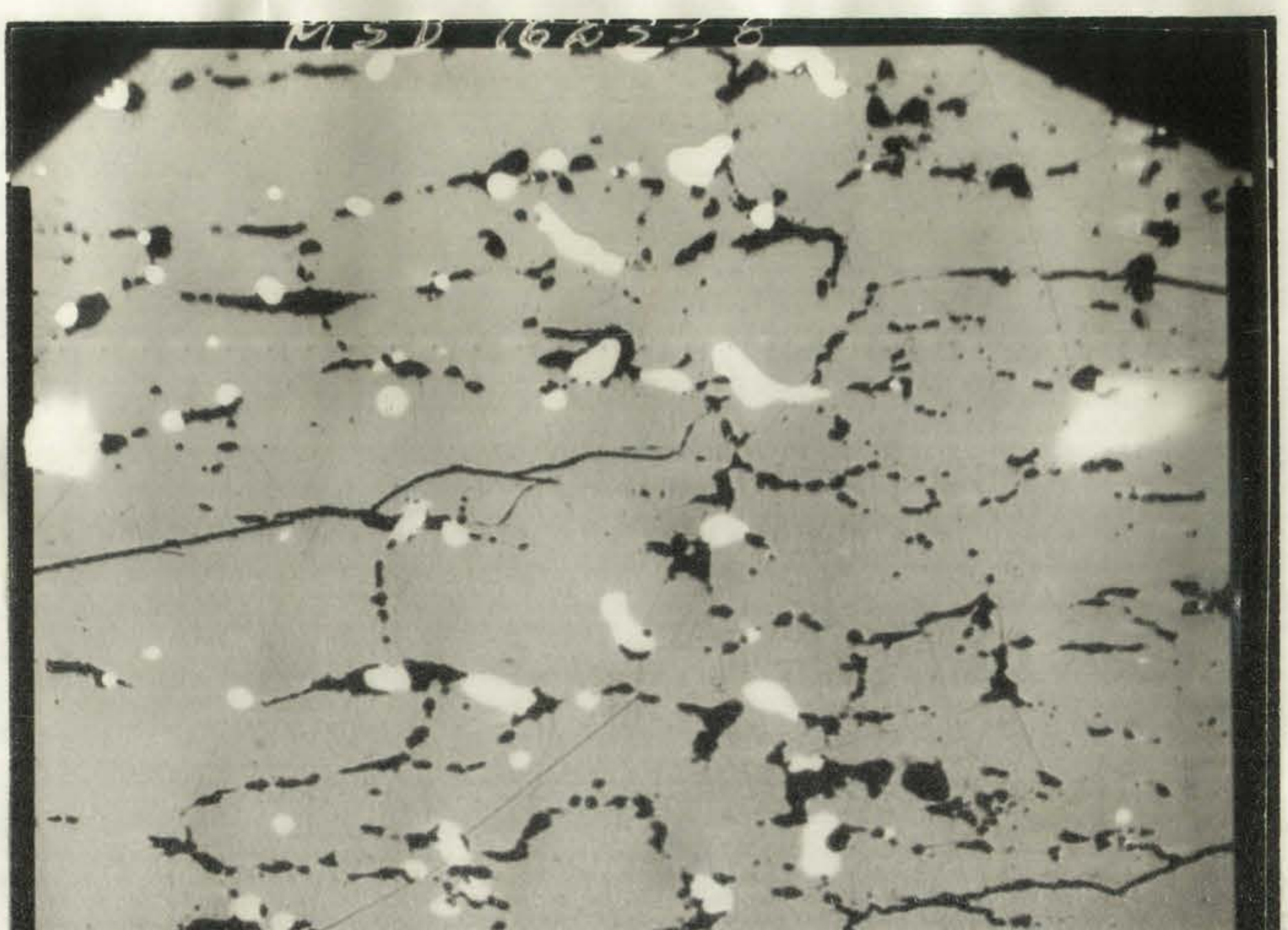

Figure 1.1
Micrograph showing the presence of metallic inclusions. 250 x.

REFERENCES

1. R. G. Palm, C. L. Fink, R. R. Stewart, S. M. Gehl, and A. B. Rothman, "F2 Phenomenological Test on Fuel Motion," Argonne National Laboratory report ANL/RAS 76-29 (September 1976).

2. J. E. Harson and J. H. Field, "Experimental Studies of Transient Effects in Fast Reactor Fuels Series III, Preirradiated Mixed Oxide (PuO_2-UO_2) Irradiations Final Report, Transient Irradiation," General Electric Company report GEAP-4469 (July 1967).

3. G. R. Thomas, J. H. Field, "Oxide Fuel Behavior During Transient Overpower Conditions," Proc. Int. Conf. Fast Reactor Fuel Element Technology, American Nuclear Society (New Orleans, Louisiana, April 1971).

4. T. Hidiko and J. H. Field, "Molten Fuel Movement in Transient Overpower Tests of Irradiated Oxide Fuel," General Electric Company report GEAP-13543 (September 1969).

5. J. T. A. Roberts, D. T. Eggen, C. D. Livengood, G. G. Trantina, D. Stahl, P. P. Lambropoulos, L. A. Neimark, R. H. Shum, M. G. Stevenson, P. R. Huebotter, "Inherently Safe Fuel Development: Preliminary Analyses and Recommendations," Argonne National Laboratory report ANL-7963 (November 1972).

6. R. B. Peoppel, "An Advanced Gas Release and Swelling Subroutine," Proc. Int. Conf. Fast Reactor Fuel Element Technology, American Nuclear Society (Hinsdale, Illinois, 1971) pp. 311-326.

7. E. T. Rumble, "A Hypothetical Overpower Exclusion Model for Liquid Metal Cooled Fast Breeder Reactors," Ph.D. dissertation in Engineering, University of California Los Angeles (June 1974).

8. E. E. Gruber, "Transient Gas Release from Oxide Fuels: Parametric Representation of FRAS Results," Argonne National Laboratory report ANL/RAS 75-17 (March 1975).

9. E. E. Gruber, "A Generalized Parametric Model for Transient Gas Release and Swelling in Oxide Fuels," Argonne National Laboratory report ANL-77-2 (January 1977).

10. J. F. Jackson and R. B. Nicholson, "VENUS II: An LMFBR Disassembly Program," Argonne National Laboratory report ANL-7951 (September 1972).

11. S. Oldberg, Jr. and R. G. Stuart, "Steady-State and Transient Fuel Mechanics: The BEHAVE-3 Code," General Electric Company report GEAP-14021 (August 1974).

12. H. J. Willenberg, et al. "Dynamics of Molten Fuel Motion During Fast-Reactor Overpower Transient," Proc. Int. Conf. Fast Reactor Safety Meeting (Beverly Hills, California, April 1974).

13. R. G. Stuart and G. R. Thomas, "Effects of Fission Gas on Transient Overpower Fuel Rod Failure," Trans. of Am. Nuc. Soc., 13, (1970) p. 654

2. FISSION PRODUCT CHARACTERIZATION

In order to determine the possible contribution of fission products to accident scenerios, the location, quantity, and physical and chemical state of these products must be known. The quantity of fission products is dependent on fuel burnup and the fission product yield of the fuel species. The location and physical and chemical state is dependent on the oxygen potential and other thermodynamic properties of the individual fission products. These areas are discussed to determine the fission products that will be of concern in this work.

2.1 Fission Product Yield

The proportion of the various fission and decay products in the fuel at any given time depends on the particular fissile materials and flux/energy spectrum. For a short period of time after startup the fission product yield also depends on flux levels and irradiation time, but this is not important for fuels irradiated longer than 100 days. The fission product yield distribution does not change appreciably within the neutron energy range, a few Kev - few Mev, of concern with fast reactors, but does depend on the fissile composition as seen in Fig. 2.1.[1]

The yield of mixed oxides, (U, Pu) O_2, is weighted somewhat to the heavy metal elements, i.e. atomic masses 100-110, at the expense of light elements due to the upward shift of the lower yield curve of

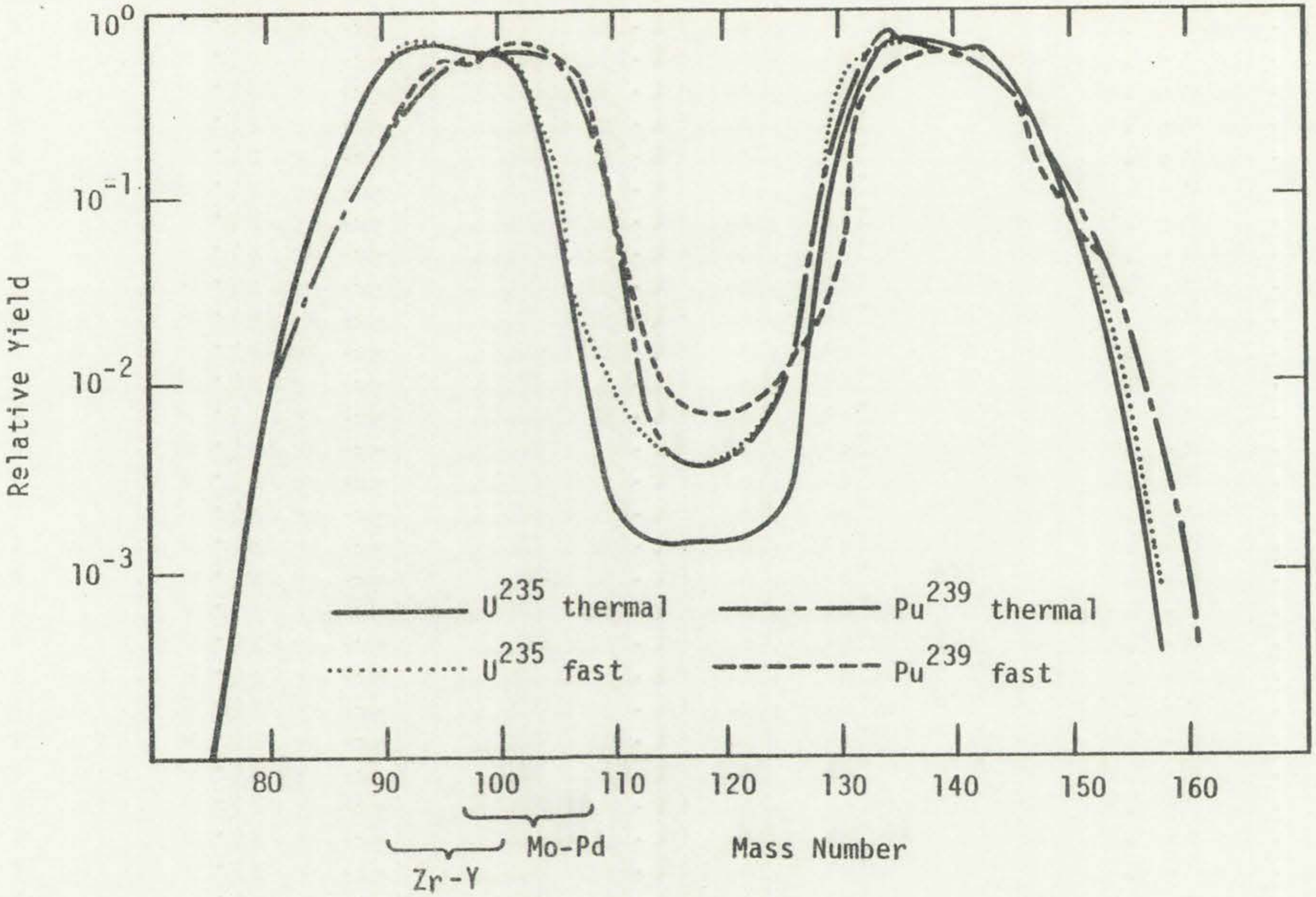

Figure 2.1.
Fission yield spectra of U^{235} and Pu^{239}.

Pu^{239} vs U^{235}. For example, in the fissioning of Pu^{239} compared to U^{233} or U^{235}, there is a drop in the yield of zirconium isotopes from about 30% to 20% as well as a drop in the light elements cerium, strontium, with a corresponding increase in the noble metal products, rhodium, ruthenium, and palladium, as shown in Table 2.1.a[1] and Table 2.1.b[2]

Fission product yields have been calculated for oxide and mixed oxide fuels and various irradiation spectrums.[2-7] Computations have shown that the effect of power rating and cooling time on composition are negligible for irradiations longer than 100 days. Obviously short lived products build up to very low equilibrium values, and it is the long half-life and stable products that become important. However, as will be mentioned later, the precursors of the stable or long lived products can have an effect on where their daughter nuclei will be spatially located in the fuel pin for the case where the diffusion time is shorter than the decay time. A few of these yield curves will be used in later analysis.

2.2 Oxygen Potential

The oxygen potential controls the chemical state of the fission products, and their interaction with and distribution throughout the fuel.

The valency, thus the oxygen requirements for the fuel and fission products, is controlled by the partial molar free energy or oxygen potential for the reaction:

Table 2.1a

Atom Percent of Final Fuel Composition at 10% Burn-up.

Element	Thermal Fission $(^{238}U_{.70}, ^{235}U_{.30})O_2$	Thermal Fission $(U_{.70}, Pu_{.30})O_2$	Fast Fission $(U_{.85}, Pu_{.15})O_2$
Y	.195	.084	.078
La	.216	.199	.177
Ce	.840	.691	.446
Pr	.139	.123	.164
Nd	.373	.328	.514
Pm	.063	.059	.063
Sm	.063	.106	.119
Eu	.006	.021	.021
Ba	.232	.215	.212
Zr	1.085	.740	.685
Sr	.416	.125	.140
Nd	.047	.038	.021
Mo	.676	.678	.665
Tc	.202	.197	.190
Ru	.444	.851	.695
Rh	.050	.099	.167
Pd	.042	.425	.419
Xe	.703	.755	.696
Cs	.625	.647	.605
Rb	.123	.049	.072

Table 2.1b

Atoms Per 100 Atoms Fast Fissioned,
135 Days Irradiated, 0 Days Cooling

Element	U^{235}	Pu^{239}
Zr	29.510	20.650
Ce	15.852	13.403
Sr	9.875	4.418
Ba	6.910	6.304
Mo	21.394	20.098
Tc	6.010	5.835
Ru	16.091	24.736
Rh	2.450	5.458
Pd	1.600	15.500

$$M(s) + \frac{x}{2} O_2\ (g) \rightarrow MO_x(s) \quad . \tag{2.1}$$

The free energy of formation for various fission product oxides and fuel systems are calculated from Eq. (2.2), based on the thermochemical constants given in Ref. 8;

$$\Delta F = \Delta H_{f,298} - (2.303\ \Delta a)\ T \log T - \tfrac{1}{2}\ (\Delta b \times 10^{-3})\ T^2 - \frac{1}{6}\ (\Delta c \times 10^{-6})\ T^3 - \frac{\tfrac{1}{2}\ (\Delta d \times 10^5)}{T} - T\ \Delta(B - a) + \Delta A \quad , \tag{2.2}$$

where

ΔF = free energy of formation at T,

T = temperature,

$\Delta H_{f,298}$ = heat of formation of the oxide under consideration from the elements at 298 K,

$\Delta a, \Delta b, \Delta c, \Delta d, \Delta(B-a), \Delta A$ = empirical constants.

The derivation of Eq. (2.2) can be found in Appendix A. Figure 2.2 shows the results for representative fission products. For a system in thermodynamic equilibrium, the free energy is a minimum, thus allowing a prediction of the chemical state of the various fission products. Complicating factors exist in this prediction, however. First, the initial state of the fuel has a large effect on its oxygen potential. As shown in Fig. 2.3[9] the oxygen potential of UO_2 and PuO_2 is strongly dependent on whether the fuel is hypo- or hyperstoicheometric. The oxygen potential undergoes a rapid change

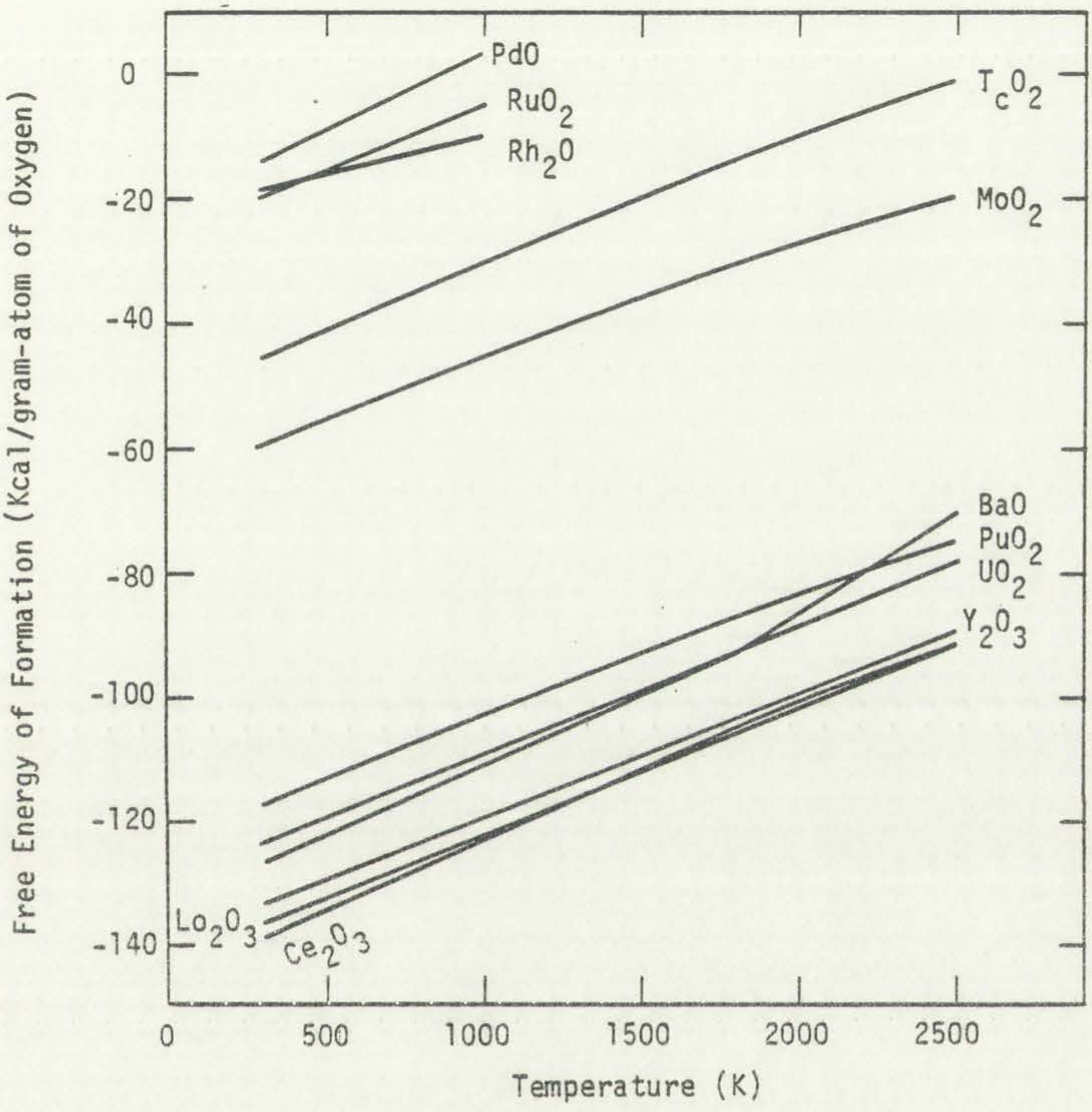

Figure 2.2.
Free energy of formation for various
fuels and fission products.

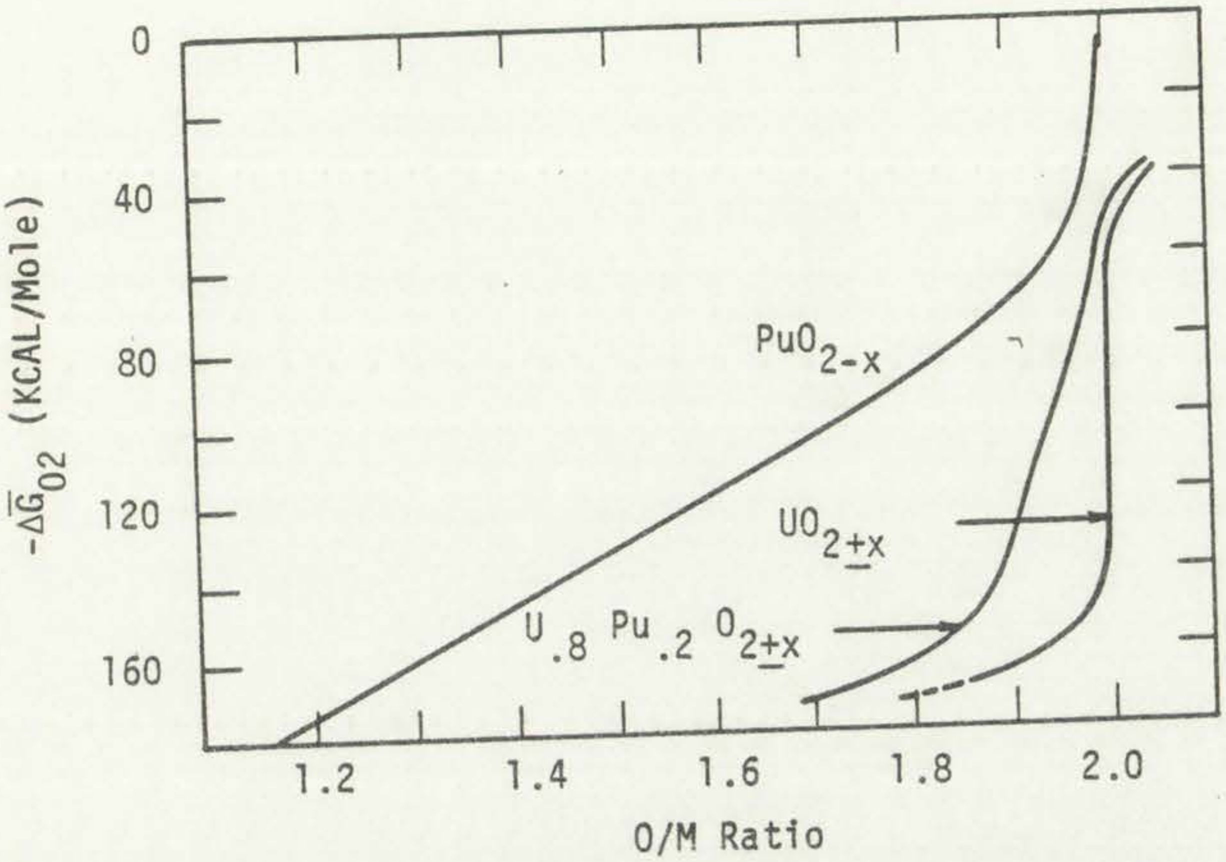

Figure 2.3.
Calculated oxygen potentials at 2513 K for $UO_{2\pm x}$, PuO_{2-x}, and $(U_{.8}Pu_{.2})O_{2\pm x}$.

between $MO_{1.99}$ and $MO_{2.01}$. In addition to the oxygen-to-metal (O/M) ratio, the total number of moles of uranium and plutonium, and the quantity of fission product elements available to go into solid solution in the flourite phase change with burnup. The rate at which the O/M ratio increases with burnup is dependent on the fuel composition. Plutonium, with its increased yield of noble metals at the expense of lighter elements, has a lower average valency per fission product than U, i.e. 1.3^+ vs 1.7^+,[10] leading to a larger increase in stoichiometry per atom % burnup.

As seen in Fig. 2.2, the oxygen potentials for the various fission products vary approximately linearly with temperature but have

differing slopes. Thus, a fuel pin having a temperature gradient leads to a gradient in the oxygen potential. Figure 2.4[9] illustrates calculated and measured oxygen potentials vs temperature for $(U_{.8}Pu_{.2})O_{2\pm x}$ for various investigators. Such a gradient provides a driving force for the oxygen, U, Pu, and fission product concentrations to redistribute, involving a combination of solid-state diffusion and gaseous transport processes.[*] Figure 2.5 illustrates the effect on the oxygen distribution as calculated by Rand and Markin[11] for the various stoichiometries of fuel.

Using the oxygen potentials, the fission products can be broken into four groups:

A. Those that form stable oxides.

B. Those that exist as stable gases at normal fuel operating temperatures.

C. Molybdenum, which has an oxygen potential very close to that of stoichiometric UO_2 and $(Pu, U)O_2$.

D. Those that remain stable in their elemental form (metallics).

2.3 Stable Oxides.

Besides the fission products which remain in their elemental form or exist as gases, a certain portion of the fission yield products, $\simeq$ 45%,[12] interact with the fuel to form stable oxides. Such elements as Y, La, Zr, and the rare earths (Ce, Pr, Nd, Pm, Sm, Eu, and Gd) form

---

[*] By solid-state diffusion one is referring to individual atom or molecule diffusion through the lattice. In the gaseous transport process, atoms are swept through the fuel columnar region by lenticular pores. Gas or vapor also aggregates into bubbles in other fuel regions and can form interconnecting pores along the grain boundaries.

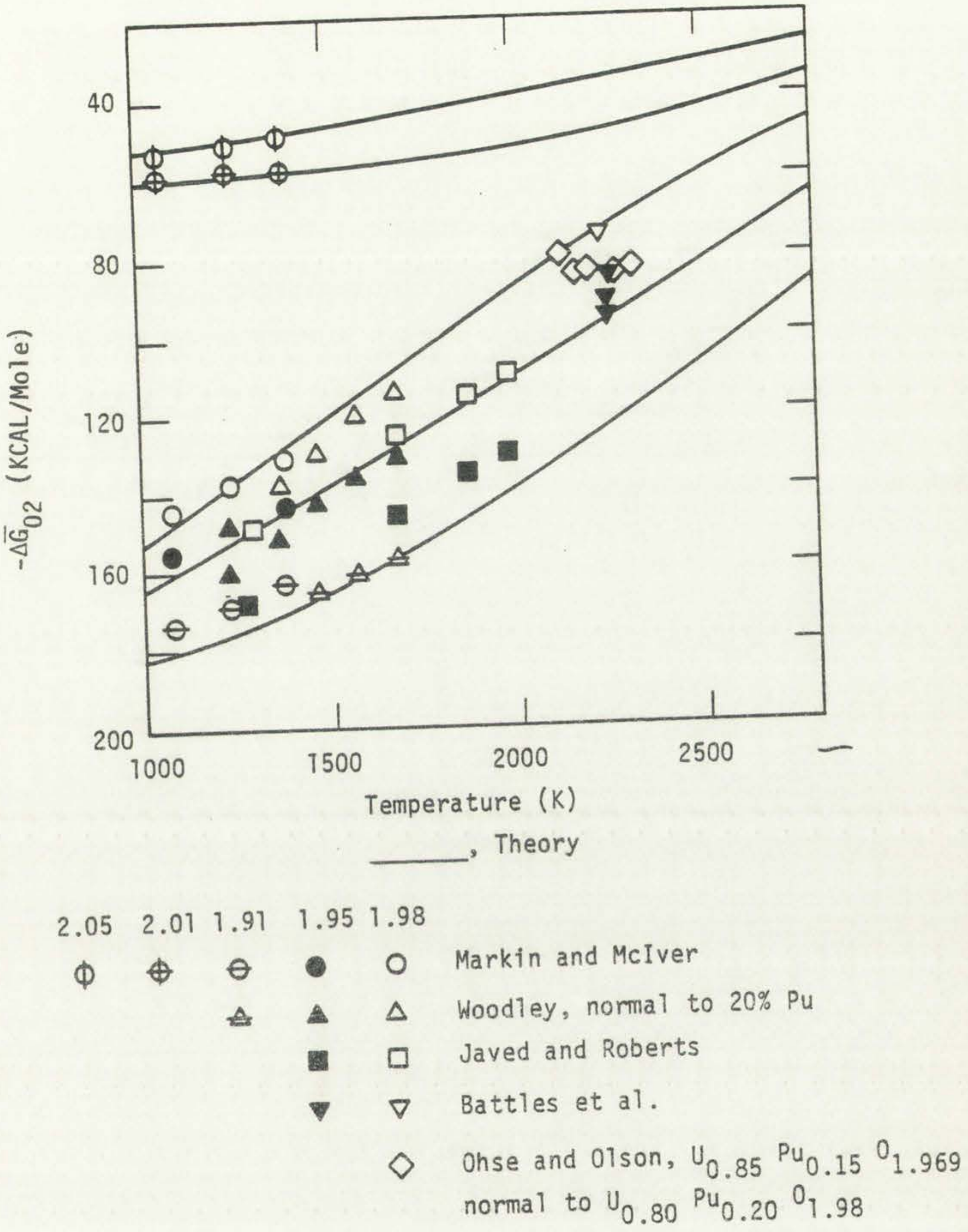

Figure 2.4.
Calculated and measured oxygen potential vs temperature curves for $(U_{.8}Pu_{.2})O_{2\pm x}$.

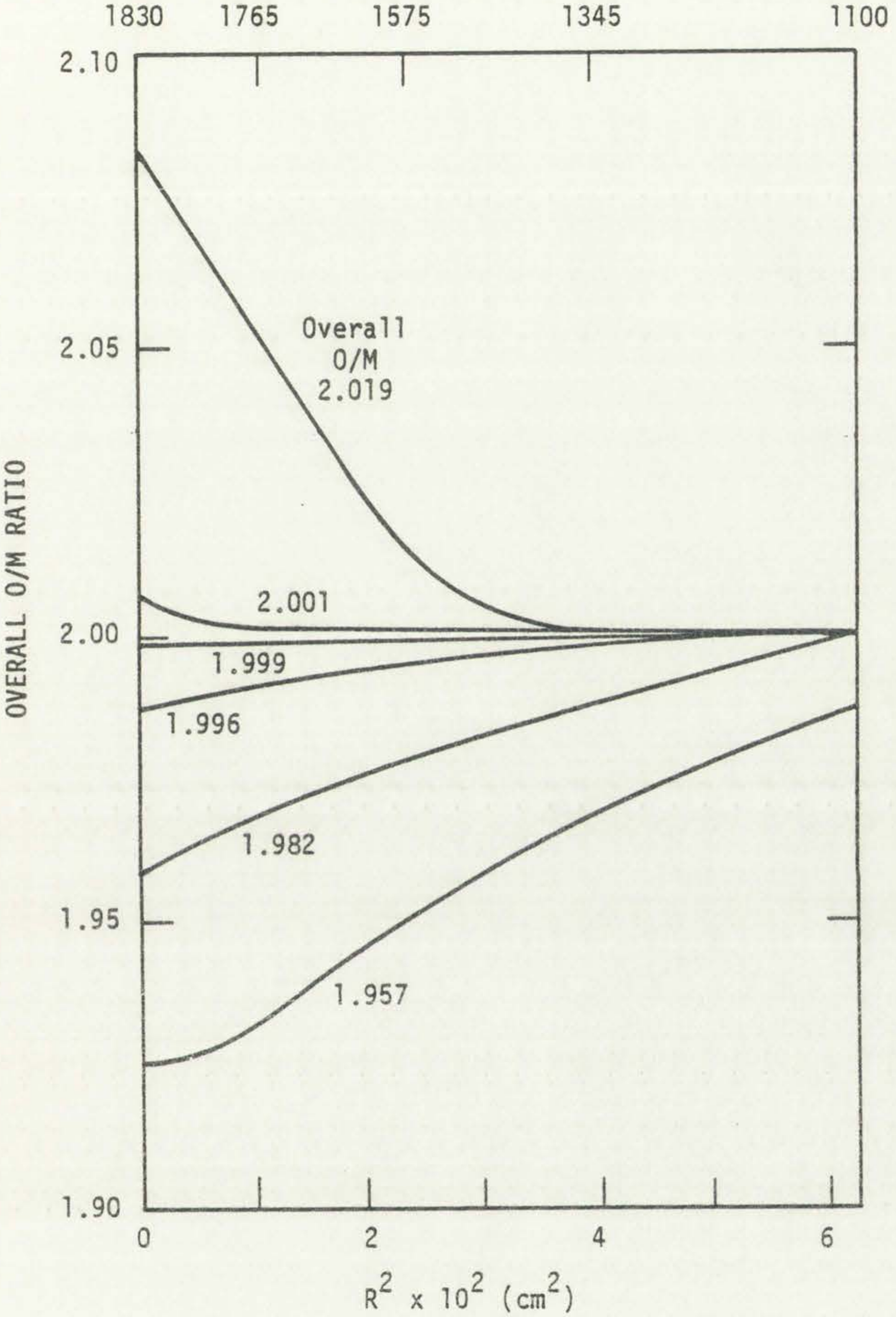

Figure 2.5
Oxygen distribution in $(U_{.85}\,Pu_{.15})\,O_{2\pm x}$ as computed by Rand and Markin.

oxides of greater stability than the initial UO_2 or $(U, Pu)O_2$. Even if there is not enough oxygen freed during the fission process, these elements will reduce the fuel matrix. Such elements are soluble fission products and their oxides enter the fuel crystalline structure.

Ba, Sr, and Nb also form stable oxides BaO, SrO, NbO_2 but are not in solid solution with the fuel,[1] but can be expected to form a separate oxide phase. As the fission product elements accumulate in the oxide matrix, however, physical-chemical phases most stable under the local conditions will form. As the concentration of Sr, Ba, and Zr increases, the tendency to form a separate phase of $SrZrO_3$ and $BaZrO_3$ will increase via the following reactions:

$$SrO + ZrO_2 = SrZrO_3$$

$$BaO + ZrO_2 = BaZrO_3$$

It can be shown that at even 1 atom %, the mole fraction solubility products of the zirconates, ($BaZrO_3$, $SrZrO_3$), exceed their activity solubility products. Thus, it is expected that both solid phases will tend to form early in the irradiation life of the fuel.

In the metallurgical analysis of irradiated oxide and mixed oxide fuels, two separate types of solid fission product states were observed:

1. small, $\simeq$ 5 -$\simeq$10 m dia., metallic inclusions to be discussed later,
2. a separate gray phase.

This separate gray phase had been observed by various investigators.[12-17] O'Boyle[12] found this phase in the equiaxed region immediately adjacent to the columnar grains. Analysis of this gray

phase yielded a high concentration of Ba and Ce. Concentrations of U and Zr were low, but some Sr was present. The analysis does not support the formation of zirconates, where equal concentrations of Ba plus Sr, and Zr are expected. O'Boyle[12] believes the Ba and Sr existed in their oxide state. The Ce in or near Ba concentration is not unusual since La and Ce are daughter products of Ba-140 and Ba-142. During normal operation La and Ce from the decaying Ba redissolve into the fuel matrix. After shutdown, however, the migration and resolution processes virtually cease. Thus, in the analysis of this separate phase after shutdown, Ce is associated with the Ba.

The yields of Sr and Ba are fairly close; therefore, one would expect a measured concentration of Sr very close to that of Ba in the gray phase. This was not the case in any of the observed analyses,[10,12,16,17,18] and may be due to the very short half life of the volatile precursors of Sr-90, i.e. 33 s for Kr, 2.74 m for Rb, and 28 y for Sr, which makes up approximately 60% of the total Sr yield. The volatile precursors of Ba-138, 5.9 s for I, 17 m for Xe, 32 m for Cs-Ba(stable), are much longer lived. Not only the volatility but also the decay time of precursors is important in determining the form and location of daughter products.

Kleykamp's[15] analysis of the gray phase indicated that is predominantly metallic (Mo, Tc, Ru, Rh) in nature; thus the assumption that the gray phase is made up of fission product oxides or zirconates phase exhibits a high concentration of [illegible] and Ba. [illegible] for [illegible] was [illegible] present. The [illegible] does not support the formation of [illegible], where equal concentrations of Ba, Sr, and Zr are expected. [illegible][38] [illegible] the Ba and Sr [illegible] in their [illegible] states. The Sr-to-Ba [illegible] concentration is not unusual since Ce and [illegible] daughter products of Xe-140 and Xe-143. During normal operation Xe and Cs [illegible] into the fuel matrix. After shutdown, however, the [illegible] and [illegible] processes [illegible] cease. Thus, in the analysis of this [illegible] phase after shutdown, Ce is associated with the Ba.

The yields of Sr and Ba are fairly close; therefore, one would expect a measured concentration of Sr very close to that of Ba in the gray phase. This was not the case in any of the observed analyses,[10,38,16,17,18] and may be due to the very short half life of the volatile precursors of Sr-90, i.e. 33 s for Kr, 1.23 m for Rb, and [illegible] for Sr, which makes up approximately 20% of the total Sr yield. The volatile precursors of Ba-140, [illegible] for I, [illegible] for Xe, [illegible] for Cs, are much longer lived. Not only the volatility but also the decay time of precursors is important in determining the form and location of daughter products.

Kleykamp's[38] analysis of the gray phase indicated that it predominantly contains (Ba, Sr, [illegible]) [illegible] from the assumption that the gray phase is made up of fission product [illegible] or [illegible] cannot be made. The analysis of fuel microstructure by Hanson[14] found the gray phase located in the cooler portion of the fuel near the clad; thus, it could contain not only fission products, but also could be due to cladding attack. This phase, however, was not analyzed.

There have been analyses that support the formation of zirconates. Bazin[17] did find a gray phase in UO_2 that had concentrations of Ba, Zr, and O very close to that needed for $BaZrO_3$. HEDL-TME 76-16[16] also reported a ring of Ba-Zr deposits in the columnar grain region of the fuel. Bradbury[19] analyzed inclusions that contained Ba and Zr in a 1:1 ratio. Jeffery[18] in his inclusion analysis found a type of inclusion which contained Ba and Zr in a 4:5 ratio which is close to 1:1.

From the above analysis, it is known that a large portion of the stable oxides are in solution within the fuel structure, with Ba and Sr, however, tending to form a separate oxide or zirconate phase. From the experimental evidence, it appears that a high concentration of Ba is present in the gray phase, but one cannot make a conclusion about its state (oxide or zirconate).

2.4 Stable Gases

Elements that exist as vapor in the fuel include the inert gases Xe, Kr; the halogens Br, I; and the highly volatile elements (Ce, Te, Rb, Cd, Sn, Se, and Sb). It should be noted that Cd, Sn, Te, and Sb are listed both under stable metallics and also under stable gases. This is due to the fact that their vaporization temperatures are in the

range between the expected maximum and minimum fuel temperature at steady state operation. Since these elements exist as vapors in the columnar region they migrate by the same mechanism as the inert gases. Some of the fission products such as Cs are swept out with the Xe and Kr and condense in the cooler regions of the fuel, i.e., at the clad-fuel interface.

A radial concentration profile of Cs in a fuel pin shows high concentration of cesium in the unrestructured region of the fuel and in the region of the fuel-clad interface. Cs was not detected within the columnar grains but was found in the cracks and voids in this region, supporting the idea that redistribution of cesium occurs by vaporization rather than by diffusion through the matrix.

2.5 Molybdenum

The chemical state of Mo and the oxygen balance in the fuel are interdependent. The extent of MoO_2 formation depends on such factors as temperature, fuel composition, oxygen potential, and initial O/M ratio.

As seen in the Ellingham diagram, Fig. 2.6,[1,11,20] the oxygen potential of MoO_2 is very close to that of stoichiometric fuel. The free energy of formation of Mo oxide is of the same order of magnitude as the fuel at low temperatures but increases rapidly with increasing temperature. It can also be seen that the oxygen potential of the fuel decreases as the fuel becomes more hypostoichiometric. Thus for hypostoichiometric fuel at temperatures of relevance to reactor range between the operating surface and maximum fuel temperatures at steady state operation. Since these elements exist as vapors in the columnar region they migrate by the same mechanism as the fuel. Since some of the fission products such as Cs are swept out with the Xe and Kr and condense in the colder regions of the fuel, i.e., at the clad-fuel interface.

A radial concentration profile of Cs in a fuel pin shows high concentration of cesium in the low-temperature region of the fuel and in the region of the equiaxed structure. Cs was not detected within the columnar grains but was found in the cracks and voids in this region, supporting the fact that redistribution of cesium occurs by vaporization rather than by diffusion through the matrix.

2.3 Molybdenum

The chemical state of Mo and the oxygen balance in the fuel are interdependent. The extent of MoO_2 formation depends on such factors as temperature, fuel composition, oxygen potential, and initial O/M ratio.

As seen in the Ellingham diagram, Fig. 2.6.[illegible] the oxygen potential of MoO_2 is very close to that of stoichiometric fuel. The free energy of formation of Mo oxide is of the same order of magnitude as the fuel at low temperatures but increases rapidly with increasing temperature. It can also be seen that the oxygen potential of the fuel decreases as the fuel becomes more hypostoichiometric. Thus for hypostoichiometric fuel at temperatures of relevance to reactor

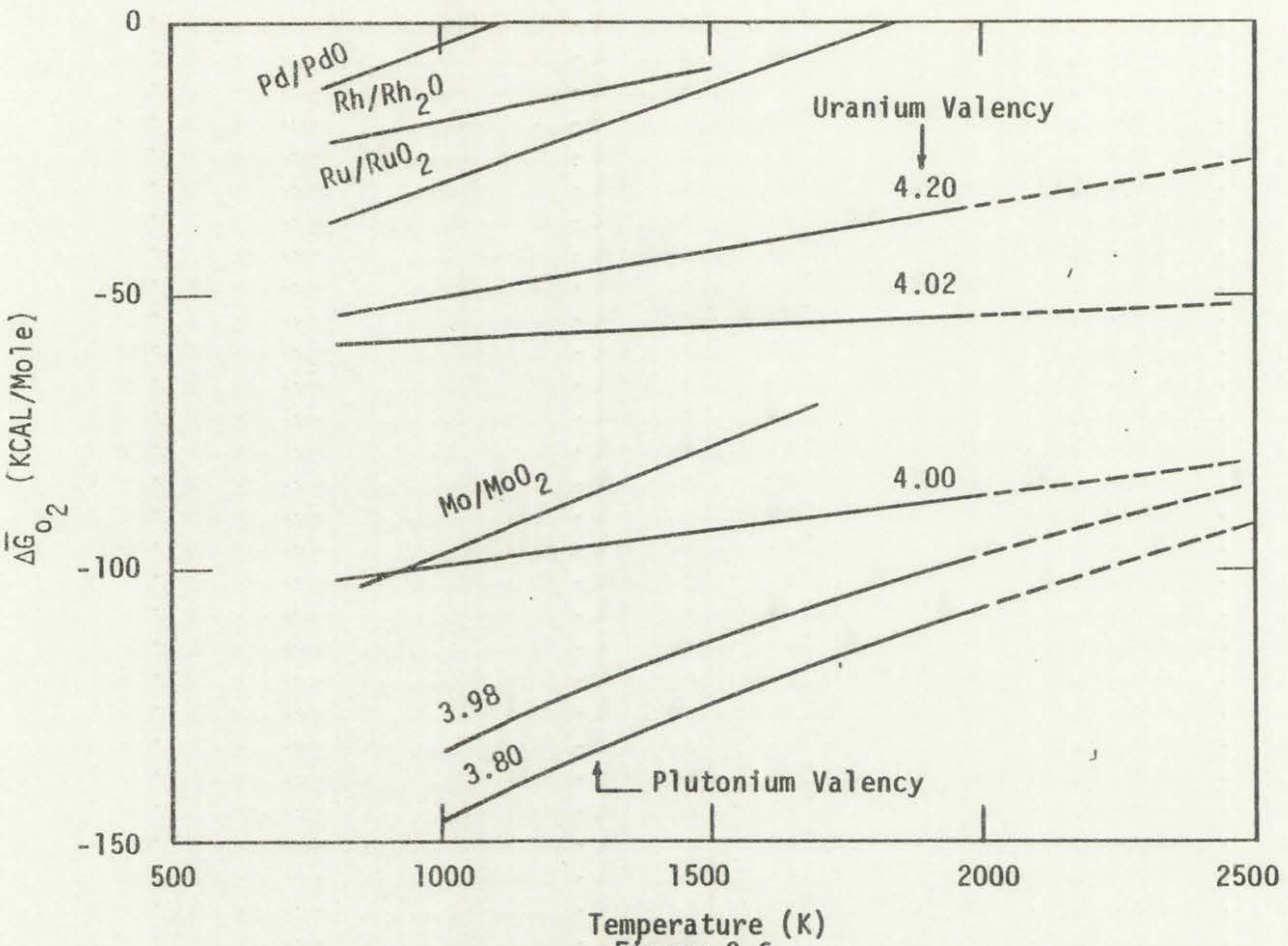

Figure 2.6

Ellingham diagram comparison of oxygen potentials of uranium, plutonium oxides as a function of U valency ($\geq$ 4.00) and Pu valency ($\leq$ 4.00) and some fission product metal/metal oxide couples.

operation, i.e. > 1000 K, one would expect only the existence of elemental Mo. In the burnup of U^{235} and Pu^{239}, the fissile phase is replaced with fission products of an average valency of 1.68^+ and 1.29^+ respectively.[10] The oxygen released has a mean valency of 2^-.[10] This leads to an increase in stoichiometry of approximately 0.012 for U^{235} fission and 0.028 for Pu^{239} fission at 4 atom % (a/o) burnup,[10] or 0.021 for $(U_{.85}, Pu_{.15})O_2$.[1] Thus, in substantially hypostoichiometric oxide, one would not expect any molybdenum oxide to form. Experiments reported by Davis and Ewart[1] support this.

Molybdenum may also react with Cs to form Cs_2MoO_4 which, because of its volatility, will deposit on the cooler cladding. Out of pile results suggest that significant quantities of Cs_2MoO_4 will not form inside irradiated fuel rods unless the fuel O/M is high (≥ 2). It is possible, however, (for low O/M) that part of the Cs released from the interior of the fuel will combine with $MoO_2(V)$, $MoO_3(V)$, and $O_2(V)$ to form $Cs_2MoO_4(V)$. This vapor phase reaction would result in an outward radial transport of a small fraction of the fission products Cs and Mo, but appears to have little impact on the total Mo distribution.[16,21]

Thus for hypostoichiometric fuel, Mo remains essentially in elemental form. Since stoichiometry increases with burnup, one must assure that for a given burnup that hypostoichiometric conditions still exist if the assumption of elemental Mo is made.

2.6 Stable Metallic State

The fission products As, Ge, Nb, Tc, Ru, Rh, Pd, Ag, Cd, In, Sn, Sb, and Mo exist in the metallic state or have oxides that are easily reduced at fuel operating temperatures. This is due to the fact that these elements have free energies of formation higher, and are thus less stable, than UO_2 and PuO_2. Since the free energy of formation of some of the fission product oxides (Pd, Rh, Ru, Tc, etc.) is positive in the temperature range of interest (2000 to 2500 K), energy must be provided to form these oxides.

Microanalysis of irradiated fuel[1,9,10,12-18,21-29] shows the presence of small inclusions, approximately 5 to 10 μm in diameter, believed to be the aggregation of these insoluble solid fission products (see Fig. 1.1). This form of fission products is a logical target for possible contribution to fuel swelling during an overpower transient. The inclusions are distributed throughout the columnar and equiaxed portion of the fuel pin and if vaporization or even partial vaporization of these inclusions occur, fuel foaming as a driving force for axial and/or radial fuel motion is a distinct possibility.

The composition of these metallic inclusions have been investigated by a number of people. Bradbury[25] analyzed inclusions found in UO_2, irradiated in the thermal flux, PLUTO reactor to 4.6 atom % burnup with an estimated center temperature of 1720 K. He found two types of inclusions: one containing molybdenum and ruthenium and the other barium and traces of cerium; the two never combined. In a later

3.6 Stable Metallic Phase

The fission products As, Sb, Mo, Tc, Ru, Rh, Pd, Ag, Cd, In, Sn, Zr, and Nb exist in the metallic state or combinations that are readily reduced at fuel operating temperatures. This is due to the fact that these elements have free energies of formation higher, and are thus less stable, than UO_2 and PuO_2. Since the free energy of formation of some of the fission product oxides (Mo, Rh, Ru, Tc, etc.) is positive in the temperature range of interest (2000 to 2500 K), energy must be supplied to form these oxides.

Microanalysis of irradiated fuel[1,2,10,12-16,21-29] shows the presence of small inclusions, approximately 5 to 10 μm in diameter, believed to be the aggregation of these insoluble solid fission products (see Fig. 3.11). This form of fission products is a logical target for possible contribution to fuel swelling during an overpower transient. The inclusions are distributed throughout the columnar and equiaxed portion of the fuel pin and if vaporization or even partial vaporization of these inclusions occurs, fuel foaming as a driving force for axial and/or radial fuel motion is a distinct possibility.

The composition of these metallic inclusions have been investigated by a number of people. Bradbury[26] analyzed inclusions found in UO_2 irradiated in the Shannon Fire, PLUTO reactor to 4.6 atom % burnup with an estimated center temperature of 2200 K. He found two types of inclusions: one containing molybdenum and ruthenium and the other barium and traces of cesium; the two never combined. In a later report,[19] however, he stated that all inclusions contained molybdenum, ruthenium, technetium, and rhodium and that only 80 out of the 3723 inclusions contained in addition, barium, cerium, strontium, and zirconium. The relative concentrations of Mo, Ru, and Tc were estimated from count rate measurements using an electron microprobe and found to be

Mo:Ru:Tc = 3.7:1.6:1

which agrees well with the values calculated from fission product yield[4] of 4.1:1.8:1. This leads one to conclude that the segregation of these fission products is almost total and that very little of these elements remains in solution in the fuel matrix.

Jeffery,[18] using an electron microprobe, analyzed the same batch of 4.6% burnup material. He found the inclusions to be small (on the average less than 5 m in diameter). His microprobe analysis of 26 different inclusions revealed 3 basic types:

1. 70% contained Mo without Ba. Rhodium, ruthenium, technetium, and neodynium were always detected in the presence of Mo.
2. 15% of the inclusions contained both Mo and Ba. Rhodium, ruthenium, and technetium were also detected along with trace amounts of other elements.
3. 15% contained Ba without Mo. Cerium, neodynium, zirconium, and strontium were also detected.

Table 2.2 contains the average weight percents of the three type of inclusions. This low irradiation temperature fuel is nonprototypic, and Jeffery does not indicate in which section of the fuel pin either axially or radially these 26 inclusions were found. This may or may

TABLE 2.2

COMPARISON OF INCLUSION COMPOSITIONS

Investigator	Fuel Description	Type of Inclusion	Consituent Weight %								Other Consituents
			Mo	Ru	Tc	Rh	Ba	Pd	Zr	Ce	
Bradbury [19]	Highly enriched UO_2, thermal spectrum, low temp. (peak < 1800°k) 4.6 atom % B.U.	2%, Barium containing					Yes		Yes		Mo, Ru, Sr, Ce, Nd
		98% Barium free	Yes	Yes	Yes	Yes					
Jeffery [18]	Highly enriched UO_2, thermal spectrum, low temp. (peak < 1800°k) 4.6 atom % B.U.	70% Type 1	41	18	13	5	-		-	-	Te, Pd, Nd < 5 w/o
		15% Type 2	21	9	6		20		10	6	Sr, Nd, Rh < 5 w/o
		15% Type 3					25		10	5	Sr, Nd, Mo < 5 w/o
Bramman [29]	$(U_{.85}, Pu_{.15})O_2$, fast spectrum 8 - 8.5 atom % B.U. 2000°C < T < T melt	1 mm inclusion at central void	41.	32	15	7		≅2			
		5-10 volume % of above incl.		2.5		11.9		38.4			
	$(U_{.85}, Pu_{.15})O_2$, fast spectrum 4.9 atom % B.U.	5µm Dia. inclusions	35	35	20	10					
O'Boyle [12]	$(U_{.8}, Pu_{.2})O_{2.0}$, fast spectrum 2.7 atom % B.U.	6µm inclusions	25	48	17						Rh + Pd ≈ 10 w/o (Based on yield data of Burris[2] split is ≈ 5 w/o Rh, 5 w/o Pd; using RIBD code[7] split can be estimated as 7.5 w/o Pd, 2.5 w/o Rh)
Johnson [26]	$(U_{.8}, Pu_{.2})O_2$ fast spectrum 9.5 atom % B.U.	Averaged Type 1 inclusion from Pin, C-11, C-15	14.5	43.3	20.	17.6		2.1			Fe ≈ 2.45
		Type 2						≈72			Fe 13-30, Sb 1-2, Te .3-1.7
		Type 3	> 90								

not have influenced the much higher percentage of barium rich inclusions found by Jeffery in the same fuel analyzed by Bradbury.

Jeffery compared the experimentally determined ratios of the concentrations of rhodium: ruthenium: technetium: molybdenum: barium (1:3.6:2.5:8.3:1.7) to the theoretical yield determined by Katcoff[4] (1:3.6:2.0:8.1:1.9). Such agreement suggests that all five elements segregate almost completely into inclusions or at least do so in the same ratio as their fission yield. This applies only to regions where inclusions are formed, i.e. columnar and equiaxed.

In the work by Bramman et al.[29] $(U_{.85}\ Pu_{.15})O_2$ was irradiated to a maximum burnup of 8-8.5 atom % in the Dounreay Fast Reactor. The center temperature of the fuel was greater than 2273 K but less than the melting temperature of the fuel, hence representing more realistic operating conditions than the fuel analyzed by Jeffery. Microanalysis was performed on small metallic particles on the order of 1 mm diameter attached to the wall of the center void. X-ray analysis of one of the particles indicated the presence of Mo, Ru, Tc, and Rh with the following approximate concentrations:

Mo 41.0 wt. %, Ru 31.9 wt. %, Tc 14.9 wt. %, Rh 7.6 wt. %

Palladium was thought to be present in about 2 wt. %, but U and Pu, if present, were in a concentration less than .5 wt. % in the section exposed.

A separate phase existed adjacent to the fuel and constituted approximately one-tenth of the whole inclusion. Quantitative analysis

of this phase gave the composition as 25.4 wt. % U, 13.5 wt. % Pu, 38.4 wt. % Pd, 11.9 wt. % Rh, and 2.5 wt. % Ru. Tc and Mo were not present. Both phases contained no significant amount of oxygen and no other elements were present in excess of .5-1. wt. %.

Another interesting aspect of Bramman's work was the analysis of inclusions approximately 5 μm in diameter found within the fuel. A sample of $(U_{.85}\ Pu_{.15})O_2$ fuel irradiated in the Dounreay Reactor to 4.9% burnup was dissolved in nitric acid yielding an insoluble residue of the inclusions. These particles were analyzed with an electron microprobe and yielded the following composition:

35 wt. % Mo, 35 wt. % Ru, 20 wt. % Tc, 10 wt. % Rh.

As stated by Bramman, a probable error of ± 5% exists on each figure because of the nature of the analysis. Palladium was also detected but only on the order of a few percent.

The initial O/M ratio of the mixed oxide was 2.004, slightly hyperstoichiometric. The relative proportion of molybdenum detected in the inclusions was approximately half of that predicted from a yield curve; therefore, as discussed in the previous section, the oxygen potential of the fuel is high enough for the formation of MoO_2.

O'Boyle et al.[12] in their electron microprobe analysis of UO_2-20 wt. % $PuO_{2.00}$, irradiated in a fast flux to a 2.7 atom % burnup, identified two separate types of solid-fission-product inclusions.

1. White metallic inclusion located in the equiaxed and columnar grain regions

2. A gray phase which was previously mentioned and located in the equiaxed grain region, thought to be insoluble oxides and zirconates.

The white metallic inclusions ranged in size up to 6μm in diameter. Ruthenium, molybdenum, and technetium account for approximately 90 wt. % of the inclusions with Rh and Pd making up the remaining 10%. The approximate concentrations can be seen in Table 2.2.

In ANL-7877[26] (Johnson) metallic inclusions from two mixed oxide pins irradiated in EBR-II were analyzed. The fuel description and irradiation history and given in Table 2.3.[26] Three distinctly different types of inclusions were found:

1. Noble-metal inclusions similar to those discussed previously found throughout the columnar-grain region and approximately midway through the equiaxed-grain region.
2. Inclusions with palladium as the principle constituent (60%-80%) alloyed with 10-30% of either iron, as an impurity in the fuel, or molybdenum or cladding constitutents. These are generally found in the cooler equiaxed and unrestructured regions of the fuel.
3. Inclusions of essentially pure molybdenum alloyed with a few percent of other fission products. Only a few of these inclusions were found and were always located in the unrestructured region.

The summary electron microprobe analysis can be found in Table 2.2

It should be noted from Table 2.2 that none of the inclusions from (U, Pu)O_2 examined thus far contain barium. Thus, it is unknown if the barium-bearing inclusions found in irradiated UO_2 occur in irradiated mixed oxide fuel. It may be possible that the increased yield of Pd at the expense of Zr in the fission of Pu may favor the formation of the palladium-rich, fissile-material phase, found by

DOCUMENT SUMMARY

Document Id:	0348A
Document Name:	Sasa Thesis
Operator:	Yvonne
Author:	Sasa
Comments:	Table 2.3 Hor Scroll

STATISTICS

OPERATION	DATE	TIME	WORKTIME	KEYSTROKES
Created	08/18/78	15:38	:16	836
Last Revised	/ /	:	:	
Last Printed	08/18/78	15:55		
Last Archived	/ /	:	onto Diskette	

Total Pages:	1	Total Worktime:	:16
Total Lines:	12	Total Keystrokes:	836

Pages to be printed: 1

TABLE 2.3

PHYSICAL CHARACTERISTICS OF NUMEC MIXED-OXIDE FUEL ELEMENTS

Fuel Element	Density, % of Theo.	O/M Ratio	Cladding Material	Burnup, at, %	Max. Linear Power Rating, kW/ft	Calculated Temp during Irradiation, (K)		
						Fuel Centerline	Fuel Surface	Cladding
C-11	90.6	2,000	316 SS	9.7	14.0	1511	1155	805
C-15	85.0	1.998	316 SS	9.4	12.9	2368	1166	814

Bramman, at the surface of metallic inclusions in preference to zirconate phases. The inclusion analysis also reflects the fact that plutonium fission favors the formation of Pd and Ru at the expense of Zr, Ce, and Sr.

In summary it can be seen that total agreement on inclusion composition has not yet been achieved. Many factors such as flux energy spectrum, original fuel stoichiometry, operating temperature, etc., affect the final composition. One does not expect total agreement, however, some inclusions differ quite markedly from the noble-metal inclusions which were found by all investigators. A graphic illustration (see Table 2.2) of this problem of fission product characterization is the nonagreement of the results of Bradbury and Jeffery analyzing the same fuel.

The mechanism by which metallic inclusions are formed is not completely understood. None of the molybdenum nuclides have volatile precursors with a half-life longer than 1 s. One the other hand, ruthenium and technetium nuclides all have molybdenum precursors. Some of the Ru and Tc nuclides are precursors of rhodium and palladium. It thus appears that molybdenum may be the diffusing species. Bramman, using an alloy of the same composition as the inclusion he found at the central void, found its melting point was between 2073-2173 K. It is possible that the inclusions close to the center may have been formed by the coalescence of molten fission products along cracks, but since inclusions have been observed in all parts of the mixed oxide fuel

Bramman, at the surface of metallic inclusions in preference to zirconate phases. The inclusion analyses also reflect the fact that plutonium fission favors the formation of Pd and Rh at the expense of Zr, Mo, and Sr.

In summary it can be seen that total agreement on inclusion composition has not yet been achieved. Many factors such as film and gap reactions, original fuel stoichiometry, operating temperature, etc., affect the final composition. One must not expect total agreement; however, some inclusions differ quite markedly from the noble-metal inclusions which were found by all investigators. A graphic illustration (see Table 5.2) of this problem of fission product characterization is the nonagreement of the results of Bradbury and Jeffery analyzing the same fuel.

The mechanism by which metallic inclusions are formed is not completely understood. None of the molybdenum nuclides have volatile precursors with a half-life longer than 1 s. On the other hand, ruthenium and technetium nuclides all have molybdenum precursors. Some of the Ru and Tc nuclides are precursors of rhodium and palladium. It thus appears that molybdenum may be the diffusing species. Bramman, using an alloy of the same composition as the inclusion he found at the central void, found its melting point was between 2073–2173 K. It is possible that the inclusions close to the center may have been formed by the coalescence of molten fission products along cracks, but since inclusions have been observed in all parts of the mixed oxide fuel.

which have exceeded 1273-1473 K, it thus appears that most of the inclusions grow by the solid state diffusion of individual atoms. The size of inclusions and their composition must depend critically upon thermal conditions in the pin during irradiation and irradiation time.

Two other factors must be known to characterize the metallic inclusions:

1. The radial concentration (number density) of metallic inclusions in the fuel.
2. Radial variation in the composition of the metallic inclusions.

In the analysis by O'Boyle,[12] inclusions were analyzed at various radial positions in the columnar region to establish the radial concentration of Mo, Tc, and Ru, as shown in Fig. 2.7. Figure 2.8 contains the radial concentrations of the inclusions analyzed in ANL-7877.[26] The general shape of the curves are similar for both investigators, and it can be seen that the concentrations do not vary dramatically with the radius. Thus, for calculational simplicity it will be assumed that the inclusion composition is independent of position.

The radial concentration of metallic inclusions is shown in Figs. 2.9[16] and 2.10.[19] Again the shapes are similar. Since the actual number density is dependent on burnup, the volume fraction of inclusions in the fuel is calculated as a function of burnup. The radial distribution as determined by Fig. 2.9 is then used to calculate the number density of inclusions at any given radius.

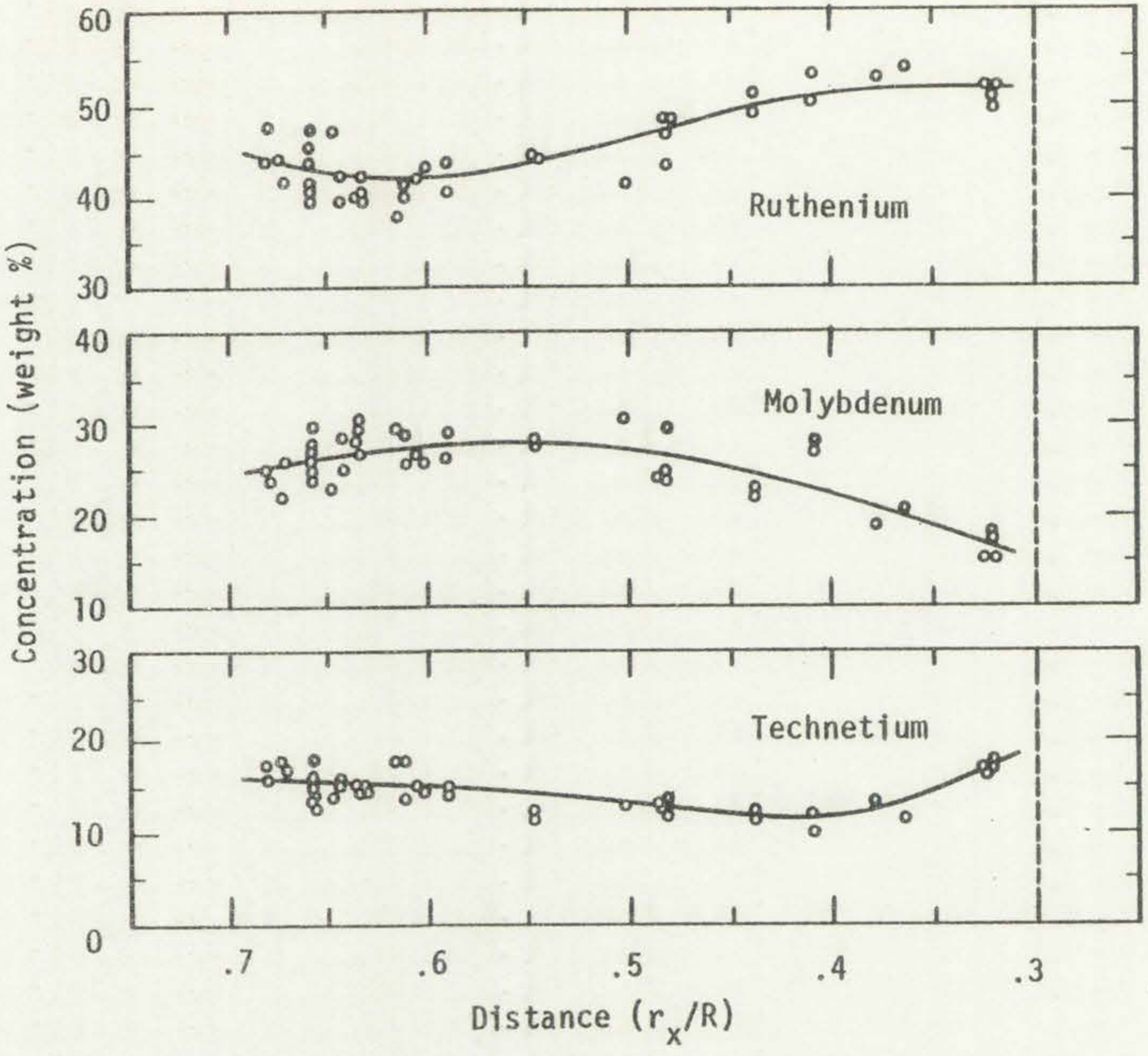

Figure 2.7.
O'Boyle's measured radial variation in Ru, Mo, and Tc concentrations in the metallic inclusions.

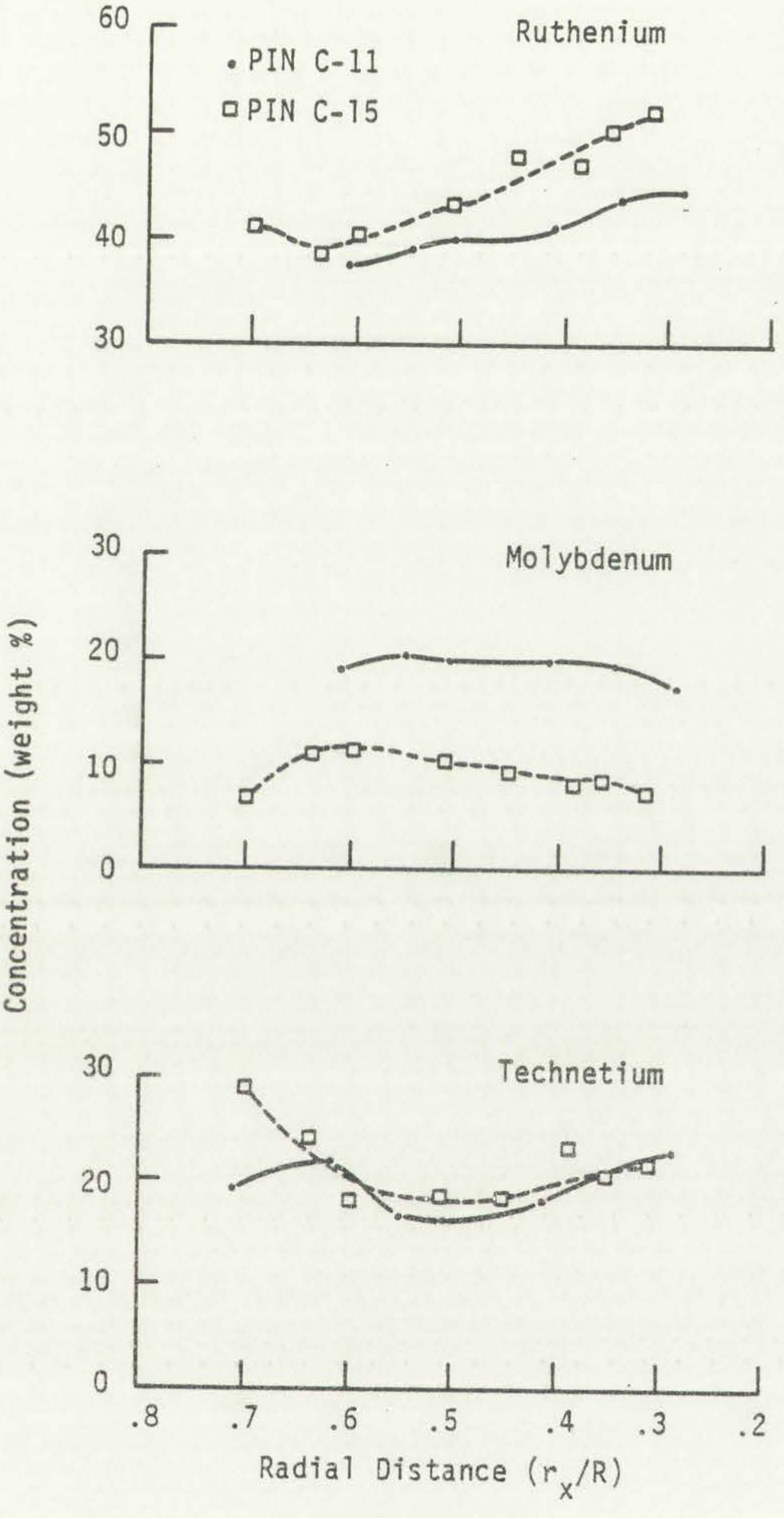

Figure 2.8.
Radial variation in composition
for Johnson inclusion.

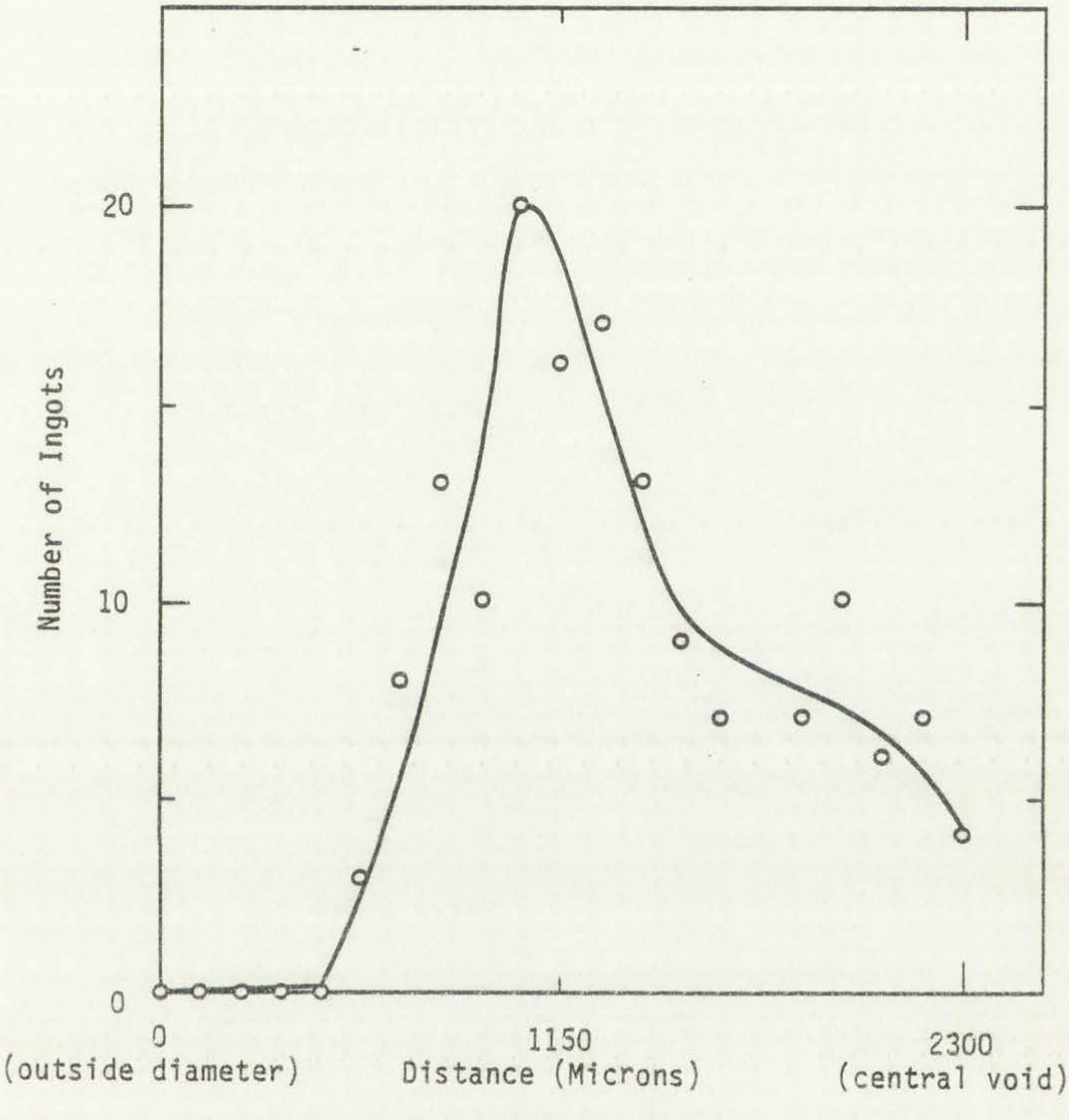

Figure 2.9.
Radial distribution of fission product ingots
in unit area found by Baird.[16]

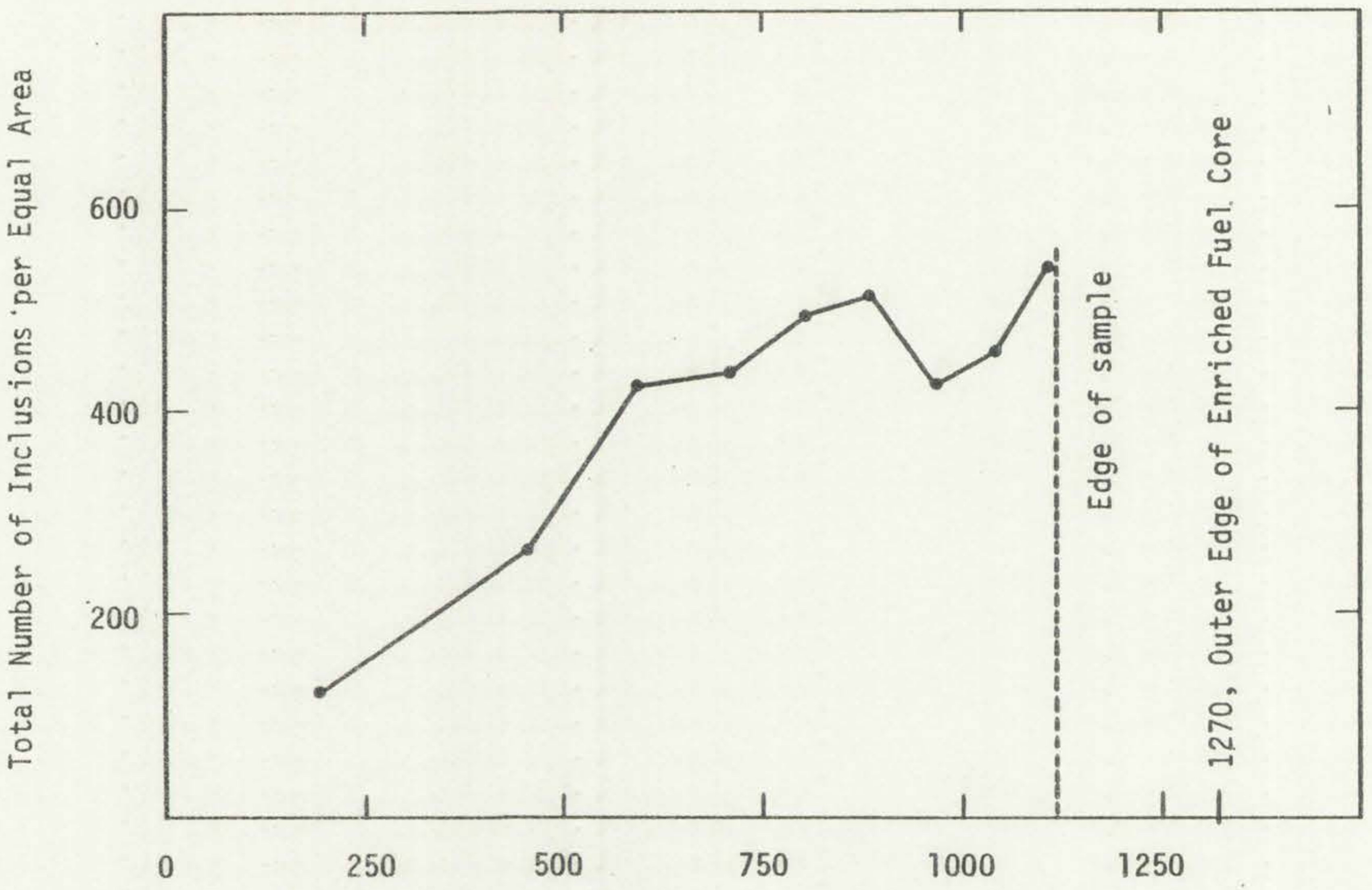

Figure 2.10.
Radial distribution of inclusions.

Knowing the composition and distribution of inclusions, the problem then becomes one of assessing an effective equation-of-state. In the following section such an assessment is made.

REFERENCES

1. J. H. Davies and F. T. Ewart, "The Chemical Effects of Composition Changes in Irradiated Oxide Fuel Materials," Journal of Nuclear Materials 41, 143-155 (1971).

2. L. Burris, Jr., and I. G. Dillon, "Estimation of Fission Product Spectra in Discharged Fuel From Fast Reactors," Argonne National Laboratory report ANL-5742 (July 1957).

3. F. L. Lisman, R. M. Abernathey, W. J. Maeck, J. E. Rein, "Fission Yields of Over 40 Stable and Long-Level Fission Products for Thermal Neutron Fissioned ^{233}U, ^{235}U, ^{239}Pu, and ^{241}Pu, and Fast Reactor Fissioned ^{235}U and ^{239}Pu," Nuclear Science and Engineering 42, (1970) pp. 191-214.

4. S. Katcoff, "Fission-Product Yields from Neutron-Induced Fission," Nucleonics, Vol. 18, No. 11, (November, 1960) pp. 201-208.

5. M. E. Meek and B. F. Rider, "Summary of Fission Product Yields for U^{235}, U^{238}, Pu^{239} and Pu^{241} at Thermal, Fission Spectrum and 14 Mev Neutron Energies," APED-5398-A (October 1968)

6. R. P. Larsen, N. D. Dudey, C. E. Crouthamel, A. D. Tevebaugh, R. C. Vogel, "Chemical Engineering Division Burnup, Cross Sections, and Dosimetry Semiannual Report July-December 1971," Argonne National Laboratory report ANL-7879 (May 1972).

7. R. O. Gumprecht, "Mathematical Basis of Computer Code RIBD," Douglas United Nuclear, Inc., report DUN-4136 (June 1968).

8. A. Glassner, "The Thermochemical Properties of the Oxides, Fluorides, and Chlorides to 2500 K," Argonne National Laboratory report ANL-5750.

9. C. E. Johnson, I. Johnson, P. E. Blackburn, and C. E. Crouthamel, "Effects of Oxygen Concentration on Properties of Fast Reactor Mixed-Oxide Fuel," Reactor Technology, Vol. 15, No. 4, (1972-1973).

10. F. Anselin, "The Role of Fission Products in the Swelling of Irradiated UO_2 and (U, Pu) O_2 Fuel," General Electric Company report GEAP-5583 (January 1969).

11. M. H. Rand and T. L. Markin, "Some Thermodynamic Aspects of (U, Pu) O_2 Solid Solutions and Their Use as Nuclear Fuels," Thermodynamics of Nuclear Materials, Symposium Proceedings, Vienna, 1967 (IAEA, Vienna, 1968) pp. 637-650.

12. D. R. O'Boyle, F. L. Brown, and J. E. Sanecki, "Solid Fission Product Behavior in Uranium-Plutonium Oxide Fuel Irradiated in a Fast Neutron Flux," Journal of Nuclear Materials, 29, 27-42 (1969).

13. J. E. Hanson and J. H. Field, "Experimental Studies of Transient Effects in Fast Reactor Fuels Series III, Preirradiated Mixed Oxide (PuO_2-UO_2) Irradiations Final Report, Transient Irradiation," General Electric Company report GEAP-4469 (July 1967).

14. J. E. Hanson and S. A. Rabin, "Experimental Studies of Transient Effects in Fast Reactor Fuels Series III Preirradiated Mixed Oxide (Pu O_2 - UO_2) Irradiations Interim Report Steady-State Irradiations, General Electric Company report GEAP-4819 (September 1965).

15. H. Kleykamp, "Formation of Phases and Distribution of Fission Products in an Oxide Fuel," Behavior and Chemical State of Irradiated Ceramic Fuels Proc. Panel, Vienna, 1972, International Atomic Energy Agency report IAEA-PL-463/8 p. 157 (1974).

16. G. R. Baird, S. A. Chastain, and R. G. Hendersen, "Fabrication, Irradiation, and Postirradiation Examination of Mixed Oxide Fuel Pins PNL 5-5, -22, -31, and -35," Hanford Engineering Development Laboratory report HEDL-TME 76-16 (April 1976).

17. J. Bazin, J. Jouan, and N. Vignesoult, "Behavior and Physico-Chemical State of Fission Products in Fuel Elements for Pressurized Water Reactors," Paris Bull. Inform. Sci. Tech. (Nuclear Regulatory Commission, 1974, translation NRC-TR-1) pp. 55-71.

18. B. M. Jeffery, "Microanalysis of Inclusions in Irradiated UO_2" Journal of Nuclear Materials 22, 33-40 (1967).

19. B. T. Bradbury, J. T. Demant, and P. M. Martin, "Solid Fission Products in Irradiated Uranium Dioxide," AERE-R5149 (1966).

20. T. L. Markin and E. J. McIver, "Thermodynamic and Phase Studies for Plutonium and Uranium-Plutonium Oxide with Application to Compatability Calculations," Plutonium 1965 Proceedings of the Third Int. Conf. on Plutonium, London, 1965 (Chapman and Hill).

21. M. Conte, M. Mouchnino, and F. K. Schmitz, "Postirradiation Observations of Mixed Oxides with Initial Addition of Fission Product Elements," Nuclear Technology, Vol. 16, (October 1972) pp. 143-155.

22. T. Hidiko and J. H. Field, "Molten Fuel Movement in Transient Overpower Tests of Irradiated Oxide Fuel," General Electric Company report GEAP-13543 (September 1969).

23. R. G. Palm, S. M. Gehl, R. R. Stewart, A. De Volpi, and A. B. Rothman, "F1 Phenomenological Test on Fuel Motion (Interim Report)," Argonne National Laboratory report ANL/RAS 76-11 (March 1976).

24. D. K. Kerwin, J. A. Ellis, W. H. McCarthy, S. K. Evans, "Performance of Encapsulated Mixed-Oxide Fuel Rods (Series F8A) Irradiated in EBR-II to 12 Atomic Percent Burnup," General Electric Company report GEAP-14126 (August 1976).

25. B. T. Bradbury, J. T. Demant, P. M. Martin, and D. M. Poole, "Electron Probe Micro-Analysis of Irradiated UO_2," Journal of Nuclear Materials 17, 227-236 (1965).

26. P. E. Blackburn, C. E. Johnson, et al. "Chemical Engineering Division Fuels and Materials Chemistry Semiannual Report, July-December 1971," Argonne National Laboratory report ANL-7877 (April 1972).

27. J. H. Davies, R. F. Boyle, B. Weidenbaum, J. E. Hanson, "On the Composition of Metallic Ingots Formed in High-Performance Ceramic Fuel Elements," Trans. American Nuclear Society, 9, (1966) p. 63.

28. D. R. O'Boyle, F. L. Brown, and A. E. Dwight, "Analysis of Fission Product Ingots Formed in Uranium-Plutonium Oxide Irradiated in EBR-II," Journal of Nuclear Materials, 35 (1970) pp. 257-266.

29. J. E. Bramman, R. M. Sharpe, D. Thom, and G. Yates, "Metallic Fission-Product Inclusions in Irradiated Oxide Fuels," Journal of Nuclear Materials 25, 201-215 (1968).

3. EQUATION-OF-STATE

One problem that must be considered in determining the contribution of volatile fission products to the fuel motion is an appropriate equation-of-state (EOS) to model the PVT behavior for the various fission products.

Very little experimental PVT data currently exists in the literature for metal vapors with the exception of mercury, sodium, and cesium. Since cesium is a volatile fission product, various EOS's are used to calculate the molar volume of cesium to compare such calculated values with existing experimental data.[1-3] This is done over a range of pressures and temperatures in order to gain insight into the expected error in the molar volumes for the rest of the volatile species where little or no experimental data exists. The equations-of-state used to calculate the molar volumes are the Ideal Gas, the van der Waals, a modified hard-sphere, and the Redlich-Kwong EOS. In addition, calculations are performed using the generalized compressibility chart. Equations-of-state such as the Beattie and Bridgeman are not considered since they contain empirical constants which do not exist in the literature for the volatiles of interest, i.e. Pd, Fe, Sb, Te, Ba, etc.

3.1 Critical Points

The critical points for the volatiles are required in order to determine constants for the Van der Waals and Redlich-Kwong EOS. Using [illegible] of state.

The problem that must be considered in [illegible] the fugaci-
[illegible] of volatile fission products at the fuel surface is to approach
the equation-of-state [illegible] to obtain the PVT behavior for the species
of the products.

Many [illegible] have been reported for gas behavior at the tempera-
tures for metal vapors with the exception of mercury, sodium, and
cesium. These are [illegible] product. Previous efforts are
used to calculate the molar volumes of [illegible] to compare such calculated
values with existing experimental values. This is done over a range
of pressures and temperatures in order to gain insight into the ex-
pected error in the molar volumes for the rest of the volatile species
where little or no experimental data exists. The equations-of-state
used to calculate the molar volumes are the ideal gas, the van der
Waals, a modified [illegible], and the [illegible]. In addition,
calculations are performed using the generalized compressibility
chart. Equations-of-state such as the Beattie and Bridgeman are not
considered since they contain empirical constants which do not exist in
the literature for the majority of elements, (i.e. Rb, Cs, Sr, Ba, Sb,
etc.

3.2 Critical Points

The critical points for the volatiles are required in order to
determine constants for the van der Waals and the Redlich-Kwong (RK) [illegible]

the technique of Young and Alder,[4] the critical points are calculated assuming a mean-field approximation of the cohesive energy[5] used in the classical van der Waals model; also required is the hard sphere atomic diameter,[6] and the molar volume.[5] The equations used and results are presented in Appendix B. Young and Alder[4] compared calculated critical points with experimentally determined values. Their results indicate that the calculated critical volumes and temperatures are fairly close, usually within 30% of the experimentally determined values. The critical pressures, however, are off by as much as 100 to 200%. The calculated critical values listed by Gates[7] differ substantially from those of Young.[4] Thus analytical agreement has yet to be established. The values calculated in Appendix B will be used since more substantiated data is not available.

3.2 Equations

As stated previously, the equations-of-state compared are the Ideal Gas, the van der Waals, the modified hard-sphere, and the Redlich-Kwong. It should be noted, however, that in analyses of the fuel pin behavior during a transient, the local pressure and temperature are usually assessed or known and used to determine the molar volume of any volatiles present. Thus, the equations-of-state are solved in terms of the molar volume, with the pressure and temperature being independent variables.

The Ideal Gas Law expression is well known. It assumes no interaction between individual molecules and assumes the molecular volume as the tendencies of Young and Alder.[4] The critical points are calculated, [illegible] a more [illegible] approximation of the [illegible] energy. Each of the classical and [illegible] models [illegible] in the hard sphere [illegible] [illegible]. The equations used and results are presented in Appendix B. Young and Alder[4] compared calculated critical points with experimentally determined values. Their results indicate that the calculated critical volumes and temperatures are fairly close, usually within 10% of the experimentally determined values. The critical pressures, however, are off by as much as 100 to 200%. The calculated critical values listed by Gates[5] differ substantially from those of Young.[4] Thus analytical agreement has yet to be established. The values calculated in Appendix B will be used since more substantiated data is not available.

3.2 Equations

As stated previously, the equations-of-state compared are the ideal gas, the van der Waals, the modified hard-sphere, and the Redlich-Kwong. It should be noted, however, that in analyses of the fuel pin behavior during a transient, the local pressure and temperature are usually assumed or known and used to determine the molar volume of any particular species. Thus, the equations-of-state are solved in terms of the molar volume, with the pressure and temperature being independent variables.

The ideal gas law expression is well known. It assumes no interaction between individual molecules and assumes the molecular volume is insignificant. Its applicability is thus for very low density gas and this equation-of-state will not be expanded upon further. By using the critical isotherm,[8] the van der Waals constants can be found in terms of the critical point as shown in Appendix C and, in particular, in terms of the more accurate V_c and T_c. The constants are put back into the general equation and solved in terms of the molar volume, yielding a cubic equation in term of the molar volume:

$$(P)v^3 - (bP + RT)v^2 + av - ab = 0 \tag{3-1}$$

where

$$b = \frac{v_c}{3} \quad , \quad a = \frac{27RbTc}{8} \quad . \tag{3-2}$$

A cubic equation solution is based on d'Alembert's Lemma[9] of algebra which states that the absolute value of a polynomial assumes a minimum if and only if it is zero. The subroutine, CUBIC, can be found in Appendix F.

Royce,[10] in his equation-of-state work for metals, used the classical hard-sphere equation of state[11,12] with a first order perturbation from a van der Waals mean-field approximation to the cohesive energy as proposed by Young and Alder.[4] A more detailed description of the equations is given in Appendix D. Due to the complexity of this equation-of-state in terms of molar volume, it is solved by an iterative process.

The Redlich-Kwong equation of state[13,14] is also included for comparison. As seen by this equation in Appendix E, its expansion is also cubic in terms of the molar volume. The numerical coefficients are determined empirically to fit moderate densities.

The generalized compressibility diagram[14] is used to hand calculate the molar volume at a few of the experimental points. The results are listed in Table 3.1. Due to the lower limits on the compressibility diagram, only the experimental data points at high pressure and temperature could be analyzed. The critical values used are those calculated via Appendix B. It should be noted that since the compressibility, Z, must be read off the diagram, this technique to generate PVT information is not easily programmable, and would thus be unusable for future modeling. It does, however, provide a few points for comparison.

3.3 Results

A program to calculate the critical values and the molar volume as a function of P and T for the various equations-of-state can be found in Appendix F. This program is run at the experimental data points of cesium, and results are compared in Table 3.2. It can be seen that the Redlich-Kwong equation-of-state comes closer to predicting the experimental molar volumes than the remaining equations-of-state. It can also be seen that, as the molar volume becomes larger, the equations-of-state and the experimental value all approach ideal gas as required. At very low molar volumes, i.e. high

The [illegible] variation of [illegible]^{7,14} is also included for comparison. As seen by this equation in Appendix C, the expression is also solved in terms of the molar volume. The numerical coefficients are determined specifically to fit methane densities.

The generalized compressibility diagram^{20} is used to hand calculate the molar volume at a few of the experimental points. The results are listed in Table 3.1. Due to the lower limits of the compressibility diagram, only the experimental data points at high pressure and temperature could be analyzed. The critical values used are those calculated in Appendix B. It should be noted that since the compressibility, Z, must be read off the diagram, this technique to generate PVT information is not easily programmable, and would thus be unusable for future modeling. It does, however, provide a few points for comparison.

3.3 Results

A program to calculate the critical values and the molar volume as a function of P and T for the various equations-of-state can be found in Appendix C. This program is run at the experimental data points of methane, and results are compared in Table 3.2. It can be seen that the [illegible] equation-of-state comes closest to predicting the experimental molar volumes than the remaining equations-of-state. It can also be seen that, as the molar volume becomes larger, the equations-of-state and the experimental [illegible] approach ideal gas, as expected. At very low molar volumes, the high

TABLE 3.1

CESIUM MOLAR VOLUMES FROM GENERALIZED COMPRESSIBLITY DIAGRAM

P_{ATM}	T °K	P_r	T_r	Z	$V = \frac{ZRT}{P}$ ℓ/g-mole	EXP. Value ℓ/g-mole	% Dev.
26.1	1533	.1155	.794	.905	4.3614	3.77	15.7
26.66	1667	.118	.864	.922	4.7303	4.406	7.36
124.13	2136.1	.549	1.107	.855	1.207	.585	106.36
64.96	1818.83	.287	.942	.860	1.976	1.442	37.01
75.07	1964.56	.332	1.018	.88	1.890	1.448	30.50
88.32	2168.61	.391	1.124	.90	1.8132	1.454	24.70

$$P_c = 226 \text{ atm}, \quad P_r = \frac{P}{P_c}$$

$$T_c = 1930\ °K, \quad T_r = \frac{T}{T_c}$$

$$R = .08205 \ \frac{\ell\text{-atm}}{°K \text{ mole}}$$

TABLE 3.2

COMPARISON OF CALCULATED AND EXPERIMENTAL RESULTS FOR CESIUM

P_{ATM}	T °K	Specific Vol. ℓ/g_{mole}										
		Experimental Value	Ideal Gas	% Variation	Van der Waals	% Variation	Modified Hard Sphere	% Variation	Redlich Kwong	% Variation	Generalized Compressibility	% Variation
10.01	1677.	12.862	13.75	6.90	13.50	4.96	13.47	4.73	13.43	4.416		
6.73	1222.3	12.70	14.91	17.40	14.54	14.49	14.48	14.02	14.36	13.071		
5.02	1201.8	17.335	19.65	13.35	19.27	11.16	19.21	10.82	19.09	10.124		
4.79	1157.9	17.316	19.84	14.58	19.44	12.27	19.38	11.92	19.24	11.111		
1.12	980.5	66.46	71.83	8.08	71.32	7.31	71.27	7.24	71.06	6.921		
12.33	1586.8	9.595	10.56	10.06	10.30	7.35	10.26	6.93	10.21	6.410		
15.24	1404.44	6.245	7.561	21.07	7.246	16.03	7.201	15.31	7.121	14.027		
19.21	1668.4	6.29	7.126	13.29	6.876	9.32	6.847	8.86	6.805	8.188		
19.26	1527.9	5.468	6.509	19.04	6.226	13.86	6.189	13.19	6.129	12.089		
26.1	1533.	3.77	4.819	27.82	4.533	20.24	4.495	19.23	4.434	17.613	4.3614	15.7
33.21	1655.4	3.222	4.090	26.94	3.830	18.87	3.799	17.91	3.754	16.511		
3.23	1101.	24.99	27.97	11.92	27.55	10.24	27.48	9.96	27.32	9.324		
26.66	1667.	4.406	5.130	16.43	4.877	10.69	4.847	10.01	4.804	9.033	4.73	7.36
25.99	1513.3	3.693	4.778	29.38	4.485	21.45	4.446	20.39	4.383	18.684		
2.01	1684.2	67.7	68.75	1.55	68.51	1.20	68.49	1.17	68.45	1.108		
5.19	1659.7	25.367	26.24	3.44	25.99	2.46	25.96	2.34	25.92	2.180		
124.13	2136.1	.585	1.412	141.37	1.216	107.86	1.211	107.01	1.194	104.10	1.207	106.36
64.96	1818.83	1.442	2.298	59.36	2.060	42.86	2.037	41.26	2.006	39.11	1.976	37.01
75.07	1964.56	1.448	2.148	48.34	1.935	33.63	1.920	32.60	1.898	31.08	1.890	30.50
88.32	2168.61	1.454	2.015	38.58	1.832	26.00	1.826	25.58	1.812	24.62	1.8132	24.70

pressure and low temperature, the equations-of-state inaccurately predict observed phenomena.

Based on this analysis, the Redlich-Kwong equation will be used. It appears from this analysis that an error in the molar volume for cesium of less than 30 to 40% can be expected in the projected temperature range, 2900 K to 6000 K, and pressure range, 25 to 100 atm., of interest. The error for the other volatiles, however, may be much higher. This depends on whether the vapor is monatomic or tends to form molecules, and on the accuracy of the calculated critical point and thus the Redlich-Kwong constants. For dense vapors, interatomic forces become important; thus the range of the quasistatic pressure used in later analysis will determine how seriously one must search for a more appropriate equation-of-state. It appears that for pressures less than 100 atms., the Redlich-Kwong equation-of-state is acceptable. One must also keep in mind that the Redlich-Kwong equation of state tends to overpredict the molar volume, and thus will tend to overpredict the quasistatic fuel motion also. A model for such fuel motion is presented in the following section.

[illegible] and the [illegible]

[illegible]

Based on this analysis, [illegible] it appears [illegible] [illegible] temperature range [illegible] [illegible] [illegible] [illegible] [illegible] [illegible] [illegible] [illegible] [illegible] [illegible] [illegible] [illegible] [illegible] [illegible] [illegible] [illegible] [illegible] is presented in the following section.

REFERENCES

1. J. P. Stone, C. T. Ewing, J. R. Spann, E. W. Steinkuller, D. D. Williams, R. R. Miller, "High Temperature Vapor Pressures of Sodium, Potassium, and Cesium," Journal of Chemical and Engineering Data, 11, No. 3, (July 1966).

2. J. P. Stone, C. T. Ewing, J. R. Spann, E. W. Steinkuller, D. D. Williams, and R. R. Miller, "High Temperature PVT Properties of Sodium, Potassium, and Cesium," Journal of Chemical and Engineering Data, 11, No. 3, (July 1966) pp. 309-314.

3. C. T. Ewing, J. R. Spann, J. P. Stone, R. R. Miller, "Pressure-Volume-Temperature Relationships for Cesium Vapor," Journal of Chemical and Engineering Data, Vol. 16, No. 1, (1971) pp. 27-30.

4. D. A. Young and B. J. Alder, "Critical Point of Metals from the van der Waals Model," Physical Review A 3, (January 1971) p. 364.

5. K. A. Gschneider, Jr., "Physical Properties and Interrelationships of Metallic and Semimetallic Elements," Solid State Physics 16, (1964) p. 275.

6. L. Pauling, The Nature of the Chemical Bond, (Cornell U. P., Ithica, New York, 1960) third edition.

7. D. S. Gates and G. Thodos, "The Critical Constants of the Elements," A. I. Ch. E. Journal, Vol. 6, No. 1 (March 1960) pp. 50-54.

8. S. Glasstone and D. Lewis, Elements of Physical Chemistry, (D. Van Nostrand Co., Inc., Princeton, New Jersey, 1960) second edition.

9. Z. C. Motteler, "A Simple Method for Finding the Zeros of Polynomials, Based on d'Alembert's Lemma," Los Alamos Scientific Laboratory report LA-3355 (August 1965).

10. E. B. Royce, "GRAY, A Three-Phase Equation of State for Metals," Lawrence Livermore Laboratory report UCRL-51121 (September 1971).

11. N. F. Carnahan and K. E. Starling, "Equation of State for Nonattracting Rigid Spheres," The Journal of Chemical Physics 51, (July 1969) p. 635.

12. B. J. Alder and T. E. Wainwright, "Studies in Molecular Dynamics II. Behavior of a Small Number of Elastic Spheres," The Journal of Chemical Physics 33, (November 1960) p. 1439.

REFERENCES

1. [illegible] [illegible], Engineering Data, Vol. [illegible], No. [illegible], [illegible]

2. [illegible] Williams, and [illegible], "High Temperature Measurements of Properties of [illegible], Molybdenum, and Tantalum," Journal of Chemical and Engineering Data, Vol. [illegible], No. [illegible], [illegible] pp. [illegible]

3. [illegible], [illegible], A. R. Miller, "Pressure-Volume-Temperature Relationships for [illegible]," Journal of Chemical and Engineering Data, Vol. [illegible], No. [illegible], [illegible]

4. D. A. Young and B. J. Alder, "Critical Point of Metals from the van der Waals Model," Physical Review A 3, (January 1971) p. 364.

5. K. A. Gschneidner, Jr., "Physical Properties and Interrelationships of Metallic and Semimetallic Elements," Solid State Physics 16, (1964) p. 275.

6. L. Pauling, The Nature of the Chemical Bond (Cornell U.P., Ithaca, New York, 1960) third edition.

7. [illegible], "The Critical Constants of the Elements," [illegible] (1960) pp. [illegible]

8. S. Glasstone and D. Lewis, Elements of Physical Chemistry, (D. Van Nostrand Co., Inc., Princeton, New Jersey, 1960) second edition.

9. [illegible], "A Simple Method for Finding the Zeros of Polynomials, Based on [illegible]," Los Alamos Scientific Laboratory Report LA-[illegible] (August 1965).

10. E. B. Royce, "GRAY, A Three-Phase Equation of State for Metals," Lawrence Livermore Laboratory report UCRL-[illegible] (September 1971).

11. N. F. Carnahan and K. E. Starling, "Equation of State for Nonattracting Rigid Spheres," The Journal of Chemical Physics 51, (July 1969) p. 635.

12. B. J. Alder and T. E. Wainwright, "Studies in Molecular Dynamics. II. Behavior of a Small Number of Elastic Spheres," The Journal of Chemical Physics 33, (November 1960) p. 1439.

13. O. Redlich and J. N. S. Kwong, "On the Thermodynamics of Solutions. V An Equation of State. Fugacities of Gaseous Solutions," Chemical Review 44, (1949) p. 233.

14. G. J. Van Wylen and R. E. Sonntag, Fundamentals of Classical Thermodynamics (John Wiley and Sons, Inc., New York, 1973) second edition.

4. FUEL MOTION MODEL

In the following sections, the input and program used to calculate axial fuel motion in a transient overpower condition will be described. The pin dimensions and inclusion compositions, input to the program, are discussed in the first two sections. The last two sections cover the subroutines used to calculate the pin temperature profiles and volume expansion that can be expected under the existing local conditions.

4.1 Fuel Pin Description

Physically the fuel pin model used in this analysis is shown in Fig. 4.1. The pin parameters used in this study are those of the Clinch River Breeder Reactor (CRBR) taken from HEDL-TME-75-12.[1] For properties not known for CRBR, the corresponding values from the Fast Flux Test Facility (FFTF) were substituted. These parameters can be found in Table 4.1.

The following assumptions were made concerning the general fuel pin description:

1. No central void was included. This assumption was made to simplify the analysis since only an order of magnitude approximation to the possible volume expansion was desired.
2. The bond gap was still present. This assumption is probably valid during steady state operation since for low power operation (≃ 7 kW/ft ave) the bond gap does not close until late in fuel life. For transient overpower accidents (TOP), however, differential temperatures between the fuel and cladding leads to rapid gap closure. For loss-of-flow (LOF) or a LOF driven TOP, the clad temperature may rise enough to keep the gap from closing.

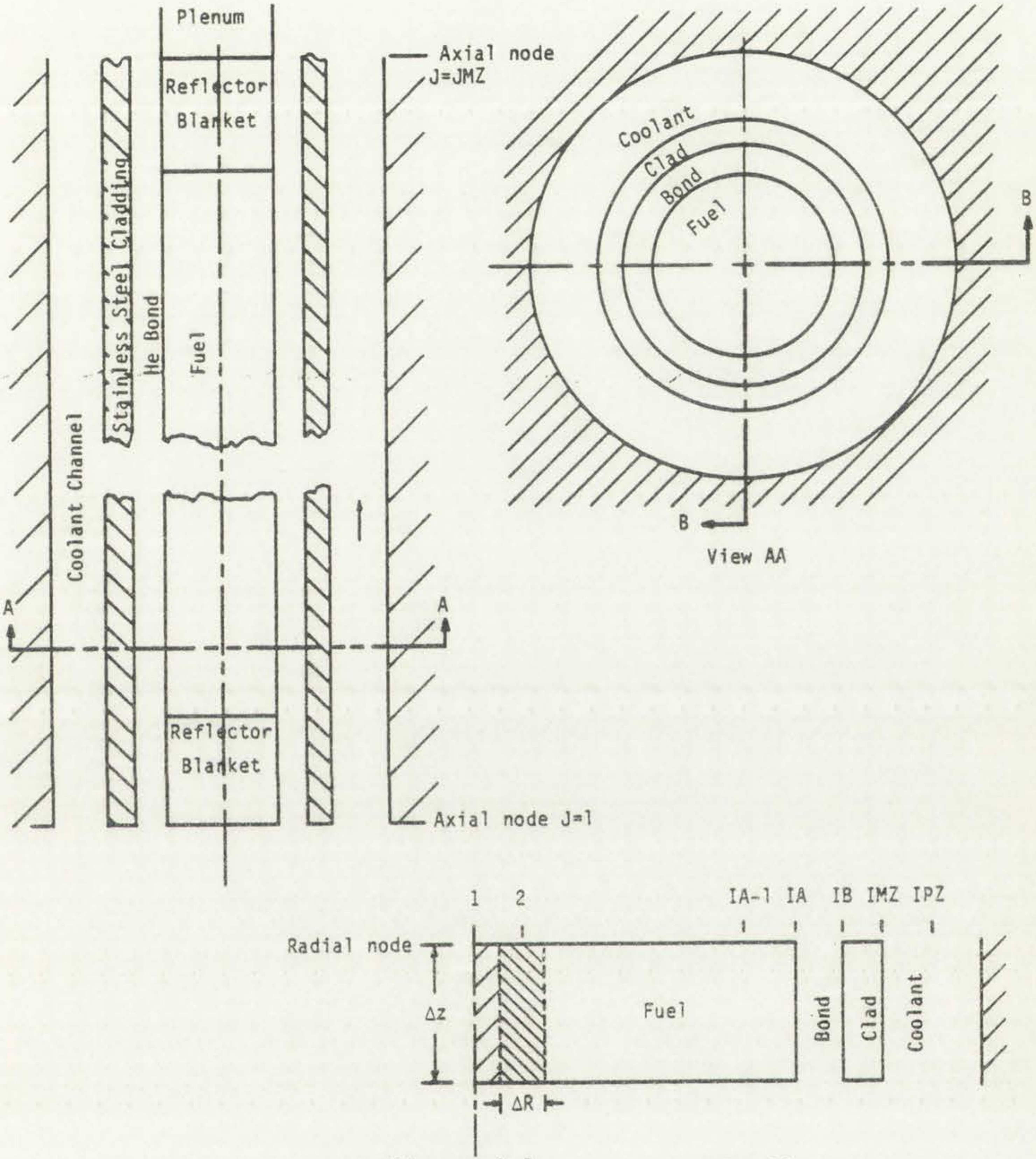

Figure 4.1.
Schematic of fuel pin.

TABLE 4.1

FUEL PIN DESCRIPTION

Description	CRBR	FFTF
A) Fuel		
Composition	UO_2 - PuO_2 (Driver Zone) UO_2 (Axial Blanket)	(U, Pu)O_2 (Driver Zone) UO_2 Insulator Pellets Inconel Reflector
Stoichiometry	Sub Stoichiometric Assume 1.96	1.96
Enrichment Pu/(U + Pu)	Depleted (Blankets) 22% (Inner Zone) 32% (Outer Zone) (U Natural)	22.43 Weight % (w/o) Inner 27.37 w/o Outer
Radius	2.3876 mm (.094 in.)	2.48 mm
Length	914.4 mm (36 in.)	910 mm (≈ 36 in.)
Axial Blanket Length	355.6 mm (14 in.) (Upper) 355.6 mm (14 in.) (Lower)	
Density	Assume 90% T.D.	85.5% T.D. Smear 90.4% T.D.
B) Cladding		
Composition	316 Stainless Steel	Stainless Steel
Outer Diameter	5.842 mm (.23 in.)	5.84 mm
Wall Thickness	.381 mm (.015 in.)	.38 mm

TABLE 4.1 (cont)

C) Bond		
Composition	Inert Gas (He)	Inert Gas
Fuel-clad gap (at beginning of life)	.1524 mm (.006 in.)	.07 mm
D) General Parameters		
Gas Plenum Length	1219.2 mm (48 in.)	940 mm
Pin Pitch	P/D = 1.26	P/D = 1.24
Core Inlet Temp.	661°K	589°K
Core Outlet Temp.	808°K	755°K
Max. Can Temp.	930.4°K	943°K (Hot Spot)
Output Power	350 MWe/975 MWt	400 MWt
	Linear 14.5 kW/ft. Max. 7 kW/ft. Ave.	.39 MW/ℓ (Density)
Coolant	Sodium	Sodium
Burnup Goal	80,000 MWD/T (≈ 8.5 atom %) Peak	80,000 MWD/T (≈ 8.5 atom %) Peak

3. Constant fuel, clad, bond, and coolant properties were assumed, i.e. temperature, pressure, or time dependence of density, heat capacity, thermal conductivity, etc., were ignored.
4. An annular flow area was used for the coolant, the equivalent cross sectional area was determined from the pin pitch. As seen in Fig. 4.1, no interchannel heat transfer was allowed.

The theoretical and 90% theoretical density for CRBR fuel is calculated in Appendix G. This was done to account for the spread in densities quoted in the literature.

4.2 Inclusion Description

In the following analyses, inclusion compositions based on the investigations of O'Boyle,[2] Johnson,[3] and Jeffery[4] were utilized. O'Boyle[2] and Johnson's[3] compositions were chosen since the pins they analyzed were of mixed oxides irradiated in a fast spectrum, thus approximating conditions in an LMFBR. Jeffery's[4] inclusion composition was included to try to obtain a comparison of both inclusion composition and expected inclusion reaction to hypothetical accident situations between an LMFBR and a light water reactor (LWR).

For use as input data, an average Jeffery[4] inclusion composition was calculated and can be found in Table 4.2. A value of 3 weight % was assigned to the constituents detected in the inclusions with a concentration of 5 weight %. It was then assumed that the fission product yield would segregate into inclusions in the weight % of Jeffery's average inclusion. The yield at 3 atom % burn-up for U, irradiated in a fast spectrum, was used. Appendix H contains the required yield data for U, Pu, and mixed oxides at 3 atom % burn-up. As

TABLE 4.2

AVERAGE JEFFERY INCLUSION COMPOSITION*

Element	Mo	Ru	Tc	Rh	Ba	Pd	Zr	Ce	Sr	U	Te	Nd
Weight %	32.2	13.95	10.0	3.95	6.75	2.1	3.0	1.65	.90	20.3	2.10	3.0

---

*based on 70% type 1; 41 w/o Mo, 18 w/o Ru, 13 w/o Tc, 5 w/o Rh, 3 w/o Te, 3 w/o Pd, 3 w/O Nd, 14 w/o U

15% type 2; 21 w/o Mo, 9 w/o Ru, 6 w/o Tc, 20 w/o Ba, 10 w/o Zr, 6 w/o Ce, 3 w/o Sr, 3 w/o Nd, 3 w/o Rh, 19 w/o U

15% type 3; 25 w/o Ba, 10 w/o Zr, 5 w/o Ce, 3 w/o Sr, 3 w/o Nd, 3 w/o Mo, 51 w/o U.

mentioned previously the yield of U in a thermal spectrum is close to its yield in a fast spectrum. The results are shown in Table 4.3. The maximum inclusion number density for both 5 and 10 μm diameter inclusions, assuming a flat distribution, was calculated along with the concentration of the constituent fission products in the fuel. It should be noted that the density of the inclusions, based on an average Jeffery inclusion was on the order of 8.5 g/cm^3 versus the measured[5] density of 11.3 g/cm^3 for UO_2 inclusions. The calculated density of Jeffery's Type 1 inclusion, disregarding the U content, is on the order of 10.5 g/cm^3. The Type 1 inclusion is very similar to the noble metal inclusions found by all investigators. It appears that the Type 2 and 3 inclusions are predominantly barium zirconates. The fuel analyzed is highly enriched UO_2 irradiated in a thermal spectrum with low center temperature, and is thus dissimilar to

TABLE 4.3

ANALYSIS OF JEFFERY'S INCLUSIONS AT 3 ATOM % BURNUP

Constituent	Weight Yield* (gms/cm^3 Fuel) for Fast Irradiated U to 3 A/O B.U.	Average Inclusion Weight %	Weight Yield Inclusion w/o	Limiting Element	Maximum Weight Concentration (gms/cm^3 Fuel)	% of Yield in Inclusions	Maximum Concentration (Moles/cm^3 Fuel)	Maximum Volume of Inclusion (cm^3 of Elem./cm^3 of Fuel)
Mo	2.29×10^{-2}	32.3	7.09×10^{-2}	Tc	2.11×10^{-2}	92.2	2.17×10^{-4}	2.04×10^{-3}
Tc	6.54×10^{-3}	10.0	6.54×10^{-2}		6.54×10^{-3}	100.0	6.61×10^{-5}	5.66×10^{-4}
Ru	1.81×10^{-2}	13.95	1.30×10^{-1}		9.12×10^{-3}	50.4	8.93×10^{-5}	7.30×10^{-4}
Rh	2.77×10^{-3}	3.95	7.01×10^{-2}		2.58×10^{-3}	93.3	2.50×10^{-5}	2.07×10^{-4}
Pd	1.86×10^{-3}	2.1	8.86×10^{-2}		1.37×10^{-3}	73.8	1.29×10^{-5}	1.15×10^{-4}
Ba	1.05×10^{-2}	6.75	1.56×10^{-1}		4.41×10^{-3}	42.0	3.19×10^{-5}	1.25×10^{-3}
Zr	3.04×10^{-2}	3.0	1.01		1.96×10^{-3}	6.5	2.09×10^{-5}	3.06×10^{-4}
Ce	2.46×10^{-2}	1.65	1.49		1.08×10^{-3}	4.4	7.63×10^{-6}	1.58×10^{-4}
Sr	9.68×10^{-3}	.90	1.08		7.06×10^{-4}	7.3	7.92×10^{-6}	2.78×10^{-4}
Nd	2.67×10^{-2}	3.0	8.9×10^{-1}		1.96×10^{-3}	7.3	1.35×10^{-5}	2.82×10^{-4}
Tc	3.37×10^{-3}	2.10	1.60×10^{-1}		1.37×10^{-3}	40.8	1.06×10^{-5}	2.17×10^{-4}
Sb	3.10×10^{-4}	< 1			3.10×10^{-4}	100.0	2.51×10^{-6}	4.57×10^{-5}
Sn	4.56×10^{-4}	< 1			4.56×10^{-4}	100.0	3.79×10^{-6}	6.14×10^{-5}
In	3.54×10^{-5}	< 1			3.54×10^{-5}	100.0	3.08×10^{-7}	4.85×10^{-6}
Nb	1.54×10^{-3}	< 1			5.22×10^{-4}	34.9	5.25×10^{-7}	6.11×10^{-5}
Ag	1.70×10^{-4}	< 1			1.70×10^{-4}	100.0	1.55×10^{-6}	1.66×10^{-5}

*Based on yield data of Burris[7] (see Appendix H).

Number Density of Inclusions† (Inclusions/cm^3 of Fuel)

Diameter of Inclusion	Average Jeffery Inclusion	Average Jeffery Inclusion + Sb, Sn, In, Nb, Ag
5μm	9.68×10^{7}	9.68×10^{7}
10μm	1.21×10^{7}	1.21×10^{7}
Calculated Inclusion Density	8.49 gms/cm^3	8.47 gms/cm^3

$$\left(\rho_{calc} = \frac{\sum_{i=1}^{n} \omega\tau_i}{\sum_{i=1}^{n} V_i}\right)$$

†U not included.

the fuel and conditions expected in CRBR, and as mentioned previously is included for comparison purposes.

O'Boyle investigated fuel more similar in composition and irradiation history to the hypothesized CRBR fuel pin. The fact that the fuel was initially stoichiometric lowered the weight % of Mo in inclusions, versus what one would expect to find in the hypostoichiometric CRBR fuel. This effect is somewhat compensated for by the fact that CRBR fuel has a larger weight % Pu which has a lower Mo yield and higher Ru yield than U.

Further analysis of O'Boyle's inclusions can be found in Table 4.4. The fission product concentration was calculated using an average O'Boyle inclusion and also by assuming that the other stable elements Sb, Sn, In, Nb, Ag were present in concentrations lower than the detection limit of the microprobe. The calculated density of an inclusion having O'Boyle's weight %, 11.64 g/cm^3, was much closer to the measured values of Bramman,[6] 12.2 g/cm,^{3} than was Jeffery's.

As mentioned previously, in ANL-7877,[3] three different types of metallic inclusions were found. Noble metal inclusions, consisting primarily of Mo, Tc, Ru, Rh, and Pd, were found throughout the columnar region and halfway through the equiaxed-grain region. The second type of inclusions was primarily Pd with small quantities of other fission products and impurities present. The second type of inclusion was found primarily in the equiaxed and unrestructured regions of the fuel. Only a few of the third type of inclusion were found and then

TABLE 4.4

ANALYSIS OF O'BOYLE'S INCLUSIONS AT 3 ATOM % BURNUP

Constituent	Weight Yield* (gms/cm^3 Fuel)	O'Boyle's Inclusion Weight %	Yield / Inclusion w/o	Limiting Element	Maximum Weight Concentration (gms/cm^3 Fuel)	% of Yield in Inclusions	Maximum Molan Concentration (Moles/cm^3 Fuel)	Maximum Volume (Alloyed) of Inclusions (cm^3/cm^3 Fuel)
Mo	2.10×10^{-2}	25.	8.4×10^{-2}	Tc	6.87×10^{-3}	32.7	7.16×10^{-5}	6.68×10^{-4}
Tc	4.67×10^{-3}	17.	2.75×10^{-2}		4.67×10^{-3}	100.0	4.77×10^{-5}	4.09×10^{-4}
Ru	2.56×10^{-2}	48.	5.33×10^{-2}		1.32×10^{-2}	51.6	1.31×10^{-4}	1.06×10^{-3}
Rh	4.97×10^{-3}	5.**	9.9×10^{-2}		1.37×10^{-3}	27.6	1.33×10^{-5}	1.10×10^{-4}
Pd	1.68×10^{-2}	5.**	3.36×10^{-1}		1.37×10^{-3}	8.2	1.30×10^{-5}	1.14×10^{-4}
Sb	3.75×10^{-4}	< 1			2.75×10^{-4}	73.3	2.24×10^{-6}	2.85×10^{-5}
Sn	9.53×10^{-4}	< 1			2.75×10^{-4}	28.8	2.31×10^{-6}	2.68×10^{-5}
In	8.84×10^{-5}	< 1			8.84×10^{-5}	100.0	7.70×10^{-7}	8.81×10^{-6}
Nb	6.85×10^{-4}	< 1			2.75×10^{-4}	40.1	2.96×10^{-6}	2.89×10^{-5}
Ag	1.35×10^{-3}	< 1			2.75×10^{-4}	20.4	2.54×10^{-6}	2.59×10^{-5}

*Based on RIBD[8] yield data (see Appendix H).

**Used more conservative O'Boyle data. If the RIBD[8] yield split is used, then the expected weight % would be 7.5% Pd and 2.5% Rh, increasing the weight % of the more volatile Pd.

Number Density of Inclusions (Inclusions/cm^3 Fuel)

Diameter of Inclusion	Average O'Boyle Inclusion	Average O'Boyle Inclusion + Sb, Sn, In, Nb, Ag
5μm	3.607×10^7	3.789×10^7
10μm	4.509×10^6	4.736×10^6
Calculated Inclusion Density	11.64 gms/cm^3	11.56 gms/cm^3

always in the unrestructured region. These consisted of almost pure Mo with a few percent of other fission products.

Due to the distribution of the three types of inclusions, it will be assumed that the noble metal inclusions are only found to some given radius R, where a step transition occurs to inclusions of the second type. The third type of inclusion will be ignored due to its location, rarity, and composition.

To determine the composition of the inclusions to be input, average values were calculated. These values can be found in Table 4.5. As stated earlier a flat compositional distribution will be initially assumed.

Using these average values of the composition, the maximum concentrations, i.e. molar, weight, and volume, were calculated for the two types of inclusions, using the RIBD yield data. The results can be found in Tables 4.6 and 4.7.

TABLE 4.5
JOHNSON'S[3] AVERAGE INCLUSION COMPOSITION

Inclusion Type	Fuel Pin Number				Weight %					
		Mo	Tc	Ru	Rh	Pd	Fe	Sn	Sb	Te
Noble Metal (Type 1)	C-11	19.5	19.0	41.0	15.0	1.0	4.5			
	C-15	9.5	21.1	45.6	20.2	3.2	0.4			
Average (Type 1)		14.5	20.05	43.3	17.6	2.1	2.45			
Palladium (Type 2)	C-15					72.55	22.25	2.8	1.3	1.1

TABLE 4.6

ANALYSIS OF JOHNSON'S INCLUSION (TYPE I) AT 3 ATOM % BURNUP

Constituent	Weight Yield* (gms/cm^3 Fuel)	Type I Inclusion Weight %	$\frac{\text{Yield}}{\text{Inclusion}}$ w/o	Limiting Element	Maximum Weight Concentration (gms/cm^3 Fuel)	% of Yield in Inclusions	Maximum Molar Concentration (Moles/cm^3 Fuel)	Maximum Volume (Alloyed) of Inclusions (cm^3/cm^3 Fuel)
Mo	2.10×10^{-2}	14.5	1.45×10^{-1}	Tc	3.38×10^{-3}	16.08	3.52×10^{-5}	3.31×10^{-4}
Tc	4.67×10^{-3}	20.05	2.33×10^{-2}		4.67×10^{-3}	100.0	4.77×10^{-5}	4.09×10^{-4}
Ru	2.56×10^{-2}	43.3	5.91×10^{-2}		1.01×10^{-2}	39.40	9.97×10^{-5}	8.15×10^{-4}
Rh	4.97×10^{-3}	17.6	2.82×10^{-2}		4.10×10^{-3}	82.48	3.98×10^{-5}	3.30×10^{-4}
Pd	1.68×10^{-2}	2.1	8.0×10^{-1}		4.89×10^{-4}	2.91	4.60×10^{-6}	4.10×10^{-5}
Fe	-	2.45	-		5.71×10^{-4}	-	1.02×10^{-5}	7.26×10^{-5}
Sn	9.53×10^{-4}	< 1			2.33×10^{-4}	24.46	1.96×10^{-6}	2.27×10^{-5}
Sb	3.75×10^{-4}	< 1			2.33×10^{-4}	62.16	1.91×10^{-6}	2.42×10^{-5}
In	8.84×10^{-5}	< 1			8.84×10^{-5}	100.0	7.70×10^{-7}	8.81×10^{-6}
Nb	6.85×10^{-4}	< 1			2.33×10^{-4}	34.03	2.51×10^{-6}	2.45×10^{-5}
Ag	1.35×10^{-3}	< 1			2.33×10^{-4}	17.27	2.16×10^{-6}	2.19×10^{-5}

*Based on RIBD[8] yield data (see Appendix H)

Number Density of Inclusions (Inclusions/cm^3 Fuel)

Diameter of Inclusion	Average Johnson (Type I) Inclusion	Average Inclusion + Sn, Sb, In, Nb, Ag
5μm	3.05×10^{7}	3.25×10^{7}
10μm	3.82×10^{6}	4.06×10^{6}

TABLE 4.7

ANALYSIS OF JOHNSON'S INCLUSIONS (TYPE II) AT 3 ATOM % BURNUP

Constituent	Weight Yield* (gms/cm^3 Fuel)	Type II Inclusion Weight %	$\frac{\text{Yield}}{\text{Inclusion}}$ w/o	Limiting Element	Maximum Weight Concentration (gms/cm^3 Fuel)	% of Yield in Inclusions	Maximum Molar Concentration (Moles/cm^3 Fuel)	Maximum Volume (Alloyed) of Inclusions (cm^3/cm^3 Fuel)
Pd	1.68×10^{-2}	72.55	2.32×10^{-2}	Pd	1.68×10^{-2}	100.0	1.58×10^{-4}	1.41×10^{-3}
Fe	-	22.25	-		5.15×10^{-3}	-	9.23×10^{-5}	6.56×10^{-4}
Sn	9.53×10^{-4}	2.8	3.40×10^{-2}		6.48×10^{-4}	68.04	5.46×10^{-6}	8.84×10^{-5}
Sb	3.75×10^{-4}	1.3	2.88×10^{-2}		3.01×10^{-4}	80.28	2.47×10^{-6}	4.50×10^{-5}
Te	4.27×10^{-3}	1.1	3.88×10^{-1}		2.55×10^{-4}	5.97	2.00×10^{-6}	4.09×10^{-5}
In	8.84×10^{-5}	< 1			8.84×10^{-5}	100.0	7.70×10^{-7}	8.81×10^{-6}
Nb	6.85×10^{-4}	< 1			2.31×10^{-4}	33.8	2.49×10^{-6}	2.43×10^{-5}
Ag	1.35×10^{-3}	< 1			2.31×10^{-4}	17.2	2.14×10^{-6}	2.18×10^{-5}

*Based on RIBD[8] yield data (see Appendix H)

Number Density of Inclusions (Inclusions/cm^3 Fuel)

Diameter of Inclusion	Average Johnson (Type II) Inclusion	Average Inclusion + In, Nb, Ag
5μm	3.42×10^{7}	3.52×10^{7}
10μm	4.28×10^{6}	4.40×10^{6}

As a comparison to the above data, Table 4.8 contains the number density of inclusions assuming complete segregation of the stable elements for the various yields. As expected Pu with its high noble metal yield has the highest number density with RIBD second and the U yield last.

In the previous calculations, it was assumed that the maximum quantity of fission products, in the appropriate weight %, segregated into inclusions, i.e. a limiting element contributed 100% of its fission yield to the inclusions. Using this principle one would expect to overestimate the inclusion density in the fuel. However, in looking at the micrographs of the inclusions in the fuel matrix by Jeffery,[4] Bramman,[6] and Bradbury[9] it appears that the inclusion volume % (v/o) is > 1%. The maximum inclusion v/o calculated, assuming the weight % of the investigators, was on the order of 0.2 - 0.6 v/o. Possible explanations of this small anomally is (1) the micrographs were taken specifically at high inclusion concentration areas, with migration of fission products occurring, and/or (2) an error existed in the measured composition of the inclusions. Due to independent analysis of composition by the various people, the last explanation probably is not valid. Errors of ± 1 w/o expected by the investigators is not sufficient to substantially increase the v/o of the inclusions.

4.3 Heat Transfer

For the heat transfer calculations, the fuel pin described in Section 4.1 was divided nodally. The pin was divided into 21 axial nodes or 20 equal segments. The plenum temperature was taken as the coolant outlet temperature, and this region was not included in the

This comparison [illegible] results of [illegible] work for the [illegible] yield per [illegible] lane.

In the [illegible] quantity of fissile [illegible] into fission [illegible] fission yield to the [illegible] to [illegible] at the micrographs of [illegible] Brenner,[illegible] and Roseberry [illegible] (v/v) is [illegible] weight % of the [illegible] possible explanations of [illegible] were taken [illegible] migration of fission [illegible] the measured [illegible] ed of [illegible] is not valid. [illegible] sufficient to [illegible]

4.3 Heat Transfer

For the heat [illegible] Section 4.1 [illegible] made of [illegible] coolant [illegible]

TABLE 4.8

INCLUSION NUMBER DENSITY FOR COMPLETE SEGREGATION

Inclusion Diameter		Inclusion Number Density (Inclusions/cm^3 Fuel)					
		Mo, Tc, Ru, Rh, Pd Segregated			Mo, Tc, Ru, Rh, Pd + Sb, Sn, In, Ag, Nb Segregated		
		RIBD[8] Yield	U[7] Yield	Pu[7] Yield	RIBD[8] Yield	U[7] Yield	Pu[7] Yield
5μm	(Pure)	9.685×10^7	7.04×10^7	1.02×10^8	1.03×10^8	7.50×10^7	1.09×10^8
	(Alloyed)	9.624×10^7	7.02×10^7	1.01×10^8	1.01×10^8	7.44×10^7	1.07×10^8
10μm	(Pure)	1.21×10^7	8.80×10^6	1.27×10^7	1.29×10^7	9.38×10^6	1.36×10^7
	(Alloyed)	1.20×10^7	8.77×10^6	1.27×10^7	1.27×10^7	9.30×10^6	1.34×10^7

analysis. Radially the fuel contained 11 nodes, or 10 equal Δr segments, with the 11th node at the fuel-bond interface. Additional nodes were at the bond-clad interface, the clad-coolant interface, and within the bulk coolant flow. The number of fuel nodes is variable and is an input quantity to the program.

A. Steady State Temperature. The steady state temperature profile was calculated using the subroutine SSTEMP. The analytical equations used in SSTEMP can be found in Appendix I. These equations were based on the following assumptions:

1. There were constant material properties such as density, heat capacity, and thermal conductivity.
2. There was no axial heat transfer. Since $z/r >> 1$, this was a realistic assumption.
3. There was no radial dependence for the volumetric heat generation. Since a fast flux was being used, this assumption should be very good.
4. Axially, a chopped cosine volumetric heat generation in the fuel and a flat distribution in the blanket-reflector region was assumed. A maximum of 575.6 cals/cm^3-s^1 (CRBR) was used with an extrapolation distance of 18.8 cms.[10] A flat 30 cals/cm^3-s, $\simeq$5% of peak value, was assumed in the blanket-reflector regions.
5. The pin dimensions at temperature were equal to those at fabrication; therefore, fuel swelling, thermal expansion, and fuel relocation were ignored.
6. The heat transfer coefficient used for the coolant was for annular flow. The derivation is in Appendix I.
7. The coolant flow rate and the maximum volumetric heat generation was adjusted to give inlet and outlet coolant temperatures close to CRBR. By using the pin pitch to calculate an equivalent annular flow, one ignores the additional coolant flow along the can wall and the possible cross channel heat transfer. Thus, the coolant velocity used, 950 cms/s, was somewhat higher than the projected CRBR flow velocity of $\simeq$ 600 cms/s.

The steady state temperature profile was generated as a starting point for the transient condition. Plots of representative axial and radial temperature profiles can be seen in Figs. 4.2 and 4.3.

B. Transient Temperature. The transient temperature profiles were calculated using subroutines POINT and TRANS. Subroutine POINT was a point kinetics routine based on the integral solution technique of Kaganove[11] and the modifications made by Burns.[10] Inputting a ramp reactivity insertion rate and a time step, Δt, POINT calculates the power amplitude at the end of the time step.

This new power amplitude, P1, was used as a multiplier of the axial volumetric power generation. The assumption was thus made that during the transient, the axial power shape remained constant and only the amplitude changed. Appendix J is an expansion of the technique.

TRANS uses an explicit finite-differencing technique to calculate the transient temperature profiles. Euler's method or forward differencing is used to approximate the time derivative of temperature, i.e.,

$$\left.\frac{dT}{dt}\right|_{n,t} = \frac{Tn^{t+\Delta t} - Tn^{t}}{\Delta t} \quad . \tag{4.1}$$

The error in forward differencing is proportional to $(\Delta r)^2$ and to Δt; thus in the program small Δt's were used for stability both in TRANS and POINT. The derivation of the finite-differencing equation can be found in Appendix K. Again, the assumption of constant material properties was used. Transient temperature profiles for both \$5/s and \$15/s ramp reactivity insertion rates can be seen in Figs. 4.4 and 4.5. Note that when the melt temperature is reached in a node,

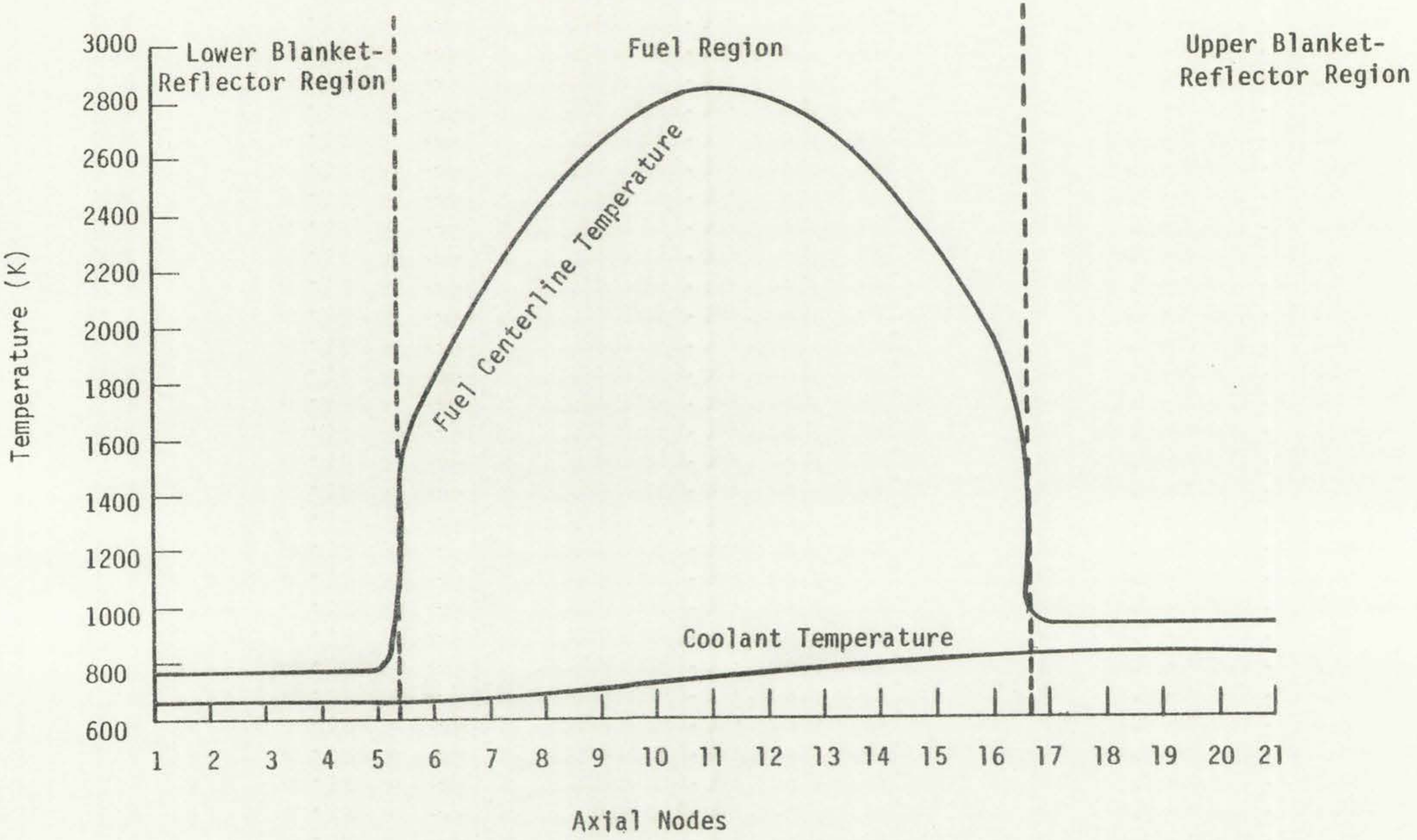

Figure 4.2.
Steady state axial temperature profiles.

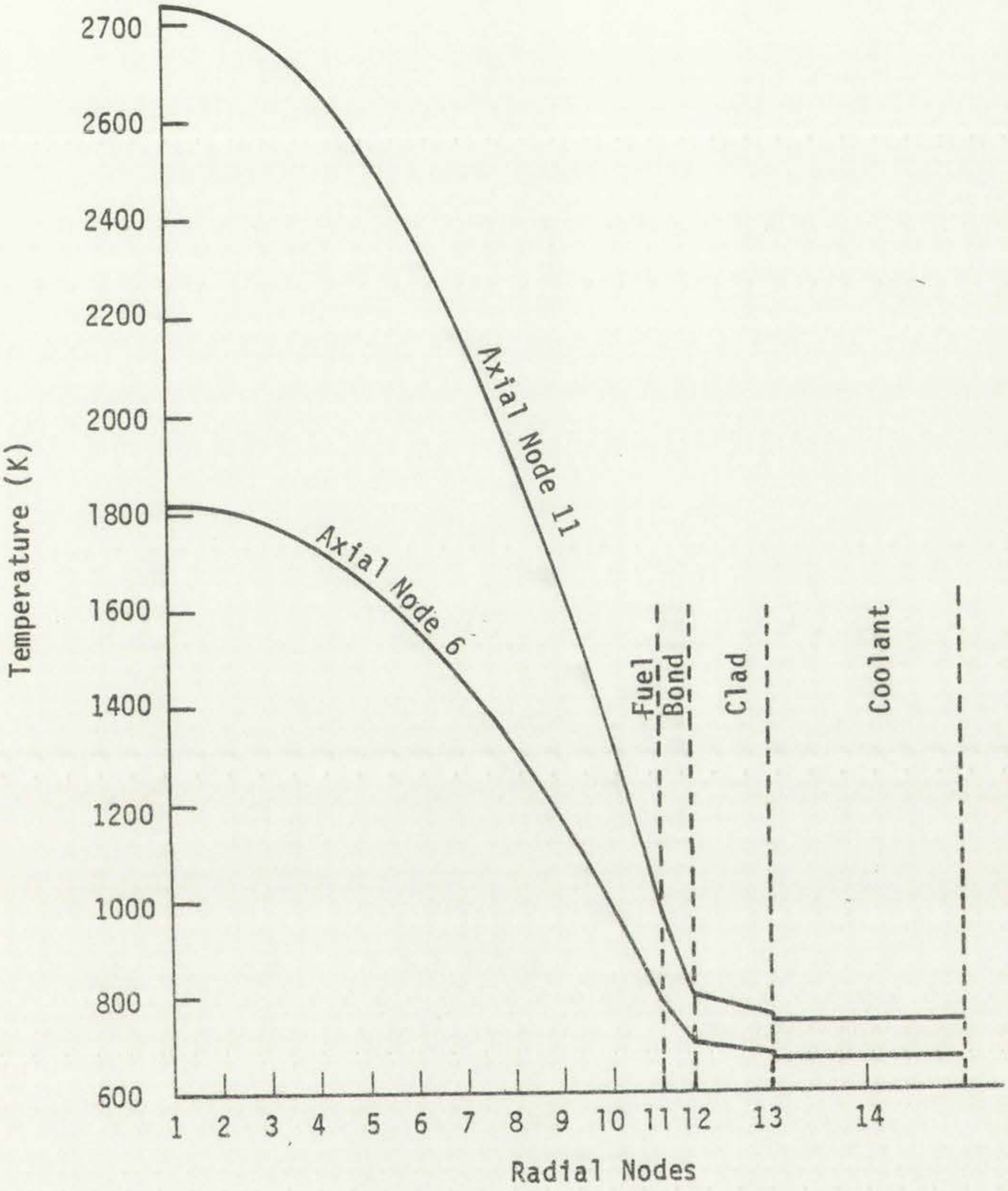

Figure 4.3.
Steady state radial temperature profiles.

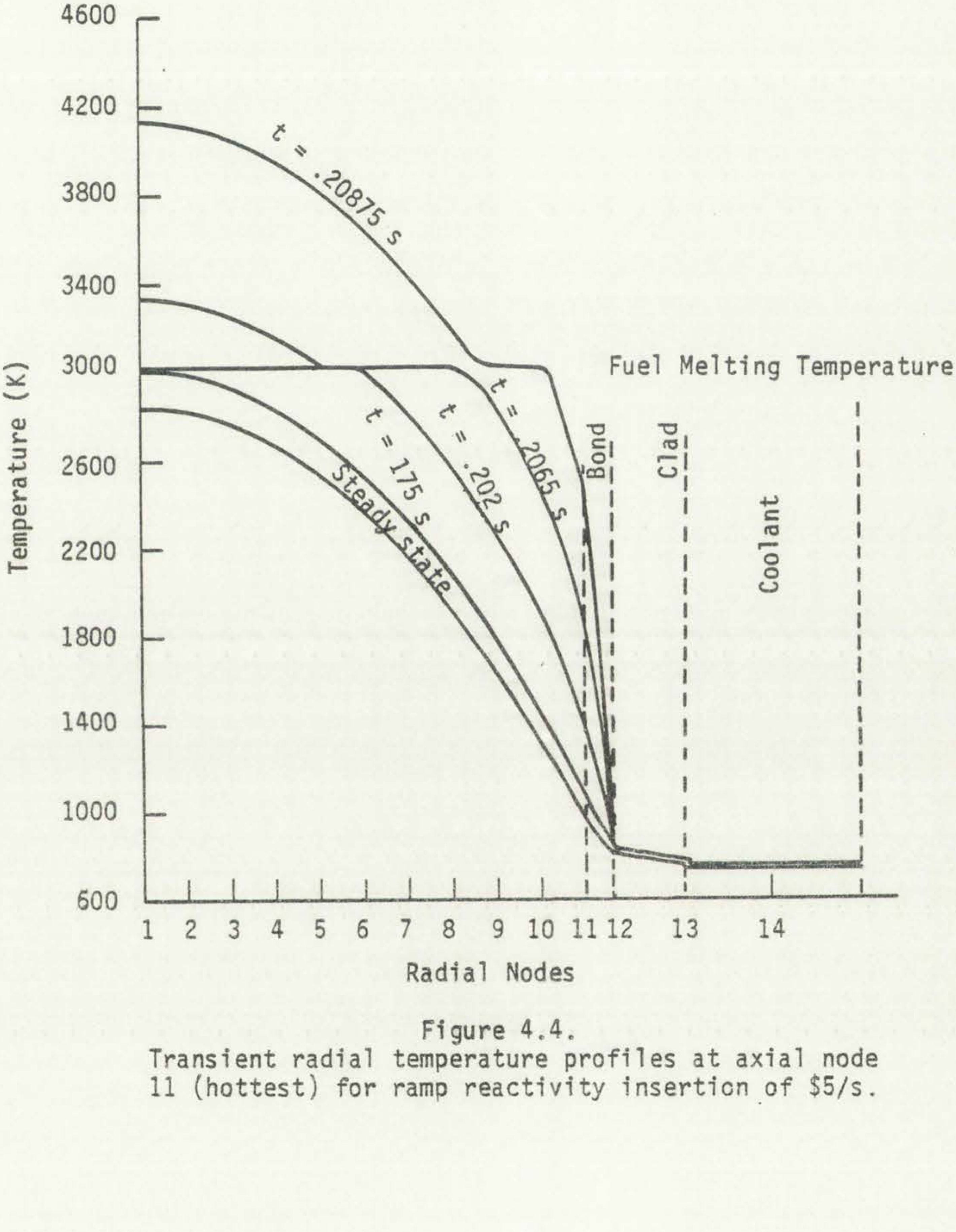

Figure 4.4.
Transient radial temperature profiles at axial node 11 (hottest) for ramp reactivity insertion of \$5/s.

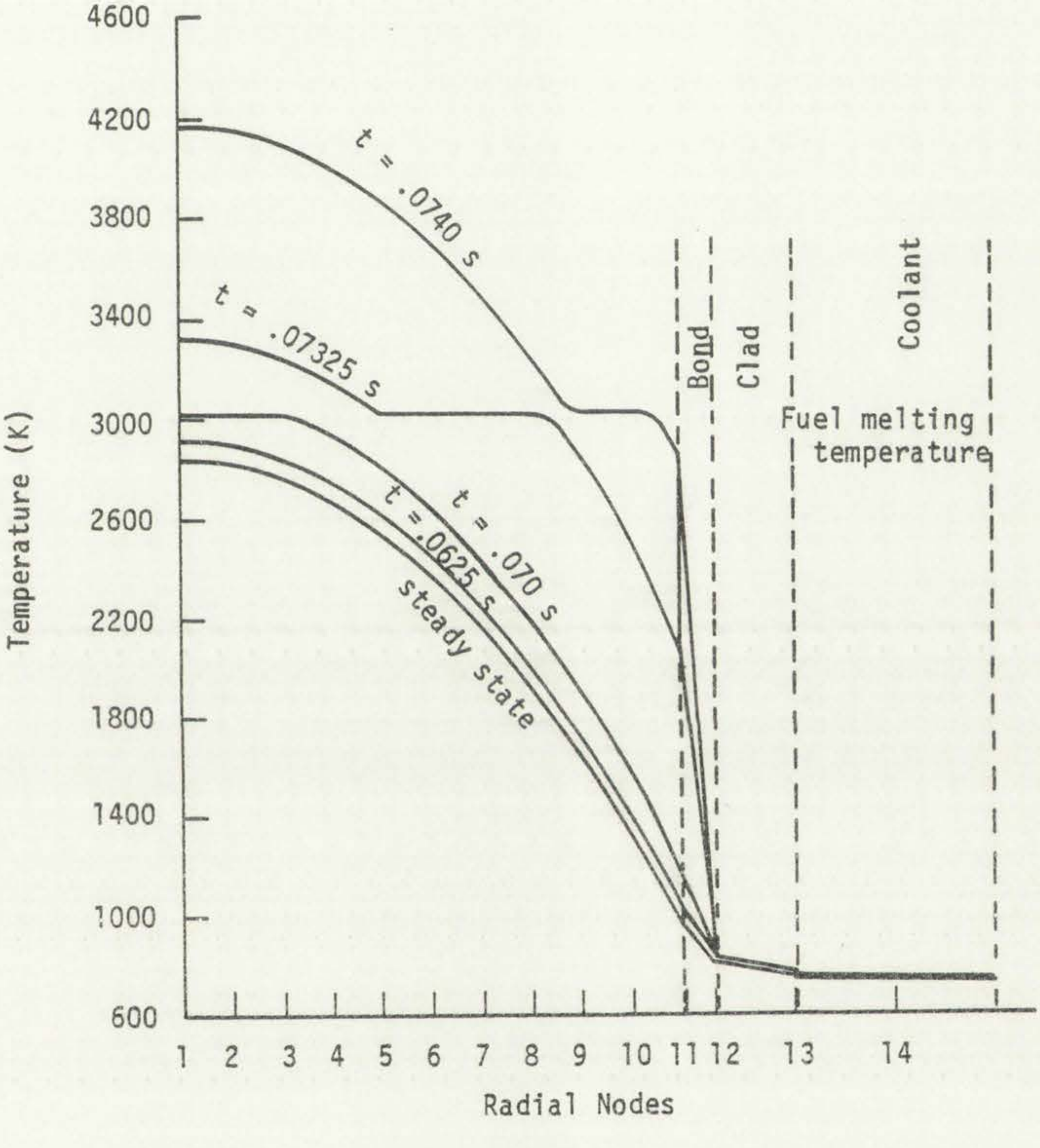

Figure 4.5.
Transient radial temperature profiles at axial node 11 (hottest) for ramp reactivity insertion of $15/s.

nodal temperature is kept at the melt temperature until the heat of fusion is acquired for all the mass in that node. Also note that the transient temperature profiles for the \$5/s and \$15/s ramp are almost identical with only the time sequence being different. The fuel edge temperature for the \$5/s ramp is slightly lower since the longer time allows some surface heat removal.

4.4 Inclusion Vaporization

Using the fuel nodal temperatures obtained by the subroutine TRANS, the subroutine VAPOR determines if inclusion vaporization occurs and, if so, the nodal volume expansion and total fuel expansion that can be expected at the end of the transient time step.

Two versions of VAPOR exist. The first version assumes the inclusion compositions are segregated elementally as shown in Fig. 4.6. The second version assumes the inclusion is a homogeneous solution of its constituents. The following assumptions are made by VAPOR:

1. The growth of the bubble upon vaporization is instantaneous. Thus any inertial or heat transfer bubble growth controlling mechanisms were assumed negligible.
2. The various vapors are noninteracting, i.e.,
   $V_T = V_1 + V_2 + \ldots$
3. Free volume expansion exists. Axial fuel-clad drag, solid fuel constraint (pressure bottle), etc., are assumed nonexistent.

Since the first version assumes segregated inclusion composition, species K vaporizes when its vapor pressure exceeds the bulk pressure. In the second version, inclusion vaporization does not occur until the inclusion vapor pressure determined by Raoult's Law, i.e.,

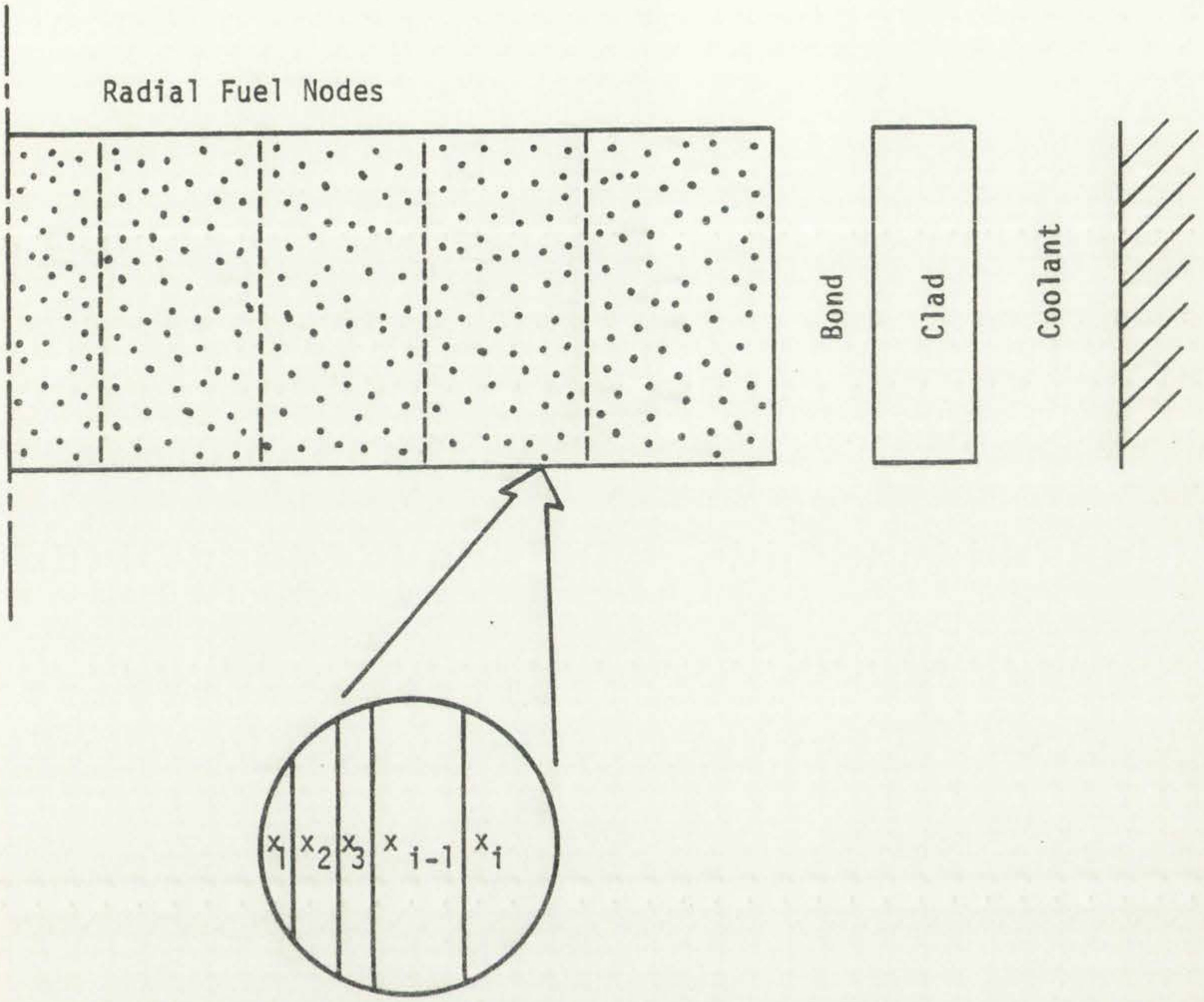

Compositional Segregated Inclusion Weight Percent for:

O'Boyle Inclusion: Mo-25%, Tc-17%, Ru-48%, Rh-5%
Pd-5%, Sb~1%

Johnson Inclusion (Type I): Mo-14.5%, Tc-20%, Ru-43.3%, Rh-17.6%
Pd-2.1%, Fe-2.45%, Sb~1%

Jeffery Inclusion: Mo-32.3%, Tc-10%, Ru-13.95%, Rh-3.95%,
Pd-2.1%, Ba-6.75%, Zr-3%, Ce-1.65%,
Sr-.9%, Nd-3%, Te-2.1%

Figure 4.6
Segregated inclusions.

the sum of the partial pressures (see Sec. 5.2), exceeds the bulk pressure.

In the above calculations, saturation vapor pressure curves for the appropriate volatiles must be known. Experimentally and theoretically determined vapor pressure curves can be found in Appendix L. If the data did not exist, it was extrapolated to the pressure range of interest, i.e. 25 to 100 atm. Table 4.9 contains a listing of the saturation pressure-temperature relations for the elements of interest, used in this analysis.

Hornung[12] in extrapolating his data assumes a linear relationship Log $P \propto \frac{1}{T}$ over a large temperature range. He also states that one must be careful in extrapolating vapor-pressure equations that contain additional phenomenological terms, i.e.,

$$\text{Log } P \propto A - \frac{B}{T} + CT + D \log T \quad , \tag{4.2}$$

since no physical basis exists for these terms. This equation can, however, be derived as shown in Appendix M, if one assumes a temperature dependent latent heat of vaporization, ΔH. Nesmeyanov[13] uses this equation in his work to represent the saturation vapor pressure curves.

The subroutines along with the driver program can be found in Appendix N.

TABLE 4.9

ESTIMATED SATURATION PRESSURE (atm) FOR ELEMENTS OF INTEREST PIN METALLIC INCLUSION ANALYSIS

Element	TEMPERATURE (K)						
	1000	1500	2000	2500	3000	3500	4000
Ba	1.8×10^{-4}	.0964	2.224	14.62	51.3	2.7×10^{4}	
Ce		2.84×10^{-9}	9.23×10^{-6}	1.18×10^{-3}	3.00×10^{-2}	.302	1.71
Pd		1.95×10^{-9}	1.68×10^{-6}	6.44×10^{-2}	.944	6.43	27.1
Fe		2.29×10^{-7}	3.4×10^{-4}	.0273	.507	4.09	19.57
Te	5.59×10^{-2}	5.25	46.77	165.	370.	643.	957.
Sb	1.03×10^{-3}	8.92×10^{-2}	.876	3.46	8.65	16.64	27.2
Cs	1.69	27.3	105.2	230.	380.	538.	691.
Mo			5.84×10^{-15}	1.12×10^{-10}	8.06×10^{-8}	8.84×10^{-6}	3.00×10^{-4}
Ru				1.48×10^{-6}	2.44×10^{-4}	9.08×10^{-3}	.131
Rh				9.98×10^{-5}	6.14×10^{-3}	.109	.696
Tc				1.50×10^{-6}	1.31×10^{-4}	3.19×10^{-3}	3.5×10^{-2}

REFERENCES

1. E. A. Appleby, "Compilation of Data and Descriptions for United States and Foreign Liquid Metal Fast Breeder Reactors," Hanford Engineering Development Laboratory report HEDL-TME-75-12 (August 1975).

2. D. R. O'Boyle, F. L. Brown, and J. E. Sanecki," Solid Fission Product Behavior in Uraniun-Plutonium Oxide Fuel Irradiated in a Fast Neutron Flux," Journal of Nuclear Materials 29 27-42 (1969).

3. P. E. Blackburn, C. E. Johnson, et al. "Chemical Engineering Division Fuels and Materials Chemistry Semiannual Report, July-December 1971," Argonne National Laboratory report ANL-7877 (April 1972).

4. B. M. Jeffery, "Microanalysis of Inclusions in Irradiated UO_2," Journal of Nuclear Materials 22 33-40 (1967).

5. J. H. Davies, R. F. Boyle, B. Weidenbaum, J. E. Hanson, "On the Composition of Metallic Ingots Formed in High-Performance Ceramic Fuel Elements," Trans. American Nuclear Society, 9, (1966) p. 63.

6. J. E. Bramman, R. M. Sharpe, D. Thom, and G. Yates, "Metallic Fission-Product Inclusions in Irradiated Oxide Fuels," Journal of Nuclear Materials, 25 201-215 (1968).

7. L. Burris, Jr., and I. G. Dillon, "Estimation of Fission Product Spectra in Discharged Fuel From Fast Reactors," Argonne National Laboratory report ANL-5742 (July 1957).

8. R. O. Gumprecht, "Mathematical Basis of Computer Code RIBD," June 1968 (DUN-4136).

9. B. T. Bradbury, J. T. Demant, P. M. Martin, and D. M. Poole, "Electron Probe Micro-Analysis of Irradiated UO_2," Journal of Nuclear Materials, 17 227-236 (1965).

10. R. D. Burns, "A Parametric Approach to LMFBR Safety Evaluation," Purdue University, PNE-76-110 (August 1976).

11. J. J. Kaganove, "Numerical Solution of the One-Group, Space-Independent Reactor Kinetics Eqiations for Neutron Density Given the Excess Reactivity," Argonne National Laboratory report ANL-6132 (February 1960).

12. K. Hornung, "Liquid Metal Coexistence Properties from Corresponding States and Third Law," Journal of Applied Physics, 46, No. 6 (1975).

13. A. N. Nesmeyanov, Vapor Pressure of the Chemical Elements, (Elsevier Publishing Co., 1963).

5. DISCUSSION OF RESULTS

In this section, the local (nodal) and total fuel volume expansion are calculated for a hypothetical transient overpower excursion. The results of the calculations depend strongly on the physical-chemical state of the inclusions. The physical state with respect to the solubility of the inclusion constituents in one another is uncertain. Thus calculations are done assuming: (1) the inclusion constituents are totally segregated from one another (immiscible) and (2) the inclusion constituents are in solid solution with one another (miscible).

5.1 Segregated Inclusions

The nodal and fuel volume expansions are calculated assuming the inclusion constituents are immiscible. This assumption implies that species k vaporizes when its vapor pressure exceeds the local bulk pressure, taken as the plenum pressure in these analyses. In addition, the following assumptions are made:

1. The various vapors are noninteracting, i.e., V_T(total volume) = $V_1 + V_2 + \ldots, V_i$
2. The growth of the bubbles upon nucleation is instantaneous; thus, inertial and heat transfer controlling mechanisms are ignored.
3. As mentioned previously, the inclusions are considered identical in terms of size and composition, both in the radial and axial direction. The size assumed is 5 μm in diameter[1-3] and the composition based on O'Boyle[3] and Johnson's[4] average inclusion compositions are used.

Two additional assumptions were made for simplicity in the initial runs. These are:

1. The number density of inclusions is constant in the radial and axial direction. The density assumes total segregation of pertinent fission products.
2. An Ideal Gas equation-of-state is used for the metallic fission product vapor.

In the following calculations the percent volume expansion, $\frac{\Delta V}{V}$ x 100%, is computed for both the entire fuel pin and for each individual node. Within any given node it is assumed that the temperature profile is flat, and that volatile species k will vaporize when the nodal temperature reaches its vaporization temperature. This leads to step jumps in the nodal volume expansion at the various vaporization temperatures. The contribution of each inclusion constituent is monitored. These calculated volume expansion are then compared to the volume expansion due to the phase change upon fuel melting and the expansion due to fission gas.

Figures 5.1-5.7 show the results using the above assumptions. If one assumes Sb is present in the inclusions at a level of 1 wt%, an additional 3-4% nodal volume expansion can be expected. Consequently the presence of Sb, Nb, Ag, and other stable metallics mentioned previously, in levels under the 0.5 to 1 wt% detection limit of the ion microprobe could substantially increase the expected fuel volume expansion. Future calculations will be done with and without Sb present in order to obtain an order of magnitude approximation to the possible contribution of nondetected metallics. Whether these elements actually

The additional assumptions have been made in [illegible]

initial runs. These are:

1. The thermal analysis of the [illegible] is computed in the radial and axial direction. The [illegible] behavior [illegible] of [illegible] fission products.

2. At least one equilibrium state is reached [illegible] fission product vapor.

In the following calculations the percent volume expansion, $\Delta V/V \times 100\%$, is computed for both the entire fuel pin and for each individual node. Within any given node it is assumed that the temperature profile is flat and that volatile species [illegible] once the nodal temperature reaches its vaporization temperature. This leads to step jumps in the nodal volume expansion at the various vaporization temperatures. The contribution of each volatile species is then found. These individual volume expansion are then compared to the volume expansion due to the phase change upon fuel melting and the expansion due to fission gas.

Figures 6.1-6.3 show the results using the above calculations. [illegible] was assumed to be present in the inclusions [illegible] at 1 000 [illegible] additional 3-4% nodal volume expansion can be expected [illegible] the presence of Cs, Rb, Ag, and other [illegible] fission products [illegible] yields [illegible] and 0.1 to 1 wt% [illegible] elements could substantially increase the overall [illegible] pansion. Future calculations will be done [illegible] in order to obtain an order of magnitude approximation of the [illegible] contribution of undissolved metallics. [illegible]

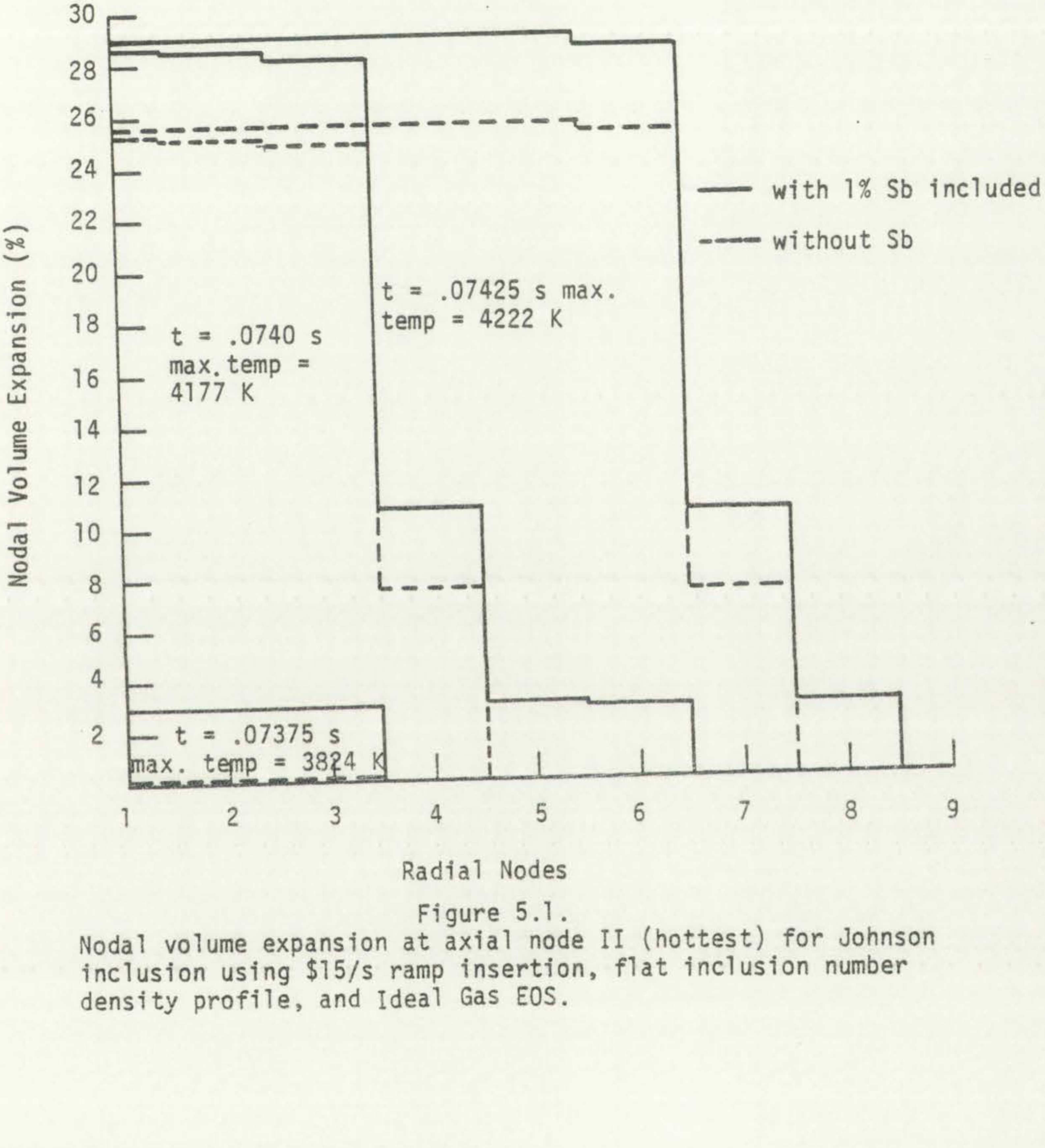

Figure 5.1.
Nodal volume expansion at axial node II (hottest) for Johnson inclusion using $15/s ramp insertion, flat inclusion number density profile, and Ideal Gas EOS.

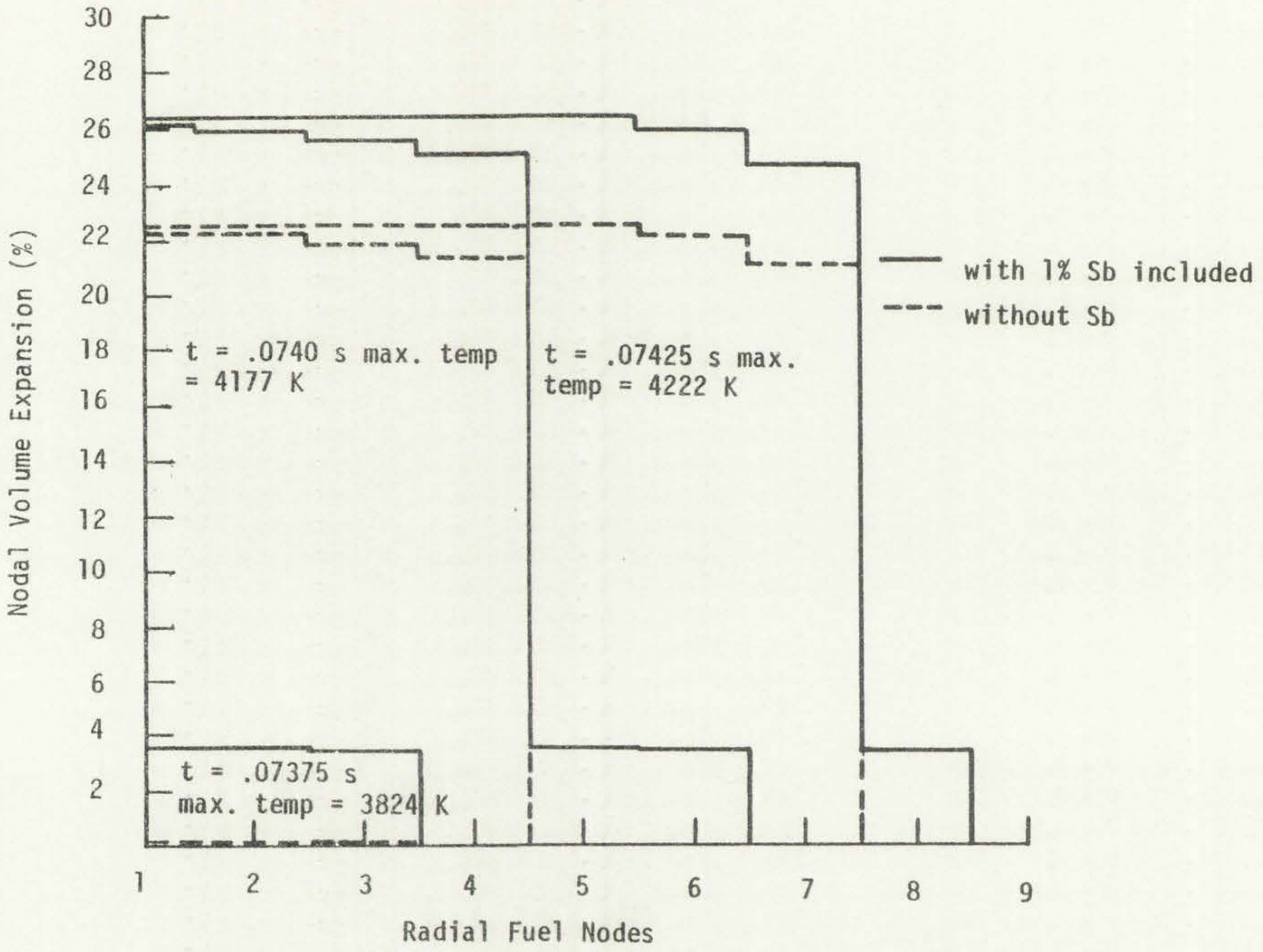

Figure 5.2
Nodal volume expansion at axial node II (hottest) for O'Boyle inclusions using \$15/s ramp insertion, flat inclusion number density profile, and Ideal Gas EOS.

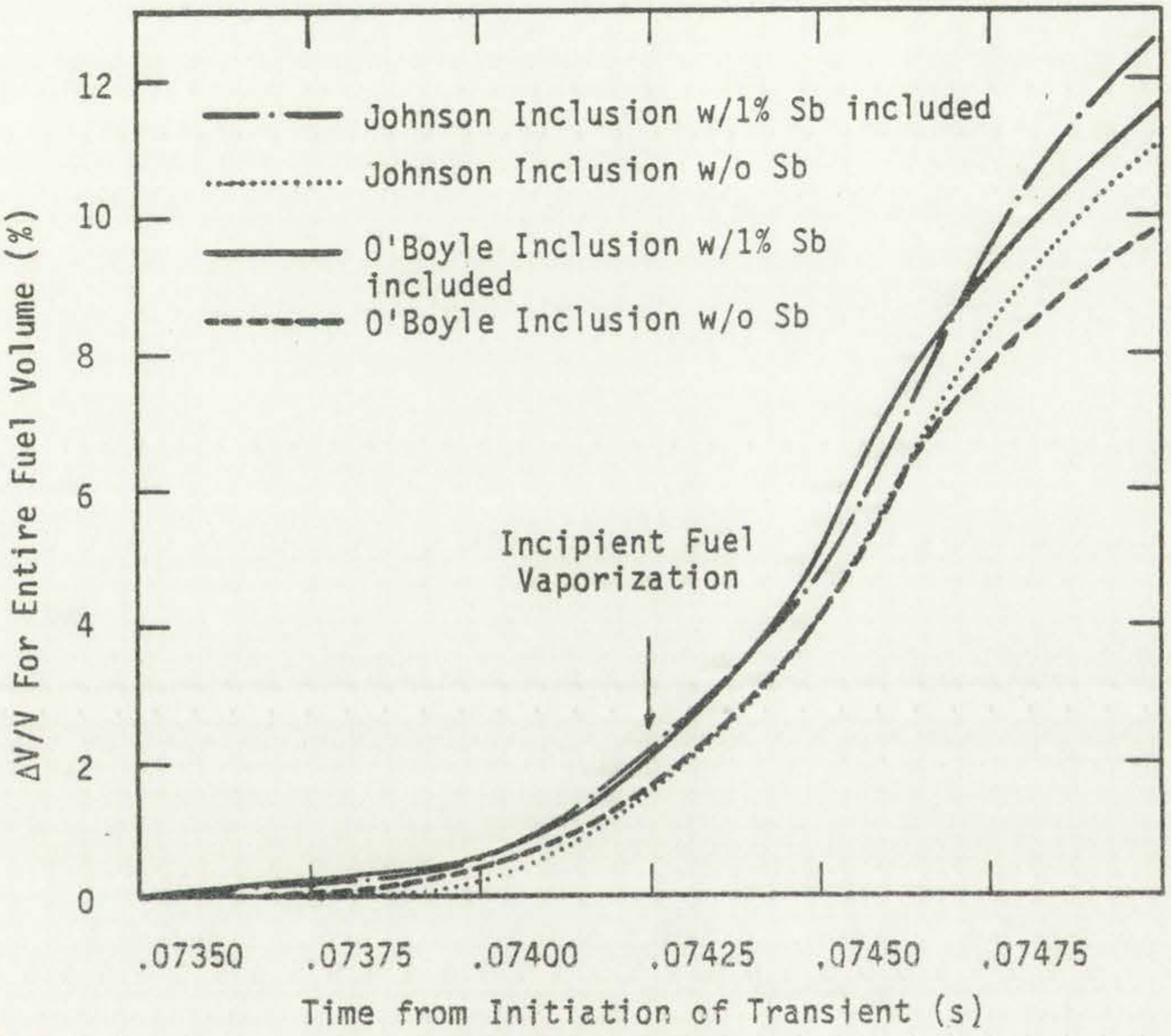

Figure 5.3
Total fuel volume expansion for \$15/s ramp insertion, flat inclusion number density profile, and Ideal Gas EOS.

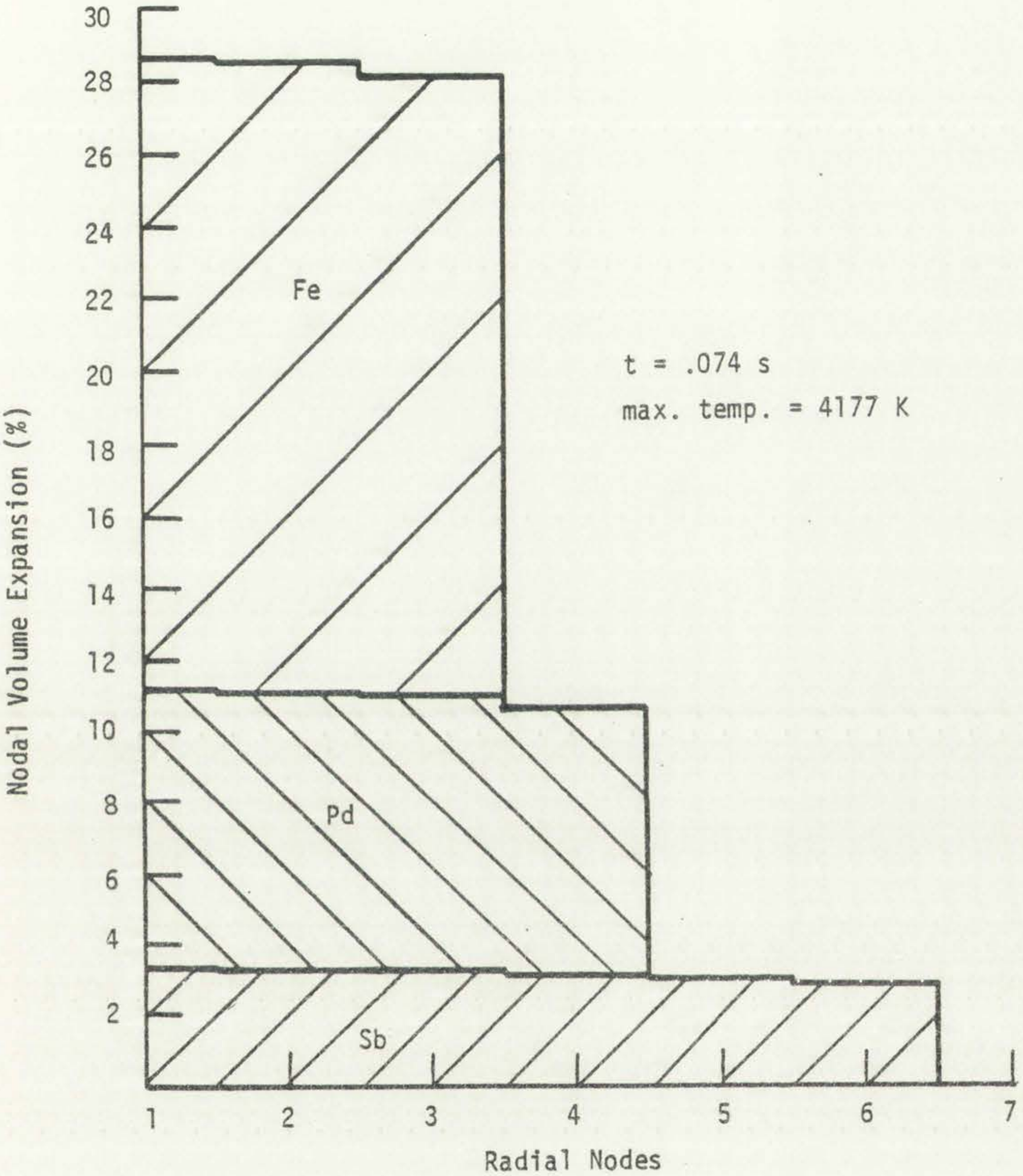

Figure 5.4
Nodal volume expansion contribution from the various constituents of Johnson's inclusions for \$15/s ramp insertion at axial node 11 (hottest).

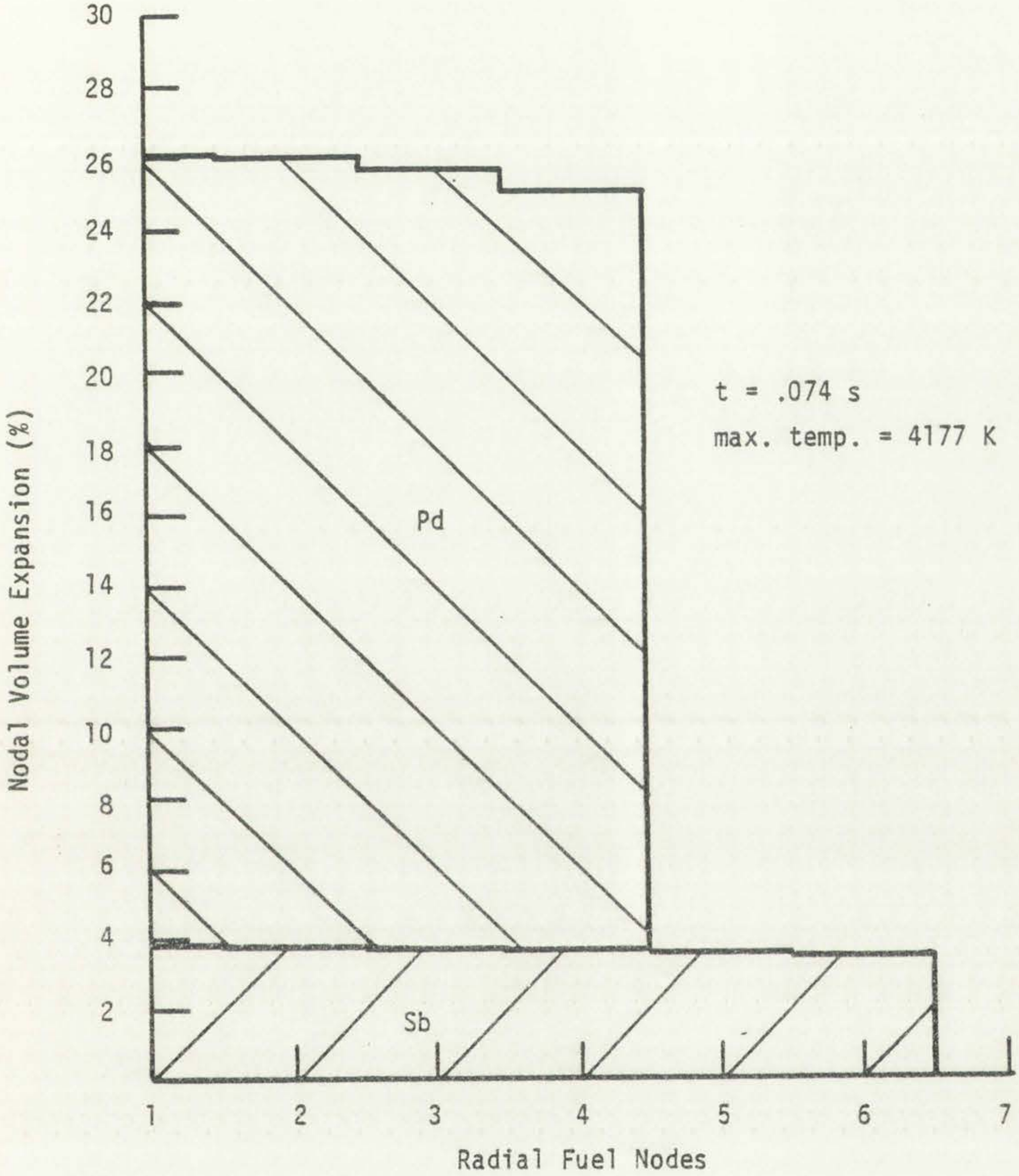

Figure 5.5
Nodal volume expansion contribution from the various constituents of O'Boyle's inclusions at $15/s ramp insertion.

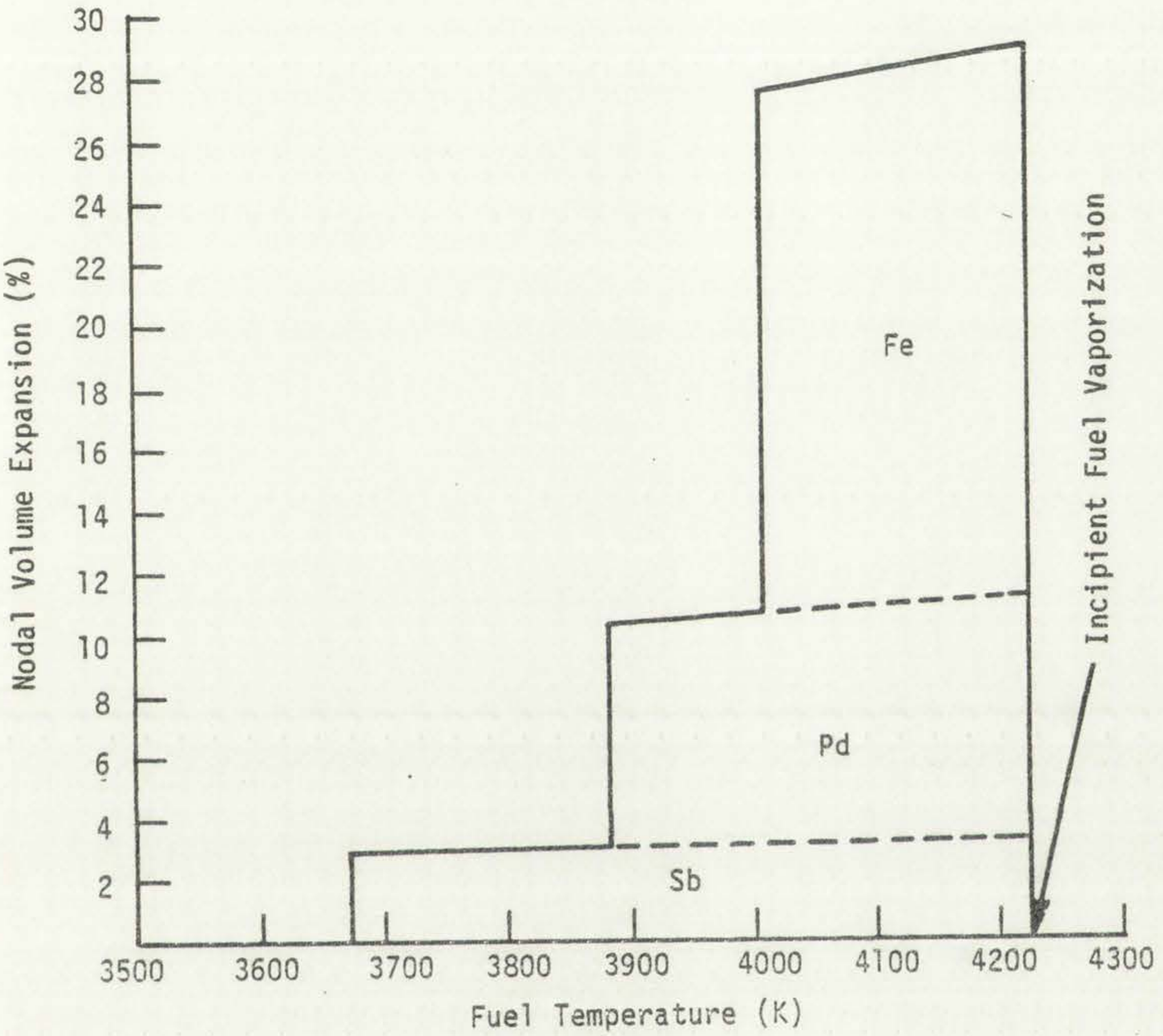

Figure 5.6
Nodal volume expansion for Johnson inclusions using a flat inclusion number density profile and Ideal Gas EOS.

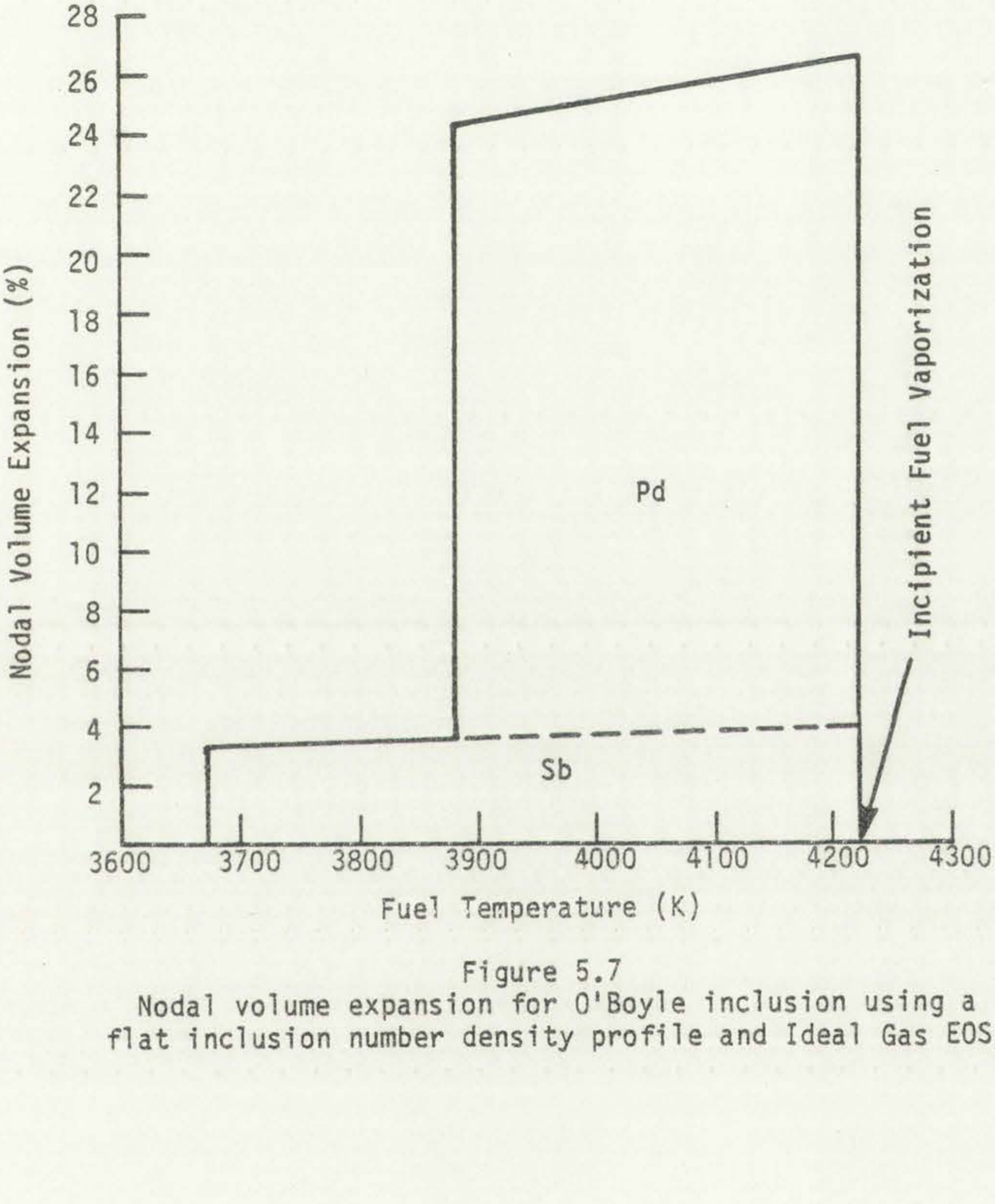

Figure 5.7
Nodal volume expansion for O'Boyle inclusion using a flat inclusion number density profile and Ideal Gas EOS.

exist in the inclusions at levels < 1% depends on the mechanism of inclusion formation. One investigator[5] postulated that all elements are daughter products of Mo isotopes which form aggregates before decaying, in which case, Sb, Sn, Ag, Cd, etc., would not be present due to their decay chains. Since the mechanism is not known and since Sb was detected by Johnson[4] in his type 2 inclusion found in the equiaxed region of the fuel, the potential Sb contribution is a logical choice to use as an indicator.

As can be seen from the figures, without the Sb contribution, a nodal volume expansion of 25 and 22% can be expected for Johnson's[4] and O'Boyle's[3] inclusions respectively. Due to the radial temperature profile and flat inclusion profile, the maximum nodal volume expansion occurs in the hottest (center) nodes. In addition, a total fuel volume expansion of 1.5 to 2% can be expected at incipient fuel vaporization. The Redlich-Kwong equation-of-state is more applicable to the temperature-pressure range of interest than the Ideal Gas equation-of-state. Using the same assumptions as above except with the Redlich-Kwong EOS instead of the Ideal Gas EOS, the nodal and total fuel volume expansion were recalculated. As can be seen from Figs. 5.8 and 5.9, the Redlich-Kwong EOS lowers the predicted nodal volume only on the order of a few tenths of a percent. The Redlich-Kwong EOS will be more applicable if higher pressures are assumed.

As seen in Figs. 2.9 and 2.10, the inclusion number density is not constant in the radial direction as assumed above. A radial

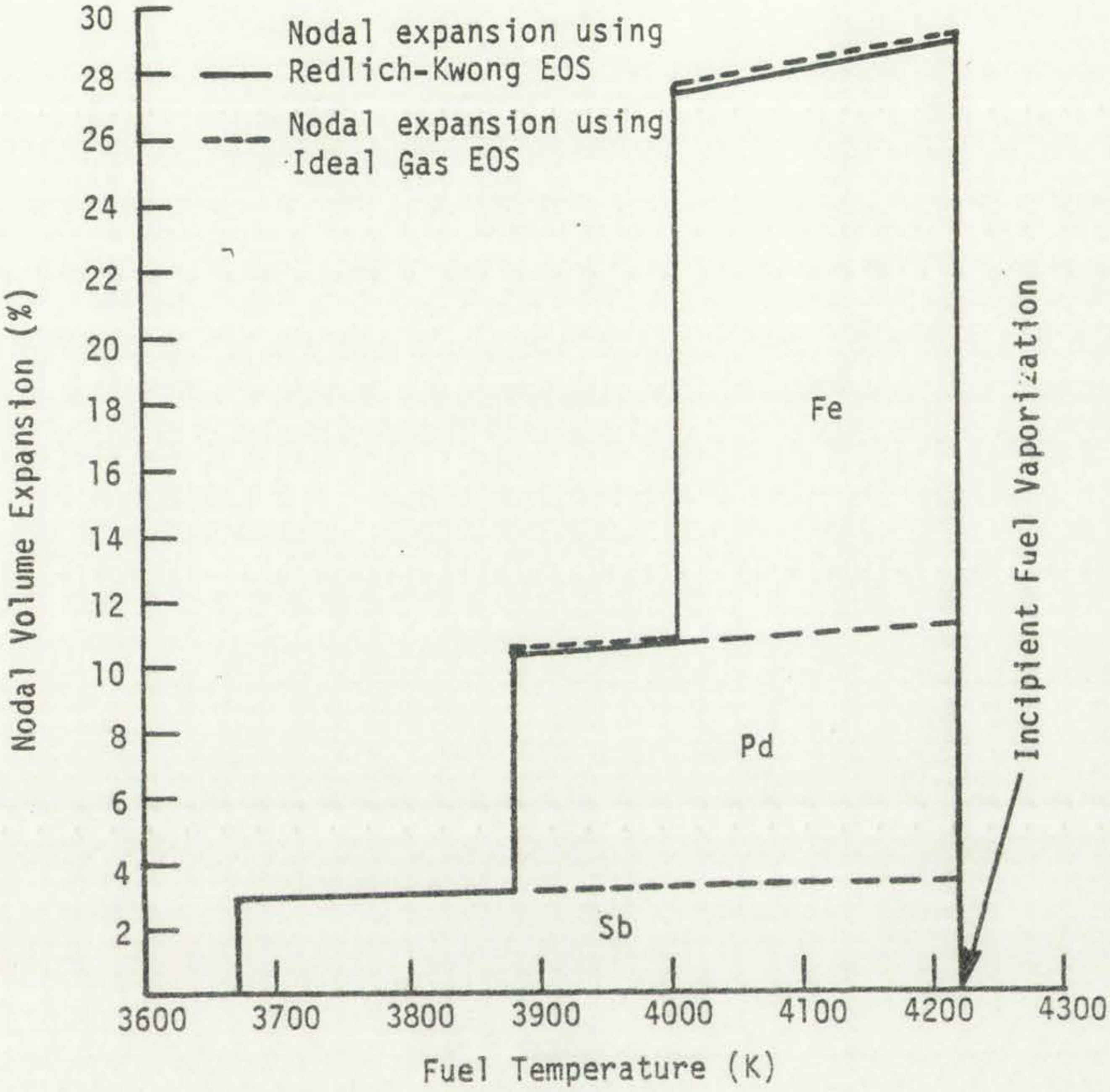

Figure 5.8
Nodal volume expansion for Johnson inclusions using
a flat inclusion number density profile
and Redlich-Kwong EOS.

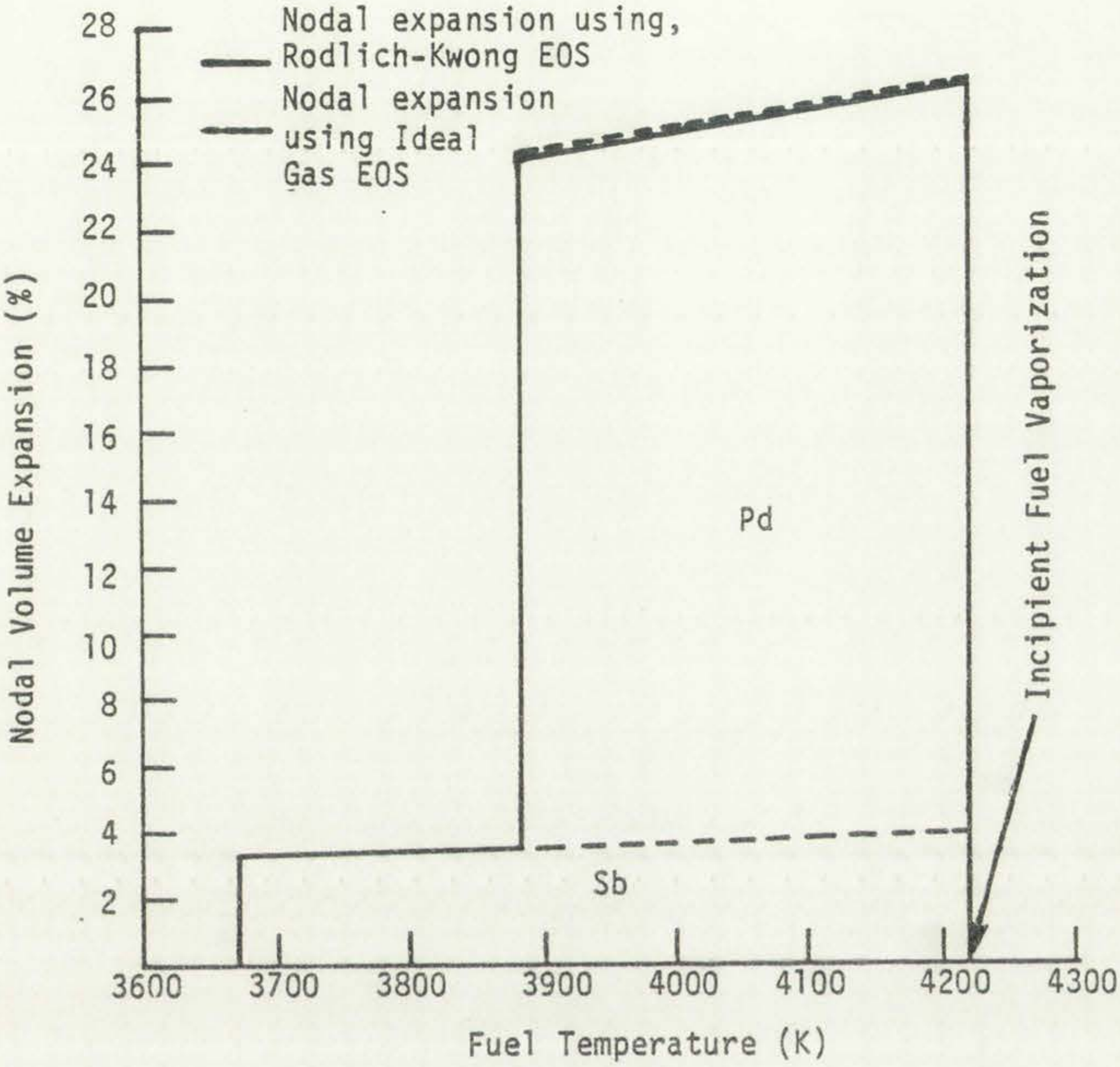

Figure 5.9
Nodal volume expansion for O'Boyle inclusion
using a flat inclusion number density
profile and Redlich-Kwong EOS.

inclusion density distribution based on work of Baird,[6] Fig. 2.9, was used to create a normalized inclusion distribution curve found in Fig. 5.10. It should be noted that the inclusion density is zero in the unrestructured region as per experimental evidence. Since, in this analysis a central void is not used, the measured inclusion density at the central void edge was assumed for this region. A multiplication factor is used such that the volume integral of the calculated inclusion density is equal to the volume integral assuming a flat distribution, i.e., for nodal notation:

$$\pi\Delta z \left[\frac{\Delta r}{2}\right]^2 x_1 D + \pi\Delta z \sum_{i=1}^{n} \left[(r_i + \frac{\Delta r}{2})^2 - (r_i - \frac{\Delta r}{2})^2\right] x_i D$$

$$= \Delta z\ \pi\overline{D}\ (R_n + \frac{\Delta r}{2})^2 \qquad (5.1)$$

where:

x_i = distribution factors from Fig. 5.10

$\overline{D}$ = inclusion number density assuming flat distribution

Δr = radial nodal width

Δz = axial nodal width

r_i = radius of ith node

n = outermost node in the equiaxed grain region

R_n = radius of nth node

D = $A \cdot \overline{D}$ where A is the multiplication factor

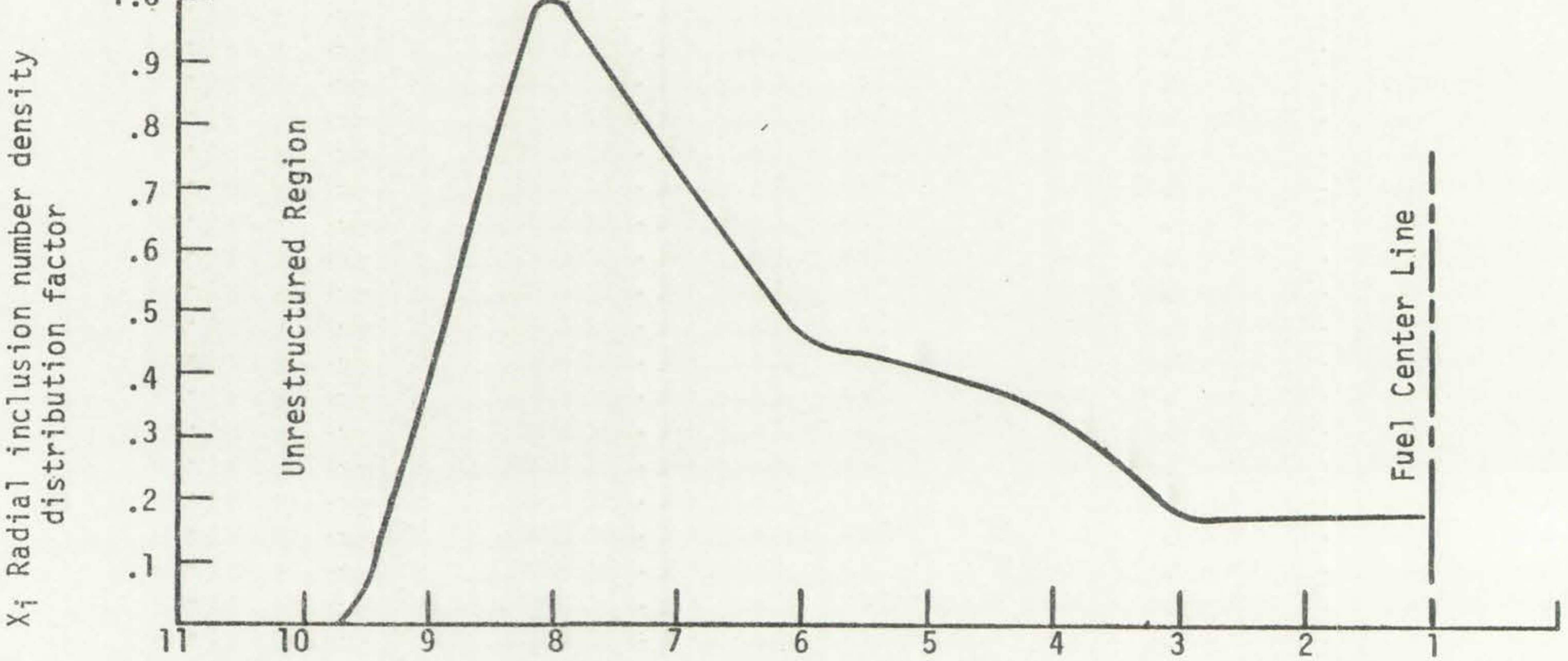

Figure 5.10
Radial inclusion number density profile.

Figures 5.11-5.15 show the effect of the radial distribution in inclusion number density. The combination of the cosine shaped radial temperature profile and the number density profile in Fig. 5.10 causes the maximum nodal volume expansion to move outwards, but not to the maximum point in inclusion number density. It actually increases the maximum nodal volume expansion from 26.4% to 28.6% for O'Boyle type inclusion. However, due to the higher vaporization temperature of Fe the maximum nodal volume expansion for Johnson's inclusions decreases from 29% to 20%, both assuming Sb present. The total fuel volume expansion also decreased approximately 0.75-.1% at incipient fuel vaporization. It thus appears that the radial distribution decreases potential fuel motion up to incipient fuel vaporization.

5.2 Homogeneous Inclusions

A more realistic approximation to the physical state of the inclusions is to consider the inclusions as a homogeneous solution of the constituent elements, i.e., miscible and thus in a single phase. This assumption is supported by the experimental work of Bramman[5] whose X-ray examination found the inclusions to be single phase with a hexagonal structure, i.e. as stated by Bramman, "It was found that insoluble residues contained small particles of the order of 5μm in dia., and X-ray examination showed these particles to have a hexagonal structure with $a_o = 2.756 \pm .001\text{Å}$, $C_o = 4.426 \pm .002\text{Å}$."[5] No other investigators reported finding more than one phase.

The Hume-Rothery rule[7] was also used to investigate solubility. This rule states that substitutional solubility is not found if:

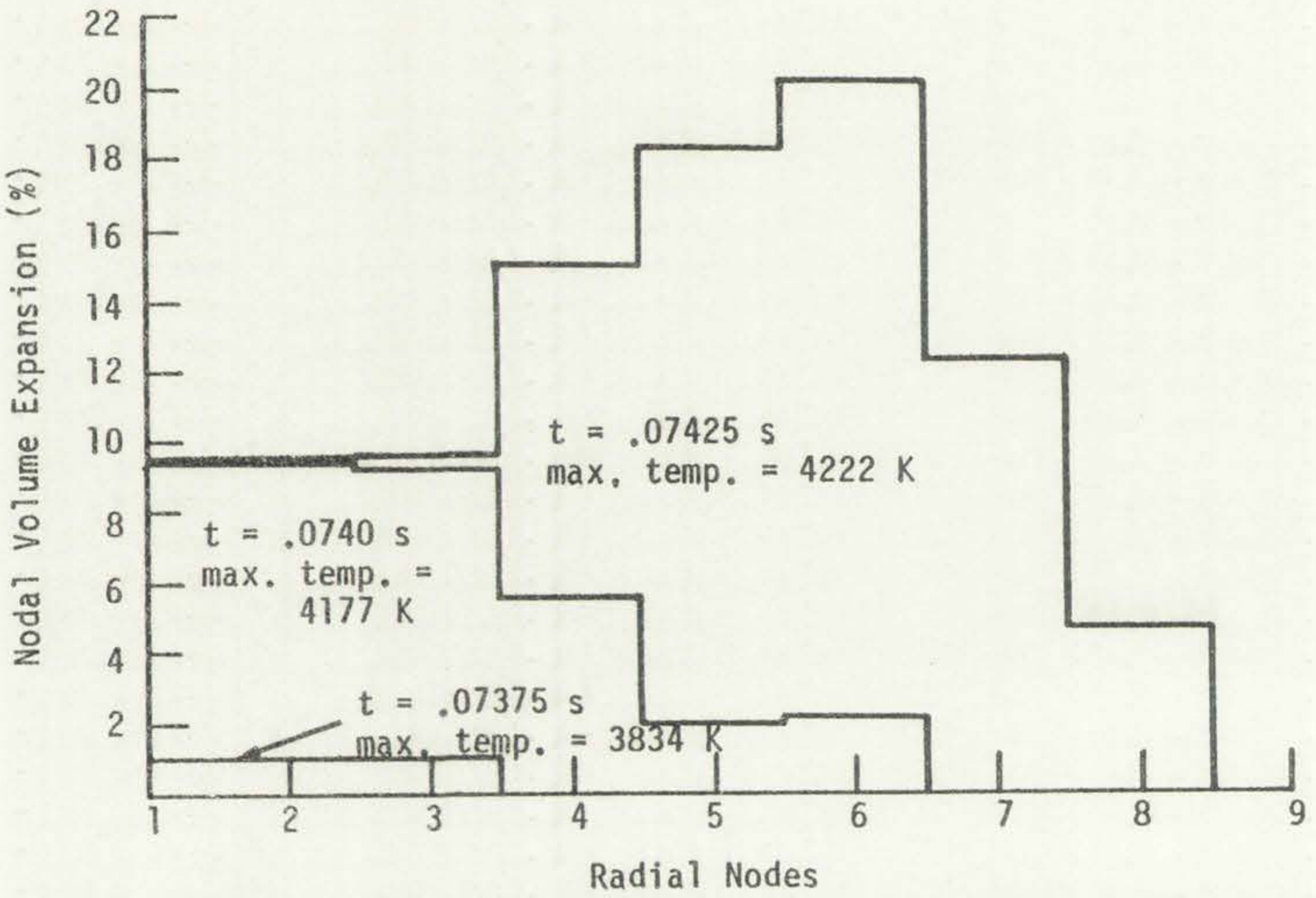

Figure 5.11
Nodal volume expansion for Johnson inclusions at $15/s ramp insertion, axial node 11 (Hottest) using radial inclusion distribution.

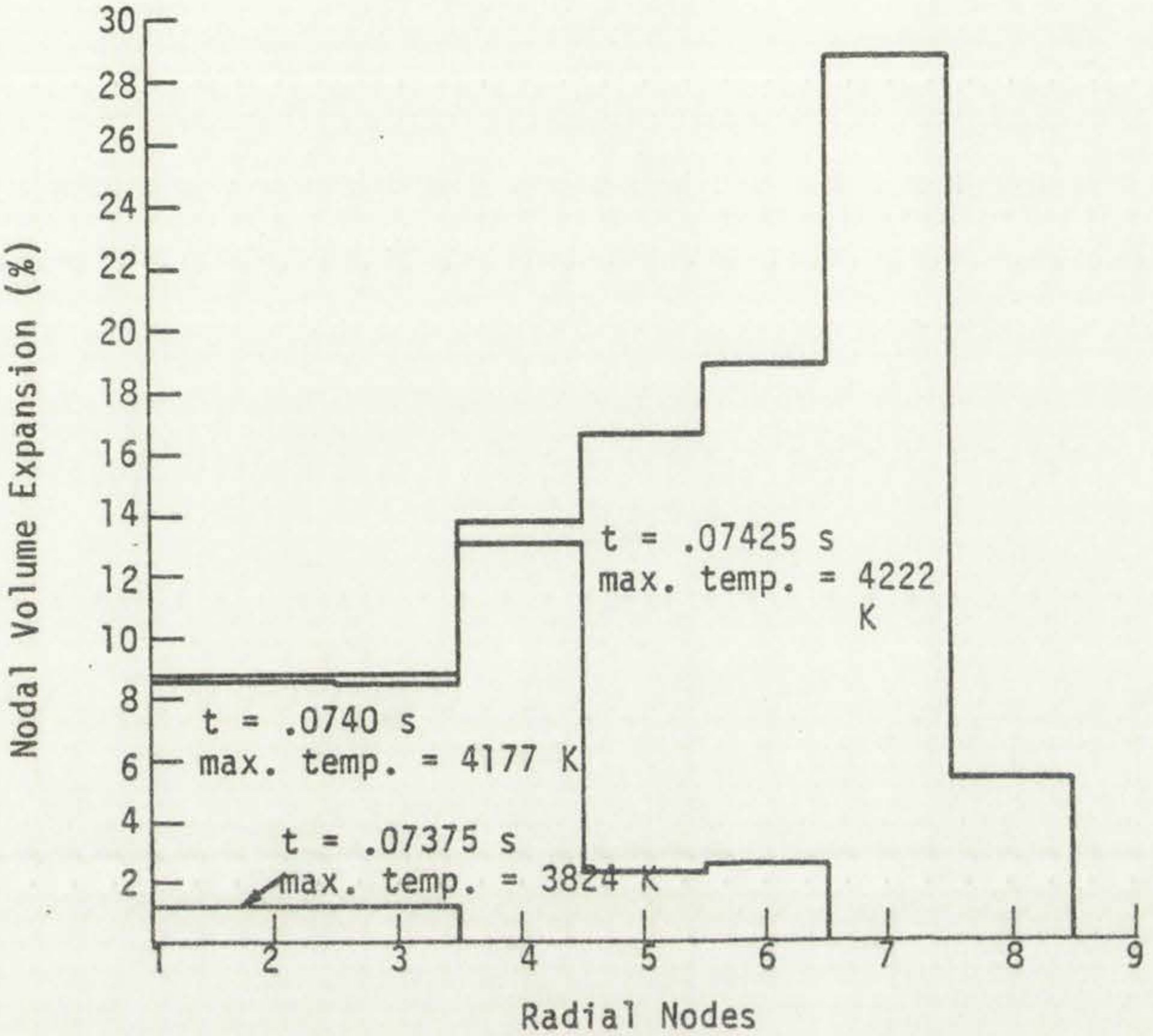

Figure 5.12
Nodal volume expansion for O'Boyle inclusion for \$15/s ramp insertion at axial node 11 (Hottest) using radial inclusion distribution.

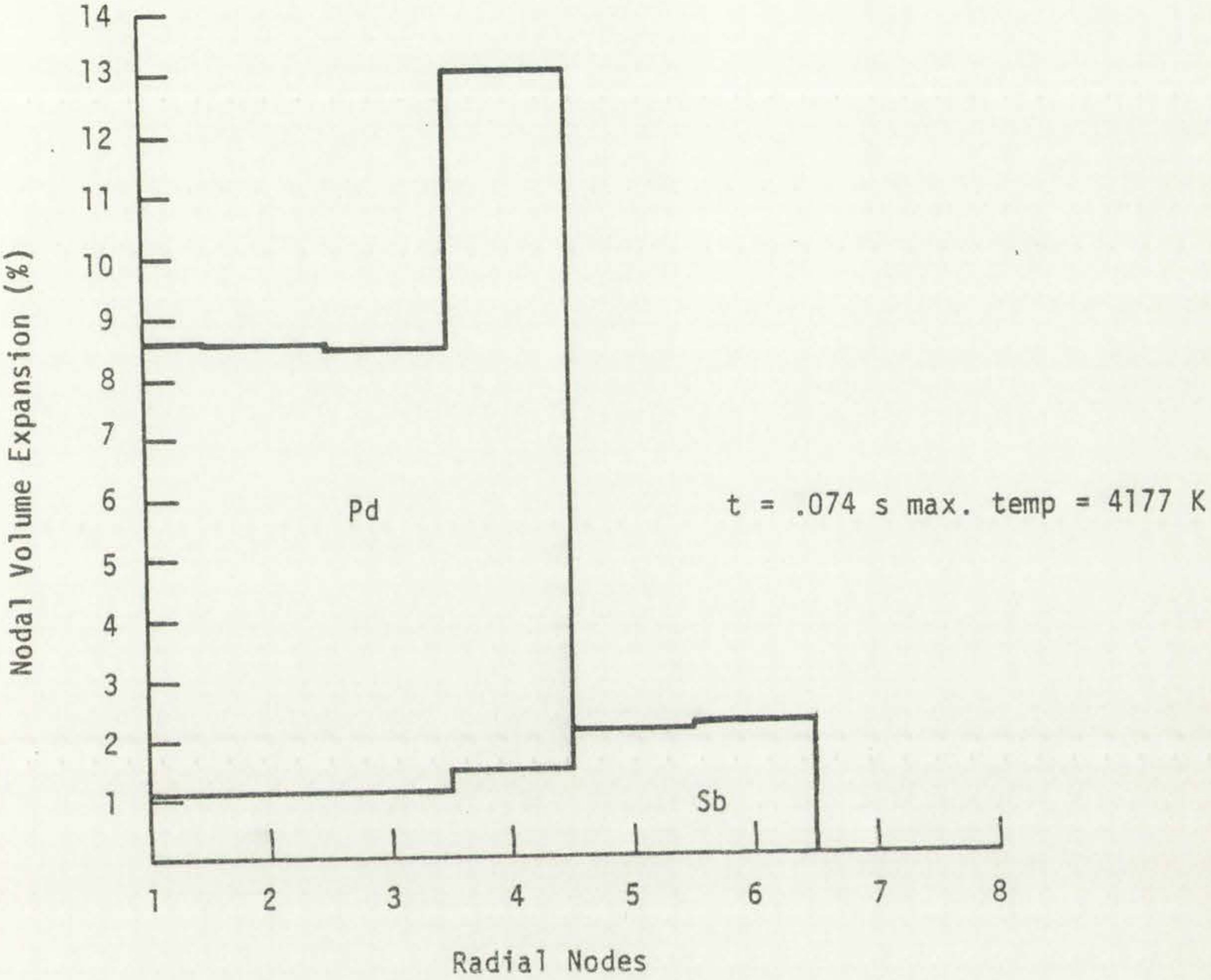

Figure 5.13.
Nodal volume expansion for $15/s ramp insertion at axial node II (hottest) using the radial inclusion distribution in number density in O'Boyle inclusions.

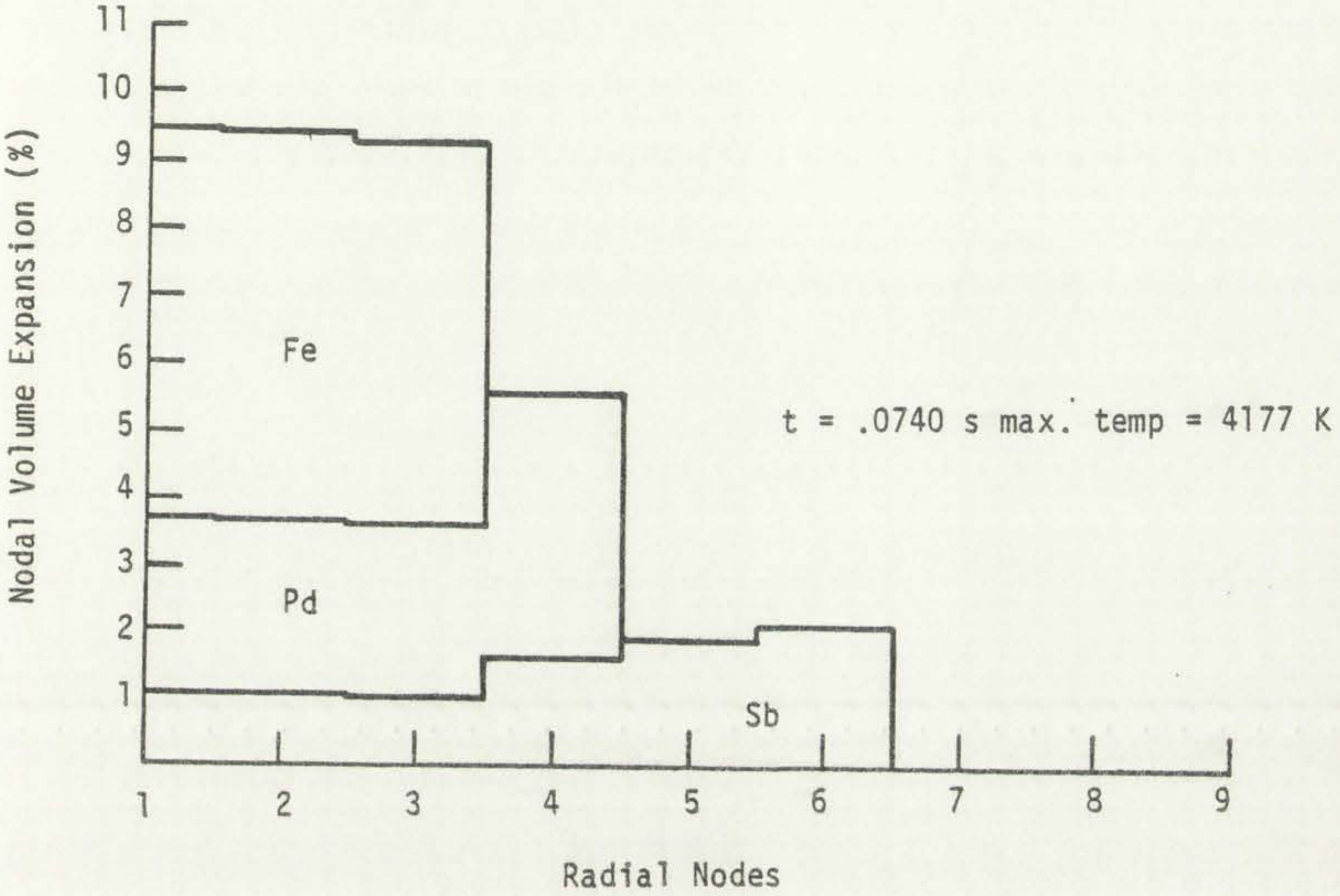

Figure 5.14.
Nodal volume expansion for \$15/s ramp insertion at axial node II (hottest) using radial inclusion distribution in number density for Johnson's inclusions.

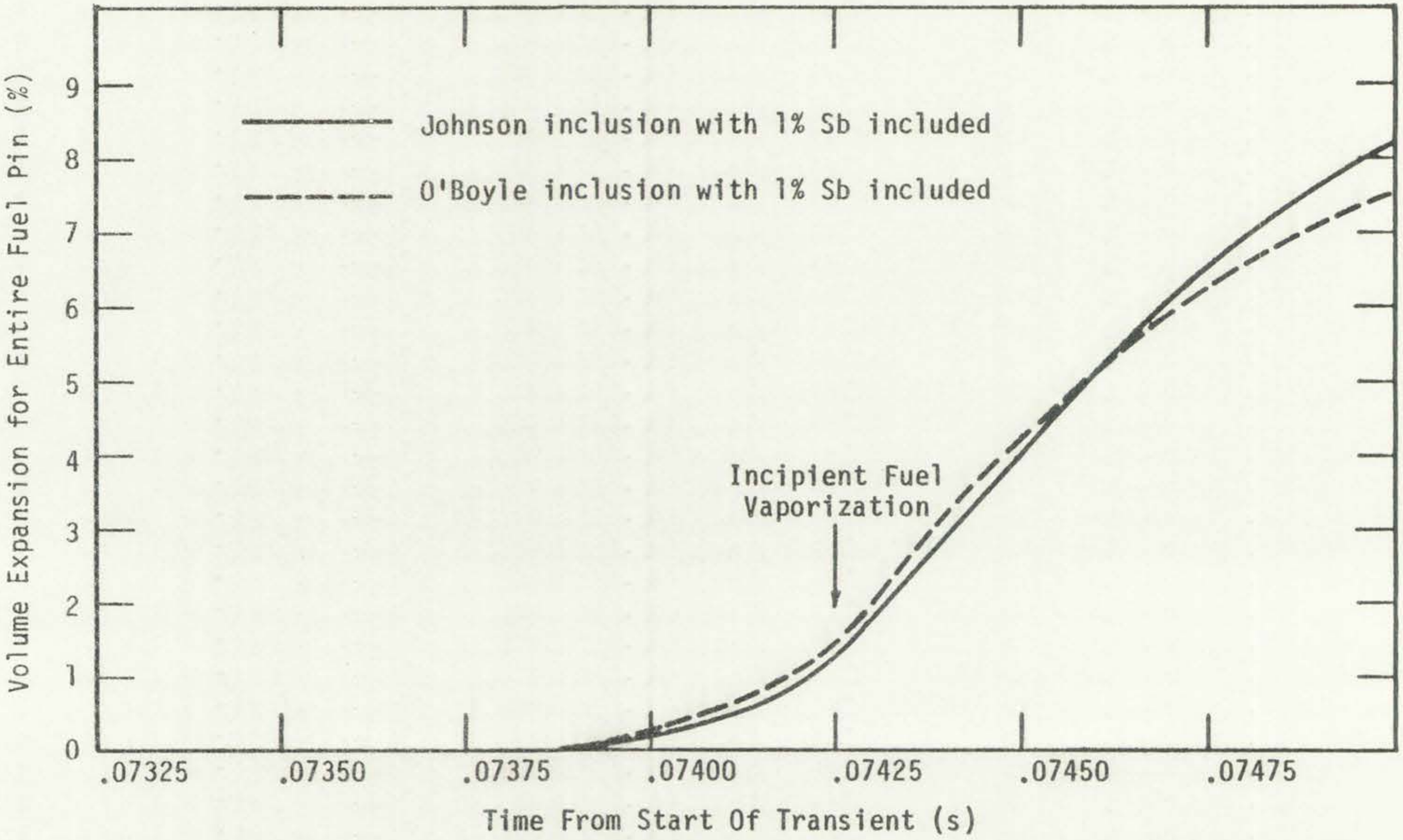

Figure 5.15
Total fuel volume expansion for \$15/s ramp insertion
using radial inclusion distribution in number density.

a. Atom size difference exceeds 15%.

b. Large electronegativity difference (ionic compound likely) exists.

c. Large valence difference exists.

d. Different in crystal structures.

In Table 5.1 is a comparison of the appropriate variables. It can be seen that rules a. thru c. are not violated. There is, however, different crystalline structure for the various constituents. From this, one cannot infer immiscibility or solubility, but can only say that three Hume-Rothery rules for solubility are satisfied.

Metallic phase diagrams also support the homogeneous inclusion assumption. A ternary phase diagram[8] of Mo, Ru, and Rh shown in Fig. 5.16 indicates that the Johnson and O'Boyle inclusion compositions are in the single phase, region, at least at the 1798 K isotherm. By comparing Fig. 5.16 to a ternary phase diagram at 1413 K, it appears that the phase increases with temperature. This should only be taken as an "in general" assumption since phase diagrams are empirical and cannot be predicted or constructed on a theoretical basis.

In addition, Johnson's and O'Boyle's inclusions contain 17 and 20 wt% (w/o) Tc, and 2 and 5 w/o Pd respectively. Johnson's inclusions also contain 2.5 w/o Fe. It is not known how this affects the Mo, Ru, Rh ternary diagram, since pentary phase diagrams do not exist. However, from binary phase diagrams,[9-11] Tc, Pd, and Fe are soluble at least to some degree in Mo, Ru, and Rh. Tc has a restricted solubility of $\simeq$ 5 atom % (A/o) in Rh but is soluble up to 50 a/o in Mo and

TABLE 5.1

COMPARISON OF PARAMETERS FOR HUME-ROTHERY RULE

Element	Metallic[13] Radius (Å)	Electronegativity[14]	Valency[13]	Crystal Structure[14-16]
Mo	1.296	1.8	6	Body centered cubic
Ru	1.246	2.2	6	Hexagonal
Rh	1.252	2.2	6	Face centered cubic
Pd	1.283	2.2	6	Face centered cubic
Tc	1.271	1.9	6	Hexagonal

according to Shunk[9] and Darby[12], totally in Ru. Pd has restricted solubility, ≃ 5 A/o, in Mo but is totally soluble above 1118 K in Rh, and is soluble to some extent in Ru. It is also soluble in Tc. Fe has restricted solubility in Mo, ≃ 22 A/o at 1813 K, but is totally soluble in Rh and Ru. Thus via phase diagrams there is no basis to assume that Tc, Pd, and Fe are not in solid solution with Mo, Ru, and Rh. Unfortunately one cannot conclude categorically that they are in solid solution; however, this assumption of some degree of solubility seems reasonable and is thus considered here by assessing the upper limit of complete solubility.

The vapor pressure of the homogeneous inclusions was determined from the sum of the constituent partial pressures. The constituent partial pressures were calculated using Raoult's Law[17] as stated in Eq. (5.2)

$$P_i = Y_i P_{oi} \qquad (5.2)$$

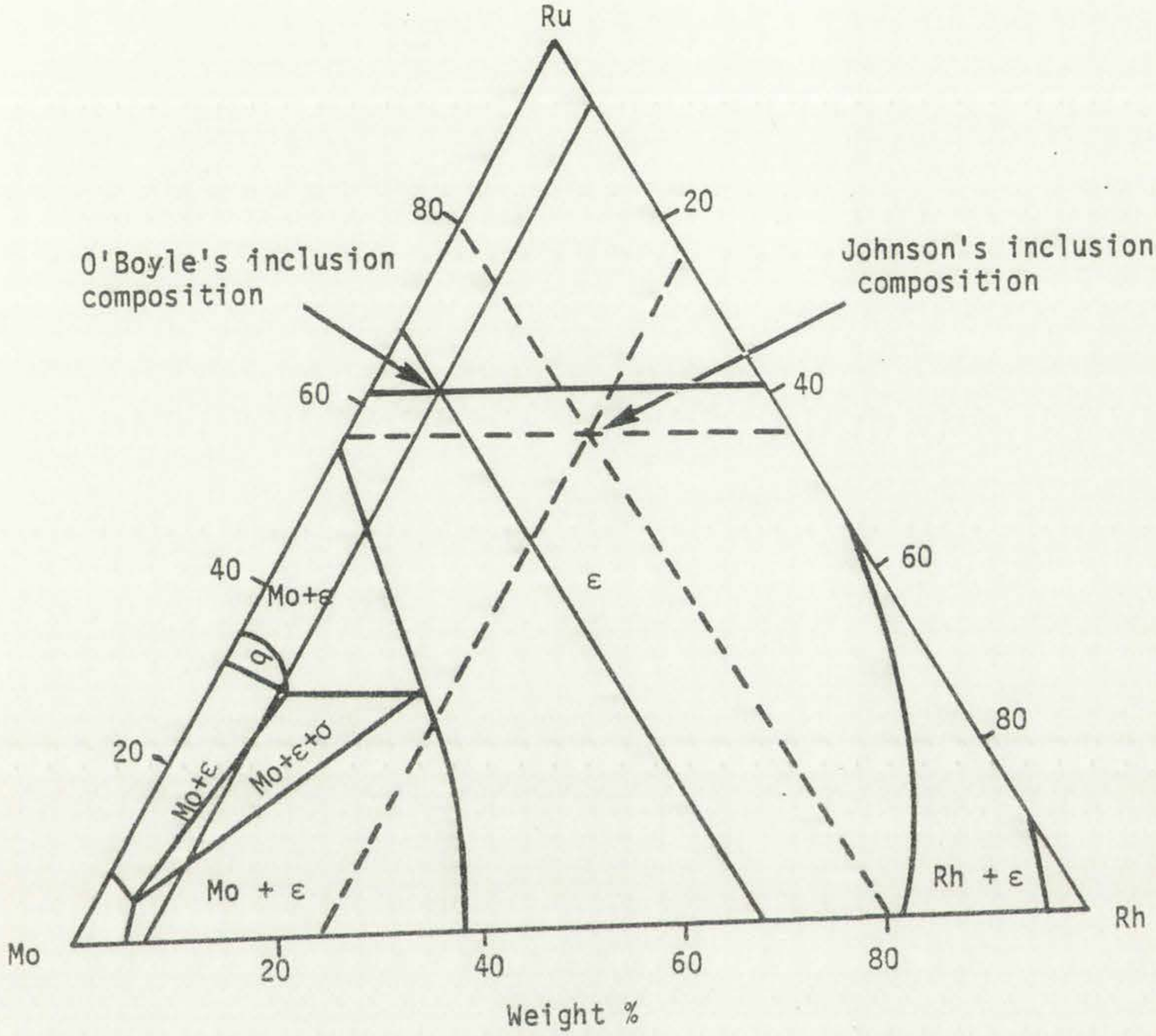

Figure 5.16
1798 K Isotherm of Mo-Ru-Rh ternary phase diagram.

where:

P_i = partial pressure of constituent, i

Y_i = mole fraction of constituent i = $\dfrac{n_i}{\sum_{i=1}^{x} n_i}$,

n_i = moles of constituent, i

P_{oi} = vapor pressure of pure constituent, i.

thus

$$P(\text{total inclusion}) = \sum_{i=1}^{x} \frac{n_i}{\sum_{i=1}^{x} n_i} P_{oi} \tag{5.3}$$

Raoult's Law is based on an ideal system of liquids, i.e., the presence of molecules of other species has no effect on the intramolecular forces of another species. The species must be completely miscible, and there is no volume or heat change upon mixing. However, if the attraction between molecules of species "B" is much stronger than that between molecules of species "A," and if the intermolecular forces are either repulsive or nonexistent, the effect is to force the molecules of "A" out of the liquid into the vapor. In other words, the vaporization of species "A" is increased by the presence of "B." This results in a positive deviation from Raoult's Law. However, if the intermolecular force between species "A" and "B" are attractive or if

compounds between "A" and "B" are formed in the liquid, negative deviation, i.e. suppression of the total vapor pressure line in Raoult's Law will occur.[18-20]

The internal pressure for the various inclusion elements was calculated to assess the magnitude of the intramolecular forces. This information can then be used to approximate solubility for metal in the liquid state, as seen in Fig. 5.17 from Hildebrand.[21] The internal pressure is proportional to σ/v where v is the molar volume and σ is the surface tension which was calculated from the heat of vaporization[22] via the equations in Appendix O. Tables 5.2 thru 5.4 contain: (1) the parameters to calculate σ at the melting temperatures; (2) the calculated values of σ; (3)experimental values of σ; and (4) the calculated internal pressure.

The internal pressure cannot predict tendencies toward the formation of compounds or abnormally great attractions between atoms of unlike metals. About all that can be said is that insolubility cannot occur unless there is a sufficient difference in internal pressure, and even then it may not occur if compounds are formed. Table 5.5 shows the magnitude of the calculated internal pressures of interest as compared to elements in Fig. 5.2 from Hildebrand.[21] Looking at Table 5.5, one would expect that only the volatile Fe and possibly Pd would be soluble in Mo, Ru, Rh, and Tc which make up a large weight percent of the inclusion. Hildebrand, however, feels a separation of about 100% difference in internal pressure is required for insolubility. If compounds between [illegible] and [illegible] have formed [illegible]

other, the concentration of the [illegible]

can still occur.[19-22]

The internal pressure for the various [illegible]

calculated to assess the magnitude of the [illegible]

information can then be used to approximate [illegible]

liquid state, as seen in Fig. 6.12 from [illegible]. The internal

pressure is proportional to [illegible]

the surface tension which was calculated from the [illegible]

[illegible] via the equations in Appendix D. [illegible] 6.4

below: (1) the parameters to calculate [illegible]

(2) the calculated values of [illegible]

the calculated internal pressure.

The internal pressure cannot predict [illegible] the

formation of compounds or abnormally great solubility [illegible]

metals. About all that can be said [illegible]

occur unless there is a sufficient difference [illegible]

[illegible] does not occur if compounds are formed. [illegible]

the magnitude of the calculated internal pressures of [illegible]

based on elements in Fig. 6.8 from solubilities [illegible]

6.5, one would expect that only the elements [illegible]

be soluble in Re, Ru, Rh, and Tc which have [illegible]

of the lanthanides. [illegible], however, [illegible]

100% difference in internal pressure is expected for [illegible]

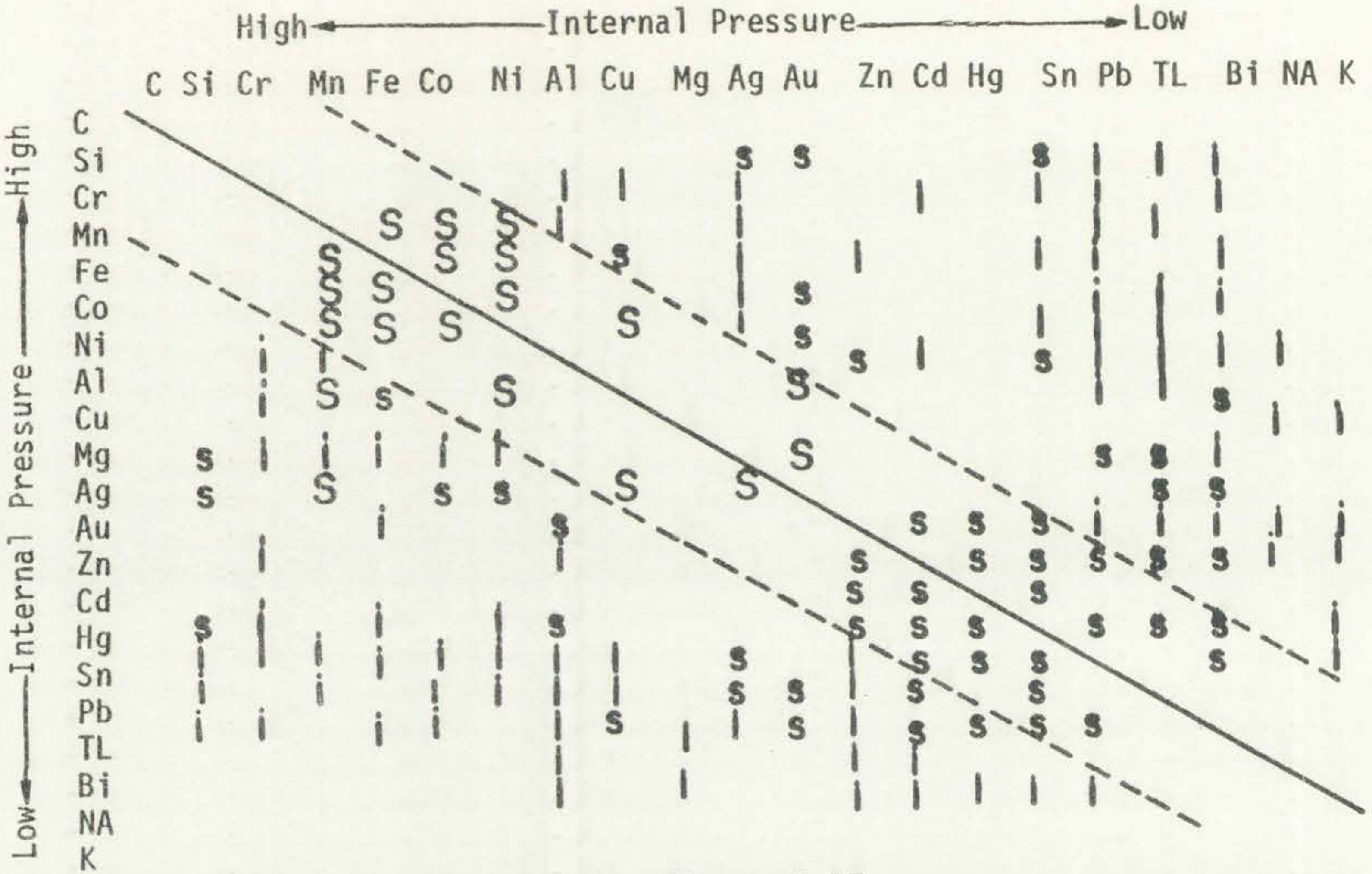

Figure 5.17
Internal pressure series for liquid metals

i: 2 Liquid Phases (immiscible)
S: Complete solubility in the solid state
s: Limited solubility in the solid state

TABLE 5.2

PHYSICAL PARAMETERS TO CALCULATE SURFACE TENSION, σ

				Heat of Vaporization, ΔH_{vap} (ergs/g-mole)					
Element	Molecular Weight	Density, ρ, at Melting Temp.[23] (g/cm^3)	Crystal Structure[24,25]	Handbook of Chemistry & Physics[23]	Nesmeyanov[26]	Stull[27]	Hultgren[28]	Hampel[29]	Others
Ba	137.34	3.32	BCC	1.49×10^{12}	1.74×10^{12}	1.51×10^{12}	1.54×10^{12}	1.51×10^{12}	
Ce	140.12	≈6.6	BCC	3.06×10^{12}	3.10×10^{12}	3.14×10^{12}	3.89×10^{12}	3.98×10^{12}	
Pd	106.4	10.7	FCC	3.73×10^{12}	3.93×10^{12}	3.93×10^{12}	3.52×10^{12}	3.93×10^{11}	
Fe	55.847	≈7.04	BCC	3.54×10^{12}	4.05×10^{12}	3.51×10^{12}	4.14×10^{12}	3.54×10^{12}	
Te	127.60	5.77	Hexagonal	4.98×10^{11}	1.61×10^{12}	5.07×10^{11}		5.72×10^{11}	
Sb	121.75	6.49	Rhombohedral	1.95×10^{12}	2.04×10^{12}	6.79×10^{11}	5.25×10^{11} (Sb_4 only)	1.95×10^{12}	9.28×10^{11}[30]
Cs	132.905	1.845	BCC	6.83×10^{11}	7.71×10^{11}	6.59×10^{11}	7.82×10^{11}	8.12×10^{11}	
Mo	95.94	9.34	BCC		6.63×10^{12}	5.94×10^{12}	6.63×10^{12}	4.91×10^{12}	
Ru	101.07	≈10.9	Hexagonal		6.68×10^{12}	5.68×10^{12}	6.47×10^{12}	5.67×10^{12}	
Rh	102.905	≈10.7	FCC	5.32×10^{12}	5.54×10^{12}	4.96×10^{12}	5.56×10^{12}	5.78×10^{12}	
Tc	99.0	≈11.5	Hexagonal	≈5.02×10^{12}	6.49×10^{12}	5.78×10^{12}			
Zr	91.22	5.8	BCC	4.19×10^{12}	6.10×10^{12}	5.82×10^{12}	6.09×10^{12}	5.95×10^{12}	
Sr	87.62	2.375	BCC	1.41×10^{12}	1.64×10^{12}	1.39×10^{12}	1.65×10^{12}	1.40×10^{12}	
Nd	144.24	6.8	BCC	≈2.55×10^{12}	3.21×10^{12}	2.84×10^{12}	3.24×10^{12}	2.89×10^{12}	

TABLE 5.3

COMPARISON OF CALCULATED AND EXPERIMENTAL VALUES OF SURFACE TENSION

Element	Range of Heat of Vaporization, ΔH_{vap} (ergs/g-mole)	Corresponding Range of Calculated (Appendix O) Surface Tension (ergs/cm^2)	Experimentally Determined Surface Tension (ergs/cm^2)
Ba	1.49×10^{12}	197.6	276[14] (Tm), 224[30] (Tm)
	1.74×10^{12}	230.7	
Ce	3.0×10^{12}	620.2	
	3.9×10^{12}	806.3	
Pd	3.9×10^{12}	1384.2	1475[31] (Tm), 1500[32] (Tm)
	3.5×10^{12}	1233.0	
Fe	3.5×10^{12}	1394.8	1788[30] (Tm), 1850[33] (Tm), 1710[34]
	4.1×10^{12}	1633.9	1800[32] (Tm)
Te	5.0×10^{11}	112.7	
	1.6×10^{12}	360.5	
Sb	2.0×10^{12}	573.3	357[35] (Tm), 383[30] (Tm), 384[33,36] (Tm)
	6.8×10^{11}	194.4	
Cs	6.6×10^{11}	60.4	69.5[37] (Tm), 67[30] (Tm), 68[36] (Tm)
	7.8×10^{11}	71.4	
Mo	4.9×10^{12}	1643.7	2045[38], 2250[32] (Tm)
	6.6×10^{12}	2213.9	
Ru	5.7×10^{12}	2292.7	2250[32] (Tm)
	6.6×10^{12}	2654.7	
Rh	5.0×10^{12}	1800.7	2000[32] (Tm)
	5.5×10^{12}	1980.8	
Tc	5.8×10^{12}	2451.4	
	6.5×10^{12}	2747.2	
Zr	4.2×10^{12}	1060.5	1430[32] (Tm)
	6.1×10^{12}	1540.3	
Sr	1.4×10^{12}	200.2	
	1.64×10^{12}	234.6	
Nd	2.84×10^{12}	587.5	
	3.2×10^{12}	661.9	

TABLE 5.4

CALCULATED INTERNAL PRESSURES

Element	Melting Temperature[23] Tm(°K)	Surface Tension at Tm[23] (ergs/cm^2)	Calculated Surface Tension at Tm (ergs/cm^2)	Molar Volume at Tm (cm^3/g-mole)	Internal Energy ($\sigma/V^{1/3}$)
Si	1683	≈725		11.15	324.52
Cr	2130	1700		8.05	847.12
Mn	1517	1030		8.54	503.91
Co	1768	≈1800		7.65	913.52
Ni	1726	1725		7.48	882.04
Al	933	860		11.24	383.92
Cu	1356	≈1300		8.00	650.00
Mg	922	583		15.29	234.89
Ag	1235	920		11.56	405.83
Au	1337	1130		11.40	502.08
Zn	693	760		9.95	353.35
Cd	594	590		14.01	244.74
Hg	234	≈490		14.75	199.80
Sn	505	≈550		16.98	213.99
Pb	601	470		19.37	175.01
Tl	576	465		18.10	177.10
Bi	544	380		20.86	138.04
Na	371	200		24.73	68.65
K	337	110		47.68	30.34
Ba	998	276	≈215	41.37	79.80
Ce	1072	---	≈700	21.07	253.44
Pd	1825	1500	≈1310	9.94	697.64
Fe	1800	≈1770	≈1510	7.94	887.22
Te	723	180	≈236	22.0	64.24
Sb	904	380	≈383	18.79	142.94
Cs	301	70	≈65	71.84	16.84
Mo	2890	2250	≈1928	10.27	1035.12
Ru	2583	2250	≈2473	9.27	1071.08
Rh	2239	2000	≈1900	9.53	943.34
Tc	2446	----	≈2600	8.61	1268.54
Zr	2125	1400	≈1300	15.73	558.75
Sr	1042	300	≈220	36.97	90.05
Nd	1294	688	≈625	20.58	251.06

TABLE 5.5

COMPARISON OF INTERNAL EXERGIES

Elements in Descending Internal Pressure from Fig. 5.16[21]	Internal Energy Calculated in Hildebrand[21]	Internal Energy Calculated in Table 5.3	Placement and Internal Energy of Elements of Interest
			Tc(1268),Ru(1071), Mo(1035),Rh(943)
Si		324	
Cr		848	
Mn		503	
Fe	490	887	
Co		913	
Ni		882	
Al		384	
			Pd(700)
Cu	294	650	
Mg		235	
			Zr(558)
Ag	348	405	
Au	282	502	
Zn	350	353	
			Ce(253),Nd(251)
Cd	256	245	
Hg	157	200	
Sn	198	214	
Pb	163	175	
Tl		177	
			Sb(142)
Bi		138	
			Sr(90),Ba(80), Te(64)
Na		68	
K	114	30	Cs(17)

this is the criteria Fe, Pd, and Zr should all be soluble in Mo, Ru, Rh, and Tc.

Using Raoult's Law means that the low vapor pressure elements (Mo, Ru, Rh, Tc) that make up a large portion of the inclusions, are weighted accordingly, depressing the total inclusion vapor pressure.

To determine if the homogeneous inclusions can contribute to fuel swelling and frothing, one must know what the relationship is between the inclusion vapor pressure and that of the fuel. Table 5.6 and Fig. 5.18 contain the vapor pressures of an average Johnson, O'Boyle, and Jeffery homogeneous inclusion based on Raoult's Law. Both Johnson's and O'Boyle's inclusion are assumed to contain 1 w/o Sb, thus maximizing their vapor pressure. Tables 5.7 thru 5.10 contain fuel vapor pressure data from Gabelnick,[39] Bogensberger,[40] and Leibowitz[41] which are plotted on Figs. 5.18 and 5.19. Leibowitz's UO_2 data is based on the work of Gillian[42] and his mixed oxide work on that of Breitung.[43] Above 5000 K Bogensberger's extrapolated curve is used, which deviates greatly from his measured values. It was felt that this deviation may have been caused by a high dynamic pressure preventing free evaporation from the laser heated section.

From Figs. 5.18 and 5.19, it can be seen that the vapor pressures from the homogeneous metallic inclusions for both Johnson and O'Boyle type are less than the oxide and mixed oxide vapor pressure curves. If one of these fuel vapor pressure curves is close to reality in the temperature range of interest, 3000-6000 K, and if Raoult's Law is

TABLE 5.6

VAPOR PRESSURE DUE TO INCLUSIONS ASSUMING 100% SOLUBILITY OF THE FISSION PRODUCTS

Temperature (K)	Vapor Pressure (atm)		
	Johnson	O'Boyle	Jeffery
10,029.0	2,898.8	5,251.2	
8,490.6	781.4	1,079.6	
6,950.6	180.9	225.1	
5,413.0	26.1	35.1	1,436.8
4,221.6	2.93	4.4	584.5
3,607.8	.73	1.2	320.2
3,015.2	.12	.21	118.4
2,736.3			67.3
2,074.6			9.7
1,690.9			1.6
1,316.3			.107

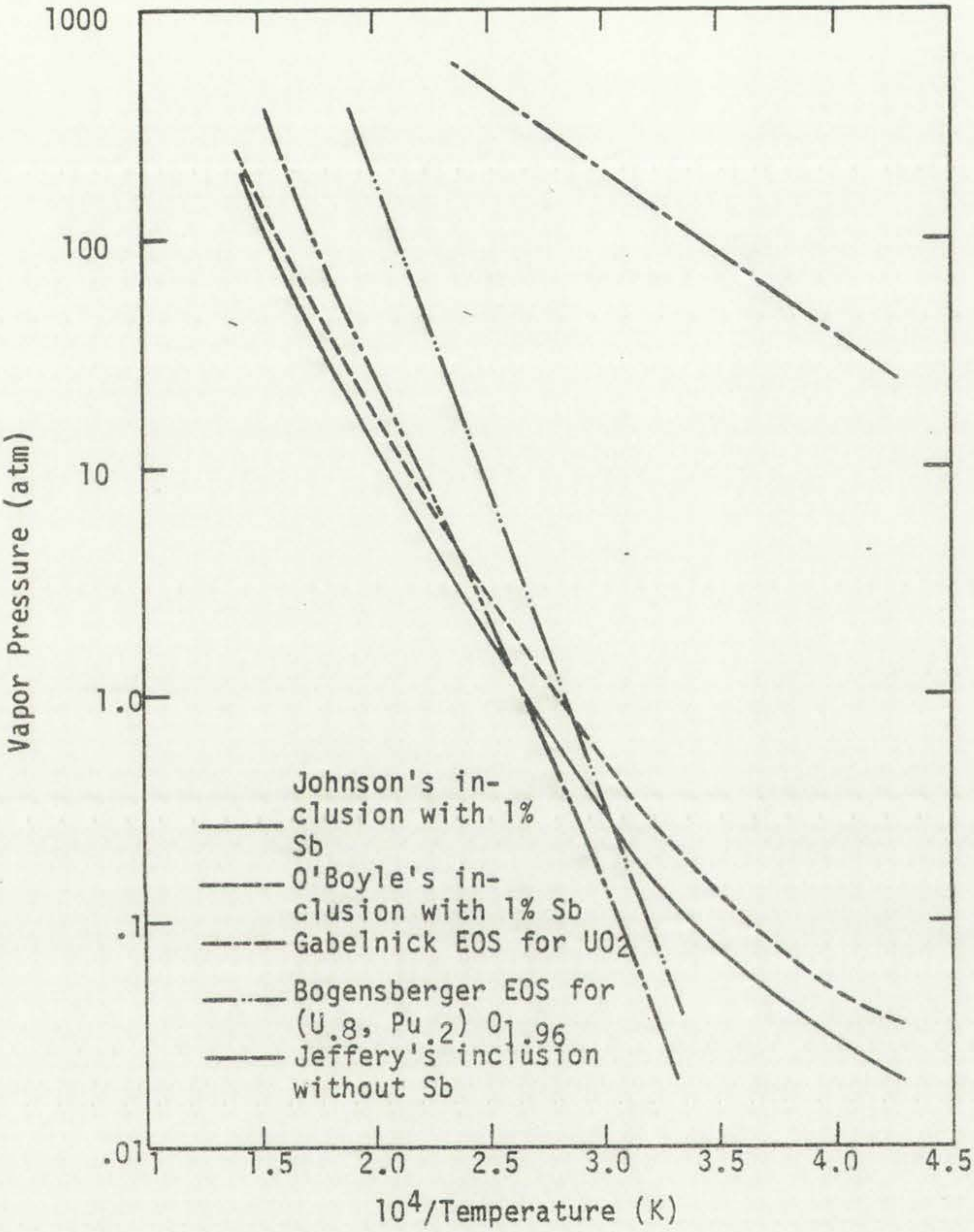

Figure 5.18
Comparison of inclusion and fuel vapor pressures.

TABLE 5.7

GABELNICK[39] VAPOR PRESSURE OF UO_2

Temperature (°K)	$\frac{10^4}{T}$	Vapor Pressure (atm)	
		$6 g/cm^3$ Smear Density	$7 g/cm^3$ Smear Density
3000	3.333	.0191	.0191
3500	2.857	.321	
4000	2.500	2.24	2.24
4500	2.222	9.45	
5000	2.000	29.1	29.1
5500	1.818	74.6	
6000	1.667	173.	
6500	1.538	375	

TABLE 5.8

VAPOR PRESSURE OF UO_2 AND $(U, Pu)O_2$ BASED ON EXPERIMENTAL WORK OF BOGENSBERGER[40]

Temperature (K)	$\frac{10^4}{T}$	Vapor Pressure (atm) UO_2	Vapor Pressure (atm) $(U,Pu)O_2$ *
3000	3.333	.025	.0386
3500	2.857	.535	.845
4000	2.500	5.31	8.546
4600	2.174	43.13	70.67
5000	2.000	131.82†	218.1†
6000	1.667	1122.†	1890.†
7000	1.429	5179.†	8840.†

* For 20 atom % Pu and oxygen-to-metal ratio (O/M) of 1.96

† Calculated from following empirical formula based on lower temperature experimental points:

For UO_2 above melting temperature

$$P_{(atm)} = 10^{(7.7-27900/T)}$$

For $(U,Pu)O_2$ above melting temperature

$$P_{(atm)} = 10^{(7.966-28137/T)}$$

TABLE 5.9

LEIBOWITZ[41] VAPOR PRESSURE FOR UO_2

Temperature (K)	Vapor Pressure (atm)
2000	9.29×10^{-8}
2500	1.25×10^{-4}
3000	1.52×10^{-2}
3500	.344
4000	2.45
4500	10.7
5000	33.1
5500	77.6
6000	151

TABLE 5.10

LEIBOWITZ[41] VAPOR PRESSURE FOR $(U_{.8}Pu_{.2})O_{1.96}$

Temperature (K)	Vapor Pressure (atm)
2000	1.2×10^{-7}
2500	2.1×10^{-4}
3000	3.6×10^{-2}
3500	.91
4000	9.1
4500	49
5000	170
5500	500*
6000	1000*

*Extrapolated from low temperature data

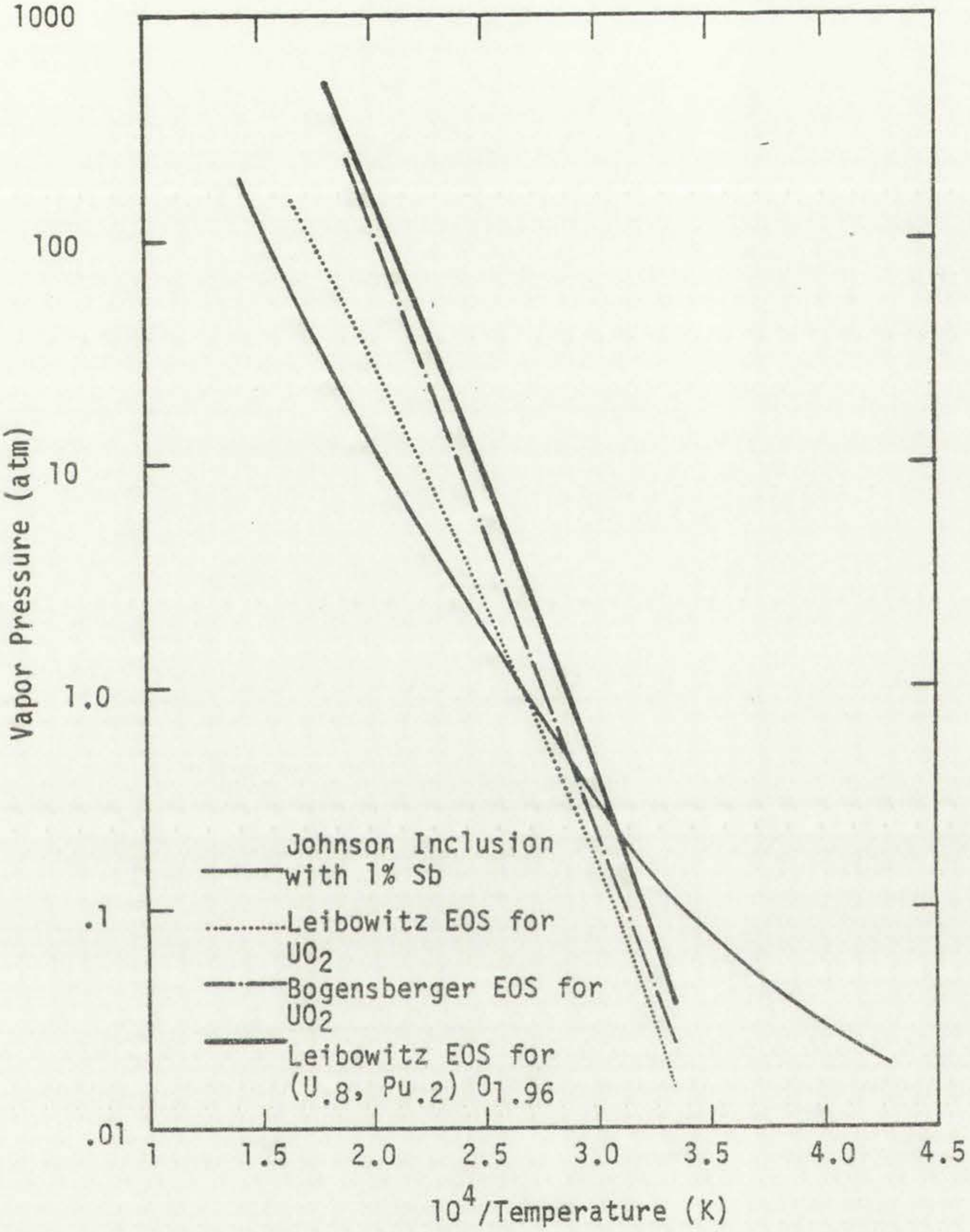

Figure 5.19
Comparison of additional fuel EOS with inclusion vapor pressure.

applicable, the homogeneous metallic inclusions are of no consequence as far as a fuel driving force is concerned. They are still important if one considers their application as decay heat and neutron precursors.

The above two assumptions, total miscibility and total immiscibility, represent limiting conditions on the state of the metallic inclusions. If partial solubility occurs, and occurs in the same molar ratio as the inclusion, it will have a linear effect on the expected nodal expansion.

Table 5.11 contains the fuel vapor pressure, homogeneous inclusion vapor pressure, and the vapor pressure of the segregated volatiles at temperatures from 3000-7000 K. From Fig. 5.20 one additional feature should be noted. Due to the differing slopes of the fuel and individual constituent vapor pressure curves, if the pin internal pressure reaches on the order of hundredsd of atmospheres or higher, the fuel may reach incipient vaporization at a lower temperature than some or all of the segregated volatiles depending on the specific local pressure. If this were the case, then even segregated inclusions would not be of importance for prepin failure fuel motion. After pin failure, however, as the pin pressure drops they could still provide a fuel expulsion-foaming force.

5.3 LWR Inclusion

Figure 5.18 also contains the inclusion vapor pressure for a homogeneous, average, Jeffery[1] inclusion. As seen from Table 2.2, applicable, the fuel vapor pressure at the [illegible] temperatures of the [illegible] [illegible] [illegible] [illegible] [illegible]. [illegible] if the coolant [illegible] application of [illegible] heat and [illegible] . . . The [illegible], [illegible] volatile fission products [illegible] bility, [illegible]. [illegible] conditions at the state of [illegible] the [illegible]. If [illegible], and [illegible] in the [illegible] ratio [illegible], it will have a [illegible] effect on the [illegible] model [illegible].

Table 5.11 contains the fuel vapor pressure, [illegible] inclusion vapor pressure, and the vapor pressure of the [illegible] volatiles at temperatures from 2000-4000 K. From Fig. 5.[illegible] one additional feature should be noted. Due to the differing slopes of the fuel and individual constituent vapor pressure curves, if the pin internal pressure reaches on the order of hundreds of atmospheres or higher, the fuel may reach incipient vaporization at a lower temperature than some or all of the [illegible] volatiles, depending on the specific local pressure. If this were the case, then even segregated inclusions would not be of importance for [illegible] failure [illegible]. After pin failure, however, as the pin pressure drops they could still provide a fuel expulsion-causing force.

5.[illegible] [illegible] Inclusion

Figure 5.13 also contains the inclusion vapor pressure for a homogeneous, average, [illegible] inclusion. As seen from Table 5.11,

TABLE 5.11

COMPARISON OF THE VAPOR PRESSURES OF SOLUBLE INCLUSIONS, VOLATILE CONSTITUENTS, AND FUEL

Temperature (°K)	Soluble Vapor Pressure (atm) (Raoult's Law)		Individual Constituent Vapor Pressure (atm)			Fuel Vapor Pressure (atm)		
	Johnson	Boyle	Pd	Sb	Fe	Gabelnick (UO_2)	Bogensberger	Leibowitz
3000	.115	.2056	.9455	8.647	.507	.0191	.0251 UO_2	.0152 UO_2
							.0386 $(U,Pu)O_2$	.036 $(U_{.8}Pu_{.2})O_{1.96}$
4000	1.83	2.87	27.133	27.174	19.567	2.24	5.31 UO_2	2.45 UO_2
							8.546 $(U,Pu)O_2$	9.1 $(U_{.8}Pu_{.2})O_{1.96}$
5000	13.0	17.6	203.3	54.0	175.1	29.1	131.8 UO_2	33.1 UO_2
							218.1 $(U,Pu)O_2$	170. $(U_{.8}Pu_{.2})O_{1.96}$
6000	57.	77.	778.6	85.4	754.9	173.	1122 UO_2	151 UO_2
							1890 $(U,Pu)O_2$	1000 $(U_{.8},Pu_{.2})O_{1.96}$
7000	190	240	2031.7	118.4	2143.5	740 .	5179 UO_2	325 UO_2
							8840 $(U,Pu)O_2$	2200 $(U_{.8},Pu_{.2})O_{1.96}$

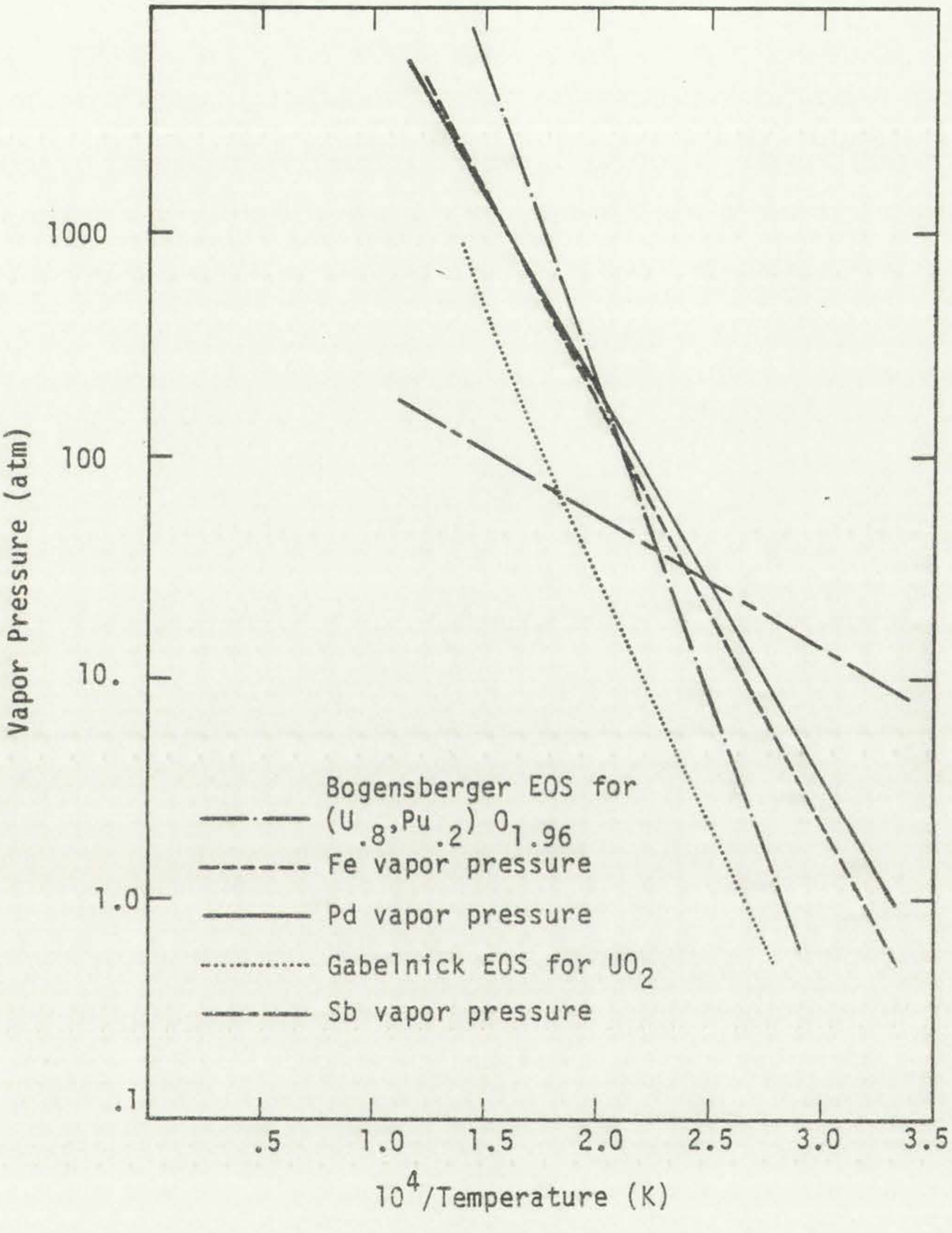

Figure 5.20
Comparison of fuel EOS and vapor pressures of individual constituents.

the UO_2 fuel was irradiated in a thermal spectrum and the inclusion composition differed substantially from the mixed oxide, fast spectrum inclusions of Johnson[4] and O'Boyle.[3] From Figs. 5.18 and 5.19, it appears that thermal reactor fuel analysis may have to consider possible contribution to accident scenerios from the metallic inclusions. The homogeneous inclusion vapor pressure is much higher than the EOS for UO_2, leading to a large, i.e. 40% $\Delta V/V$, for the entire fuel pin at 20 atm. and peak temperature of 2800 K. Using a $15/s ramp insertion of reactivity, the total fuel volume expansion increases to 360% at incipient fuel vaporization. From Figs. 5.21 and 5.22, it can be seen that if one assumes Jeffery's inclusions to be in the segregated form vs homogeneous form, a nodal volume expansion on the order of 100% and a total fuel pin volume expansion of 37% can be expected at incipient fuel vaporization. This is assuming a flat distribution in the inclusion number density and using the Ideal Gas EOS. Tellurium, strontium, and barium are constituents not found in the fast reactor fuel metallic inclusions. These three elements are more volatile than the palladium, iron, and antimony and contributes a minimum of 75% of the nodal volume expansion. The high volatility also causes expansion to occur much earlier in the transient. It thus appears that thermal reactor fuel may swell due to volatilization during a transient if either segregated or homogeneous inclusions are assumed.

Two questions, however, must be addressed before a definitive statement to that effect can be made. First, the electron microprobe

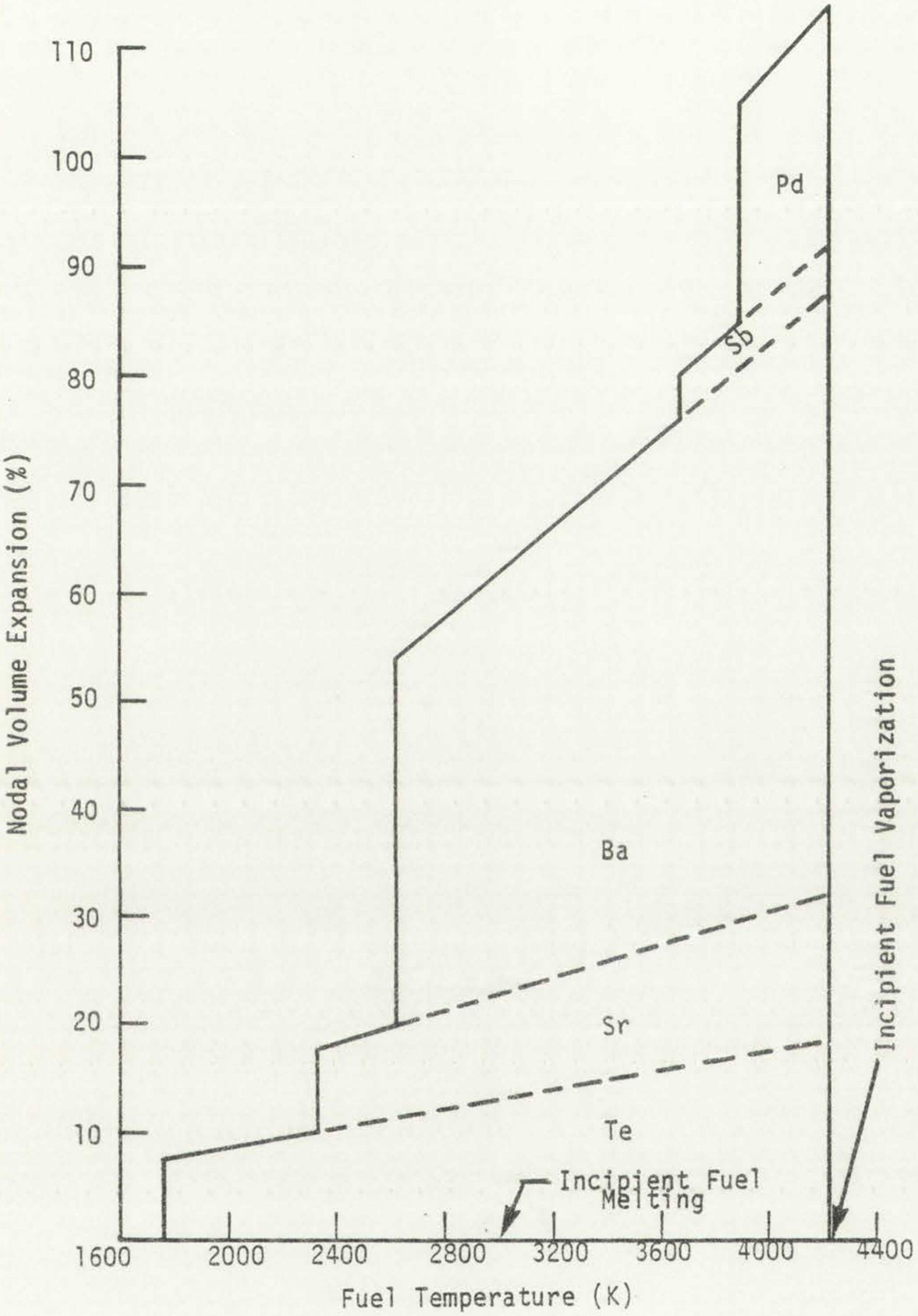

Figure 5.21
Nodal volume expansion for Jeffery inclusions using
a flat inclusion number density profile and Ideal Gas EOS.

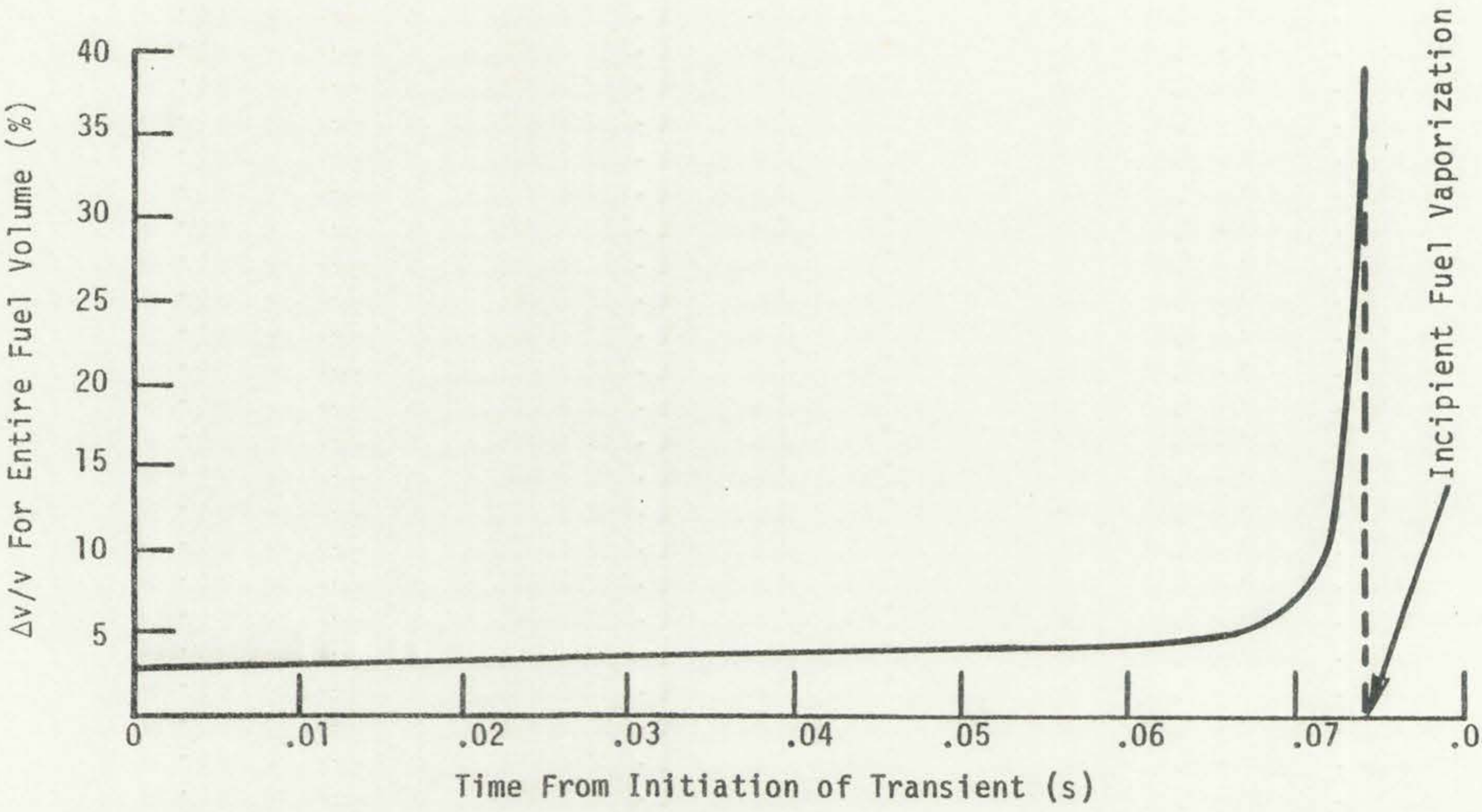

Figure 5.22
Total fuel volume expansion for Jeffery inclusion using \$15/s ramp insertion, flat inclusion number density profile, and Ideal Gas EOS.

used by Jeffery only looks for the existence of elements. It does not determine whether the constituents are in elemental form or whether compounds exist; thus, the Ba and Sr found in the inclusions may be in oxide or zirconate form. Secondly, the fuel analyzed was irradiated at somewhat lower temperature, than that for typical LWR condition, i.e., the test fuel centerline temperature being $\simeq$ 1800 K, while typical present day commercial boiling and pressurized reactors operate characteristically within the range of 1900 K to 2100 K centerline temperature, depending on linear power level. However, since LWR fuel rods are normally partially prepressurized during fabrication to about 30 atm (at 300 K) to compensate for high system hydraulic pressure (e.g. $\simeq$ 70 atm for BWR; $\simeq$ 160 atm for PWR, vs. 2-5 atm for LMFBR designs). Thus, the highly volatile constituents found in Jeffery's inclusion (i.e. Ba with a vaporization temperature of 1913 K at 1 atm Sr at 1657 K, BaO at 3000 K, and SrO at 2703 K) would be expected to be found in typical LWR inclusions. To determine if metallic fission products are of importance in pre- or postcladding failure fuel motion, one must compare it to the fuel motion driving potential of fission gas. The following section discusses expected fission gas contributions.

REFERENCES

1. B. M. Jeffery, "Microanalysis of Inclusions in Irradiated UO_2," Journal of Nuclear Materials 22 33-40 (1967).

2. B. T. Bradbury, J. T. Demant, and P. M. Martin, "Solid Fission Products in Irradiated Uranium Dioxide," AERE-R5149 (1966).

3. D. R. O'Boyle, F. L. Brown, and J. E. Sanecki," Solid Fission Product Behavior in Uraniun-Plutonium Oxide Fuel Irradiated in a Fast Neutron Flux," Journal of Nuclear Materials 29 27-42 (1969).

4. P. E. Blackburn, C. E. Johnson, et al. "Chemical Engineering Division Fuels and Materials Chemistry Semiannual Report, July-December 1971," Argonne National Laboratory report ANL-7877 (April 1972).

5. J. E. Bramman, R. M. Sharpe, D. Thom, and G. Yates, "Metallic Fission-Product Inclusions in Irradiated Oxide Fuels," Journal of Nuclear Materials, 25 201-215 (1968).

6. G. R. Baird, S. A. Chastain, and R. G. Henderson, "Fabrication, Irradiation, and Postirradiation Examination of Mixed Oxide Fuel Pins PNL 5-5, -22, -31, and -35," Hanford Engineering Development Laboratory report HEDL-TME 76-16.

7. A. Prince, Alloy Phase Equilibria, (Elsevier Publishing Company, 1966).

8. A. E. Dwight and D. R. O'Boyle, "Reactor Development Program Progress Report February 1970," Argonne National Laboratory report ANL-7669, pp. 105-107 (March 1970).

9. F. A. Shunk, Constitution of Binary Alloys, Second Supplement, (McGraw-Hill Book Company, 1969).

10. R. P. Elliot, Constitution of Binary Alloys, First Supplement, (McGraw-Hill Book Company, 1965).

11. M. Hansen, Constitution of Binary Alloys, (McGraw-Hill Book Company, 1958).

12. J. B. Darby, Jr., D. J. Lam, L. J. Norton, and J. W. Downey, "Intermediate Phase in Binary Systems of Technetium - 99 with Several Transition Elements," Journal of the Less-Common Metals 4, pp. 558-563 (1962).

13. L. Pauling, The Nature of the Chemical Bond, (Cornell U. P. Ithica, New York, 1960) third edition.

14. Sargent-Welch, Table of Periodic Properties of the Elements (1968).

15. W. B. Pearson, A Handbook of Lattice Spacing and Structures of Metals and Alloys, Vol. 2, (Pergamon Press, 1965).

16. W. Hume-Rothery, Electrons, Atoms, Metals, and Alloys, (Dover Publications, Inc., 1963).

17. M. J. Sienko, R. A. Plane, Chemistry, 2nd Edition, (McGraw-Hill Book Company, 1961).

18. R. H. Parker, An Introduction to Chemical Metallurgy (Pergamon Press, 1967).

19. G. M. Barrow, Physical Chemistry Third Edition (McGraw-Hill Book Company, 1973).

20. O. Kubaschewski and E. L. Evans, Metallurgical Thermochemistry (Pergamon Press, 1958).

21. J. H. Hildebrand, Solubility, (The Chemical Catalog Company, Inc., 1924).

22. S. H. Overbury, P. A. Bertrand, G. A. Somorjai, "The Surface Composition of Binary Systems. Prediction of Surface Phase Diagrams of Solid Solutions," Chemical Reviews, Vol. 75, No. 5, (October 1975).

23. R. C. Weast, CRC Handbook of Chemistry and Physics, 53rd Edition, (The Chemical Rubber Co., 1972).

24. D. T. Hawkins, Metals Handbook Vol. 8 Metallography, Structures, and Phase Diagrams, American Society for Metals (1973) pp. 242.

25. W. Hume-Rothery, Elements of Structural Metallurgy, The Institute of Metals (1961).

26. A. N. Nesmeyanov, Vapor Pressure of the Chemical Elements, (Elsevier Publishing Co., 1963).

27. J. P. Stone, C. T. Ewing, J. R. Spann, E. W. Steinkuller, D. D. Williams, R. R. Miller, "High Temperature Vapor Pressures of Sodium, Potassium, and Cesium," Journal of Chemical and Engineering Data, 11, No. 3 (July 1966).

28. R. Hultgren, R. Orr, P. D. Anderson, K. K. Kelley, Selected Values of Thermodynamic Properties of Metals and Alloys, (John Wiley and Sons, Inc., 1963).

29. C. A. Hampel, Rare Metals Handbook Second Edition (Reinhold Publishing Corporation, 1961).

30. A. A. V. Grosse, "The Relationship Between Surface Tension and Energy of Liquid Metals and Their Heat of Vaporization at the Melting Point," Journal of Inorganic and Nuclear Chemistry, Vol. 26 1349-1361 (1964).

31. V. F. Ukhov, N. A. Vatolin, and V. P. Chentsov, "Temperature Dependence of the Surface Tension of Palladium - and Silver-Based Melts," Tr. Inst. Met., Akad. Nauk SSSR, Ural. Nauch. Tsentr No. 25 (Pt. 3), (1971) pp. 30-36.

32. B. C. Allen, "The Surface Tension of Liquid Transition Metals at Their Melting Points," Trans. of the Metallurgical Society of AIME, Vol. 227, (October 1963) pp. 1175-1183.

33. Y. Waseda and K. Suzuki, "Interionic Potentials in Liquid Metals Including Liquid Noble and Transition Metals," Phys. Stat. Sol. (6) 57 (1973) pp. 351-367.

34. K. Ogino, A. Adachi, K. Nogi, "Wettability of Solid Oxides by Liquid Iron," Tetsu to Hagana, 59(9) (1973) pp. 12337-1244.

35. V. K. Semenchenko, Surface Phenomena in Metals and Alloys," (Pergamon Press, 1961).

36. Y. Waseda, M. Ohtani, "Effective Interionic Potentials and Properties of Molten Metals," Journal of the Japan Institute of Metals, 36, No. 10, 1016-1025 (October 1972).

37. J. Bohdansky, H. E. J. Schins, "The Surface Tension of the Alkali Metals," Journal of Inorganic and Nuclear Chemistry, Vol. 29, 2173-2179 (1967).

38. V. S. Chernov, F. I. Busol, B. P. Nam, "Inoculation Mechanism of Molybdenum During Vacuum Melting with Boron," Izv. Akad. Nauk SSSR, Met. Vol. 6, (1974) pp. 116-121.

39. M. G. Chasanov, D. F. Fischer, D. R. Fredrickson, S. D. Gabelnick, R. Kumar, L. Leibowitz, G. T. Reedy, F. A. Cafasso, and L. Burris, "Chemical Engineering Division Reactor Safety and Physical Property Studies Annual Report, July 1973 - June 1974" Argonne National Laboratory report ANL-8120 (1974).

40. H. G. Bogensberger, E. A. Fischer, P. G. Berrie, P. R. Kinsman, R. W. Ohse, "Vapor Pressure Measurements to 7000 K and Equation of State of Oxide Fuels for Fast Reactor Safety Analysis," KFK2272, EUR5501e (May 1976).

41. L. Leibowitz, E. C. Chang, M. G. Chasanov, R. L. Gibby, C. Kim, A. C. Millunzi, D. Stahl, "Properties for LMFBR Safety Analysis," Argonne National Laboratory report ANL-CEN-RSD-76-1 (March 1976).

42. M. J. Gillian, "Thermodynamics of Nuclear Materials 1974," Vol. I, International Atomic Energy Agency, Vienna, p. 269 (1975).

43. W. Breitung, "Calculation of Vapor Pressure of Oxide Fuels up to 5000 K for Equilibrium and Nonequilibrium Evaporaton," KFK2091 (1975).

44. D. R. Sageman and G. Burnet, "Predicting the Surface Tension of Liquid Metals," Journal of Inorganic and Nuclear Chemistry, Vol. 36, 1105-1107 (1974).

6. FISSION GAS

To determine whether the metallic inclusion contribution to fuel motion and expansion is of importance, one can compare to the expected range of volume expansion from fission gas.

Fission gas retention is temperature dependent and thus varies radially across the fuel pin. In Fig. 6.1,[1] the radial distribution for a mixed oxide fuel pin irradiated in EBR-II at a peak power level of ≃ 10 kW/ft to an average burnup of ≃ 3.2 atom % is shown. This distribution was determined by measuring the activity of Kr-85 The fission gas retention varies from 4% in the columnar region to 64% in the unrestructured region yielding a volume average fission gas retention of 42.2%. Due to the low irradiation power, these gas retention numbers should be at the high end of expected values.

Table 6.1 contains the yield data for 3 atom % burnup for Xe, Kr, and I based on Burris.[2] The totals in Table 6.1 are close to the ≃ 1.99×10^{20} atoms/cm^3 fuel, value obtained from Stahl.[1] The gas exists in solution or in small (unresolvable) bubbles within the matrix, in intragranular bubbles (≃ 650 Å[1] in diameter), and at the grain boundaries (intergranular bubbles). Intragranular bubble size seems to decrease with increase in fission rate, i.e. 300 Å diameter for 17 kW/ft. and 1000-1800 Å diameter for ≃ 8.9 kW/ft.

In the hand calculations presented here, to obtain the maximum fuel volume expansion due to fission gas, it was assumed that during a

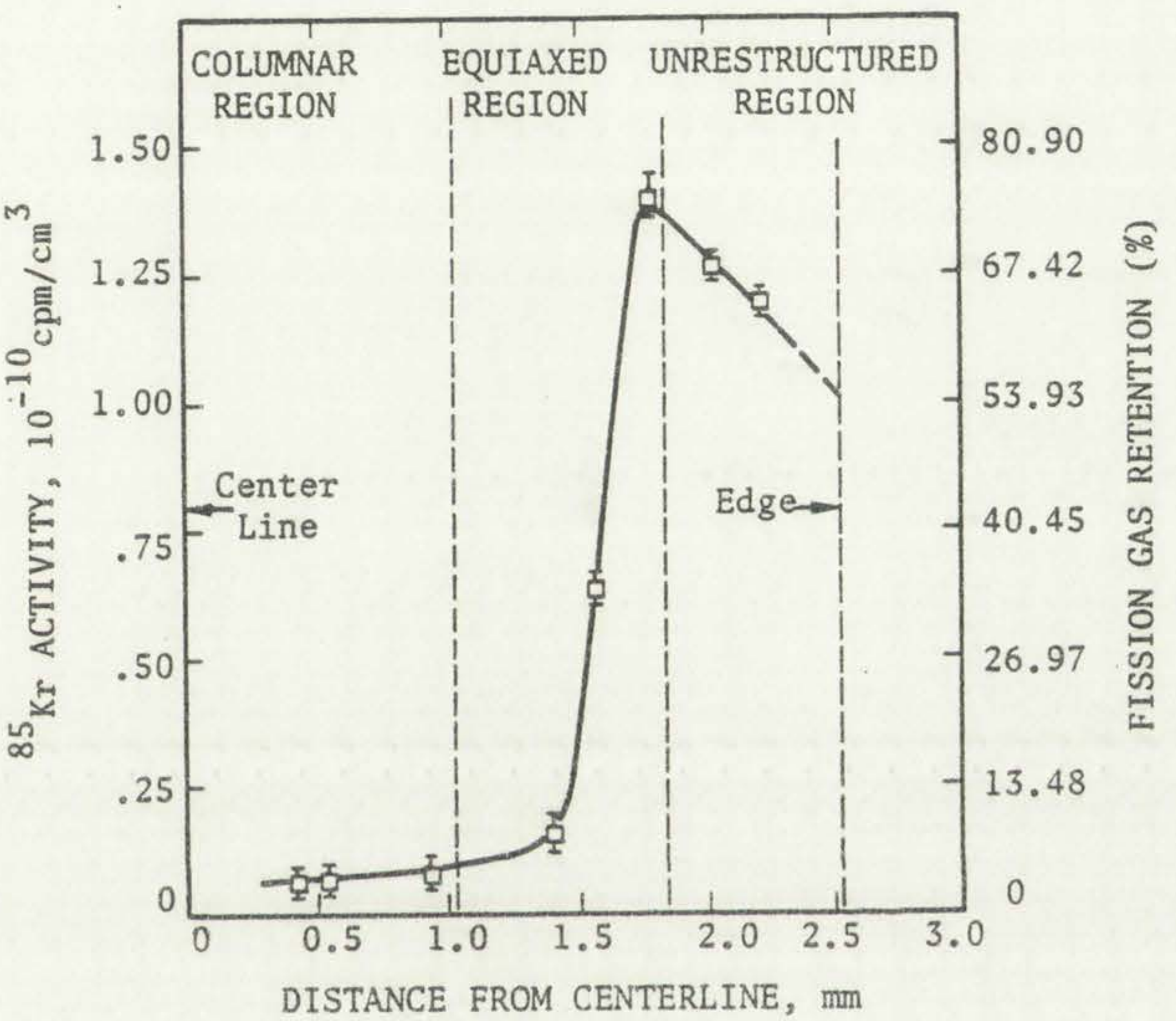

Figure 6.1
Fission gas retention.

TABLE 6.1

FISSION GAS YIELD FOR 3 ATOM % BURNUP
($\simeq 6.624 \times 10^{20}$ FISSION/cm^2 FUEL) BASED ON BURRIS

	Yield (Atoms/cm^3 Fuel)			Total	
Fuel Species	Kr	Xe	I	(Atoms/cm^3 Fuel)	(Moles/cm^3 Fuel)
U^{235}	1.97×10^{19}	1.441×10^{20}	8.737×10^{18}	1.7254×10^{20}	2.865×10^{-4}
Pu^{239}	6.001×10^{18}	1.566×10^{20}	1.796×10^{19}	1.806×10^{20}	2.999×10^{-4}

transient no further fission gas release occurred and all existing gas is precipitated into large bubbles (i.e. ignoring surface tension effects). Using the Ideal Gas EOS (Eq. (6.1)) and a bulk pressure of 20 atm. the volume % occupied by fission gas in the various grain regions was calculated.

$$V = \frac{nRT}{P}, \; V_2 - V_1 = nR \left(\frac{T_2}{P_2} - \frac{T_1}{P_1}\right) \quad . \tag{6.1}$$

These results can be found in Table 6.2 and Fig. 6.2. They indicate that the maximum fission gas contribution to fuel expansion varies from 10% in the columnar region to 260% near the radius of maximum fission gas retention.

As mentioned above, in actuality the fission gas is in solution, in intragranular bubbles, and in intergranular bubbles. During a fast transient ($15/s ramp insertion) intragranular bubble coalescence and diffusion due to temperature gradients has little effect. Even if coalescence occurs, pressure equilibration does not occur in very short time frames. The rate of bubble migration is on the order of 4 μm/s,[1,3] and the diffusion coefficient for a single atom at 1773 K is $\simeq 1.3 \times 10^{-15}$ cm^2/s.[4,5] Also gas in solution precipitates into extremely small intragranular bubbles which do not significantly contribute to fuel expansion due to the large internal bubble pressure from surface tension effects. Stahl[1] in his experimental work determined the quantity of gas in inter- and intragranular bubbles. To

TABLE 6.2

MAXIMUM POSSIBLE VOLUME EXPANSION FOR 3 ATOM % BURNUP

Fuel Region	Average % Gas Retention	Moles gas/cm^3 Fuel (Pu^{239})	Approximate Average Region Steady State Temp (K)	Volume Expansion (%) 20 Atm			
				3023 K	3824 K	4177 K	4222 K
Columnar	3.9	1.17×10^{-5}	1920	5.3	9.1	10.8	11.0
Equiaxed	32.	9.60×10^{-5}	1520	59.2	90.7	104.6	106.4
Unrestructured	64.	1.92×10^{-4}	870	169.6	232.7	260.5	264.0
Maximum Expected Retention	74.97	2.25×10^{-4}	1470	143.4	217.3	249.9	254.0
Volume Average	42.2	1.27×10^{-4}	1270	91.3	133.1	151.5	153.8

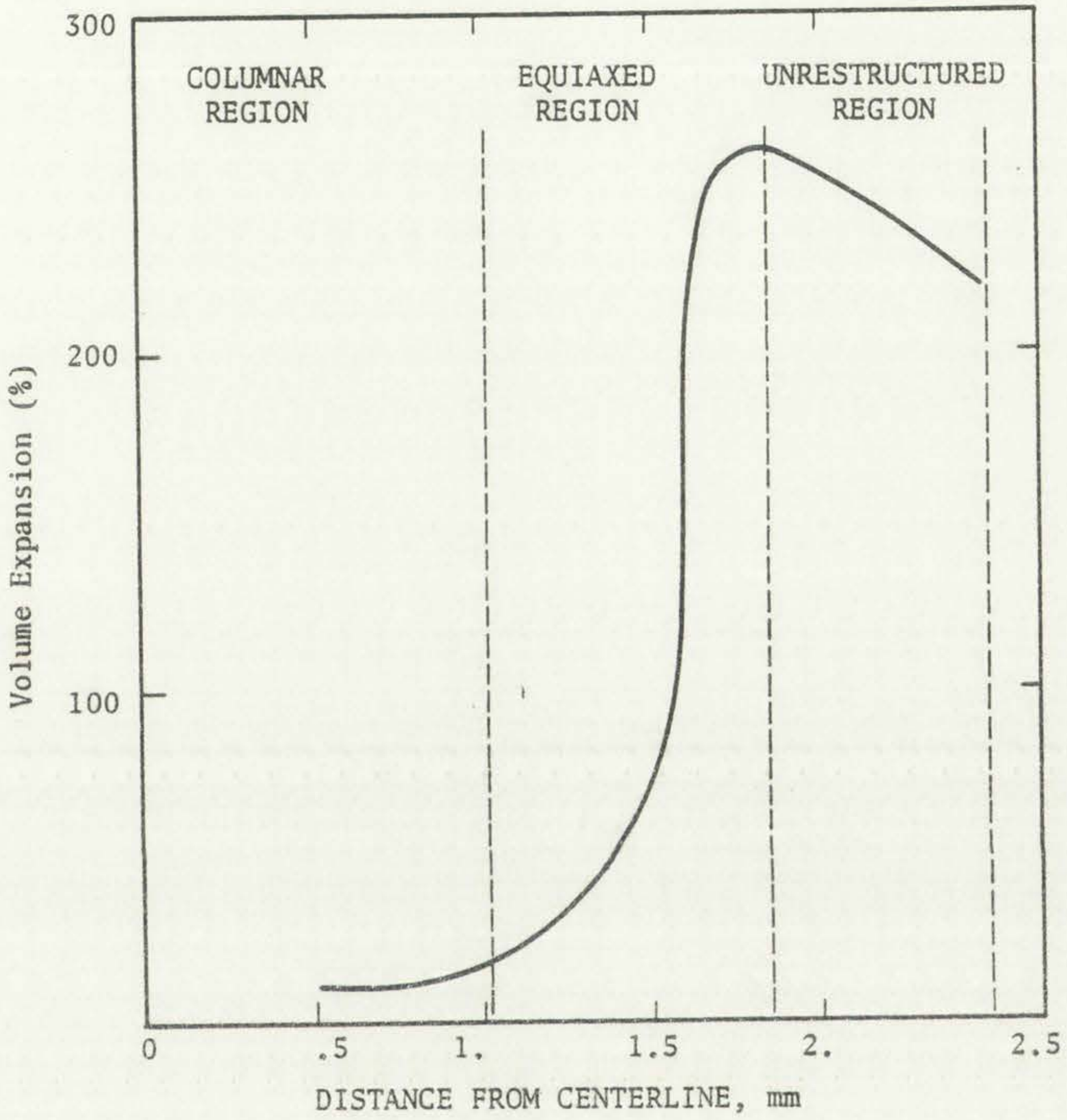

Figure 6.2
Maximum fuel volume expansion due to fission gas at P = 20 atms, T = 4222 K

obtain the possible contributions from the various grain regions, the maximum fission gas expansions are calculated via Eq. (6.1) and the results listed in Table 6.3. Again this maximum possible contribution ignores surface tension and the usual transient gas release of 8%[1] - 16%.[6] Transient gas release is usually associated with intergranular gas and the interlinking of bubbles, forming paths to the central void. The degree of linkage is a function of burnup, power, and the transient conditions, but is not considered here except to say that a substantial portion of intergranular gas can be expected to be released, especially in a slow transient.

As seen in Table 6.3, the majority of the fission gas in the columnar and equiaxed region is in bubble form. In the unrestructured region, however, the major portion of the gas is in solution or unresolvable intragranular bubbles. For the unrestructured region Ronchi and Matzke[7] calculated that 0.8% of the fission gas was in intragranular bubbles, 3-17% in grain boundaries, and 97-75% in solution, which is not much different than the results of Stahl.[1] The volume expansion calculations in Tables 6.2 and 6.3 were done using the Ideal Gas EOS. This tends to underestimate the volume expansion as can be seen in Table 6.4 which compares the Ideal Gas EOS to Harrison's tabular EOS[8] for Xe, for temperature-pressure ranges as close as can be found to those of interest. Thus the fuel swelling due to existing bubbles is only on the order of 2 to probably 40% if the transient is rapid enough that coalescence and precipitation have a negligible effect.

TABLE 6.3

VOLUME EXPANSION FOR 3 ATOM % BURNUP FROM EXISTING FISSION GAS BUBBLES

Fission Gas Description	Fuel Region	Approximate Ave. Region Steady State Temp (K)	Gas Density (Atoms/cm^3 Fuel)	% of Gas in Region	Volume Expansion (%), 20 Atms.			
					3023 K	3824 K	4177 K	4222 K
Intergranular (.5-5μm dia.)	Columnar	1920	1.8×10^{18}	25.6	1.4	2.3	2.8	2.8
	Equiaxed	1520	3.01×10^{19}	52.5	31.1	47.6	54.9	55.9
Intragranular (.065μm dia.)	Columnar	1920	4.5×10^{18}	63.9	3.4	5.8	6.9	7.1
	Equiaxed	1520	1.01×10^{19}	17.5	10.4	15.9	18.3	18.6
	Unrestructured	870	3.75×10^{18}	3.2	5.5	7.5	8.4	8.6

TABLE 6.4

COMPARISON OF IDEAL GAS EOS AND HARRISON'S EOS FOR XENON

T(K)	P(atm)	Harrison v (cm^3/mole)	Ideal Gas v (cm^3/mole)
2028	306.6	597.3	542.7
2028	660.9	298.7	251.8
2028	1075.	199.1	154.8
1160	170.1	597.3	559.5
1160	357.8	298.7	266.0
1160	570.5	199.1	166.8
1160	818.7	149.3	116.3
1160	1116.	199.5	85.3

The surface tension of the fuel will affect the fuel swelling. Using a solid UO_2 surface tension of 750 ergs/cm^2,[9,3] one can calculate the internal pressure of the bubble using:

$$P_{int} - P_{bulk} = \frac{2\sigma}{r} , \tag{6.2}$$

where

P_{int} = internal pressure of the bubbles,

P_{bulk} = bulk pressure,

σ = surface tension ($\simeq$ 750 ergs/cm^2), and

r = bubble radius ($\simeq$ 325 Å).

One obtains $P_{int} = P_{bulk} + 455.5$ atms, for an intragranular bubble. In molten UO_2, the surface tension has a value of only 450 ergs/cm^2.[9,3] Thus upon the change of phase the surface tension pressure (thus the bubble internal pressure) will drop to 273 atm + P_{bulk}, leading to a 30%[10] increase in the gas volume due to surface tension effects only. To demonstrate, however, the overall effect of surface tension, the intragranular, equiaxed volume expansion (10.4%) is recalculated using Eq. (1) with $P_1 = 475.5$ atm, $T_1 = 1520$ K, $P_2 = 293$ atm, and $T_2 = 3023$ K, obtaining a volume expansion of only 1%.

Experimentally a 3.6 volume % expansion[6] was attributed to fission gas during an overpower transient in TREAT. The 25% PuO_2 mixed oxide fuel was irradiated at 9 kW/ft to a burnup of 8250 MWd/MTM ($\simeq$ 1 atom %) in EBR-II. The transient irradiation produced a peak pin power of 75 kW/ft with a pulse duration measured at half-peak of .97 s resulting in the inner 50 areal percent of the fuel being within 270 K of fuel melting temperature. Approximately 8% of the fission gas generated was released during steady state with an additional 16% released during the transient. The intragranular bubble size was 1000 Å compared to 650 Å found by Stahl.[1] Calculated maximum expected swelling in the unrestructured region was done by Stahl[1] yielding a volumetric swelling of 1%. GRASS calculations by Dias[4] for a hypothetical FFTF fuel pin at 6 atom % burnup undergoing a \$5/s ramp insertion of reactivity lead only to a .05% volume expansion if hydrostatic pressure (fuel constraint, cladding constraint, etc.) is

included. However, if hydrostatic pressure is ignored and the calculation done with a constant 10 atm bulk pressure, a swelling of 3.17% occurs at incipient fuel melting. Calculations done by Makenas and Poeppel reported by Dias[4] for the same transient conditions gave an unrestrained (10 atm.) fission gas swelling of 34.8% and a restrained swelling of 3.4%.

Further parametric work by Dias[4] indicates that for short transients, as investigated in this work, re-solution of fission gas, thermal gradients, and initial bubble-size distribution have little effect on the final swelling.

Gruber[11] also calculated intragranular fission gas swelling for 50, 500, and 5000 K/s fuel temperature rises using FRAS2 and obtained swelling of 6.8%, 10.6%, and 10.9% respectively. At the even higher rates, expected for $15/s ramp insertion, the volume expansion is expected to be lower. The gas in solution precipitates into extremely small bubbles, thus with very high internal pressure due to surface tension effects, and does not contribute substantially to volume expansion. Also the fast transient does not allow time for bubble coalescence to occur.

Prediction of fission gas swelling is very difficult. Parameters such as burnup, irradiation power and temperature, initial porosity, etc., effect the quantity and form of gas retention. The transient preheat, time and power scale, hydrostatic forces (such as cladding and solid fuel), fuel temperature and thus surface tension, irradiation time, axial and radial restraints, etc., all effect gas release, bubble

coalescence and growth, and thus fuel swelling due to fission gas. Most of the relationship of the above parameters to fuel swelling are not fully understood making the swelling predictions difficult.

However, from above, it appears that fission gas expansion on the order of 1-10% can be expected, with an unrestrained expansion of 3-30%. Again, if metallic inclusion are assumed segregated, its expected volume expansion is significant when compared to the fission gas expansion and the $\simeq$ 10% volume expansion upon fuel melting.

REFERENCES

1. D. Stahl, and T. J. Patrician, "Fission-Gas Behavior During a Mild Overpower Transient," Argonne National Laboratory report ANL-8069 (February 1974).

2. L. Burris, Jr., and I. G. Dillon, "Estimation of Fission Product Spectra in Discharged Fuel from Fast Reactors," Argonne National Laboratory report ANL-5742 (July 1957).

3. P. S. Maiya, "Surface Diffusion, Surface Free Energy, and Grain-boundary Free Energy of Uranium Dioxide," Journal of Nuclear Materials, 40(1) 57-65 (1971).

4. J. W. Dias and R. B. Poeppel, "Transient Swelling Studies with the GRASS Code," Argonne National Laboratory report ANL-7992 (January 1973).

5. R. M. Cornell, "Growth of Fission Gas Bubbles in Irradiated Uranium Dioxide," Phil. Magazine, 19, 539 (1969).

6. G. E. Culley, J. E. Hanson, R. D. Leggett, and F. E. Bard, "Response of an EBR-II Irradiated, Mixed Oxide Fuel Pin to an Overpower Transient in TREAT," Proc. Conf. on Fast Reactor Fuel Element Technology, ANS, (1971) pp. 657-678.

7. C. Ronchi and H. J. Matzke, "Calculations on the In-pile Behavior of Fission Gas in Oxide Fuels," EUR-4877E, Karlsruhe (1972).

8. J. W. Harrison, "An Extrapolated Equation of State for Xenon for Use in Fuel Swelling Calculations," Journal of Nuclear Materials, 31, 99-106 (1969).

9. L. Leibowitz, E. C. Chang, M. G. Chasanov, R. L. Gibby, C. Kim, A. C. Millunzi, D. Stahl, "Properties for LMFBR Safety Analysis," Argonne National Laboratory report ANL-CEN-RSD-76-1 (March 1976).

10. L. W. Deitrich and R. W. Ostensen, "An Assessment of Fission-Gas-Driven Fuel Disruption and Dispersal in a Hypothetical LMFBR Loss-of-Flow-Accident," Argonne National Laboratory report ANL/RAS 77-4 (February 1977).

11. E. E. Gruber, "Modeling Breeder Reactor Transient Fission Gas Behavior: Bubble Equilibration Effects," ANS Transactions, San Diego, California, 28, (June 1978) pp. 236.

7. EXPERIMENTAL COMPARISON

In order to determine possible contributions to pre- and postclad failure fuel motion from metallic fission products and/or fission gases, a number of experiments on fuel motion were investigated. Both transient overpower and undercooling tests have been performed using fresh and preirradiated fuel. From such experiments only qualitative results could be drawn due to the difficulty of transient instrumentation and the resolution of hodoscope and other current techniques.

7.1 E and H Series

In the Argonne National Laboratory (ANL) E and H transient overpower test series,[1-3] both fresh and preirradiated fuel rods were subject to 50¢-\$1/s and \$3-\$5/s reactivity ramp insertions respectively. The H-series was largely intended to determine the failure threshold for FTR-type fuel pins with energy input not much in excess of the failure energy for 50¢-\$1/s ramp reactivity transients. The E-series was intended to examine not only the failure threshold, but events subsequent to failure, including fuel motion. Tests H4, E6, and E7 used high-power-preirradiated (10-11.6 kW/ft) pins with a burnup of $\simeq$ 4.5 atom %. Tests H3 and H5 used intermediate-power-irradiated fuel with a burnup of $\simeq$ 3.4 atom %. Table 7.1 summarizes fuel rod descriptions for the various tests.

TABLE 7.1

SUMMARY OF TRANSIENT TESTS

Test	Fuel Description	Fuel Motion Restraints (Axial)	Transient Description	Results
E1	Fresh UO_2	None	Transient overpower, no preheat TREAT high heating rate, burst max. 1800 (MW) total energy 500 (MW-s), rise period .064 (s).	Prefailure fuel motion.
H2	Fresh $(U_{.75}, Pu_{.25}) O_2$	½" insulator pellet.	Transient overpower; no preheat, TREAT low heating rate, burst max. 1518 (MW), total energy 490 (MW-s), rise period .080 (s).	Prefailure fuel motion.
E4	Fresh $(U_{.75}, Pu_{.25}) O_2$	½" insulator pellet.	Transient overpower; no preheat, TREAT high heating rate, burst max. 2584 (MW), total energy 700 (MW-s), rise period .066 (s).	Possible prefailure fuel motion.
E2	Fresh UO_2	½" depleted UO_2 2" stainless steel	Transient overpower; no preheat, TREAT high heating rate, burst max. 2865 (MW), total energy 750 (MW-s), rise period .050 (s).	Compressed spring .3 in. before failure, no other significant prefailure axial motion.
H3	$(U_{.75} Pu_{.25}) O_2$ Irradiated in EBR-II (fast), 3.4 atom % burnup at intermediate power.	½" insulator pellet	Transient overpower; preheat 160 (MW) for 3 (s), TREAT (50¢-\$1/s ramp) burst max. 425 (MW), total energy 810 (MW-s), rise period .9 (s).	No clad failure. No transient fuel or clad swelling. No fuel melting.

TABLE 7.1 (cont)

Test	Fuel Description	Fuel Motion Restraints (Axial)	Transient Description	Results
H4	$(U_{.75}, Pu_{.25})O_2$ irradiated in EBR-II 4.5 atom % burnup at high power	7" insulator pellets 5" inconel reflector.	Transient overpower; preheat 235 (MW) for 2.5 (s), TREAT (50¢/s ramp), burst max. 650 (MW), total energy 1250 (MW-s), rise period .96 (s).	No prefailure fuel motion.
H5	$(U_{.75}, Pu_{.25})O_2$ irradiated in EBR-II 3.4 atom % burnup at intermediate power.	½" insulator pellet	Transient overpower; preheat 115 (MW) for 3 (s), TREAT (50¢/s ramp), burst max. 650 (MW), total energy 1090 (MW-s), rise period 1.1 (s).	No prefailure fuel motion.
E6	$(U_{.75}, Pu_{.25})O_2$ irradiated in EBR-II 4.5 atom % burnup at high power.	7" insulator pellets 5" inconel reflector.	Transient overpower; preheat 167 (MW) for 3 (s), TREAT ($3/s ramp), burst max. 2250 (MW), total energy 1211 (MW-s), rise period .188 (s).	No prefailure fuel motion (preliminary, neutron radiography only).
E7	$(U_{.75}, Pu_{.25})O_2$ irradiated in EBR-II 4.5 atom % burnup at high power.	7" insulator pellets 5" inconel reflector.	Transient overpower; preheat 142 (MW) for 2.4 (s), TREAT ($3/s ramp), burst max. 2468 (MW), total energy 1450 (MW-s), rise period .180 (s).	No prefailure fuel motion.
E3	UO_2 irradiated in MTR (thermal) 4.82-6.33 atom % burnup.	No axial restraint.	Transient overpower; no preheat, TREAT ($3-$5/s ramp), burst max. 6500 (MW), total energy 1250 (MW-s), rise period (.035 s).	Pin failure prior to fuel melting.
F1	$(U_{.75}, Pu_{.25})O_2$ irradiated in EBR-II at 12 kW/ft to 2.55 atom % burnup.	6.7" depleted UO_2 insulator pellets 5" inconel reflector. No coolant channel restraint.	Loss-of-flow treat at pin design power level. Axial peak flat topped at 11-12 kW/ft. duration 11 s.	Clad melting and drainage, fuel swelling and axial fuel drainage through central region.

TABLE 7.1 (cont)

Test	Fuel Description	Fuel Motion Restraints (Axial)	Transient Description	Results
F2	$(U_{.75}, Pu_{.25}) O_2$ irradiated in EBR-II at 11.6 kW/ft to .35 atom % burnup.	5.4" natural UO_2 insulator pellets. No coolant channel restraint.	Loss-of-flow; TREAT at design level to 10 times design level. Axial peak linear power generation of 12.5 kW/ft for 6.5 s, followed by power burst of 135 kW/ft (11 x) over 1 s.	Early clad melting and drainage. Fuel dispersal during burst portion of transient believed driven by fuel vaporization.
EOS-1	$(U_{.75}, Pu_{.25}) O_2$ Fresh	.5" Boron nitride insulator pellets. No coolant channel Axial constraint.	No preheat Burst max. power 1302 kw/ft, duration .25 s (100 x nominal design).	Fuel dispersal Believed stainless steel driven.
EOS-2	$(U_{.75}, Pu_{.25}) O_2$ irridiated in EBR-II at 11.3 kW/ft to .85 atom %	Same as EOS-1.	No preheat. Burst max. 1236 kW/ft, duration .25 s (100 x nominal design).	Fuel Dispersal. Earlier in transient than EOS-1. Believe fission gas effect.
EOS-3	$(U_{.75}, Pu_{.25}) O_2$ irradiated in EBR-II at 8.12 kW/ft to .81 atom % burnup.	Same as EOS-1.	No preheat. Burst max. 978 kW/ft, duration .3 s.	Fuel dispersal. Slightly earlier in transient than EOS-2. Believe fission gas effect.
C5A	UO_2 irradiated in General Electric test reactor (thermal) at low power (12 kW/ft peak) to 2 atom % burnup.	14.25" natural uranium blanket (solid).	Preheat fuel to 500 K, TREAT transient initial period .131 s, reactivity insertion 1.37%, duration 1 s, peak power 160 kW/ft intergrated power 338 MW/s.	Clad failure post axial fuel motion in coolant channel.

TABLE 7.1 (cont)

Test	Fuel Description	Fuel Motion Restraints (Axial)	Transient Description	Results
C5B	UO_2 irradiation same as C5A.	14.25" natural uranium annular blanket (.07" i.d.).	preheat fuel to 500 K, TREAT transient initial period .136 s, reactivity insertion 1.35% duration 1 s, peak power 155 kw/ft integrated power 339 MW/s.	no clad failure axial expulsion of fuel (10") into annular blanket pellets.
L5	$(U_{.75}, Pu_{.25}) O_2$ in General Electric test reactor (thermal) at 12.2 kw/ft to 8 atom % burnup.	.5" UO_2 insulator pellets, 3" inconel reflector, no coolant channel restraint.	TREAT transient 1) 9 s at nominal power (11 kW/ft) 2) followed by burst peak power 66 kW/ft (6x) rise period 835 ms.	Sodium voiding, clad failure, mild fuel dispersal at or after scram.

Concerning fuel motion behavior prior to cladding failure, which is of interest in the present work, using hodoscope analysis, posttest examination, and/or neutron radiography, fuel motion prior to cladding failure occurred in the E1, H2, and possibly E4 experiments. These three tests had several features in common. All three were fresh pins, thus the fuel-clad gap was present at initiation of the transient with the resulting effect of greatly reducing axial fuel-cladding drag. Pin pressurization and fuel swelling from fission gas was essentially nonexistent which most likely extends the time-to-failure allowing a high areal fraction (≈75-100%) of the fuel to be above solidus, again reducing fuel self-constraint to axial motion. In addition, a fairly uniform axial power distribution led to uniform axial melting, helping to eliminate solid end-of-fuel-column blocks. Finally, axial expansion space for the molten fuel was readily available and no axial inertial restraint was present. In test E1, virtually nothing separated the fuel and the plenum, and in H2 and E4 only .5 in. of insulator pellets separated the active fuel from the plenum as shown in Fig. 7.1. Because such fuel was previously unirradiated, fuel motion with respect to volatile and gaseous fission products is nonexistent. However, the results indicate that for free expansion the $\simeq$ 10% volume expansion due to the change of phase, i.e. solid to liquid, can provide a driving force for axial fuel motion.

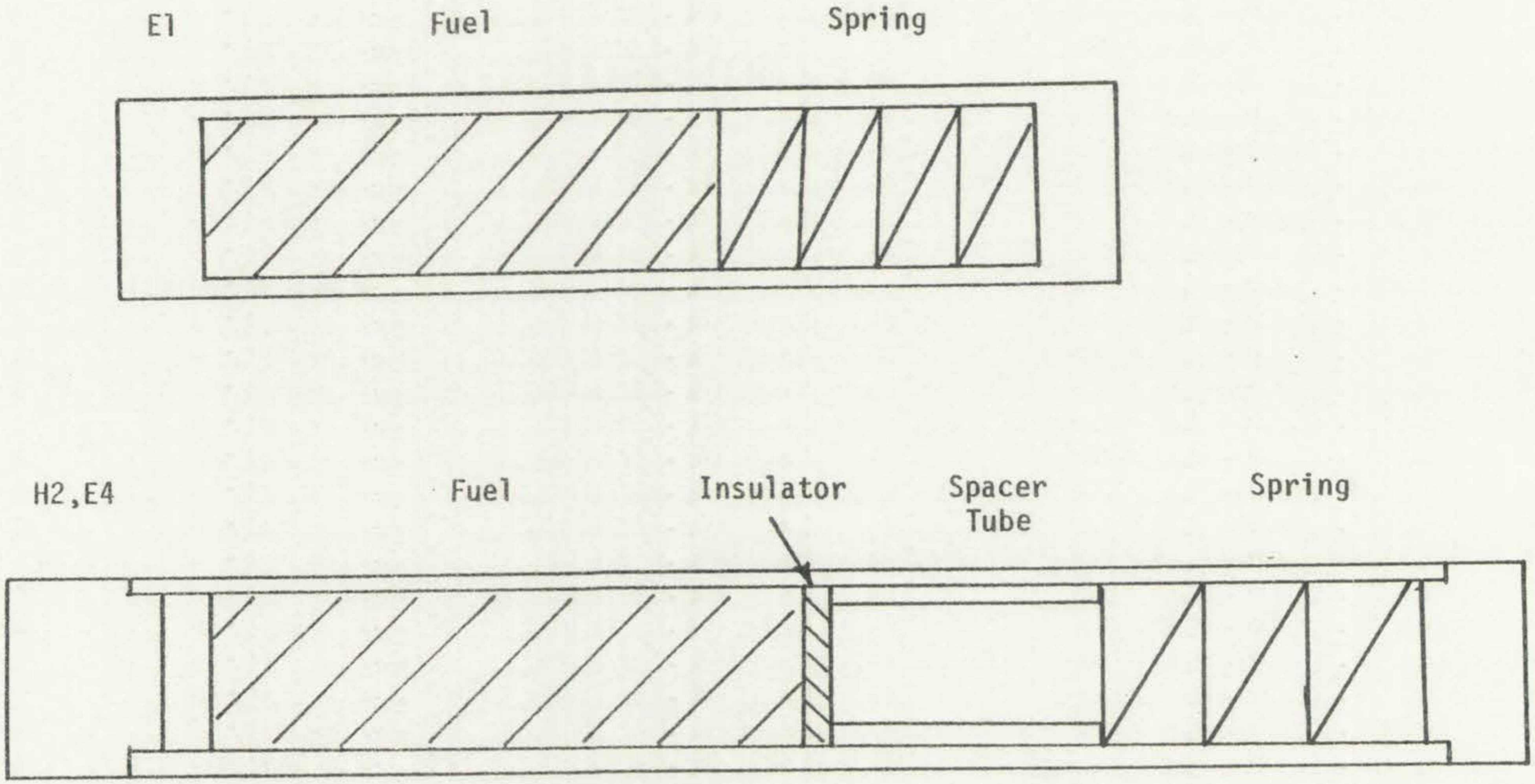

Figure 7.1.
Schematic of E1, H2, and E4 fuel rods.

In the remaining tests (pre-irradiated fuel), H3, H4, H5, E3, E6, E7, and E8, hodoscope analysis, posttest examination, and/or neutron radiography suggest that prefailure axial fuel motion did not occur. However in some cases the results were inconclusive. Again as seen in the summary Table 7.1, this includes intermediate and high power irradiated fuel subjected to transients both in the 50¢-\$1/s and \$3-\$5/s ramp ranges. The power distribution was more cosine-shaped leading to less melting at the end of the pins, with the consequence of additional mechanical constraint at the fuel column extremities. In addition preirradiation leads to fuel swelling and fuel-cladding gap closure, thus increasing the potential for drag effects. Three out of the four test in this preirradiated group that experienced fuel melting and clad failure had thick insulator pellets and reflectors with hold down springs providing additional inertial and mechanical restraints to axial fuel motion. The melt fraction upon cladding failure was $\simeq$ 20% for H4 and $\simeq$ 25% for H5, corresponding to the situation where the melt front reachs the area of large fission gas retention as can be seen in Fig. 6.1. Gas release could contribute to pin pressurization and cladding failure or could coincide with the cladding stress due to differential thermal expansion of the fuel and cladding. Since more prototypic (inertial and axial constraints) fresh fuel pins, run with the preirradiated fuel pin tests, did not exhibit prefailure fuel motion,

it thus appears for the E- and H-series tests, that prefailure fuel motion only occurs for unrestrained fuel. Fission gas and other volatile fission products appear not to be able to overcome the axial mechanical constraints for fuel motion prior to clad failure as seen in Fig. 7.2. They may however, contribute to radial swelling, clad failure, and possible postfailure fuel movement. The spring compression force, F_s, is probably minimal. After only hours in the irradiation environment, the spring anneals and loses much of its compressive force. However, due to fuel restructuring and swelling and fuel-cladding gap closure, the frictional forces, F_f and F_g, become significant. Unfortunately, the magnitude of this force is not known, but it will depend on initial fuel conditions the steady state irradiation, and the transient conditions. Due to differential thermal expansion between the fuel and cladding during a TOP accident this force will become very large and as mentioned above the resulting cladding stress could lead to cladding failure.

7.2 F-Series

The TREAT F-series tests were simulated loss-of-flow (LOF) or transient undercooling accidents to provide data for possible LMFBR fuel motion. The LOF test condition is achieved by surrounding a single fuel element with an annular nuclear heated wall in a dry (no sodium) test capsule (Mark-II loop as seen in Fig. 7.3). The F1 it has already shown that the IC and W contact loads, [illegible] motion only occurs for unrestrained fuel. Fission gas and other [illegible] this fission products appear not to be able to overcome the [illegible] chemical constraints for fuel motion prior to cladding failure as seen in Fig. 7.2. They may however, contribute to cladding [illegible] failure, and possible postfailure fuel movement. The spring compression force, F_s, is probably minimal. After many hours in the irradiation environment, the spring anneals and loses much of its compressive force. However, due to fuel restructuring and cladding and fuel-cladding gap closure, the frictional forces, F_f and F_c, become significant. Unfortunately, the magnitude of this force is not known, but it will depend on initial fuel conditions, the [illegible] ation, and the transient conditions. Due to differential expansion between the fuel and cladding during a TOP accident, this force will become very large and as mentioned above the resulting cladding stress could lead to cladding failure.

7.4 F-Series

The TREAT F-series tests were completed [illegible] transient overpower accidents to provide data for [illegible] LMFBR fuel [illegible]. The TOP test condition is achieved by [illegible] single fuel element with an annular coolant [illegible] annual test capsule [illegible] as seen in Fig. 7.3.

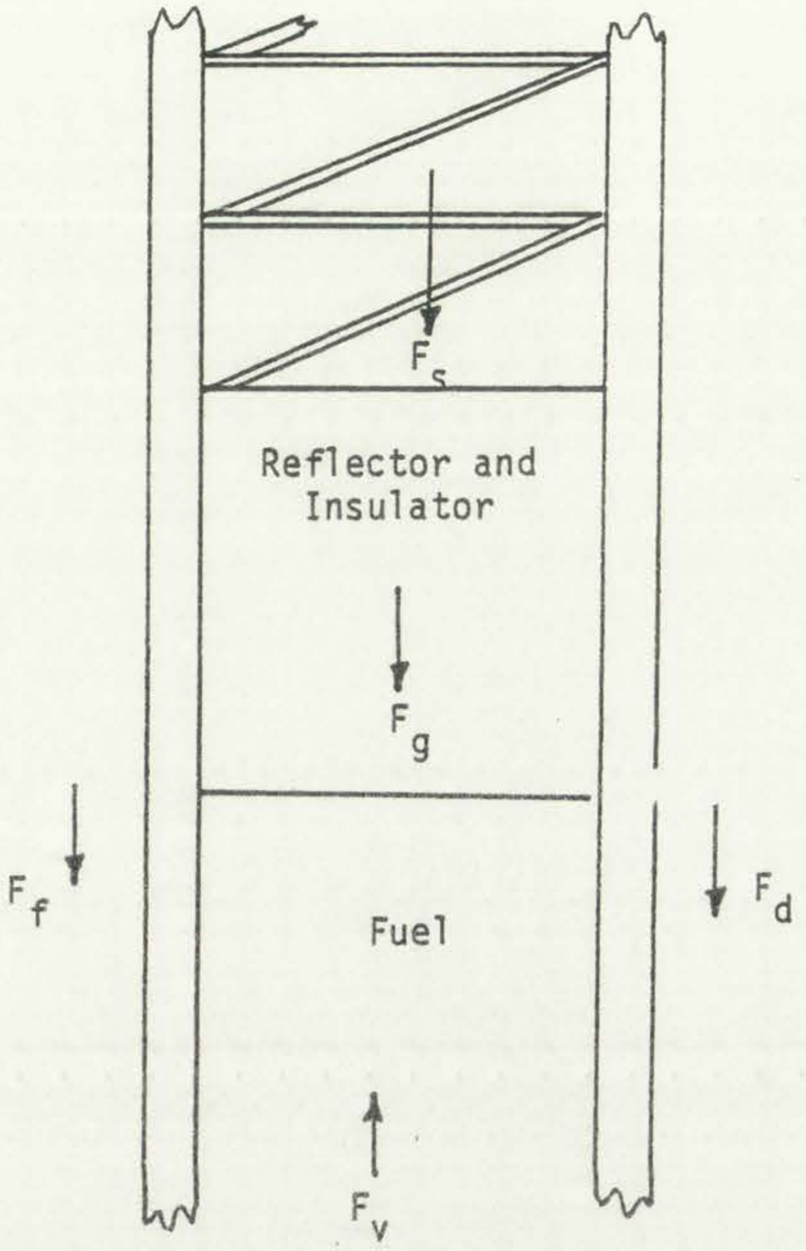

F_s = force due to spring compression,

F_g = gravitational force due to mass of reflector and insulator,

F_d = drag force (=0 for zero velocity)

F_f = static friction force due to fuel swelling and closure of fuel-cladding gap,

F_v = force due to fission gas, volatiles, and fuel = P_vA,

A = cross-sectional area, and

P_v = total vapor pressure of fission gas, volatiles, and fuel.

Figure 7.2.
Forces affecting fuel motion prior to cladding failure.

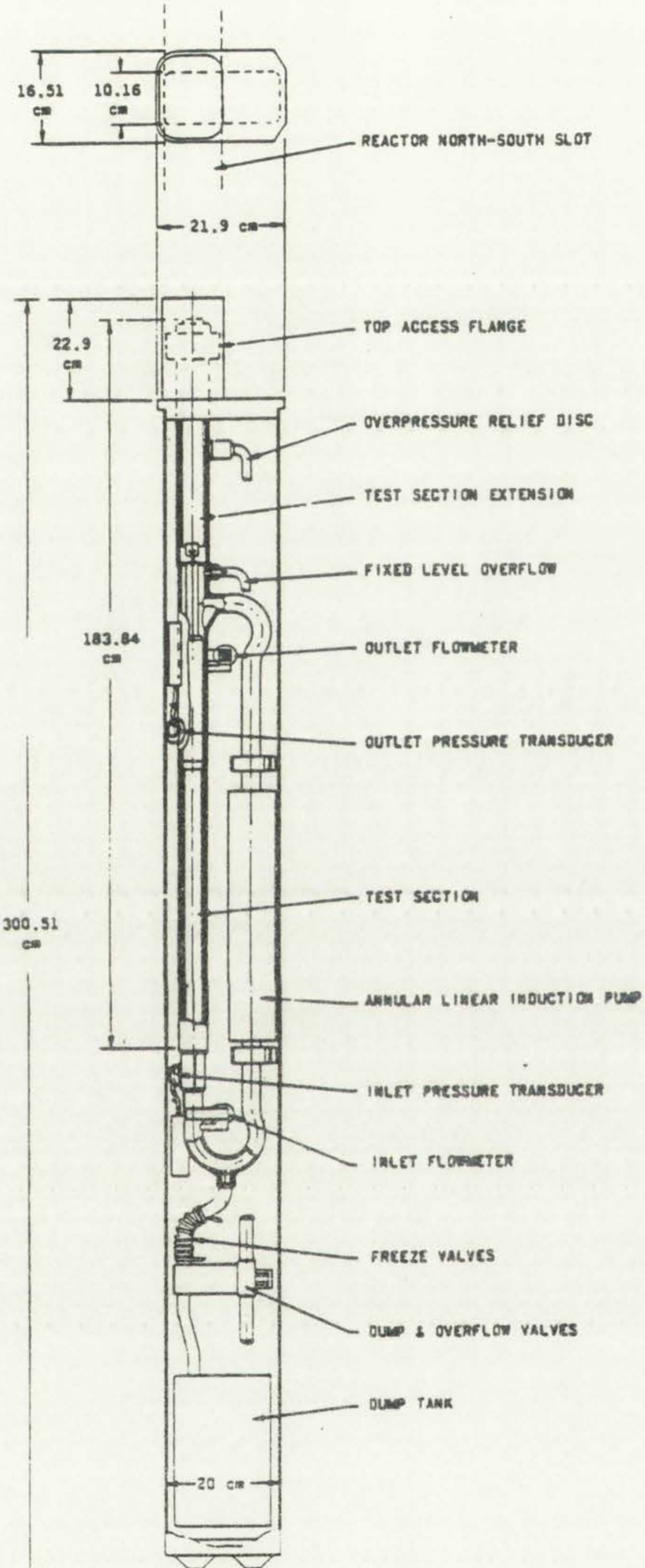

Figure 7.3.
Mark-II loop.

test[4,5] was performed to investigate the effect of fission gas on fuel motion at design power levels following clad melt and drainage. The F1 test fuel contained $(U_{.75}, Pu_{.25}) O_2$ irradiated at 12 kW/ft to 2.55 atom % burnup and was fully restructured. Axial motion of the entire fuel pin was constrained by a tungsten pin through the lower fuel pin and plug, and a fuel pin retainer on the top end plug which restricted downward but allowed upward movement of the top end plug. Internal to the cladding, 6.7 in. of insulator pellets and 5 in. of Inconel reflector was above the active fuel column as seen in Fig. 7.3. However, these axial constraints were not important as far as axial fuel motion was concerned since cladding melting and drainage occurred prior to fuel melting.

The TREAT transient, at the test pin axial peak power, was approximately flat-topped at 11 to 12 kW/ft (design power levels) and lasted $\simeq$ 11 s. The TREAT reactor can be seen in Fig. 7.4. Hodoscope, neutron radiography, and posttest examination showed that only downward fuel motion was experienced, with no upward fuel motion detected at any time. Fission gas and volatiles did cause axial and radial fuel swelling to occur, as evidenced by posttest photomicrographs,[4] however, bubble release to the central void region allowed fuel drainage to occur versus a "foaming" axial driving situation. It was concluded that retained fission gas and volatiles did not prevent an axial

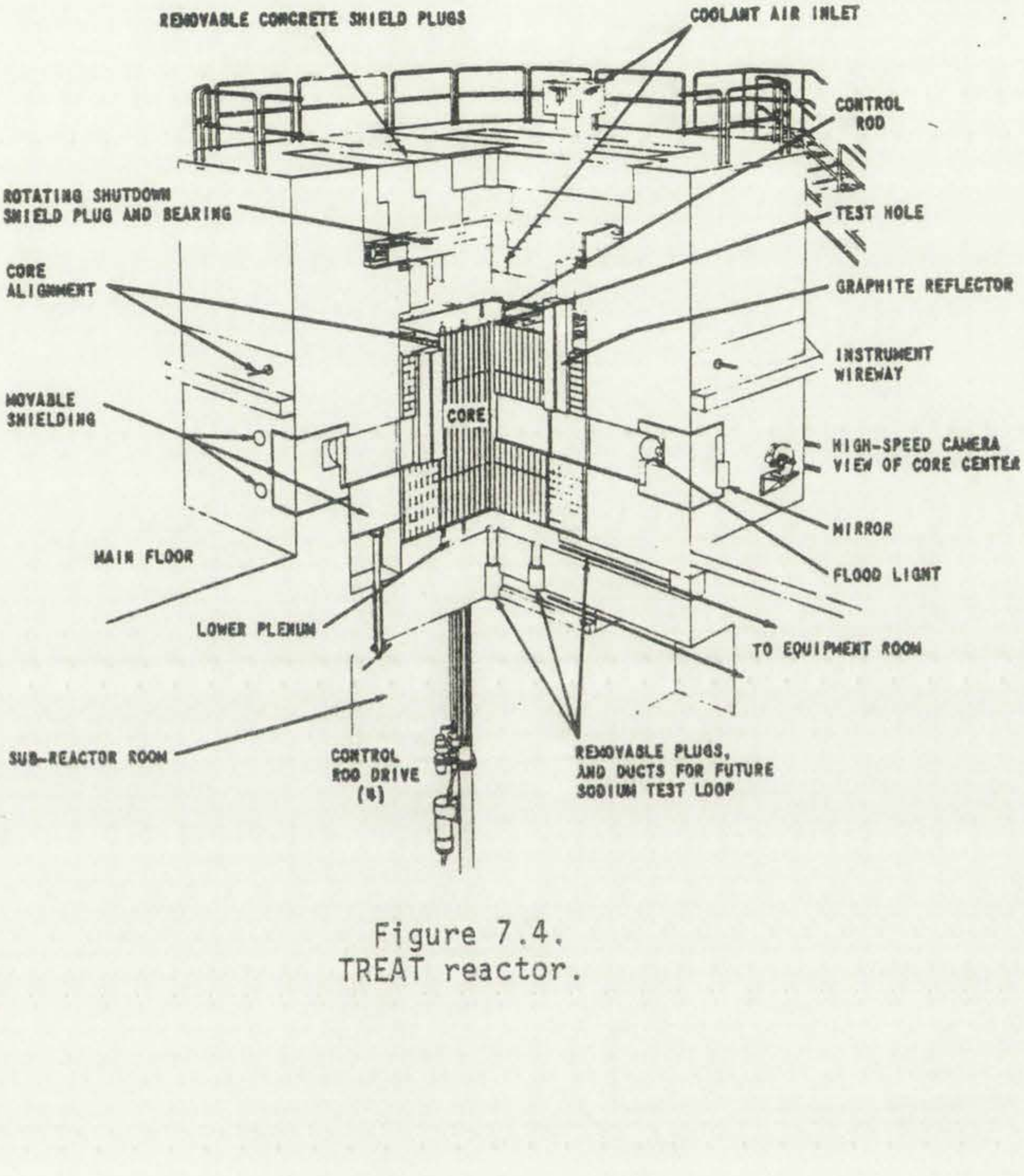

Figure 7.4.
TREAT reactor.

drainage or cause axial fuel dispersion for power-time scales as in the F1 test.[4] The transient was slow enough that fission gas bubble escape was occurring at least as rapidly as bubble growth.

The F2[6,7] test was performed to evaluate the motion of high power fuel in a hypothetical LOF accident. The F2 test train was similar to that used in F1, consisting of a single test pin surrounded by a nuclear heated wall in a dry test capsule. The fuel pin was $(U_{.75}Pu_{.25})O_2$, irradiated in EBR-II at 11.6 kW/ft to .35 atom % burnup and was restructured. This test pin contained a 34.4 cm active fuel column with 13.8 cms of natural UO_2 insulator pellets above. No reflector was present, but a 26.8 cm annular stainless steel spacer tube separated the insulator pellets from the compression spring. The TREAT transient consisted of a constant axial peak linear power generation of 12.5 kW/ft for 6.5 s, followed by a power burst of $\simeq$ 135 kW/ft (11 x design) over approximately 1 s. At the power burst initiation ($\simeq$ 10.5 s after the transient initiation), the hodoscope indicated that the fuel column was erect, heat transfer calculations indicated that the fuel did not reach the molten state, and lower thermocouple burnout signified clad drainage had occurred. The hodoscope also indicated that no fuel motion was observed during the flattop portion of the test transient. During the power burst two major upward fuel movements occurred based on hodoscope information, moving fuel to

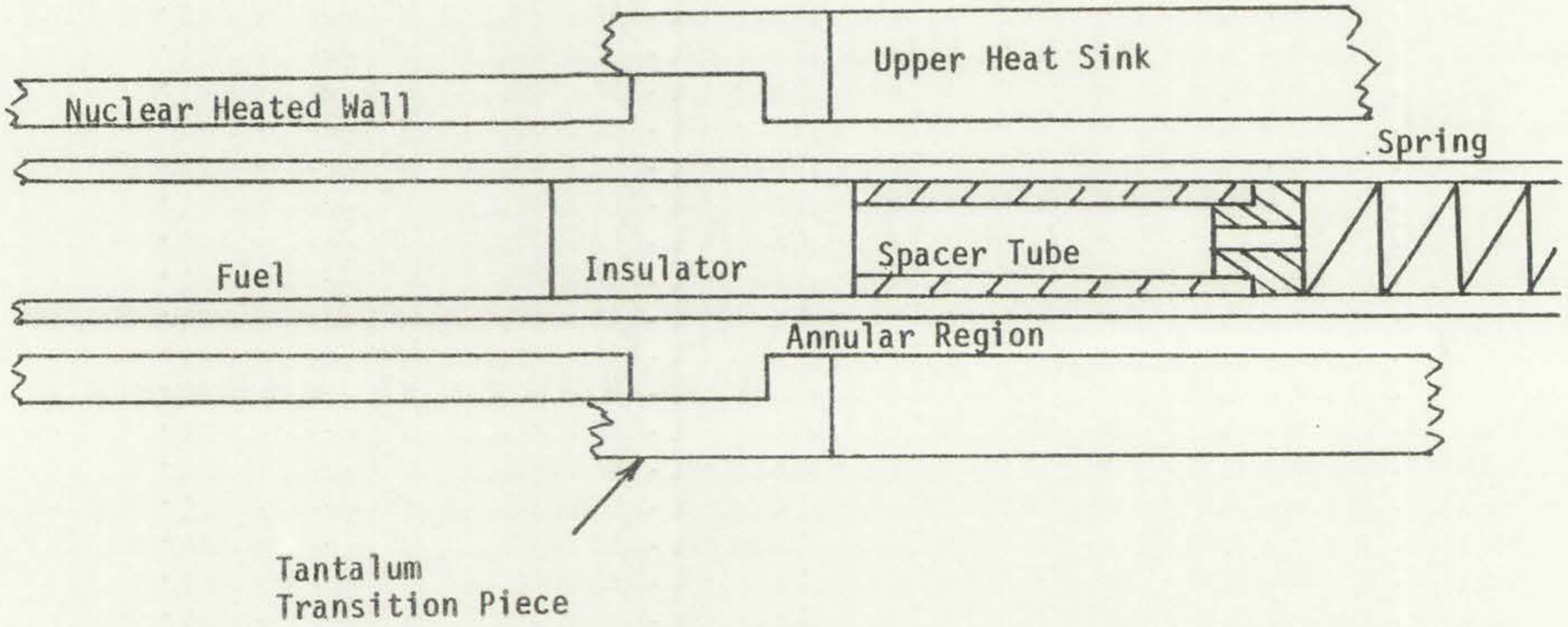

Figure 7.5.
Test F2 annular region.

a maximum of 19 cms above the active fuel column into the annular region formed by the upper insulator and spacer portion of the fuel pin and the upper heat sink as shown in Fig. 7.5. The first upward dispersal occurred at 11.04 s into the transient and consisted of the top $\simeq$ 10 cm portion of the fuel pin. The hodoscope indicated the second dispersion occurred at 11.18 s into the transient and was located at the center of the active fuel column, moving an additional 5-8 cms of fuel upward. About 17 grams of fuel froze in the cool annular region, but the remaining fuel drained back into the lower half of the fuel pin. At fuel ejection, all the fuel was calculated to be at or above the solidus temperature.

To determine the driving species for this upward fuel dispersal, the maximum fuel temperature and the pressure required to overcome the head pressure and frictional loss were calculated.[6] A pressure of 1.5 atm. (22 psi) at a maximum temperature of 3273 K was obtained. As demonstrated in Table 7.2 under these temperature conditions, fission gas, cladding, volatile fission products, and fuel species could be responsible for the dispersion. The inclusion of the fuel species assumes the maximum temperature is not well defined but may be off by as much as 300 K. Also from Table 7.2, it can be seen that the homogeneous inclusion composition of O'Boyle[8] and Johnson[9] could not have driven the dispersal. Their individual volatile constituents (segregated compositionally) as well as Jeffery's[10] homogenous inclusion

TABLE 7.2

DETERMINATION OF POSSIBLE F2 FUEL DISPERSAL DRIVING SPECIES

Species Description	Temperature (K)	Pressure (atm)
A. Inclusions		
Johnson inclusion composition (Homogenous)	3273	.26
O'Boyle inclusion composition (Homogenous)	3273	.45
Jeffery inclusion composition (Homogeneous)	3273	180
B. Segregated Inclusion Volatiles		
Sb	3273	13
Ba	3273	97
Te	3273	512
Pd	3273	3
C. Cladding		
Fe	3273	1.8
D. Gases		
Noble gases (Xe, Kr)	3273	100

TABLE 7.2 (cont)

Species Description	Temperature (K)	Pressure (atm)
E. Fuel EOS		
Bogensberger EOS $(U_{.8}, Pu_{.2})\ O_{1.96}$	3600	1.5
Bogensberger EOS UO_2	3700	1.5
Gabelnick EOS UO_2	3900	1.5
Leibowitz EOS UO_2	3800	1.5
Leibowitz EOS $(U_{.8}, Pu_{.2})\ O_{1.96}$	3570	1.5

composition, however, have a high enough vapor pressure to cause ejection. The authors believe that the stainless steel clad probably would not have been intimately mixed in the fuel at the ejection time. Thus fission product pressurization and fuel vapor pressure are considered the primary causes for fuel dispersal. From Sec. 5, evidence supports homogeneous inclusion composition, leaving fission gas and fuel species as the most probable driving forces. From the results in Sec. 6, at .35 atom % burnup and assuming a radial average fission gas retention of 42%, approximately 1.47×10^{-5} moles of gas/ cm^3 of fuel exists. Using the Ideal Gas Law, a $\Delta T = 3273$ K - 1270 K (average steady state temperature), and ignoring the surface tension, one could expect a 160% volume expansion at the peak temperature location due to fission gas. Since the F2 transient radial temperature profiles are very flat, not much gas release is expected, i.e. no driving potential, except from interlinking porosity and cracks (8-16% as discussed in Sec. 6). However, a minimum of 40% of the gas in the various fuel regions is in solution versus existing intra- and intergranular bubbles. Also surface tension effects on the fission gas bubble increase the pressure felt by the gas from 1.5 atm. to 1.5 +273 atm.* If one considers these factors the expected volume expansion

---

*As shown in Sec. 6, the liquid fuel surface tension increases the fission gas intragranular bubble (650 Å dia.) pressure by 273 atms.

at the peak fuel temperature is approximately .5%; far less than that needed for fuel dispersal. Even if the expected volume expansion at fuel melting due to surface tension effects is taken into account, the volume expansion is still only a few percent. It thus appears that the unknowns in the transient and heat transfer calculations were sufficient to encompass the required fuel temperature, and that the fuel vapor was the driving species. The fission gas pressure was high enough, it just appears that not enough gas is available to cause the fuel dispersion.

7.3 EOS Test Series

TREAT tests EOS-1, EOS-2, and EOS-3[11] were performed to determine LMFBR irradiated fuel behavior to a rapid energetic power burst following coolant voiding and clad relocation (LOF driven TOP). The fuel was of the mixed oxide type, $(U_{.75}\ Pu_{.25})\ O_2$, with EOS-1 being fresh fuel, EOS-2 preirradiated at high power (11.3 kW/ft) in EBR-II to a burnup of .85 atom %, and EOS-3 preirradiated at intermediate power (8.12 kW/ft) to a burnup of .81 atom %. The active fuel column had a .5 in. boron nitride insulator pellet separating it from the hold down spring. The test train consisted of the test pin mounted in a dry capsule with 1.7 mm between the clad (5.33 mm O.D. for EOS-1 and EOS-2, 5.79 mm O.D. for EOS-3) and a boron nitride crucible. Room thus existed for radial expansion. Also, once cladding failure or

melting occurred, axial expansion into an upper test train plenum region was possible. The temperature limited TREAT transient was similar for the EOS-1 and EOS-2 tests. In the EOS-1 test, the transient consisted of a step reactivity insertion of 4.66% $\Delta K/K$ with an initial period of 22.9 ms. This led to a power burst of $\simeq$ 0.25 s with a maximum of 1302 kW/ft. The EOS-2 transient consisted of a step reactivity insertion of 4.42% $\Delta K/K$ with an initial period of 24.3 ms, leading to a power burst of $\simeq$ 0.25 s with a maximum of 1236 kW/ft. Both tests thus reached the desired level of $\simeq$ 100 x nominal design. The EOS-3 transient also was similar except the initial period was slightly longer (26.8 ms) and the peak power was lower, 978 kW/ft.

In the transient test of EOS-1 upward fuel dispersal occurred, based on preliminary hodoscope data and pressure and themocouple traces. Such upward fuel motion was believed to have been driven by stainless steel vapor pressure. The shortness of the test fuel, 4 in. active fuel length and 5.8 in. total test pin length, and the fact that the boron nitride crucible enclosed the bottom portion of the test volume, indicates that the drained cladding was in intimate contact with the hot fuel. In the F-series, the drained cladding settled around the bottom cooler fuel pellets and thus was not considered the principal dispersed species. The vapor pressure of iron is $\simeq$ 1 atm. at the fuel melting temperature (3023 K) and is $\simeq$ 4 atms. at 3500 K, sufficient to cause fuel dispersal.

In the EOS-2 test, fuel dispersal occurred earlier in the transient, i.e. about half the elapse time, than EOS-1, indicating fission gas may have a significant effect on fuel dispersal. The test pins were evacuated to 20 Pascals (2×10^{-4} atm.) prior to the test, and Xe (boiling point of 166 K, at 1 atm.) has a high enough vapor pressure as seen in Table 7.2 to cause dispersal. Again from the results in Sec. 6, at 0.85 atom % burnup and assuming a radial average fission gas retention of $\simeq 40\%$[1,12] (high power irradiation), approximately 3.4×10^{-5} moles of fission gas/cm^3 of fuel exists. Using the Ideal Gas Law and a ΔT of 2000 K one obtains a maximum possible fission gas contribution to fuel expansion of 550%. If one assumes 8% gas release during the transient, only 60% of the gas in bubbles (rest in solution), and also takes into account surface tension increasing the intragranular bubble pressure by about 273 atms., one gets a fission gas volume expansion of $\simeq 1\%$. Gas precipitation into bubbles will not be important in transients this rapid and thus in-solution gas can be ignored. Since the fuel must expand over 100% to fill the cladding-crucible volume, if the fission gas is contributing to earlier fuel dispersal, it cannot be due to simple expansion (assuming the rough estimate of 1% is close). Intergranular bubbles, however, may be causing grain boundary separation, fuel breakup, and more intimate mixing of fuel and stainless steel, leading to greater heat transfer and stainless steel entrainment.

In the [illegible] fuel [illegible] [illegible] of [illegible] Fission gas may have a [illegible] the [illegible] of [illegible] and to fission-gas of [illegible] as shown in Table 7.1 [illegible] in [illegible] 0.20 [illegible] Fission gas [illegible] of [illegible] × 10 [illegible] of fission gas [illegible] The [illegible] fission gas could [illegible] to the [illegible] gas release during the transient, [illegible], and [illegible] the in-reactor [illegible] fission gas-vapor [illegible] to [illegible] Since the [illegible] of the [illegible] fuel [illegible] of [illegible] mixing of fuel and stainless steel [illegible] and stainless steel [illegible].

In the EOS-3 transient, which was at lower power than EOS-2, fuel dispersal appeared to occur slightly sooner in the transient than the EOS-2 test. This may be attributed to the larger fission gas retention in the intermediate power preirradiated test pin. From these tests it appears that for LOF and LOF driven TOP accidents with relatively low burnup fuel, fission gas and other volatiles potential for fuel motion appears to be in the form of fuel breakup for very rapid transients and for some fuel swelling (< 10%) for slower transients. Little potential appears to exist, however, for axial dispersal, since for LOF accidents clad melt allows expansion into the coolant channel.

7.4 Series V Tests

The General Electric Series V tests[13] were designed to investigate the effects of molten fuel movement, fission product gases, and fuel and blanket length, on transient failure thresholds and mechanisms. Two test pins, C5A and C5B, consisted of UO_2 fuel irradiated at low power (12 kW/ft peak) in the General Electric Test Reactor (GETR) to a burnup of $\simeq$ 20,000 Mwd/Te ($\simeq$ 2 atom %). Both pins had an active fuel length of 24 in. with a 14.25 in. natural uranium blanket between the fuel and the gas plenum (He at 1 atm.). The test pins in this series were identical except the C5A blanket was composed of solid pellets, and the C5B blanket had annular pellets with a .07 in. I.D. (see Fig. 7.6). Due to the low power steady state irradiation ($\simeq$ 1840

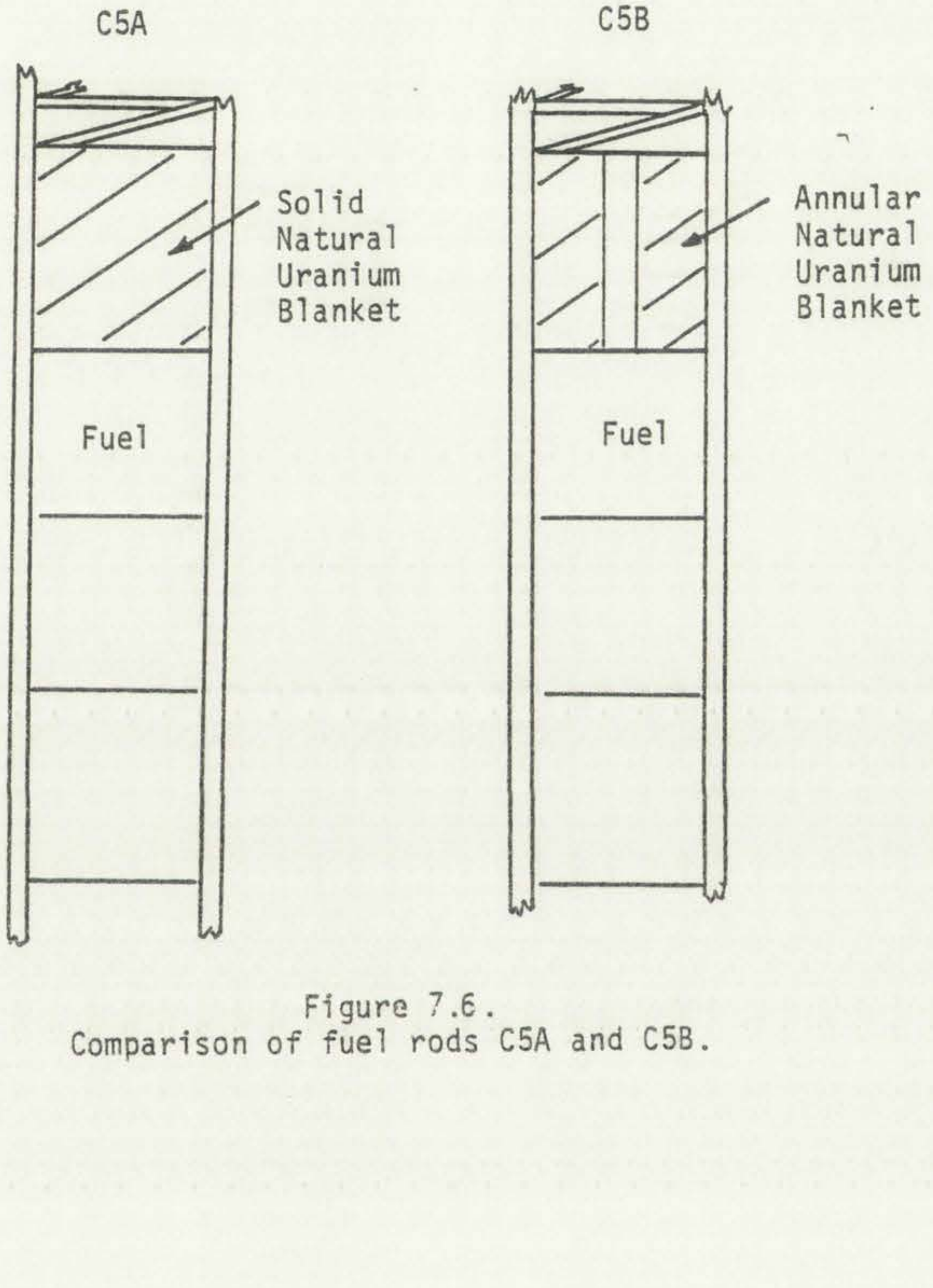

Figure 7.6.
Comparison of fuel rods C5A and C5B.

K peak fuel temperature and 850 K peak fuel surface temperature) no central void was formed; the fuel consisted of equiaxed and unrestructured grain regions, and thus the fission gas retention was high ($\simeq$ 32% equiaxed, 64% unrestructured[12]). The test train contained NaK between the test pin cladding and the heat sink.

The TREAT transients for the two tests were nearly identical. The transients had initial periods of 0.136 and 0.131 s with reactivity additions of 1.35% and 1.37% for test C5B and C5A respectively. This led to peak powers of 160 kW/ft for C5A and 155 kW/ft for C5B and maximum fuel temperature of $\simeq$3310 K. The pin was preheated to about 500 K, the transient duration was $\simeq$ 1 s and the integrated power was 339 cal/gm.

In test C5A (solid blanket pellets) cladding failure occurred, resulting in the expulsion of fuel into the coolant channel. Pin C5B, however, survived the transient intact and had extensive upward movement ($\simeq$ 10 in.) of molten fuel into the annular blanket. Posttest neutron radiography and inspection indicated that for both pins the central core of the fuel was molten ($\simeq$ 35%). As in Sec. 6 if one then assumes 2 atom % burnup, a fission gas retention of $\simeq$32% (melt region in equiaxed grain area), a surface tension of 450 ergs/cm[14,15] and 100% of the equiaxed gas in inter- and intragranular bubbles[12] (very little in solution), a possible volume expansion of 6% is calculated.

A post test examination was not a good [illegible] surface temperatures [illegible] control [illegible] the fuel [illegible] structural [illegible] the fission gas release [illegible] [illegible] agreement with [illegible]. The [illegible] between the [illegible] cladding and the heat sink.

The TREAT transients for the two tests were [illegible]. The transients had initial periods of [illegible] by additions of [illegible] for test CEN and CEB [illegible]. This led to peak powers of [illegible] for CEN and [illegible] and maximum fuel temperatures of [illegible]. The pin was preheated to about 500 K, the transient duration was [illegible] and the integrated power was 335 cal/gm.

In test CEN (solid blanket pellets) cladding failure occurred resulting in the expulsion of fuel into the coolant channel. [illegible] however, survived the transient intact and had extensive internal movement [illegible] of molten fuel into the annular channel. [illegible] neutron radiography and inspection indicated that the [illegible] central core of the fuel was molten [illegible]. As in [illegible] annular [illegible] however, [illegible] in [illegible] of the captured gas [illegible] little in solution), a possible [illegible]

This is also assuming no bubble coalescence or release. Release is very possible since ≃90% of the equiaxed gas is intergranular, however since no central void was initially present, it can be assumed that the gas remained trapped in the molten fuel volume. If one uses the higher surface tension (750 ergs/cm^2) of solid fuel and recalculate the volume expansion at fuel melting, taking into account the drop in surface tension, i.e. from 750 ergs/cm^2 for solid fuel to 450 ergs/cm^2 for liquid fuel with a corresponding drop in bubble pressure and corresponding increase in bubble radius, an additional increase of only a few percent can be expected. The fission gas expansion along with the expected 10% volume expansion upon fuel change of phase could be the driving force for the axial fuel motion. The annular blanket accommodated ≃ 11% of the molten fuel volume (≃ 4% of the total fuel volume) which apparently was sufficient to prevent clad failure. In this test it appears that fission gas is the most probable cause of axial fuel motion.

7.5 Test L5

The L5 test[16] was performed to simulate the behavior of moderate power fuel subjected to a hypothetical loss-of-flow driven transient overpower accident in an LMFBR. Three $(U_{.75}, Pu_{.25}) O_2$ fueled test elements irradiated in the General Electric Test Reactor (thermal) at 12.2 kW/ft to 8 atom % burnup were arranged in a triangular pattern in a closed sodium loop test train (MARK-II C). The test

pin plenums were bled to 1 atm. pressure and resealed to prevent premature cladding failure. The test pins consisted of a 34 in. active fuel length with 0.5 in. of UO_2 insulator pellets, and 3 in. of Inconel reflector separating it from the plenum. The sodium flow area (0.63 cm^2) is somewhat larger than the combined cross-sectional area (0.57 cm^2) of the three fuel elements.

To simulate the LOF driven TOP, the TREAT transient consisted of a constant power portion (nominal power of $\simeq$ 11 kW/ft) that lasted approximately 9 s. During this period flow coastdown was initiated and sodium boiling and flow reversal occurred. After channel voiding and at the calculated time of incipient clad melting, the pins were subjected to an assymetrical power burst. This was equivalent to about a 1% $\Delta k/k$ reactivity step, causing an average period in the rising portion of the power burst of about 835 ms. The target peak burst power of 10x nominal was not reached; in actuality the peak power was approximately 6x nominal (66 kW/ft). The burst was planned to keep the fuel temperature below 3870 K so that the dispersive effects of fuel vapor pressure would be relatively insignificant. Even at 3870 K the vapor pressure is on the order of 2-3 atms.

During the burst the fuel underwent a mild dispersal at or after (from hodoscope observations) the scram. This dispersal centered at the fuel column center, moved approximately 15% of the test fuel

axially in both directions 4-8 in. Again if one ignores surface tension effects and assumes 25% precipitation into bubbles, the fission gas may cause up to 1400% volume expansion assuming a bulk pressure of 1 atm. and a temperature rise of $\simeq$ 2000 K. If surface tension effects and are taken into account and if coalescence and equilibration effects ignored a volume expansion of 6% is obtained. These calculations are shown here.

exactly in both directions and the [illegible] of [illegible] surface
tension effects [illegible] 2% [illegible] the case of [illegible]
[illegible] pressure of
1 atm. and a temperature rise of ~ 2000 K. If surface tension effects
are taken into account and if coalescence and equilibration effects
[illegible], a better agreement of [illegible] is obtained. These calculations are
given below.

From Eq. (6.1)

$$V_2 - V_1 = nR\ (\frac{T_2}{P_2} - \frac{T_1}{P_1}) \quad .$$

At 8 atom % burnup (Table 6.1) assuming 42.2% average fission gas retention, assuming conservative 25%[12] of available gas in bubbles, ignoring surface tension effects, and assuming a bulk pressure of 1 atm.,

$$n = (2.999 \times 10^{-4} \text{ moles gas/cm}^3)\ (\tfrac{8}{3})\ (.42)\ (.25) \quad .$$

Assume

T_2 = 3023 K (Fuel melting temperature)

T_1 = 1000 K.

Then

$$V = (2.999 \times 10^{-4})\ (\tfrac{8}{3})\ (.422)\ (.25)\ (82.05\ \frac{\text{cm}^3\ \text{atm}}{\text{K}})\ (\frac{2023\ \text{K}}{1\ \text{atm}}) \times 100\%$$

$$= 1400\%$$

Using same assumptions, except taking into account surface tension effects, i.e. from Sec. 6,

$P_1 = 455$ atm

$P_2 = 273$ atm

Then

$$V = (2.999 \times 10^{-4})\ (\tfrac{8}{3})\ (.422)\ (.25)\ (82.05)\ (\tfrac{3023}{273} - \tfrac{1000}{455}) \times 100\%$$

$$= 6\%.$$

For a transient such as this where the temperature rise is rapid, coalescence and precipitation probably can be ignored in the initial short time span. However, since the transient analysis continues past scram and the fuel remains at elevated temperatures, coalescence, bubble growth, precipitation, etc. become important and may lead to substantial swelling in later stages of the transient as observed in this test. Since the fuel vapor pressure was deliberately kept low and since the dispersal seems to have occurred after peak power, it appears that fission gas was the mild dispersing force. The bubble pressure equilibration time of .1 to 1 s[17] for the coalescence of 2, 100 nm dia. bubbles at 3070 K is the right time frame for the dispersal experienced in this test. Microanalysis of the L5 fuel indicates that precipitation and growth of intragranular bubbles occur.

The vapor pressure of the fuel as well as that of the mixed oxide homogeneous metallic inclusions discussed previously, are both on the order of 1-2 atm. As stated in Sec. 2, the fuel composition and irradiation temperature affect the final inclusion composition more than the irradiation spectrum. One thus would not expect the LWR inclusions found by Jeffery.[10] If Jeffery's type of inclusion were present, their high vapor pressure (see Fig. 5.18) and the high burnup would have led to a rapid and large fuel dispersal which was not experienced in this test.

For a transient such as this one where the power change rate is rapid, this behavior and precipitation probably can be ignored in the initial short time span. However, since the transient analysis continues past scram and the fuel reaches a liquid temperature, coalescence, bubble growth, precipitation, etc. become important and may lead to substantial swelling in later stages of the transient as observed in this test. Since the fuel vapor pressure was sufficiently high too and since the dispersal seems to have occurred after peak power, it appears that fission gas was the main dispersing force. The bubble pressure was likely on the order of .1 to 1 s.[17] For the coalescence of 2, 100 nm dia. bubbles at 2000 K is the right time frame for the dispersal experienced in this test. Microanalysis of the fuel indicates that precipitation and growth of large, smaller bubbles occur.

The vapor pressure of the fuel as well as that of the mixed oxide nongaseous metallic inclusions discussed previously, are both on the order of 1-2 atm. As stated in Sec. 2, the fuel composition and irradiation temperature affect the final inclusion composition more than the irradiation spectrum. One thus would not expect the LMR inclusions found by Jeffery.[16] If Jeffery's type of inclusion were present, their high vapor pressure (see Fig. 2.18), and the high barium would have led to a rapid and large fuel dispersal which was not experienced in this test.

The above experimental analyses is summarized in Table 7.3 and support the fact that fission gas and other highly volatile fission products (Cs, etc.) may contribute to fuel dispersal. However, in tests C5B, F1, E7, and H4 metallic inclusions were present in the post-test metallographic examination. No microprobe analysis was done to assure that the inclusions were in fact solid fission products of roughly the same composition as found in "as irradiated" fuel. Their size, i.e. microns in diameter, support solid fission product inclusions rather than dispersed clad and their posttransient presence supports the homogeneous inclusion state.

TABLE 7.3

SUMMARY OF EXPERIMENTAL FUEL MOTION

Test	Pre- or Postfailure Motion	Postulated Mechanisms
E1	Prefailure	~10% volume expansion due to fuel change of phase, possibly fuel vapor pressure.
H2	Prefailure	Same as E1.
E4	Prefailure	Same as E1.
F2	Postfailure (LOF)	Fuel vapor pressure.
EOS-1	Postfailure (LOF)	Stainless steel vapor pressure.
EOS-2	Postfailure (LOF)	Fission gas fuel breakup, stainless steel vapor pressure.
EOS-3	Postfailure (LOF)	Fission gas fuel breakup stainless steel vapor pressure.
C5B	Prefailure	Fission gas.
L5	Postfailure (LOF)	Fission gas.

REFERENCES

1. L. W. Deitrich, R. C. Doerner, T. H. Hughes, A. E. Wright, "Summary and Evaluation - Fuel Dynamics Transient Overpower Experiments," Argonne National Laboratory report ANL/RAS 74-8 (June 1974).

2. R. C. Doerner, W. F. Murphy, G. S. Stanford, and P. H. Froehle, "Final Summary Report of Fuel Dynamics Test E7," Argonne National Laboratory report ANL/RAS 76-32 (November 1976).

3. A. E. Wright, C. L. Fink, L. R. Kelman, L. W. Deitrich, R. T. Purviance, R. W. Mouring, A. B. Rothman, and C. E. Dickermann, "Transient Overpower Meltdown Test H4 on FFTF-Type, High-Power Irradiated Fuel," Argonne National Laboratory report ANL/RAS 76-9 (December 1976).

4. R. G. Palm, S. M. Gehl, R. R. Stewart, A. De Volpi, and A. B. Rothman, "F1 Phenomenological Test on Fuel Motion (Interim Report)," Argonne National Laboratory report ANL/RAS 76-11 (March 1976).

5. R. G. Palm, R. R. Stewart, S. M. Gehl, A. B. Rothman, A. De Volpi, "Loss-of-Flow Test F1 on a FFTF-Type Fuel Element," ANS Trans. San Francisco. California, 22, (November 16-21, 1975) pp. 427-428.

6. R. G. Palm, C. L. Fink, R. R. Stewart, S. M. Gehl, and A. B. Rothman, "F2 Phenomenological Test on Fuel Motion (Interim Report)," Argonne National Laboratory report ANL/RAS 76-29 (September 1976).

7. R. G. Palm, S. M. Gehl, C. L. Fink, R. R. Stewart, A. B. Rothman, A. De Volpi, "F2 Phenomenological Test on Fuel Motion," ANS Trans. Toronto, Canada, 23, (June 14-18, 1976) pp. 354-356.

8. D. R. O'Boyle, F. L. Brown, and J. E. Sanecki, "Solid Fission Product Behavior in Uranium-Plutonium Oxide Fuel Irradiated in a Fast Neutron Flux," Journal of Nuclear Materials 29, (1969) pp. 27-42.

9. P. E. Blackburn, C. E. Johnson, et al., "Chemical Engineering Division Fuels and Material Chemistry Semi-annual Report, July-December 1971," Argonne National Laboratory report ANL-7877 (April 1972).

10. B. M. Jeffery, "Microanalysis of Inclusions in Irradiated UO$_2$," Journal of Nuclear Materials 22, (1967) pp. 33-40.

11. J. P. Tylka, A. B. Rothman, and P. H. Froehle, "Preliminary Data Report TREAT Tests EOS-1, EOS-2, and EOS-3," Argonne National Laboratory report ANL/RAS 78-17 (March 1978).

12. D. Stahl and T. J. Patrician, "Fission-Gas Behavior During a Mild Overpower Transient," Argonne National Laboratory report ANL-8069 (February 1974).

13. T. Hidiko and J. H. Field, "Molten Fuel Movement in Transient Overpower Tests of Irradiated Oxide Fuel," General Electric Company report GEAP-13543 (September 1969).

14. L. Leibowitz, E. C. Chang, M. G. Chasanov, R. L. Gibby, C. Kim, A. C. Millunzi, D. Stahl, "Properties for LMFBR Safety Analysis," Argonne National Laboratory report ANL-CEN-RSD-76-1 (March 1976).

15. P. S. Maiya, "Surface Diffusion, Surface Free Energy, and Grain-Boundary Free Energy of Uranium Dioxide," Journal of Nuclear Materials 40, (1971) pp. 57-65.

16. R. Simms, S. M. Gehl, R. K. Lo, and A. B. Rothman, "Loss-of-Flow Test L5 on FFTF-Type Irradiated Fuel," Argonne National Laboratory report ANL/RAS 77-24 (July 1977).

17. L. W. Deitrich and R. W. Ostensen, "An Assessment of Fission-Gas-Driven fuel Disruption and Dispersal in a Hypothetical LMFBR Loss-of-Flow-Accident," Argonne National Laboratory report ANL/RAS 77-4 (February 1977).

8. SUMMARY

In analyzing the free energy of formation of the various fission products of UO_2 and $(Pu, U)O_2$, their general chemical state can be determined. the fission products can be broken into four general categories:

1. stable gases,
2. stable oxides,
3. stable metallics, and
4. molybdenum, which has an oxygen potential very close to that of the fuel.

Of interest here are metallic fission products which exist as aggregrate inclusions throughout the fuel, and which upon heating can vaporize, providing a possible driving force for fuel motion. Fission products that exist as gases during normal reactor operating temperatures such as xenon and krypton, are swept out of the columnar and equiaxed fuel regions and are analyzed as a comparison contribution to fuel swelling. The stable oxides in general, are present in solution form within the fuel matrix and thus, cannot volatilize preferentially. However, in the metallurgical analysis of irradiated nuclear reactor fuel rods, fission product inclusions, approximately 5 microns in diameter, consisting mainly of molybdenum and stable metallic elements, have been found both in LMFBR (mixed oxide) and LWR (uranium

dioxide) fuels. since some metallic fission products have lower vaporization temperatures than the fuel itself, such metallic inclusions have the potential to volatilize during overheating events. An assessment of the potential contribution of such metallic inclusions to fuel motion, during postulated accident overheating events, was assessed for the first time in this work.

For an LMFBR inclusion (Johnson type), if the metallic constituents are assumed completely immiscible and for a bulk fuel rod internal pressure of 20 atm a maximum inclusion nodal volume expansion of $\simeq$ 26% and a total fuel column volume expansion of $\simeq$ 1-1/2$ was calculated at incipient fuel vaporization. This is based on an assumption of a flat distribution profile in the number density of inclusions and the Ideal Gas EOS for the vapor. The Redlich-Kwong EOS, which appears more applicable than the Ideal Gas, van der Waals, or the modified hard-sphere EOS, did not change the results significantly. However, when a representative radial distribution in the inclusion number density is incorporated, a maximum nodal volume expansion of $\simeq$ 11.5% can be expected. If the radial inclusion number density profile is used, the total fuel pin volume expansion also drops from 1.5 to 1% at incipient fuel vaporization.

If the inclusion constituents are assumed to be completely miscible in one another, the vapor pressure of the such single-phase inclusions are calculated using Raoult's Law of Partial Pressure. This assumption is supported by thermodynamic solution consideration and by established binary and tenary phase diagrams. The vapor pressure for

such miscible inclusions is assessed to be less than the fuel vapor pressure, in the temperature and pressure ranges of interest. As a result, incipient fuel vaporization is expected prior to metallic inclusion volatilization. If partial solubility is assumed in the same molar ratio as the original inclusion composition, the insoluble fraction will have a linear effect on the volume expansion of the inclusion.

For inclusions found in typical LWR fuel (Jeffery type), the miscible inclusion vapor pressure was assessed to be much greater than that of the fuel, due to the presence of highly volatile elements including Ba, Sr, and Te, which are not found in the inclusions analyzed from LMFBR type fuel. the high vapor pressure estimate for LWR type inclusions leads to an estimated total fuel rod volume expansion of 40% at 2800 K, an estimated nodal volume expansion of 62% at incipient fuel melting, and an estimated nodal volume expansion of 114% at incipient fuel vaporization. Thus, it appears that metallic inclusions found in LWR fuel may contribute to fuel swelling during an overheating situation.

Steady-state fission gas retention (thus the amount of gas available for transient fuel swelling and dispersal) is dependent on burnup, irradiation power and temperature, and initial fuel conditions. Transient swelling is also dependent on the transient conditions experienced by fuel. Fission gas release, bubble coalescence, bubble pressure equilibration, surface tension effects, etc., are contingent upon the time-temperature (power) transient. From experimental such volatile inclusions is expected to be less than the fuel vapor pressure, in the temperature and pressure ranges of interest. As a result, inclusion fuel vaporization is expected prior to appreciable [illegible] volatilization. If partial volatility is assumed [illegible] molar ratio as the original inclusion composition, the volatile fraction will have a similar effect on the volume expansion of the inclusion.

For inclusions found in typical LWR fuel (Cubicciotti 1984), the effective inclusion vapor pressure was assessed to be much greater than that of the fuel, due to the presence of highly volatile elements, including Ba, Sr, and Te, which are not found in the inclusions analyzed from LMFBR type fuel. The high vapor pressure estimate for LWR type inclusions leads to an estimated total fuel rod volume expansion of [illegible] at 2800 K, an estimated model volume expansion of [illegible] at [illegible] melting, and an estimated model volume expansion of [illegible] at [illegible] fuel vaporization. Thus, it appears that metallic inclusions found in LWR fuel may contribute to fuel swelling during an overpower situation.

Steady-state fission gas retention (that fraction of fission gas available for transient fuel swelling and dispersal) is dependent on burnup, irradiation power and temperature, and initial fuel conditions. Transient swelling is also dependent on the transient conditions experienced by fuel. Fission gas release, [illegible] [illegible] pressure equilibration, and the transient effects of [illegible] [illegible] the high-temperature (molten) transients. [illegible] evidence it appears that for very slow transients (i.e. seconds, at or near design power), fission gas release from the fuel is greater than bubble growth, with the net result of slumping and drainage versus fuel swelling. However, for extremely rapid transients (i.e. milliseconds, at high powers 10 to 100 times design levels) it appears that intergranular fission gas may contribute to fuel breakup (dependent on steady-state irradiation history) but that coalescence and pressure equilibration of intragranular bubbles does not have time to occur during the transient itself. After scram, however, coalescence and equilibration may cause a mild dispersal or foaming of the fuel. As demonstrated by Deitrich[1] and equilibration time for the coalescence of 2 bubbles of 100 nm radius is assessed to be approximately 0.3 s. It thus appears that neither fission gas bubble growth or thermal expansion due to change-of-phase from solid to molten fuel will dominate the possible volume expansion effects from vaporization of homogeneous metallic inclusions found to occur in UO_2 fuel irradiated at thermal neutron energies. Thus, serious consideration should be given to the modeling of metallic inclusions for incorporation into LWR fuel behavior codes for accident analysis. However, this would not be the case for LMFBR fuels based on the analysis presented in this work. This is due to the fact that metals with rather high vaporization temperature are characteristically found in LMFBR type inclusion, indicating that fuel expansion by volatilization of homogeneous LMFBR type inclusions would be negligible.

evidence it appears that for very high burnups [illegible] over metal density, fission gas release from the fuel [illegible] highly probable, with the net result of [illegible] swelling. However, for extremely rapid [illegible] at high powers 10 to 100 times design [illegible] effect of fission gas may contribute to [illegible] steady-state irradiation history) but that [illegible] and formation of [illegible] bubbles does not [illegible] during the transient itself. After which, however, [illegible] equilibrium may cause a mild dispersal or [illegible] demonstrated by [illegible] and equilibration [illegible] of 2 bubbles of 100 [illegible] radius is [illegible] It thus appears that neither fission gas bubble [illegible] part of due to change of phase from solid to [illegible] the possible volume expansion effects from [illegible] metallic inclusions tend to occur in UO2 fuel [illegible] reactor samples. Thus, melting considerations [illegible] modeling of metallic inclusions for incorporation [illegible] earlier model for accident analysis. However, [illegible] tion for LMFBR fuels based on the analysis [illegible] This is due to the fact that metals with [illegible] temperature are characteristically found in LMFBR [illegible] indicating that fuel expansion by solidification [illegible] type inclusions would be negligible.

REFERENCE

1. L. W. Deitrich and R. W. Ostensen, "An Assessment of Fission-Gas-Driven Fuel Disruption and Dispersal in a Hypothetical LMFBR Loss-of-Flow Accident," Argonne National Laboratory report ANL/RAS 77-4 (February 1977).

9. CONCLUSIONS AND RECOMMENDATIONS

The question of assessing the effect of metallic inclusions, found to occur in irradiated fuel, on fuel motion during an overpower transient depends upon an accurate understanding of constituent solubility. The question of whether the various metal species found within the inclusions of irradiated nuclear fuel elements are either segregated or in a homogeneous solution cannot be answered theoretically, since an analytical basis does not exist to construct multicomponent phase diagrams from first principles. Thus, such a question must be resolved experimentally if one is to be able to accurately assess with assurance the role metallic inclusion volitalization has on fuel behavior phenomena for high temperature overheating reactor transients. It is suggested that a metallurgical sample be prepared of the same metal species composition as found to occur for the inclusion of typical irradiated fuel rods. This sample could be heated to *in situ* temperatures and analyze to determine its metallographic structure, i.e. its phases and transition temperatures, as well as the total vapor pressure vs. temperature characteristics.

Based upon existing information an educated guess can be made that the metallic inclusions will not contribute to fuel motion for LMFBR type inclusions. The assumption that the inclusions are single-phase, i.e. totally miscible, is strongly supported not conclusively proven. However, fuel behavior assessment for LWR accident analysis

[illegible] CONCLUSIONS AND RECOMMENDATIONS

[illegible]

found to occur in irradiated fuel, a great deal [illegible]

predicted through such an approach (calculations of [illegible]

ability. The question of whether the various metal [illegible]

the behavior of irradiated nuclear fuel elements are [illegible]

metal or in a homogeneous solution cannot be answered [illegible]

Since an analytical basis does not exist to construct multi[illegible]

phase diagrams from first principles. Thus, such a question [illegible]

resolved experimentally if one is to be able to accurately [illegible]

estimate the role metallic inclusion solidification has in [illegible]

reactor performance for high temperature overheating reactor [illegible]

It is suggested that a metallurgical sample be prepared of the exact

metal inclusion composition as found to occur for the inclusion of [illegible]

cal irradiated fuel rods. This sample would be heated to [illegible]

temperatures and analyzed to determine its metallographic [illegible]

i.e., its phases and transition temperatures, as well as [illegible]

pressure vs. temperature characteristics.

Based upon existing information an educated guess can be made

that the metallic inclusions will not contribute to fuel melting [illegible]

LMFBR type fuel pins. The assumption that the inclusions are [illegible]

phase, [illegible] totally miscible, is strongly supported [illegible]

present. However, fuel behavior [illegible] for the [illegible] may have to consider the metallic inclusion contribution to fuel swelling during an accident transient. Large fuel volume expansion due to the vaporization of the inclusions, both assuming the inclusion constituents are totally miscible and immiscible, can be expected, due to the presence of the highly volatile species of Barium, Strontium, and Tellurium found to exist in LWR type inclusions (which are not found in LMFBR type inclusions). Further investigation, however, should be done in the area of inclusion composition assessment. Comparison of expected volume expansion due to LWR type inclusion vaporization with fission gas bubble expansion and volume expansion due to UO_2 change-of-phase from solid to melt, indicates that inclusion volatilization may be as great or greater than these two effects, thus, metallic LWR type inclusions may provide a substantial fuel motion driving force during a transient overheating situation.

Other factors which were not included in this analysis, but should be considered in future work in this area are:

1. Separate oxide inclusion contribution.
2. Bubble growth dynamics at inclusion vaporization.
3. More realistic fuel pin geometry, i.e., central void, fuel swelling and closure of bond gap, fuel cracking and thus possible communication of central void and outer fuel surface.
4. Differential thermal expansion of fuel and clad and thus differing geometry.
5. Fuel-clad shear drag opposing free expansion of fuel nodes.
6. Temperature dependence of physical parameters, i.e., heat capacity, density, thermal conductivity, etc.
7. Time (temperature) dependence of bulk and local pressures.
8. Inclusion volitalization analysis for such advanced concept fuels as UC, which have higher fission product retention characteristics.

APPENDIX A

DERIVATION OF THE FREE ENERGY OF FORMATION (Eq. 2.1)

From Gibb's free energy,

$$\Delta F = \Delta H - T\Delta S \quad , \qquad \text{(A-1)}$$

where

ΔF = free energy,

ΔH = enthalpy,

T = temperature,

ΔS = entropy.

Let heat capacity, C_p, be represented in the form of a power series

$$C_p = f(T) = \Delta a + (\Delta b \times 10^{-3})\ T + (\Delta c \times 10^{-6})\ T^2 + \frac{\Delta d \times 10^5}{T^2} \quad , \qquad \text{(A-2)}$$

where Δa, Δb, Δc, Δd are empirical coefficients. Thus,

$$\Delta H = \Delta H_T - \Delta H_{298} = \int_{298}^{T} C_p dt = \Delta a\ (T - 298) + \tfrac{1}{2}\ (\Delta b \times 10^{-3})\ (T^2 - 298^2)$$

$$+ \frac{1}{3}\ (\Delta c \times 10^{-6})\ (T^3 - 298^3) - (\Delta d \times 10^5)\ (\frac{1}{T} - \frac{1}{298}) \quad ,$$

$$= (\Delta a)T + \tfrac{1}{2}\ (\Delta b \times 10^{-3})\ T^2 + \frac{1}{3}\ (\Delta c \times 10^{-6})\ T^3 - \frac{\Delta d \times 10^5}{T} + \Delta A \ , \quad \text{(A-3)}$$

DERIVATION OF THE FREE ENERGY OF FORMATION EQN. (A-3)

From Gibb's free energy,

$$\Delta F = \Delta H - T\Delta S \; , \qquad (A-1)$$

where

ΔF = free energy,

ΔH = enthalpy,

T = temperature,

ΔS = entropy.

Let heat capacity, C_p, be represented in the form of a power series

$$C_p = f(T) = \Delta a + (\Delta b \times 10^{-3})\,T + (\Delta c \times 10^{-6})\,T^2 + \frac{\Delta d \times 10^5}{T^2} \; , \qquad (A-2)$$

where Δa, Δb, Δc, Δd are empirical coefficients. Thus,

$$\Delta H = \Delta H_T - \Delta H_{298} = \int_{298}^{T} C_p\,dT = \Delta a\,(T - 298) + \tfrac{1}{2}\,(\Delta b \times 10^{-3})\,(T^2 - 298^2)$$

$$+ \tfrac{1}{3}\,(\Delta c \times 10^{-6})\,(T^3 - 298^3) - (\Delta d \times 10^5)\left(\frac{1}{T} - \frac{1}{298}\right)$$

$$-\Delta H(T) = \tfrac{1}{2}\,(\Delta b \times 10^{-3})\,T^2 + \tfrac{1}{3}\,(\Delta c \times 10^{-6})\,T^3 - \frac{\Delta d \times 10^5}{T} + \Delta H_0 \qquad (A-3)$$

where

$$\Delta A = -298\ \Delta a - \tfrac{1}{2}\ (\Delta b \times 10^{-3})\ (298^2) - \frac{1}{3}\ (\Delta c \times 10^{-6})\ (298^3)$$

$$+ \frac{\Delta d \times 10^5}{298}\ , \qquad \text{(A-4)}$$

$$\Delta S = \Delta S_T - \Delta S_{298} = \int_{298}^{T} \frac{c_p}{T}\, dT\ ,$$

$$= \Delta a\ \ell n\ \left(\frac{T}{298}\right) + (\Delta b \times 10^{-3})\ (T - 298) + \tfrac{1}{2}\ (\Delta c \times 10^{-6})\ (T^2 - 298^2)$$

$$- \tfrac{1}{2}\ (\Delta d \times 10^5)\ \left(\frac{1}{T^2} - \frac{1}{298^2}\right)\ ,$$

$$= \Delta a\ \ell n\ T + (\Delta b \times 10^{-3})\ T + \tfrac{1}{2}\ (\Delta c \times 10^{-6})\ T^2 - \frac{\tfrac{1}{2}\ (d \times 10^5)}{T^2} - B' \qquad \text{(A-5)}$$

$$B' = \Delta a\ \ell n\ (298) + (\Delta b \times 10^{-3})\ (298) + \frac{1}{2}\ (\Delta c \times 10^{-6})\ (298^2)$$

$$- \frac{1}{2}\ (\Delta d \times 10^5)\ \left(\frac{1}{298^2}\right)\ , \qquad \text{(A-6)}$$

$$\Delta S_T = 2.303\ \Delta a\ \log T + (\Delta b \times 10^{-3})\ T + \tfrac{1}{2}\ (\Delta c \times 10^{-6})\ T^2$$

$$- \frac{\tfrac{1}{2}\ (\Delta d \times 10^5)}{T^2} - B\ , \qquad \text{(A-7)}$$

where

$$B = B' - \Delta S_{298},$$

since

$$\Delta F_T = \Delta H_T - T\Delta S_T,$$

$$\Delta F_T - \Delta H_{298} = (\Delta H_T - \Delta H_{298}) - T\Delta\, S_T = -(2.303\ \Delta a)\ T \log T$$

$$- \tfrac{1}{2}\,(\Delta b \times 10^{-3})\ T^2 - \frac{1}{6}\,(\Delta c \times 10^{-6})\ T^3 \qquad \text{(A-8)}$$

$$- \frac{\tfrac{1}{2}\,(\Delta d \times 10^5)}{T} - T\Delta\,(B - a) + \Delta A \quad .$$

APPENDIX B

CALCULATION OF CRITICAL POINT OF METALS

From Young and Alder[1]

$V_c = 2.417 \times 10^{24}\ \sigma^3$ $T_c = .7232\ a/RV_c$,

$P_c = .2596\ a/V_c^2$ $Z_c = P_cV_c/RT_c = .3590$,

$a = -\ E_oV_o$,

where

R = gas constant = .08205 ℓ-atm/K mole,

σ = diameter of metal atoms*,

E_o = molar cohesive energy in solid state,

V_o = molar volume of the metal in solid state,

---

*Young and Alder[1] calculated σ by fitting the first peak of the Percus-Yevick Hard-sphere structure factor S(K) to the experimental curves for liquid metals,[2] finding

$$\nu \simeq .45 = \frac{1}{6}\pi N_o\sigma^3/V_L \quad .$$

The molar volume V_L of the metal must be known at the melting point to find σ. It was found that the metallic diameters given in Ref. 3 were very close to those calculated by Young and Alder and thus were used.

TABLE B.1

CALCULATED CRITICAL VALUES

Element	E_o(cal)	V_o(cm^3)	(cm)	V_c (cm^3/mole)	P_c(atm)	T_c(K)	Z_c
TE	4.66E+04	2.05E+01	2.74E-08	4.97E+01	4.13E+03	6.98E+03	3.59E-01
BA	4.28E+04	3.81E+01	3.96E-08	1.50E+02	7.76E+02	3.95E+03	3.59E-01
CE	9.79E+04	2.07E+01	3.29E-08	8.61E+01	2.93E+03	8.57E+03	3.59E-01
FE	9.94E+04	7.09E+00	2.34E-08	3.10E+01	7.88E+03	8.28E.03	3.59E-01
PD	8.99E+04	8.88E+00	2.57E-08	4.10E+01	5.08E+03	7.08E+03	3.59E-01
SB	6.23E+04	1.82E+01	2.78E-08	5.19E+01	4.51E+03	7.95E+03	3.59E-01
HG	1.54E+04	1.41E+01	2.77E-08	5.14E+01	8.81E+02	1.54E+03	3.59E-01
CS	1.92E+04	6.92E+01	4.70E-08	2.51E+02	2.26E+02	1.93E+03	3.59E-01

REFERENCES

1. D. A. Young and B. J. Alder, "Critical Point of Metals from the van der Waals Model," Physical Review A, Vol. 3, No. 1, (January 1971) pp. 364-371.

2. N. W. Ashcroft and J. Lekner, "Structure and Resistivity of Liquid Metals," Physical Review, Vol. 145, No. 1, (May 1966) pp. 83-90.

3. L. Pauling, The Nature of the Chemical Bond (Cornell U. P., Ithica, New York, 1960) third edition.

APPENDIX C
VAN DER WAALS EQUATION-OF-STATE

The van der Waals equation-of-state takes into account the attractive force between molecules as well as the finite size of the molecules. The pressure exerted by a gas is due to molecular collision with the boundary. The attractive force, however, pulls molecules away from the boundary, due to the nonisotropic conditions which exist at the boundary and is proportional to n, molecules/unit volume. The number of molecules striking the boundary is also proportional to n, thus the total force $\propto n^2 \propto \frac{1}{v^2}$, where v is the molar volume.

Thus,

$$\text{corrected ideal pressure} = P\ (\text{observed pressure}) + \frac{a}{v^2}\ . \qquad (C\text{-}1)$$

Also, to take into account the finite volume of the molecules,

$$\text{corrected ideal volume} = V(\text{total molar volume}) - b\ (\text{correction term due to the volume of the molecules}). \qquad (C\text{-}2)$$

Using Ideal Gas equation:

$$(\text{ideal volume})\ (\text{ideal pressure}) = RT, \qquad (C\text{-}3)$$

one obtains the van der Waals equation

$$(v - b)\left(P + \frac{a}{v^2}\right) = RT \quad , \qquad \text{(C-4)}$$

or

$$P = \frac{RT}{v - b} - \frac{a}{v^2} \quad . \qquad \text{(C-5)}$$

The critical isotherm passes through a point of inflection at the critical point, where the slope is zero; thus from Eq. (C-5)

$$\left.\frac{\partial P}{\partial v}\right)_T = \frac{-RT}{(v - b)^2} + \frac{2a}{v^2} = 0 \quad , \qquad \text{(C-6)}$$

$$\left.\frac{\partial^2 P}{\partial v^2}\right)_T = \frac{2RT}{(v - b)^3} - \frac{6a}{v^4} = 0 \quad . \qquad \text{(C-7)}$$

Also from Eq. (C-5), at the critical point

$$P_c = \frac{RT_c}{(v_c - b)} - \frac{a}{v_c^2} \quad . \qquad \text{(C-8)}$$

Using Eqs. (C-6), (C-7), and (C-8) solve for a and b

$$a = \frac{27\ RbT_c}{8} \quad , \qquad \text{(C-9)}$$

$$b = \frac{v_c}{3} \quad . \qquad \text{(C-10)}$$

[illegible]

The critical isotherm passes through a point [illegible]

critical point, where the slope is zero; thus from [illegible]

[illegible]

[illegible]

With from Eq. (C-8), at the critical point

[illegible]

Using Eqs. (C-9), (C-10), and (C-11), solve for a and

[illegible]

[illegible]

In a rearrangement of the equations, one obtains

$$\frac{RT_c}{P_c V_c} = \frac{8}{3} = 2.67 \quad , \qquad \text{(C-11)}$$

thus if the van der Waals EOS is accurate, $\frac{RT_c}{P_c V_c}$ is approximately constant irrespective of the nature of the substance. However, values of 3.18 for He,[1] 3.42 for oxygen,[1] and 2.79 for Pd (using the critical values calculated previously) have been found, indicating that a more complicated function for the attractive-repulsive forces between molecules is required. The van der Waals EOS is more appropriate for higher pressures than the Ideal Gas EOS, but still its error is significant far below the critical point conditions.

REFERENCE

1. S. Glasstone and D. Lewis, Elements of Physical Chemistry (D. Van Nostrand Co., Inc., Princeton, New Jersey, 1960) second edition.

APPENDIX D

EOS CALCULATION USING HARD-SPHERE PRESSURE MODIFIED BY VAN DER WAALS MEAN-FIELD APPROXIMATION TO COHESIVE ENERGY

The mean field approximation of the cohesive energy used in the classical van der Waals model is:

$$E = -a/ac \quad , \qquad \text{(D-1)}$$

where

a = positive constant.

The free electron theory for the cohesive energy generally assumed for a dense metallic phase, is of the form:

$$E = \frac{A}{V^{1/3}} + \frac{B}{V^{2/3}} + \frac{c}{ac} + D \quad , \qquad \text{(D-2)}$$

and provides a fairly accurate description at high fluid density. At lower densities, substantial deviation of the theoretical and experimental values occur since the electrons attach themselves to the ions. There is evidence that this metal-nonmetal transition occurs near the critical density. At metal vapor densities lower than the critical density, which will be the expected range of interest in this study, the vapor will behave like a normal imperfect gas and at very low

densities the energy will vary as V^{-1} rather than $V^{-1/3}$, thus supporting the use of the mean-field approximation.

A refined equation for the energy, based on the free electron theory,

$$E = \frac{A}{V^{1/3}} + \frac{B}{(V - V_i)^{2/3}} \quad , \tag{D-3}$$

includes the volume, V_i, excluded from the electrons by the ion cores. It represents a more realistic behavior at the energy minimum but still fails at low density.

Due to the uncertainty in the validity of the free-electron theory and the lack of experimental data in the critical region, the use of the mean-field approximation to the cohesive energy appears justified. The mean-field approximation yields a pressure, using Eq. (D-1) of

$$\frac{-\partial E}{\partial V} = \frac{-a}{V^2} \quad , \tag{D-4}$$

so that the first-order perturbation theory is

$$P = P_o - a/V^2 \quad , \tag{D-5}$$

where

P_o = hard-sphere pressure,

duct that the energy will vary as $V^{-1/2}$ rather than $V^{-1/3}$, thus supporting the use of the mean-field energy equation.

A refined equation for the energy, based on the free-electron theory,

$$E = \frac{A}{V^{2/3}} + \frac{B}{(V - V_c)^{1/3}} \qquad (5\text{-}43)$$

includes the volume V_c excluded from the electrons by the ion cores. It represents a more realistic behavior of the energy minimum but still fails at low density.

Due to the uncertainty in the validity of the free-electron theory and the lack of experimental data in the critical region, the use of the mean-field approximation to the cohesive energy appears justified. The mean-field approximation yields a pressure, using Eq. (5-3) of

$$-\frac{a}{V^2} \qquad (5\text{-}44)$$

so that the first-order perturbation theory is

$$P = P_0 - a/V^2 \qquad (5\text{-}45)$$

where

P_0 = hard-sphere pressure.

$$P_o = \frac{RT}{V} \quad \frac{1 + \nu + \nu^2 - \nu^3}{(1 - \nu)^3} , \qquad \text{(D-6)}$$

where

$$\nu = \frac{\pi N_o \ \sigma^3}{6V} ,$$

where

σ = hard-sphere diameter,

N_o = avogadro's number,

a(from Eq. D-1) = $-E_o \ V_o$.

The subscripts on the molar cohesive energy and molar volume refer to a reference state where the hard spheres are uninfluenced by the attractive potential. Since almost no experimental data is available for supercritical fluid near normal liquid density for metals, values for E_o and V_o for metals in the solid state are used. This approximation is supported by the closeness of "a" for solid and liquid mercury.

Thus

$$P = \frac{RT}{V} \quad \frac{1 + \nu + \nu^2 - \nu^3}{(1 - \nu)^3} - \frac{E_o \ V_o}{V} ,$$

where the first order perturbation term includes the attractive potential found to be significant for liquid metals.

$$\rho_0 = [illegible]$$

where

$$[illegible]$$

where

σ [illegible] = hard-sphere diameter,

N_0 = Avogadro's number,

Also from Eq. (9.1) [illegible]

The subscripts on the solar cohesive energy and [illegible] refer to the reference state where the hard spheres are under [illegible] of the attractive potential. Since almost no [illegible] a conventional fluid mean [illegible] liquid [illegible] ϵ_c and [illegible] for metals in the solid state are [illegible] which is supported by the closeness of [illegible] for solid and liquid mercury.

Thus

$$[illegible]$$

where the first order perturbation term [illegible] to be significant for liquid metals.

Due to the above assumptions one would expect this EOS to be more accurate at low densities, where the mean-field approximation is more appropriate. For higher densities, however, the modified free electron theory may be more suitable.

APPENDIX E
REDLICH-KWONG EQUATION-OF-STATE

The Redlich-Kwong is a generalized equation-of-state, Eq. (1) that is more accurate than the van der Waals EOS.

$$P = \frac{RT}{v-b} - \frac{a}{v(v+b)\,T^{\frac{1}{2}}} , \qquad \text{(E-1)}$$

where

$$a = .4275 \frac{R^2 \; T_c^{5/2}}{P_c} ,$$

$$b = .0866 \frac{RT_c}{P_c} ,$$

and subscripts denote critical value. The numerical values have been determined empirically to give a good fit at moderate densities. Expanding Eq. (1) in terms of v:

$$(P)v^3 + (-RT)\;v^2 + \left(\frac{a}{T^{\frac{1}{2}}} - Pb^2 - RTb\right)\,v + \left(-\,\frac{ab}{T^{\frac{1}{2}}}\right) = 0 \;. \qquad \text{(E-2)}$$

This EOS has been used frequently for hydrocarbons and mixture calculations.

APPENDIX F

PROGRAM COMPARING VARIOUS EQUATIONS-OF-STATE

```
      PROGRAM SKI (INPUT,TAPE11)
      DIMENSION EO(12),VO(12),SIG(12),ELEM(12),A(12),VC(12),TC(12),
     1PC(12),ZC(12),BB(12),AA(12),PCHK(12),C(4),E(6),VM(3),PCALC(3),
     1ZERO(3),CRK(4),ERK(5)
      CALL CHANGE(2R+B)
C     NN=NUMBER OF ELEM. IN INPUT
      NN=8
      AV=6.023E23
      PI=3.14159
      SM=1.E-4
      R=82.05
C
C     UNITS:V IN CMS**3, P IN ATM, T IN DEG. K
C
C     READ INPUT, CALC. CRIT. VALUES, AND VAN DE WAALS CONSTS.
C     E IN CAL., VO IN CMS**3, SIG IN CMS.
   10 DO 15 I=1,NN
      READ(2,210) ELEM(I),EO(I),VO(I),SIG(I)
      A(I)=EO(I)*VO(I)
      VC(I)=2.417E24*SIG(I)**3
      TC(I)=.7232*A(I)/(1.987*VC(I))
      PC(I)=.2596*A(I)*82.05/(1.987*VC(I)**2)
      ZC(I)=PC(I)*VC(I)/(TC(I)*82.05)
      BB(I)=VC(I)/3.0
      AA(I)=276.92*BB(I)*TC(I)
      PCHK(I)=AA(I)/(27.*BB(I)**2)
   15 CONTINUE
      WRITE(11,215)
C
C     INPUT P ,T-START, T-END,AND STEP SIZE OF T.
C     IF P SET LE 0. , PROG. WILL CALL NEXT ELEM.
C     IF T2(TEND) IS SET LE 0., WILL PRINT CRIT VALUES AND END
C     PROG. WILL END AUTO. AFTER LAST ELEM. HAS BEEN CALC AND P SET 0.
C
      N=0
    5 N=N+1
      IF(N.GT.NN) GO TO 40
      WRITE(11,220) ELEM(N)
      WRITE(11,225)
      WRITE(11,230)
      WRITE(11,235)
   20 WRITE(59,220) ELEM(N)
      WRITE(59,240)
      READ(59,245) P
      IF(P.LE.0.) GO TO 5
      WRITE(59,250)
      READ(59,255) T1
      WRITE(59,260)
      READ(59,265) T2
      IF(T2.LE.0.) GO TO 40
      WRITE(59,270)
      READ(59,275) DELTT
C
C      CALC. IDEAL GAS VOL.
       T=T1
   30 VIDL=82.05*T/P
C
C      CALC MODIFIED VAN DE WAALS VOL.
       IFLAG1=0
       IFLAG2=0
```

```
      CON=(PI*AV*SIG(N)**3)/6.0
      GUESS=VIDL
      VINCR=100.0
      COMP=1.E-5
  410 IF(IFLAG1.LT.5) GO TO 411
      IF(IFLAG2.GT.0) GO TO 411
  420 IFLAG1=0
      VINCR=8.*VINCR
      GO TO 430
  411 IFLAG1=IFLAG1+1
  430 VM(1)=GUESS
      VM(2)=GUESS-VINCR
      VM(3)=GUESS+VINCR
      DO 431 I=1,3
      GAM=CON/VM(I)
      TGAM=(1.+GAM+GAM**2-GAM**3)/(1.-GAM)**3
      PCALC(I)=TGAM*82.05*T/VM(I)-41.293*EO(N)*VO(N)/VM(I)**2
      ZERO(I)=ABS(P-PCALC(I))
  431 CONTINUE
       IF(IFLAG2.GT.27) GO TO 440
      IF(ZERO(1).LT.SM.AND.ZERO(2).LT.SM.AND.ZERO(3).LT.SM) GO TO 440
      DIF1=ZERO(1)-ZERO(2)
      DIF2=ZERO(2)-ZERO(3)
      IF(ABS(DIF1).LT.SM.AND.ABS(DIF2).LT.SM) GO TO 420
  440 DO 460 I=1,3
      ID=I
      IF(ZERO(I).LT.COMP) GO TO 450
  460 CONTINUE
      IF(ZERO(1).LT.ZERO(2).AND.ZERO(1).LT.ZERO(3)) GO TO 463
  470 IF(ZERO(3).LT.ZERO(2)) GO TO 472
      GUESS=VM(2)
      GO TO 410
  472 GUESS=VM(3)
      GO TO 410
  463 VINCR=VINCR/2.
      IF(VINCR.LT.COMP) GO TO 451
      IF(IFLAG2.GT.50) GO TO 451
      IFLAG2=IFLAG2+1
      GO TO 430
  450 VM1=VM(ID)
      GO TO 452
  451 VM1=VM(1)
      ID=1
  452 DELP=ZERO(ID)
C
C      CALC VAN DE WAALS VOL.
C      COEFF.
       C(1)=P
       C(2)=-(82.05*T+BB(N)*P)
       C(3)=AA(N)
       C(4)=-AA(N)*BB(N)
       DELT=1.0E-6
       CALL CUBIC(C.E.DELT)
       WRITE(11,300) P,T,VIDL.VM1.DELP,E(1),E(2),E(3),E(4),E(5),E(6)
C
C      CALC REDLICH KWONG
       ARK=.4275*R**2*TC(N)**2.5/PC(N)
       BRK=.0866*R*TC(N)/PC(N)
       CRK(1)=P
       CRK(2)=-R*T
```

```
      CRK(3)=ARK/SQRT(T)-P*BRK**2-R*T*BRK
      CRK(4)=-ARK*BRK/SQRT(T)
      CALL CUBIC(CRK,ERK,DELT)
      WRITE(11,305) P,T,ERK(1),ERK(2),ERK(3),ERK(4),ERK(5),ERK(6)
      T=T+DELTT
      IF(T.LE.T2) GO TO 30
      WRITE(11,280)
      GO TO 20
C
C     OUTPUT CRIT VALUES
   40 WRITE(11,200)
      DO 50 I=1,NN
      WRITE(11,320) ELEM(I),EO(I),VO(I),SIG(I),VC(I),PC(I),TC(I),
     1ZC(I),PCHK(I)
   50 CONTINUE
C
  200 FORMAT(///," ELEM.   COH.F.(EO)  MO.VOL. DIA.SIGMA  CRIT.VOL  CRI
     1T.PRES  CRIT.TEM  COMPRES. CHK PCRIT(VDWAALS)")
  210 FORMAT(3X,A2,3E10.2)
  215 FORMAT(//," V IN CMS**3, P IN ATM, T IN DEG.K")
  220 FORMAT(///,40X," ELEMENT=",A2)
  225 FORMAT(38X,"***************")
  230 FORMAT(//," PRES.        TEMP.        ILD.VOL      MOD VDW     DELT PR.
     1         VDW VOL.1                VDW VOL.2              VDW VOL.3  ")
  235 FORMAT("--------------------------------------------------------
     1-------------------------------------------------")
  240 FORMAT(" ENTER P IN ATM  IF ENTER 0. MOVES TO NEXT ELEM.")
  245 FORMAT(F5.2)
  250 FORMAT(//," ENTER STARTING TEMP. IN DEG.K")
  255 FORMAT(F5.0)
  260 FORMAT(//,"ENTER ENDING TEMP IN DEG.K  IF ENTER 0. WILL TERM.")
  265 FORMAT(F5.0)
  270 FORMAT(//," ENTER STEP INCR. IN TEMP. IN DEG.K")
  275 FORMAT(F4.0)
  280 FORMAT(/,"_")
  300 FORMAT(11E11.3)
  305 FORMAT(8E11.3," REDLICH-KWONG ")
  320 FORMAT(A10,8E10.2)
      CALL EXIT
      END
      SUBROUTINE CUBIC(C,F,DELT)
      DIMENSION CP(4),C(4),BN(3),P(3),ABSP(3),E(6)
      GUESS=0.0
      IFLAG1=0
      IFLAG2=0
      DINCR=.5
      COMP=2.**(-16)
      CP(1)=1.0
      CP(2)=C(2)/C(1)
      CP(3)=C(3)/C(1)
      CP(4)=C(4)/C(1)
      DO 50 I=1,6
      E(I)=0.0
   50 CONTINUE
  100 IF(IFLAG1.LT.5) GO TO 110
      IF(IFLAG2.GT.0) GO TO 110
  200 IFLAG1=0
      DINCR=8.0*DINCR
      GO TO 300
  110 IFLAG1=IFLAG1+1
```

```
  300 BN(1)=GUESS+DINCR
      BN(3)=GUESS
      BN(2)=GUESS-DINCR
      DO 330 I=1,3
      P(I)=((CP(1)*BN(I)+CP(2))*BN(I)+CP(3))*BN(I)+CP(4)
      ABSP(I)=ABS(P(I))
  330 CONTINUE
      GO TO 400
  350 DO 360 I=1,2
      II=I+1
      DIF=ABSP(I)-ABSP(II)
      ABDIF=ABS(DIF)
      IF(ABDIF.GT.DELT) GO TO 400
  360 CONTINUE
      GO TO 200
  400 IF(ABSP(3).LT.COMP) GO TO 500
  600 DO 660 I=1,2
      II=I
      IF(ABSP(I).LT.COMP) GO TO 610
  660 CONTINUE
      DO 670 I=1,2
      IF(ABSP(3).GT.ABSP(I)) GO TO 700
  670 CONTINUE
      DINCR=DINCR/2.0
      IF(COMP.GT.DINCR) GO TO 500
      IF(IFLAG2.GT.50) GO TO 500
      IFLAG2=IFLAG2+1
      GO TO 300
  700 IF(ABSP(1).LT.ABSP(2)) GO TO 780
      GUESS=BN(2)
      GO TO 100
  780 GUESS=BN(1)
      GO TO 100
  500 E(1)=GUESS
      GO TO 800
  610 E(1)=BN(II)
C     SYNYHETIC DIV. AND QUAD. SOLU.
  800 B2=CP(2)+E(1)
      B3=CP(3)+E(1)*B2
      DUM=B2**2-4.*B3
      IF(DUM.GT.0.) GO TO 810
      DUM=-DUM
      COMPL=(SQRT(DUM))/2.
      REAL=-B2/2.
      E(3)=REAL
      E(4)=COMPL
      E(5)=REAL
      E(6)=-COMPL
      GO TO 820
  810 REAL1=(-B2+SQRT(DUM))/2.0
      REAL2=(-B2-SQRT(DUM))/2.0
      E(3)=REAL1
      E(5)=REAL2
  820 RETURN
      END
```

APPENDIX G
DENSITY DETERMINATION OF CRBR TYPE FUEL

The theoretical density can be calculated via Eq. (G-1).

$$\rho_T = \frac{n\ M}{N_A\ v_o}\ , \tag{G-1}$$

where

ρ_T = theoretical fuel density,

n = number of molecules/unit cell,

M = molecular weight,

N_A = Avagadro's number = 6.023×10^{23},

v_o = volume of unit cell = a_o^3,

a_o = lattice parameter,

$$a_o = 5.470 \times 10^{-8}\ (1.0 - .0133b)\left[1.0 + .0574\ (2.0 - O/M)\right]^{1} \text{ cms} \tag{G-2}$$

where

b = weight fraction of PuO_2,

O/M = oxygen-to-metal ratio.

As a check to Eq. (G-2), if one assumes pure UO_2, i.e., $b = 0$, and an $O/M = 2.00$, then $a_o = 5.470$ as reported in GEAP-5583.[2]

To find M, molecular weight, let f_1 thru f_4 be the weight fraction of U^{234} thru U^{238} (normally only f_2 and f_4 will be

significant). Let f_5 thru f_9 be Pu^{238} thru Pu^{242}.

$$\therefore \sum_{i=1}^{4} f_i = 1 \ , \qquad \sum_{i=5}^{9} f_i = 1 \ ,$$

$$M = (1 - b) \sum_{i=1}^{4} f_i \ M_i + b \sum_{i=5}^{9} f_i \ M_i + (O/M) \ M_{10} \ , \tag{G-3}$$

where

M_i = molecular weight of each isotope,

M_{10} = molecular weight of oxygen.

Since UO_2 and PuO_2 are face-centered-cubic (FCC), then:

$n = 4,$

substituting Eq. (G-3) and (G-2) into (G-1):

$$\rho_T = \frac{4}{6.023 \times 10^{23}} \ \frac{(1 - b) \sum_{i=1}^{4} f_i \ M_i + b \sum_{i=5}^{9} f_i \ M_i + (O/M) \ M_{10}}{\left\{5.470 \times 10^{-8} \ (1.0 - .0133b) \ \left[1.0 + 0.574 \ (2.0 - \frac{O}{M})\right]\right\}^3} \tag{G-4}$$

where

M_1 = 234.0409 (U^{234}) , M_5 = 238.0495 (Pu^{238}) ,

M_2 = 235.0439 (U^{235}) , M_6 = 239.0522 (Pu^{239}) ,

M_3 = 236.0456 (U^{236}) , M_7 = 240.054 (Pu^{240}) ,

M_4 = 238.0508 (U^{238}) , M_8 = 241.00 (Pu^{241}) ,

M_{10} = 15.9994 (Oxygen) , M_9 = 242.0587 (Pu^{242}) .

For CRBR

$$\frac{Pu}{Pu + U} = 22\% \text{ inner zone, } 32\% \text{ outer zone,}^{3}$$

volume average

$$\overline{\left(\frac{Pu}{Pu + U}\right)} = \frac{(.22)\ (V_{in} = 3.838 \times 10^{5}\ cm^{3}) + (.32)\ (V_{out} = 3.198 \times 10^{5}\ cm^{3})}{V_{in} + V_{out}}$$

$$= .265,$$

thus

$$b \simeq .265,$$

since CRBR O/M is unknown

$$\text{assume } \frac{O}{M} = 1.96\ (\text{FFTF})^{3} \quad .$$

Since natural U is assumed

$$f_1,\ f_3 \simeq 0 \quad .$$

Assume Pu has same initial weight fraction as the PNL-17[1] experimental fuel pin

$f_5 = .0004,$ $\qquad$ $f_8 = .0165,$

$f_6 = .8655,$ $\qquad$ $f_9 = .0015,$

$f_7 = .1161,$

substituting above values into Eq. (G-4)

$$\rho_T = 10.984 \text{ gms/cm}^3,$$

using 90% theoretical density[3]

$$= 9.886 \text{ gms/cm}^3.$$

REFERENCES

1. F. E. Bard, B. C. Gneiting, and C. M. Cox, "A Thermoelastic Material Properties Correlation for Uranium/Plutonium Mixed Oxides," Hanford Engineering Development Laboratory report HEDL-TME 74-12 (February 1974).

2. F. Anselin, "The Role of Fission Products in the Swelling of Irradiated UO_2 and (U, Pu) O_2 Fuel," General Electric Company report GEAP-5583 (January 1969).

3. E. A. Appleby, "Compilation of Data and Descriptions for United States and Foreign Liquid Metal Fast Breeder Reactors," Hanford Engineering Development Laboratory report, HEDL-TME 75-12 (August 1975).

APPENDIX H
CALCULATION OF FISSION PRODUCT CONCENTRATION IN FUEL AT 3 ATOM % BURNUP

For unit cell of CRBR Fuel (U, Pu) O_2:

$a_o \simeq 5.463 \times 10^{-8}\ \mathrm{cm}^{3}$ [1,2],

$v = a_o^3$,

Assume 90% theoretical density,

$$(.90)\ \frac{(\text{4 Fuel Atoms/Unit Cell})}{a_o^3} = 2.208 \times 10^{22}\ \text{fuel atoms/cm}^3 \quad ,$$

at 3 atom % Burnup (ignore transmutation):

$$(.03)\ (2.208 \times 10^{22}\ \text{atoms/cm}^3) = 6.624 \times 10^{20}\ \text{fissions/cm}^3\ \text{fuel} \quad ,$$

$$= 6.624 \times 10^{18}\ 100\ \text{fissions/cm}^3\ \text{fuel} \quad .$$

To obtain fission product volume:

$$\left(\frac{\text{fissions}}{\text{cm}^3\ \text{fuel}}\right)\ (\text{fission product yield})\ (\text{atomic volume}) = \frac{\text{elemental volume}}{\text{cm}^3\ \text{fuel}} \ .$$

The fission product yield and atomic volume for appropriate fission products can be found in Table H.1.

TABLE H.1

YIELD DATA

	Yield				Friedel Radii Å***		Atomic Volume $\mathring{A}^3$	
Element	RIBD*	U**	Pu^{++}	m^+	Pure Element	Alloyed Element	Pure Element	Average Volume Alloyed Element
In	.07				1.84	1.65	26.14	19.00
		.028		115.				
			.089	115.				
Sn	.73				1.86	1.66	26.88	19.20
		.345		120.2				
			.236	121.2				
Sb	.28				1.93	1.71	30.23	21.0
		.228		123.7				
			.406	124.4				
Ce	13.64				2.95^{+++}	34.32^{+++}		
		15.852		141.5				
			13.403	141.7				
Te	3.05				2.94^{+++}		33.95^{+++}	
		2.375		129.3				
			4.925	129.2				
Ba	7.27				3.66^{+++}		65.16^{+++}	
		6.91		138.2				
			6.304	138.2				
Mo	19.93				1.56	1.55	15.51	15.49
		21.344		97.3				
			18.265	93.2				
Tc	4.34				1.50	1.50	14.21	14.21
		6.01		99.				
			5.721	99.				
Ru	22.96				1.48	1.48	13.57	13.57
		16.091		102.17				
			27.267	103.17				

TABLE H.1 (cont)

	Yield				Friedel Radii Å***		Atomic Volume Å^3	
Element	RIBD*	U**	Pu^{++}	m$^+$	Pure Element	Alloyed Element	Pure Element	Average Volume Alloyed Element
Rh	4.39				1.49	1.49	13.77	13.77
		2.45		103.				
			4.033	103.				
Pd	14.35				1.52	1.52	14.79	14.65
		1.6		105.9				
			14.40	106.7				
Nb	.67				1.62	1.57	17.97	16.23
		1.473		95.0				
			1.148	95.0				
Ag	1.14				1.62	1.59	17.75	16.77
		.141		109.77				
			1.728	109.0				
Cd	1.33				1.73	1.63	21.58	18.30
		.204		113.7				
			.944	112.0				

---

*Calculation from RIBD code[3] for 20% Pu, 80% depleted U, 3% B.U. (365-day irradiation) given in atoms/100 fissions. (Changes very little with B.U. past 1%.) Note this is effectively only Pu fission since depleted U converts to Pu with very little U fission.

TABLE H.1 (cont)

**Fission product spectrum for fast fission of U^{235}, irradiated 135 days, 0 days cooling, in atoms/100 atoms fissioned, ANL-5742.[4]

***Friedel radius[2] is the radius of the sphere occupying the equivalent volume of one atom in the lattice

$$R = \left(\frac{3}{4}\,v\right)^{1/3}$$

where for a face centered cubic (FCC) crystalline structure with 4 atoms/unit cell

$$v = \frac{a_o^3}{4}\ , \qquad a_o = \text{lattice parameter} \quad .$$

$$+\bar{m} = \frac{\sum_{i=1}^{n} f_i m_i}{\sum_{i=1}^{n} f_i} \qquad \text{where } m_i = \text{molecular weight of isotope i, and} \quad f_i = \text{yield of isotope i.}$$

++Fission product spectrum for fast fission of Pu^{239}, irradiated 135 days, 0 days cooling, in atoms/100 atoms fission ANL-5742.[4]

+++Equivalent Friedel radius and volume calculation from molecular weight and density

$$v = MW\,\frac{1}{\rho}\,\frac{1}{Na}\ , \qquad R = \left(\frac{3}{4}\,v\right)^{1/3} \quad .$$

The maximum (i.e. total segregation) individual fission product volume, molar, and mass concentration for 3 atom % burnup can be found in Table H.2 thru H.4.

If one assumes total segregation of the noble metal inclusion constituents, the following weight % shown in Table H.5 are found for the above yield data.

The numbers in [illegible] in Table [illegible] tonnes, [illegible] and have been [illegible] in Table [illegible].

If one assumes total suppression of the [illegible] simultaneously, the following weight [illegible] shown in [illegible] the above yield data.

TABLE H.2

FISSION PRODUCT VOLUME CONCENTRATION FOR 3 ATOM % BURNUP

	Fission Product Volume/cm^3 Fuel					
	RIBD[3]		Uranium[4]		Plutonium[4]	
Element	Pure Element	Alloyed	Pure Element	Alloyed	Pure Element	Alloyed
Mo	2.06×10^{-3}	2.04×10^{-3}	2.21×10^{-3}	2.20×10^{-3}	1.89×10^{-3}	1.87×10^{-3}
Tc	4.09×10^{-4}	4.09×10^{-4}	5.66×10^{-4}	5.66×10^{-4}	5.39×10^{-4}	5.39×10^{-4}
Ru	2.06×10^{-3}	2.06×10^{-3}	1.45×10^{-3}	1.45×10^{-3}	2.45×10^{-3}	2.45×10^{-3}
Rh	4.00×10^{-4}	4.00×10^{-4}	2.23×10^{-4}	2.23×10^{-4}	3.68×10^{-4}	3.68×10^{-4}
Pd	1.41×10^{-3}	1.39×10^{-3}	1.57×10^{-4}	1.55×10^{-4}	1.41×10^{-3}	1.40×10^{-3}
Te	6.36×10^{-4}		5.34×10^{-4}		1.11×10^{-3}	
Ba	3.14×10^{-3}		2.93×10^{-3}		2.72×10^{-3}	
Sb	5.61×10^{-5}	3.89×10^{-5}	4.57×10^{-5}	3.17×10^{-5}	8.13×10^{-5}	5.65×10^{-5}
Ce	3.10×10^{-3}		3.60×10^{-3}		3.05×10^{-3}	
Sn	1.30×10^{-4}	9.28×10^{-5}	6.14×10^{-5}	4.39×10^{-5}	4.20×10^{-5}	3.00×10^{-5}
In	1.21×10^{-5}	8.31×10^{-6}	4.35×10^{-6}	3.52×10^{-6}	1.54×10^{-5}	1.12×10^{-5}
Nb	7.98×10^{-5}	7.20×10^{-5}	1.75×10^{-4}	1.58×10^{-4}	1.37×10^{-4}	1.23×10^{-4}
Ag	1.34×10^{-4}	1.27×10^{-4}	1.66×10^{-5}	1.57×10^{-5}	2.03×10^{-4}	1.92×10^{-4}
Cd	1.90×10^{-4}	1.61×10^{-4}	2.92×10^{-5}	2.47×10^{-5}	1.35×10^{-4}	1.14×10^{-4}

TABLE H.3

MOLAR CONCENTRATION FOR 3 ATOM % BURNUP

		Moles/cm^3 Fuel$^+$	
Element	RIBD	U	Pu
Mo	2.19×10^{-4}	2.35×10^{-4}	2.01×10^{-4}
Tc	4.77×10^{-5}	6.61×10^{-5}	6.29×10^{-5}
Ru	2.53×10^{-4}	1.77×10^{-4}	3.00×10^{-4}
Rh	4.83×10^{-5}	2.69×10^{-5}	4.44×10^{-5}
Pd	1.58×10^{-4}	1.76×10^{-5}	1.58×10^{-4}
Te	3.35×10^{-5}	2.61×10^{-5}	5.42×10^{-5}
Ba	8.00×10^{-5}	7.60×10^{-5}	6.93×10^{-5}
Sb	3.08×10^{-6}	2.51×10^{-6}	4.47×10^{-6}
Ce	1.50×10^{-4}	1.74×10^{-4}	1.47×10^{-4}
Sn	8.03×10^{-6}	3.79×10^{-6}	2.60×10^{-6}
In	7.70×10^{-7}	3.08×10^{-7}	9.79×10^{-7}
Nb	7.37×10^{-6}	1.62×10^{-5}	1.26×10^{-5}
Ag	1.25×10^{-5}	1.55×10^{-6}	1.90×10^{-5}
Cd	1.46×10^{-5}	2.24×10^{-6}	1.04×10^{-5}

$^+$Molar concentration = $\left(\frac{\text{fission}}{\text{cm}^3}\right)$ (yield) $\frac{1}{NA}$.

TABLE H.4

MASS CONCENTRATION FOR 3 ATOM % BURNUP

		gms/cm^3 Fuel	
Element	RIBD*	U**	Pu**
Mo	2.10×10^{-2}	2.29×10^{-2}	1.97×10^{-2}
Tc	4.67×10^{-3}	6.54×10^{-3}	6.23×10^{-3}
Ru	2.56×10^{-2}	1.81×10^{-2}	3.10×10^{-2}
Rh	4.97×10^{-3}	2.77×10^{-3}	4.57×10^{-3}
Pd	1.68×10^{-2}	1.86×10^{-3}	1.69×10^{-2}
Te	4.27×10^{-3}	3.37×10^{-3}	7.00×10^{-3}
Ba	1.10×10^{-2}	1.05×10^{-2}	9.58×10^{-3}
Ce	2.10×10^{-2}	2.46×10^{-2}	2.08×10^{-2}
Sb	3.75×10^{-4}	3.10×10^{-4}	5.56×10^{-4}
Sn	9.53×10^{-4}	4.56×10^{-4}	3.15×10^{-4}
In	8.84×10^{-5}	3.54×10^{-5}	1.13×10^{-4}
Nb	6.85×10^{-4}	1.54×10^{-3}	1.20×10^{-3}
Ag	1.35×10^{-3}	1.70×10^{-4}	2.07×10^{-3}
Cd	1.64×10^{-3}	2.55×10^{-4}	1.16×10^{-3}

---

*Using molecular weight from Glasstone.[5]

**Using average molecular weight yield $\overline{m}$ calculation earlier from Burris.[4]

TABLE H.5

TOTAL SEGREGATION

Element	Weight Fraction in % RIBD	U	Pu
Mo	28.75	43.89	25.13
Tc	6.39	12.54	7.95
Ru	35.05	34.69	39.54
Rh	6.80	5.31	5.83
Pd	23.0	3.57	21.56

REFERENCES

1. J. H. Davies and F. T. Ewart, "The Chemical Effects of Composition Changes in Irradiated Oxide Fuel Materials," Journal of Nuclear Materials 41, (1971) pp. 143-155.

2. F. Anselin, "The Role of Fission Products in the Swelling of Irradiated UO_2 and (U, Pu) O_2 Fuel," General Electric Company report GEAP-5583 (January 1969).

3. R. O. Gumprecht, "Mathematical Basis of Computer Code RIBD," Douglas United Nuclear, Inc. report DUN-4136 (June 1968).

4. L. Burris, Jr., and I. G. Dillon, "Estimation of Fission Product Spectra in Discharged Fuel from Fast Reactors," Argonne National Laboratory report ANL-5742 (July 1957).

5. S. Glasstone and A. Sesonske, Nuclear Reactor Engineering (Van Nostrand Reinhold Company, 1967).

APPENDIX I

DERIVATION OF STEADY STATE TEMPERATURE PROFILES

(SUBROUTINE SSTEMP)

A. Determination of heat transfer coefficient for the coolant

$$\text{Pec (Peclet number)} = \frac{D_e \, V \, \rho \, C_p}{K} , \qquad \text{(I-1)}$$

where

D_e = equivalent diameter,

V = coolant velocity,

ρ = coolant density,

C_p = coolant heat capacity,

K = coolant thermal conductivity,

for assumed flow of liquid metals in annular channels

$$\text{Nu (Nusselt number)} = .8 \left(\frac{r_o}{r_i}\right)^{.3} \left(5.1 + .028 \, \text{Pe}^{.8}\right)^{1} , \qquad \text{(I-2)}$$

where

r_i = outer clad radius (inner annulus radius),

r_o = equivalent outer radius of coolant flow.

$$Nu = \frac{h\ D_e}{K} \Rightarrow h = \frac{k\ Nu}{D_e} \quad , \qquad \text{(I-3)}$$

substituting Eqs. (I-1) and (I-2) into (I-3)

$$h \text{ (heat transfer coeff.)} = \frac{K}{D_e} .8 \left(\frac{r_o}{r_i}\right)^{.3} \cdot \left[5.1 + .028 \left(\frac{D_e\ V\ \rho\ C_p}{k}\right)^{.8}\right] \qquad \text{(I-4)}$$

B. Steady State Heat Transfer Equations

At steady state, heat stored term = 0.

1. Bulk Coolant Temperature.

$$\text{Axial heat in } = C_p \cdot V \cdot \rho \cdot AEQ \cdot T_{NA,J-1} \quad , \qquad \text{(I-5)}$$

$$\text{Axial heat out } = C_p \cdot V \cdot \rho \cdot AEQ \cdot T_{Na,J} \quad , \qquad \text{(I-6)}$$

$$\text{Radial heat in } = Q_{Ave} \cdot A_F \cdot \Delta Z \quad , \qquad \text{(I-7)}$$

where

Cp = coolant heat capacity,

V = coolant velocity,

ρ = coolant density,

AEQ = cross-sectional coolant flow-area,

$T_{Na,J}$ = axial node, J, coolant temperature,

A_F = cross-sectional area of fuel,

ΔZ = axial node length,

Q_{Ave} = average volumetric heat generation rate between axial nodes J, J-1, and

$$= \frac{Q_J + Q_{J-1}}{2} \quad ,$$

combining Eqs. (I-5), (I-6), and (I-7)

$$T_{Na,J} = T_{Na,J-1} + \frac{Q_{Ave} \cdot A_F \cdot \Delta Z}{C_p \cdot V \cdot \rho \cdot AEQ} \quad , \qquad \text{(I-8)}$$

where

T_o = coolant inlet temperature.

2. Clad Outer Surface Temperature.

At axial node, J

Radial heat in $= Q_J \cdot A_f \cdot \Delta Z$, (I-9)

Radial heat out $= h \cdot 2\,\pi R_{c1} \cdot \Delta Z\,(T_{c1,J} - T_{NA,J})$ (I-10)

Axial heat transfer = 0 (per assumptions) ,

where

h = heat transfer coefficient, Eq. (I-4),

R_{c1} = outer clad radius,

$T_{c1,J}$ = outer clad temperature,

combining Eqs. (I-9) and (I-10)

$$T_{c1,J} = T_{NA,J} + \frac{Q_J \cdot A_F}{h \cdot 2\,\pi R_{c1}} \quad . \qquad \text{(I-11)}$$

3. Clad-bond Interface Temperature.

at axial node, J

$$q = -k \cdot A \cdot \frac{dT}{dr} \quad , \qquad \text{(I-12)}$$

where

k = thermal conductivity of cladding,

A = radial heat transfer surface area = $2\pi r \Delta z$,

rearranging Eq. (I-12)

$$q \frac{dr}{r} = -k \cdot 2\pi \cdot \Delta z \cdot dT \quad , \qquad \text{(I-13)}$$

integrate Eq. (I-13) from clad inner to clad outer surface

$$q \, \ell n \left[\frac{R_{in}}{R_{cl}}\right] = -k \cdot 2\pi \cdot \Delta z \left[T_{cl,J} - T_{in,J}\right] \quad , \qquad \text{(I-14)}$$

where

R_{in} = inner clad radius,

R_{cl} = outer clad radius,

$T_{cl,J}$ = outer clad temperature,

$T_{in,J}$ = inner clad temperature,

rearranging Eq. (I-14) and since:

$$q = \pi \, R_F^2 \cdot \Delta z \cdot Q_J \quad ,$$

$$T_{in,J} = T_{cl,J} + \frac{Q_J \cdot R_F^2}{2k} \ell n \left[\frac{R_{cl}}{R_{in}}\right] . \qquad \text{(I-15)}$$

4. Fuel-bond interface

At axial node, J, assuming He bond,

$$\text{Radial heat in} = Q_J \cdot A_F \cdot \Delta z \quad , \qquad \text{(I-16)}$$

$$\text{Radial heat out} = h_{He} \cdot A_{He} \cdot (T_{F1,J} - T_{in,J}) \quad , \qquad \text{(I-17)}$$

axial heat transfer = 0 ,

where

h_{He} = helium heat transfer coefficient,

A_{He} = fuel heat transfer surface area = $2\pi \cdot R_F \cdot \Delta z$,

R_F = outer radius of fuel,

$T_{F1,J}$ = outer fuel temperature,

combining Eq. (I-16) and (I-17)

$$T_{F1,J} = T_{in,J} + \frac{Q_J \cdot R_F}{2 \cdot h_{He}} . \qquad \text{(I-18)}$$

5. Interior fuel nodes.

At axial node, J, no axial heat transfer

$$k \nabla^2 T_{i,J} + Q_J = 0 \qquad \text{(I-19)}$$

where

k = thermal conductivity of the fuel $\left[\text{assume } k \neq \text{func } (r)\right]$,

$T_{i,J}$ = fuel temperature at radial node, i, axial node, J.

$$k \left(\frac{\partial^2}{\partial r^2} + \frac{1}{r} \frac{\partial}{\partial r}\right) T_{i,J} = -Q_J \quad , \tag{I-20}$$

$$Q_J\, r = -k \left(r \frac{\partial^2}{\partial r^2} + \frac{\partial}{\partial r}\right) T_{i,J} \quad , \tag{I-21}$$

$$\frac{-Q_J r}{k} = \frac{\partial}{\partial r} \left(r \frac{\partial}{\partial r} T_{i,J}\right) \quad , \tag{I-22}$$

integrate

$$r \frac{\partial T}{\partial r} = \frac{-\,Q_J\, r^2}{2k} + C_1 \quad , \tag{I-23}$$

$$\frac{\partial T}{\partial r} = \frac{-Q_J\, r}{2k} + \frac{C_1}{r} \quad . \tag{I-24}$$

Boundary condition

$$\text{At } r = 0,\ \frac{\partial T}{\partial r} = 0 \quad C_1 = 0 \quad ,$$

integrate Eq. (I-24)

$$T = \frac{-Q_J\, r^2}{4k} + C_2 \quad . \tag{I-25}$$

Boundary condition

At $r = R_F$, $T = T_{F1,J}$

$$\therefore C_2 = T_{F1,J} + \frac{Q_J R_F^2}{4k} , \tag{I-26}$$

substituting Eq. (I-26) into (I-25)

$$T_{i,J} = T_{F1,J} + \frac{Q_J}{4k} (R_F^2 - r_i^2) . \tag{I-27}$$

APPENDIX J
POINT KINETICS SOLUTION

Point kinetics is by definition spatially independent. One can put in finiteness by including the buckling terms. What will be assumed here is that the flux is defined as

$$\Phi\,(r,t) = S(r)\,P(t) \quad ,$$

where

$S(r)$ is a shape function (in this analysis taken as a chopped cosine).

$P(t)$ is the time dependent amplitude.

As stated in the text, the flux shape will be assumed constant in time during the transient. The flux amplitude equations can then be written as

$$\Lambda \frac{dP}{dt} = \Big[\rho(t) - \beta\Big]\, P(t) + \sum_{i=1}^{n} \lambda_i\, C_i(t) \quad , \tag{J-1}$$

$$\frac{d\,C_i(t)}{dt} = -\lambda_i\, C_i(t) + \beta_i\, P(t) \quad , \tag{J-2}$$

$$\beta = \sum_{i=1}^{n} \beta_i \quad , \tag{J-3}$$

where

$\rho(t)$ = net reactivity feedback

$\Lambda = \frac{1}{v \nu \sum_f}$ = prompt neutron generation time (for this analysis $\Lambda = 3.5 \times 10^{-7}$ sec),

β = total fraction of delayed neutrons (for this analysis $\beta = 3.01 \times 10^{-3}$),

λ_i = decay constant of the ith delayed neutron precursor group, $\sec^{-1}$,

C_i = reduced concentration of the ith delayed neutron precursors group,

β_i = fraction of neutrons from the ith delayed neutron precursor group,

t = independent variable, time, sec.

At steady state:

$$P(t) = 1,$$

$$\rho(t) = 0,$$

$$C_i = \frac{\beta_i}{\lambda_i} ,$$

$$\sum \lambda_i C_i = \sum \beta_i = \beta.$$

The integral solution of Kaganove[2] is used. His method is based on representing the amplitude function as a parabola. A simplifying modification made by Burns[3] uses Lagrange interpolating polynomials to represent the amplitude function.

$$P(t) = P_i\ F_i(t) + P_2\ F_2(t) + P_3\ F_3(t) \quad , \qquad \text{(J-4)}$$

where

P_1 = power amplitude at end of current time step, $t = t_1$

P_2 = power amplitude at beginning of current time step, $t = t_2$

P_3 = power amplitude at beginning of previous time step, $t = t_3$

and

$$F_1(t) = \frac{(t - t_2)\ (t - t_3)}{(t_1 - t_2)\ (t_1 - t_3)} \quad ,$$

$$F_2(t) = \frac{(t - t_1)\ (t - t_3)}{(t_2 - t_1)\ (t_2 - t_3)} \quad , \qquad \text{(J-5)}$$

$$F_3(t) = \frac{(t - t_1)\ (t - t_2)}{(t_3 - t_1)\ (t_3 - t_2)} \quad .$$

Solving the ordinary nonhomogeneous Eq. (J-2)

$$\frac{d\ C_i(t)}{dt} + \lambda_i\ C_i(t) = \beta_i\ P(t) \quad .$$

Then

C_i = homogeneous solution + particular solution

to obtain homogeneous solution, let Eq. (J-2) be represented as

$$\frac{d\ C_i(t)}{dt} + \lambda_i\ C_i(t) = 0 \quad , \qquad \text{(J-6)}$$

and

$$C_i(t)\ \text{homo} = Ke^{-\lambda_i t} \quad , \tag{J-7}$$

to obtain the particular solution use variation of parameters

$$C_i(t)\ \text{part.} = e^{-\lambda t} \int_{t_2}^{t} e^{\lambda\tau}\ \beta_i\ P(\tau)\ d\tau \quad , \tag{J-8}$$

combining Eq. (J-7) and (J-8)

$$C_i(t) = Ke^{-\lambda_i t} + \beta_i \int_{t_2}^{t} e^{-\lambda(t-\tau)}\ P(\tau)\ d\tau \quad , \tag{J-9}$$

At $t = t_2$, $C_i(t) = C_i(t_2)$,

$C_i(t_2) = Ke^{-\lambda_i t_2} + 0$,

thus

$$K = C_i(t_2)\ e^{\lambda_i t_2} \quad , \tag{J-10}$$

and

$$C_i(t) = C_i(t_2)\ e^{-\lambda_i(t-t_2)} + \beta_i \int_{t_2}^{t} e^{-\lambda(t-\tau)}\ P(\tau)\ d\tau \quad , \tag{J-11}$$

substituting Eq. (J-11) and (J-14) into Eq. (J-1)

$$\Lambda\left[P_1\frac{d\,F_i(t)}{dt}+P_2\frac{d\,F_2(t)}{dt}+P_3\frac{d\,F_3(t)}{dt}\right]=\left[\rho(t)-\beta\right]\left[P_1F_1(t)+P_2F_2(t)\right.$$

$$\left.+P_3F_3(t)\right]+\sum_{i=1}^{k}\lambda_i\left[C_i(t_2)\,e^{-\lambda_i(t-t_2)}+\beta_i\int_{t_2}^{t}(P_iF_i(\tau)\right.$$

$$\left.+P_2F_2(\tau)+P_3F_3(\tau))e^{-\lambda_i(t-\tau)}\,d\tau\right]\quad . \qquad \text{(J-12)}$$

Let $t = t_1$, solve for P_1

$$P_1=-\Lambda P_2\,\frac{\left.\frac{dF_2}{dt}\right|_{t=t_1}-\Lambda P_3\left.\frac{dF_3}{dt}\right|_{t=t_1}+\sum_{i=1}^{k}\left[\lambda_iC_i(t_2)e^{-\lambda_i(t_1-t_2)}+\lambda_i\beta_i(P_2x_{i2}+P_3x_{i3})\right]}{\Lambda\left.\frac{d\,F_1}{dt}\right|_{t=t_1}-\rho(t_1)+\beta-\sum_{i=1}^{k}\beta_i\,\lambda_i\,x_{i1}}$$

where

$$x_{ij}=\int_{t_2}^{t_1}F_j(\tau)\,e^{-\lambda_i(t_1-\tau)}\,d\tau\ .$$

Thus P_1 can be solved directly, (t_1) is known since a ramp insertion of reactivity is used.

It should be noted that if one assumes a slow transient, i.e.,

$$\Lambda\,\frac{dp}{dt}\ll\sum_{i=1}^{k}\lambda_i\,C_i\quad ,$$

then Eq. (J-1) reduces to

$$P(t) \simeq \frac{\sum_{i=1}^{k} \lambda_i \; C_i(t)}{\beta \; - \rho(t)} \quad , \tag{J-14}$$

which is the same formula that Eq. (J-13) will reduce to for small time steps and small reactivity.

$$P_1 \simeq \frac{\sum_{i=1}^{k} \lambda_i \; C_i(t_2)}{\beta - \rho_1} \quad .$$

Convergence is determined by comparing the P_1 solution from Eq. (J-13) to solutions produced by taking smaller time steps, i.e., Eq (J-14). If the convergence criteria is not met, smaller time steps are used until the solution converges.

then the [illegible] becomes

[illegible]

which is the same formula that is, (4-11), with weights as for [illegible] the [illegible] and small respectively.

[illegible]

Convergence is determined by comparing the F_j obtained from Eq. (4-12) to solutions produced by halving smaller time steps, i.e., Eq. (3-14). If the convergence criteria is not met, smaller time steps are used until the solution converges.

REFERENCES

1. S. Glasstone and A. Sesonske, Nuclear Reactor Engineering (Van Nostrand Reinhold Company, 1967).

2. J. J. Kaganove, "Numerical Solution of the One-Group, Space-Independent Reactor Kinetics Equations for Neutron Density Given the Excess Reactivity," Argonne National Laboratory report ANL-6132 (February 1960).

3. R. D. Burns, "A Parametric Approach to LMFBR Safety Evaluation," Purdue University report PNE-76-110 (August 1976).

APPENDIX K

DERIVATION OF TRANSIENT TEMPERATURE PROFILES USING A FINITE DIFFERENCING TECHNIQUE (SUBROUTINE TRANS)

In subroutine TRANS a node-by-node, finite differencing technique is utilized. Euler's method or forward differencing is used to approximate the time derivative of temperature.

$$\left.\frac{dT}{dt}\right|_{n,t} = \frac{T_n^{t+\Delta t} - T_n^t}{\Delta t} \quad . \tag{K-1}$$

The following finite-differences equations are generated using the general energy balance:

heat in - heat out + heat generated = heat stored . (K-2)

Again axial conduction heat transfer is assumed negligible. Axial convection heat transfer in the coolant channel is taken into account. Figure 4.1 shows the location of axial and radial nodes and node boundaries.

A. Fuel Centerline

Radial heat in = 0,

$$\text{Radial heat out} = k_f \cdot A \cdot \frac{dT}{dr} = k_f \cdot 2\pi\,(\frac{\Delta r}{2})\;\Delta z\;(\frac{T_{1,j}^t - T_{2,j}^t}{\Delta r}) \;, \tag{K-3}$$

$$\text{Heat generated} = Q_J\,\Delta V = Q_J\;\;\pi\,(\frac{\Delta r}{2})^2\;\Delta z \quad , \tag{K-4}$$

$$\text{Heat stored} = \rho_F\ C_{pF}\ \Delta V\ \frac{dT}{dt} = \rho_F \cdot C_{pF} \cdot\ \pi\left(\frac{\Delta r}{2}\right)^2\ \Delta z\ \frac{T_{1,J}^{t+\Delta t} - T_{1,J}^{t}}{\Delta t} \tag{K-5}$$

note at axial nodes J=1 and J=JMZ (top and bottom axial nodes) then ΔZ is replaced with $\frac{\Delta z}{2}$.

where

k_f = thermal conductivity of the fuel,

Δr = radial node distance in the fuel,

Δz = axial node distance,

Q_J = volumetric heat generation rate at axial node, J,

ρ_F = fuel density,

C_{pF} = heat capacity of the fuel,

Δt = time step,

$T_{i,J}^{t}$ = temperature at node, i,J at time, t,

$T_{i,J}^{t+\Delta t}$ = temperature at node i,J at time, t+Δt (end of time step),

combining Eqs. (K-3) thru (K-5) one obtains

$$T_{i,J}^{t+\Delta t} = T_{1,J}^{t}\ \left(1 - \frac{4\alpha}{\Delta r^2}\ \Delta t\right) + T_{2,J}^{t}\ \ \frac{4\alpha\Delta t}{\Delta r^2} + Q_J\ \frac{\Delta t}{\rho_F\ C_{pF}}\ , \tag{K-6}$$

where

$$\alpha = \text{thermal diffusivity of the fuel} = \frac{k_F}{\rho_F\ C_{pF}}\ .$$

It can be seen from Eq. (K-6) that for stability

$$\frac{\Delta r^2}{\alpha \Delta t} >> 4 \quad \text{or} \quad \Delta t << \frac{\Delta r^2}{4\alpha} \ . \tag{K-7}$$

B. Interior Fuel Nodes

$$\text{Radial heat in} = k_F \ A_{in} \frac{dT}{r} = k_F \cdot 2\pi \ \ \Delta Z \ \ (r_i - \frac{\Delta r}{2}) \ \ (\frac{T^t_{i-1,J} - T^t_{i,J}}{\Delta r}) \ , \tag{K-8}$$

$$\text{Radial heat out} = k_F \ A_{out} \frac{dT}{dr} = k_F \cdot 2\pi \ \ \Delta Z \ \ (r_i + \frac{\Delta r}{2}) \ \ (\frac{T^t_{i,J} - T^t_{i+1,J}}{\Delta r}) \ , \tag{K-9}$$

$$\text{heat generated} = Q_J \ \Delta V = Q_J \cdot 2\pi \cdot r_i \cdot \Delta r \cdot \Delta Z \tag{K-10}$$

$$\text{heat stored} = \rho_F \ C_{pF} \ \Delta V \frac{dT}{dt} = \rho_F \ \ C_{pF} \ \ 2\pi \ \ r_i \cdot \Delta r \cdot \Delta Z \ \ (\frac{T^{t+\Delta t}_{i,J} - T^t_{i,J}}{\Delta t}) \ , \tag{K-11}$$

where

r_i = radius of ith radial node,

combining Eqs. (K-8) thru (K-11)

$$T^{t+\Delta t}_{i,J} = \frac{Q_J \ \cdot \ \Delta t}{\rho_F \ Cp_F} + T^t_{i,J} \ (1. - \frac{2.}{CM}) + \frac{T^t_{i-1,J}}{CM} \ (1 - \frac{\Delta r}{2r_i}) + \frac{T^t_{i+1,J}}{CM} \ (1 + \frac{\Delta r}{2 \ r_i}), \tag{K-12}$$

where

$$CM = \frac{\Delta r^2}{\alpha \Delta t} \text{ (i.e., stability criteria Eq. K-7)} \quad .$$

C. Fuel-Bond Interface

This node is located at the fuel surface and extends from $\frac{\Delta r}{2}$ into the fuel to half way between the fuel and clad, i.e. half the distance into the bond. The bond is assumed to be He with no heat generation occurring in the bond.

$$\text{radial heat in} = k_f \text{ Ain } \frac{dT}{dr} = k_f \cdot 2\pi \ (r_f - \frac{\Delta r}{2}) \ \Delta z \ (\frac{T^t_{i-1,J} - T^t_{i,J}}{\Delta r}) \quad , \tag{K-13}$$

heat generated = heat generated in fuel + heat generated in bond,

$$\text{heat generated} = Q_J \ \Delta z \cdot \pi \left[r_F^2 - (r_F - \frac{\Delta r}{2})^2\right] + 0 \quad , \tag{K-14}$$

heat stored = heat stored in fuel + heat stored in bond,

$$\text{heat stored} = \left[\frac{T^{t+\Delta t}_{i,J} - T^t_{i,J}}{\Delta t}\right] \pi \Delta z \ \left[\rho_b \ C_{pb} \ (r_F \cdot Thb + \frac{Thb^2}{4}) + \rho_F \ C_{pF} \ (r_F \ \Delta r - \frac{\Delta r^2}{4})\right] \quad , \tag{K-15}$$

radial heat out = radial heat out of fuel surface - heat stored in nodal bond volume,

where

(2) [illegible] , [illegible] defined by (4.5)

6. [illegible] [illegible]

[illegible] heat is [illegible] at the tool surface and [illegible] from it into the tool [illegible] between the tool and chip, [illegible] the distance into the [illegible]. The [illegible] is assumed to be [illegible] with no heat generation [illegible] in the [illegible].

[illegible] heat in = [illegible] (4.14)

heat generated = heat generated in tool + heat generated in work.

heat generated = [illegible] (4-14)

heat stored = heat stored in tool + heat stored in work.

heat stored = [illegible]

[illegible] (4.15)

[illegible] heat out = [illegible] out of tool surface – heat stored [illegible] [illegible] heat stored in nodal bond volume = $\rho_b\ C_{pb}\ (r_F \cdot \mathrm{Thb} + \frac{\mathrm{Thb}^2}{4})\ \frac{dT}{dt}\ \pi \Delta z$, (K-16)

radial heat out of fuel surface = $h_b \cdot 2\pi \cdot r_F \cdot \Delta z \left[T^t_{i,J} - T^t_{i+1,J}\right]$, (K-17)

where

r_F = fuel radius,

ρ_b = bond density,

C_{pb} = heat capacity of bond,

Thb = bond thickness,

h_b = bond heat transfer coefficient,

combining Eqs. (K-13) thru (K-17)

$$T^{t+\Delta t}_{i,J} = T^t_{i,J} + \frac{\Delta t}{\rho_F \cdot C_{pF}\ (r_F\ \Delta r - \frac{\Delta r^2}{4})} \left[\frac{2 \cdot k_F}{\Delta r}\ (r_F - \frac{\Delta r}{2})\ (T^t_{i-1,J} - T^t_{i,J}) - 2 \cdot h_b \cdot r_f\ (T^t_{i,J} - T^t_{i+1,J}) + Q_J\ (r_F\ \Delta r - \frac{\Delta r^2}{4})\right] \quad . \qquad \text{(K-18)}$$

D. Bond-Clad Interface

This node is located at the clad inner surface and extends from halfway into the bond to halfway through the clad. It is assumed that heat generation does not occur either in the bond or clad. It should be noted that the heat out of a node is equal to the heat into the adjoining node.

ment during a time step [illegible]

[illegible] . . . . (K-17)

where

r_f = fuel radius,

ρ_b = bond density,

C_{pb} = heat capacity of bond,

Δb = bond thickness,

h_b = bond heat transfer coefficient.

Combining Eqs. (K-13) thru (K-17)

[illegible]

[illegible] . . . . (K-18)

3. Bond-Clad Interface

This zone is located at the clad inner surface and extends from halfway into the bond to halfway through the clad. It is assumed that heat generation does not occur either in the bond or clad. It should be noted that the heat out of a zone is equal to the heat into the adjoining zone.

radial heat in = radial heat out of fuel surface - heat stored in nodal bond volume (see Eqs. (K-16), (K-17)),

$$\text{radial heat out} = k_c \cdot 2\pi \ \Delta z \ \left(r_c + \frac{\text{Thcl}}{2}\right) \cdot \left(\frac{T^t_{i,J} - T^t_{i+1,J}}{\text{Thcl}}\right), \qquad \text{(K-19)}$$

heat generated = 0,

heat stored = heat stored in nodal clad volume + heat stored in nodal bond volume,

$$\text{heat stored} = \left[\frac{T^{t+\Delta t}_{i,J} - T^t_{i,J}}{\Delta t}\right]\pi \cdot \Delta z \left[\rho_c \ C_{pc} \left\{\left(r_c + \frac{\text{Thb}}{2}\right)^2 - r_c^2\right\}\right]$$

$$+ \text{ heat stored in nodal bond volume.} \qquad \text{(K-20)}$$

where

r_c = clad inner radius,

k_c = thermal conductivity of the clad,

Thcl = clad thickness,

ρ_c = density of the clad,

C_{pc} = heat capacity of the clad.

Assume the heat stored in the inner half bond volume is equal to the heat stored in the outer half bond volume. This assumption is reasonable since the slight difference in volume and temperature are offsetting. Also these terms are on the order of 10^{-3} smaller than the clad storage term, making the difference insignificant.

Combining Eqs. (K-16), (K-17), (K-19), and (K-20)

$$T_{i,J}^{t+\Delta t} = T_{i,J}^{t} + \frac{2 \quad \Delta t}{\rho_c \; C_{pc} \; (r_c \cdot \text{ThcL} + \frac{\text{ThcL}^2}{4})} \left[h_b \cdot r_F \; (T_{i-1,J}^{t} - T_{i,J}^{t}) - k_c \; (r_c + \frac{\text{ThcL}}{2}) \; (\frac{T_{i,J}^{t} - T_{i+1,J}^{t}}{\text{ThcL}}) \right] \quad . \qquad \text{(K-21)}$$

E. Clad-Coolant Interface

This node is located at the clad outer surface and extends halfway through the clad. No coolant is included in this node since all the coolant is included in a bulk coolant node (see following section). Again it is assumed that heat generation only occurs in the fuel.

$$\text{radial heat in} = k_c \quad 2\pi \quad \Delta z \quad (r_c + \frac{\text{ThcL}}{2}) \; (\frac{T_{i-1,J}^{t} - T_{i,J}^{t}}{\text{ThcL}}) \quad , \qquad \text{(K-22)}$$

$$\text{radial heat out} = h_{NA} \quad 2\pi \quad r_o \quad \Delta z \; (T_{i,J}^{t} - T_{i+1,J}^{t}) \quad , \qquad \text{(K-23)}$$

heat generated = 0

$$\rho_c \; C_{pc} \; \pi \; \left[r_o^2 - (r_o - \frac{\text{Thc}}{2})^2 \right] \Delta z \; (\frac{T_{i,J}^{t+\Delta t} - T_{i,J}^{t}}{\Delta t}) \quad , \qquad \text{(K-24)}$$

where

h_{NA} = coolant heat transfer coefficient,

r_o = clad outer radius.

Combining Eqs. (K-22) thru (K-24)

$$T_{i,J}^{t+\Delta t} = T_{i,J}^{t} + \frac{2\ \Delta t}{\rho_c\ C_{pc}\ (r_o\ \text{Thcl} - \frac{\text{Thcl}^2}{4})} \left[k_c\ (r_c + \frac{\text{Thcl}}{2}) \cdot (\frac{T_{i-1,J}^{t} - T_{i,J}^{t}}{\text{Thcl}}) - h_{NA}\ r_o\ (T_{i,J}^{t} - T_{i+1,J}^{t}) \right] , \tag{K-25}$$

F. Bulk Coolant

This node is located within the bulk coolant channel and includes all the coolant within an equivalent flow annulus. The expression for the equivalent area can be found below. Cross channel flow or heat conduction is not taken into account thus it is assumed an adiabatic surface is outside the coolant flow. The additional flow along the hex can walls is also ignored, thus the coolant/pin is lower than actual conditions.

1. Equivalent flow area for coolant flow,

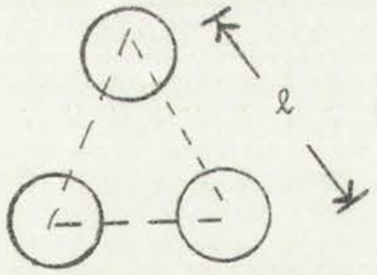

area of equilateral triangle = .43301 ℓ^2,

where

ℓ = pin pitch,

thus the area associated with ½ fuel pins = .43301 ℓ^2 - ½ π r_o^2

where

r_o = clad outer radius,

thus for 1 pin

AEQ (equivalent flow area) = $2 \cdot (.43301\, \ell^2 - \frac{1}{2} \pi r_o^2)$ (K-26).

2. Bulk coolant temperature

at bottom axial node (J=1), $T_{i,J}^{t+\Delta t}$ = coolant inlet temperature

for J > 1

$$\text{Radial heat in} = h_{NA}\ \Delta Z\ 2\pi\ r_o \left[T_{i-1,J}^{t} - T_{i,J}^{t}\right] \quad \text{(K-27)}$$

Radial heat out = 0,

$$\text{axial heat in - axial heat out} = \rho_{NA}\, C_{pNA} \cdot U \cdot AEQ \cdot \left[T_{i,J-1}^{t} - T_{i,J}^{t}\right] \quad \text{(K-28)}$$

$$\text{heat stored} = \rho_{NA}\ C_{pNA}\ \Delta z \cdot AEQ \left[\frac{T_{i,J}^{t+\Delta t} - T_{i,J}^{t}}{\Delta t}\right],$$

where

ρ_{NA} = coolant density,

C_{pNA} = coolant heat capacity,

AEQ = equivalent coolant flow area,

U = coolant velocity.

Combining Eqs. (K-27) thru (K-29)

$$T_{i,J}^{t+\Delta t} = T_{i,J}^{t} + \frac{\Delta t \quad h_{NA} \quad 2\pi \quad r_o}{\rho_{NA} \quad C_{pNA} \quad AEQ} \left[T_{i-1,J}^{t} - T_{i,J}^{t}\right]$$

$$+ \frac{U \quad \Delta t}{\Delta z} \left[T_{i,J-1}^{t} - T_{i,J}^{t}\right] \quad . \qquad \text{(K-30)}$$

APPENDIX L
VAPOR PRESSURE OF VOLATILE FISSION PRODUCTS OF INTEREST

A. Barium

The extrapolated vapor pressure of various investigators is plotted on Fig. L.1, and the tabular results are given in Tables L.1a-L.1c. Nesmeyanov's[1] curve is based on unverified experimental data in the temperature range 1333° - 1419° K. It should be noted that in this and all following partial pressure curves, theoretical or nonverified curves will be represented by dashed lines along with curves extrapolated beyond their valid or experimental limits.

Nesmeyanov's,[1] Hultgren's,[2] and the CRC's[3] data all agree fairly well in the area below 2000 K. The difference between the linear extrapolation of Hornung[4] and Hultgren, and the extrapolation containing phenomenological terms of Nesmayuanov can be seen in this Fig. L.1. The saturation curve of Hornung was determined over a larger experimental temperature range and will be used until more appropriate data can be found.

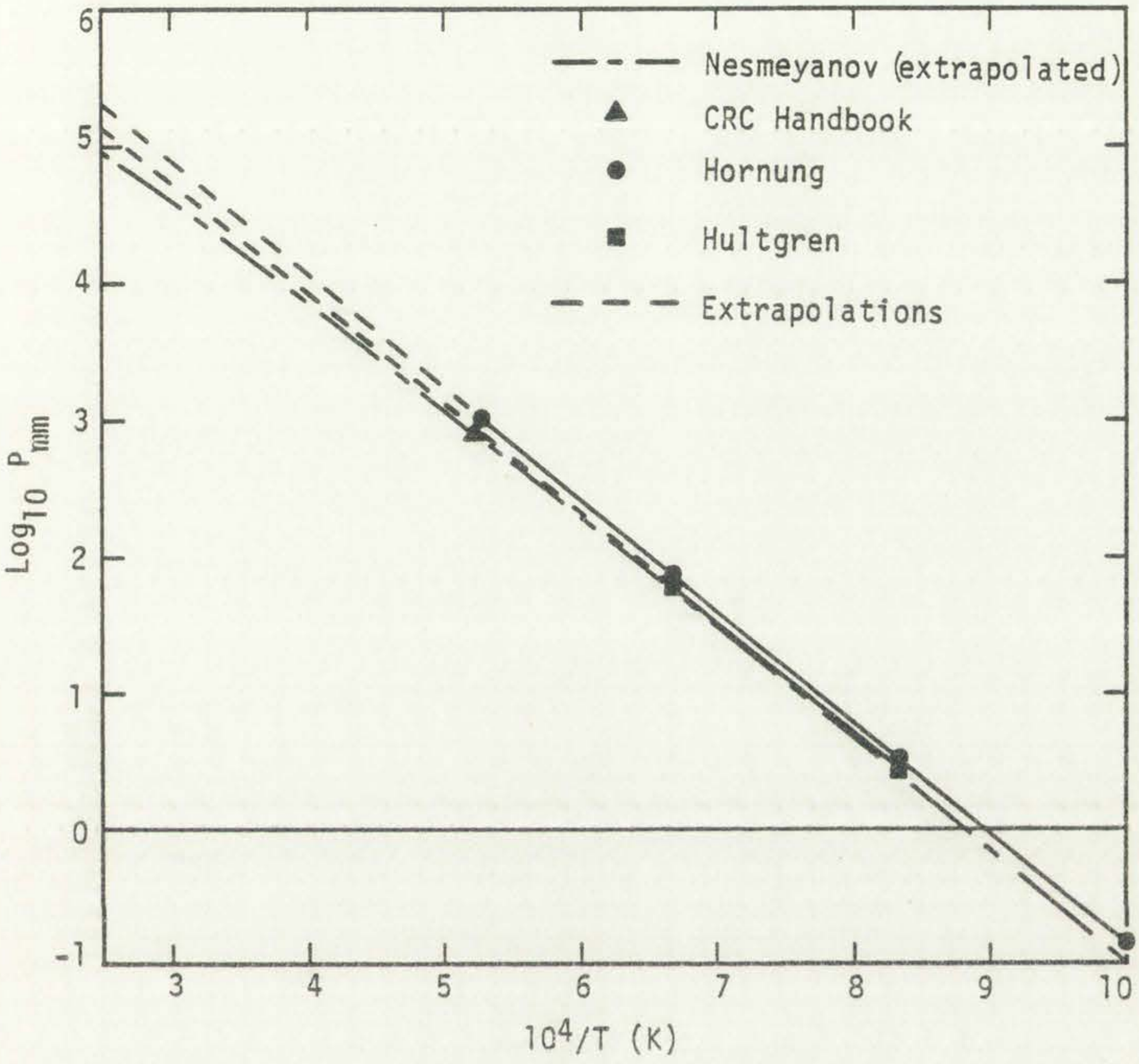

Figure L.1
Vapor pressure of barium.

TABLE L.1a
NESMEYANOV BARIUM PARTIAL PRESSURE DATA

T (K)	$\frac{10^4}{T}$	Log P_{mm}	P_{mm}
500	20.0	-9.382	4.15×10^{-10}
1000	10.0	- .977	.106
1200	8.33	.394	2.48
1500	6.67	1.747	55.80
2000	5.0	3.069	1.17×10^{3}
2500	4.0	3.838	6.88×10^{3}
3000	3.33	4.334	2.16×10^{4}

$$\text{Log } P_{mm} = 10.63717 - \frac{8703.64}{T} - .00001584\ T - .96481 \text{ Log } T \text{ (K)}$$

(Based on nonverified data)

TABLE L.1b
HULTGREN BARIUM PARTIAL PRESSURE DATA

T (K)	$\frac{10^4}{T}$	Log P_{atm}	P_{atm}	Log P_{mm}
1000	10.0	-3.79	1.63×10^{-4}	-.907
1200	8.33	-2.45	3.54×10^{-3}	.430
1500	6.67	-1.12	7.68×10^{-2}	1.77
2000	5.0	2.22×10^{-1}	1.667	3.10
2500	4.0	1.024	10.57	3.91

$$\text{Log } P_{atm} = \frac{-8020}{T} + 4.232 \text{ (1333 - 1419 K)}$$

TABLE L.1c
HORNUNG BARIUM PARTIAL PRESSURE DATA

T (K)	$\frac{10^4}{T}$	ℓn P	P_{atm}	Log P_{mm}
1000	10.0	-8.615	1.813×10^{-4}	- .86
1200	8.33	-5.477	4.18×10^{-3}	.502
1500	6.67	-2.34	.0964	1.865
2000	5.0	.799	2.224	3.23
2500	4.0	2.68	14.62	4.05
3000	3.33	3.94	51.3	4.59

$$\ell n\ P_{atm} = 10.214 - 3.621 \frac{T_c}{T} \quad (983 - 1895\ K)$$

where

T_c = 5200 K (critical temperature).

From CRC handbook

Boiling point = 1913 K

thus

$\frac{10^4}{T} = 5.227$ and log (760 mm) = 2.88

B. Cerium

Tables L.2a thru c and Fig. L.2 contain the saturation vapor pressure information for cerium. Nesmeyanov's[1] curve is based on unreliable data determined in the temperature range of 1460 - 1720 K. Hultgren[2] based his curve on the results of Daane and Spedding,[5]

and lies slightly above the curve determined by Ackermann, et al.[6] Ackermann believed that the Daane and Spedding data, and thus Hultgren's curve, is slightly erroneous, not due to weighing or temperature errors but due to the vaporization of CeO(g). Ackermann, et al. did take experimental steps to eliminate oxygen from the liquid Ce, and their data will be used until better information can be found.

TABLE L.2a
NESMEYANOV CERIUM PARTIAL PRESSURE DATA

T (K)	$\frac{10^4}{T}$	Log P_{mm}	P_{mm}
1460.	6.85	-4.447	3.57×10^{-5}
1720.	5.814	-2.025	9.45×10^{-3}
2000	5.0	- .12	.758
2500.	4.0	2.22	165.96
2690	3.717	2.88	760.0
3000	3.33	3.78	6.026×10^{3}
3500	2.857	4.89	7.84×10^{4}

$$\text{Log } P_{mm} = 11.58 - \frac{23400.}{T\ (K)}$$

Unreliable data taken in temperature range 1470 - 1720 K.

TABLE L.2b
HULTGREN CERIUM PARTIAL PRESSURE DATA

T (K)	$\frac{10^4}{T}$	P_{atm}	Log P_{mm}
1600.	6.25	5.44×10^{-8}	-4.38
1800.	5.556	1.40×10^{-6}	-2.973
2000	5.0	1.88×10^{-5}	-1.85
2038	4.91	2.90×10^{-5}	-1.66
3000	3.33	4.54×10^{-2}	1.54
3500	2.86	4.21×10^{-1}	2.51
3742	2.67	1.0	2.88

$$\text{Log } P_{atm} = \frac{-20304.}{T} + 5.4254 \quad (1611 - 2038 \text{ K})$$

TABLE L.2c
ACKERMANN CERIUM PARTIAL PRESSURE DATA

T (K)	$\frac{10^4}{T}$	Log P_{atm}	P_{mm}	Log P_{mm}
1500.	6.667	-8.547	2.158×10^{-6}	-5.667
1750.	5.714	-6.54	2.19×10^{-4}	-3.66
2000.	5.0	-5.035	7.01×10^{-3}	-2.154
2250.	4.44	-3.86	.104	-.983

$$\text{Log } P_{atm} = 5.500 - \frac{21070.}{T} \quad (1525 - 2225 \text{ K})$$

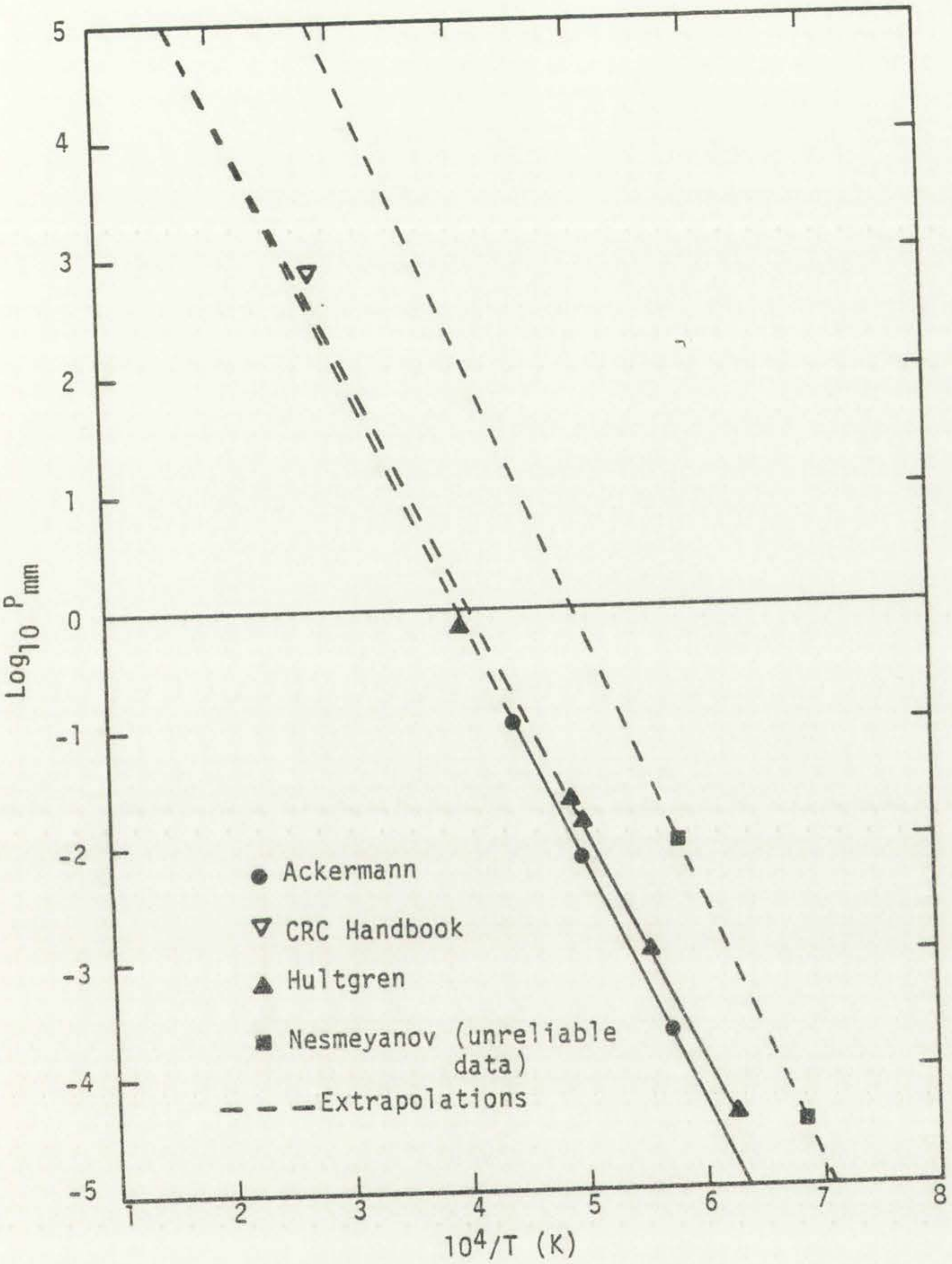

Figure L.2
Vapor pressure of cerium.

From CRC[3] handbook

Boiling Point = 3548 K

thus

$$\frac{10^4}{T} = 2.818 \quad , \log (760 \text{ mm}) = 2.88$$

C. Palladium

Tables L.3a thru L.3c and Fig. L.3 contain the saturation vapor pressure data for palladium. Nesmeyanov's[1] curve is based on theoretical work only and gives a lower partial pressure than either Hultgren[2] or Wise.[7] Wise in his book plots the saturation vapor pressure in the temperature range, 2000 - 3000 K. His plot, however, is based on the experiments of Dreger and Margrave,[8] and Hampson and Walker[9] both of which were done at temperature less than 1488 K. His curve should actually be regarded as an extrapolation. Thus Hultgren's curve will be assumed unless more suitable data is found.

TABLE L.3a
NESMEYANOV PALLADIUM PARTIAL PRESSURE DATA

T (K)	$\frac{10^4}{T}$	Log P_{mm}	P_{mm}
1500	6.67	-4.249	$5.64\text{x}10^{-5}$
2000	5.0	-1.053	.0886
2500	4.0	.868	7.376
3000	3.33	2.151	$1.415\text{x}10^{2}$
3500	2.86	3.07	$1.174\text{x}10^{3}$
4000	2.50	3.76	$5.77\text{x}10^{3}$
4500	2.22	4.30	$2.00\text{x}10^{4}$

$$\text{Log } P_{mm} = 8.76587 - \frac{19169.84}{T} + .00002347T - .08499 \text{ Log } T$$

(theoretical)

TABLE L.3b
HULTGREN PALLADIUM PARTIAL PRESSURE DATA

T(K)	$\frac{10^4}{T}$	Log P_{mm}	P_{mm}
1366	7.32	-4.12	$1\text{x}10^{-7}$
1500	6.66	-2.95	$1.48\text{x}10^{-6}$
1600	6.25	-2.2	$8.21\text{x}10^{-6}$
2000	5.00	- .012	$1.28\text{x}10^{-3}$
2600	3.85	1.95	.188
3200	3.125	3.22	2.18

$$\text{Log } P_{mm} = 8.6870 - \frac{17494}{T} \text{ (1388 - 1675 K)}$$

TABLE L.3c
WISE PALLADIUM PARTIAL PRESSURE DATA

T(K)	$\frac{10^4}{T}$	Log P_{mm}	P_{mm}
2000	5.0	- .638	.23
2273	4.40	.505	3.2
2500	4.0	1.312	20.5
2773	3.61	2.08	120.0
3077	3.25	2.792	620.0
3148	3.18	2.881	760.0

Based on experimental data.

From CRC[3] Handbook

Boiling Point = 3413 K

thus

$\frac{10^4}{T}$ = 2.93, log (760 mm) = 2.88.

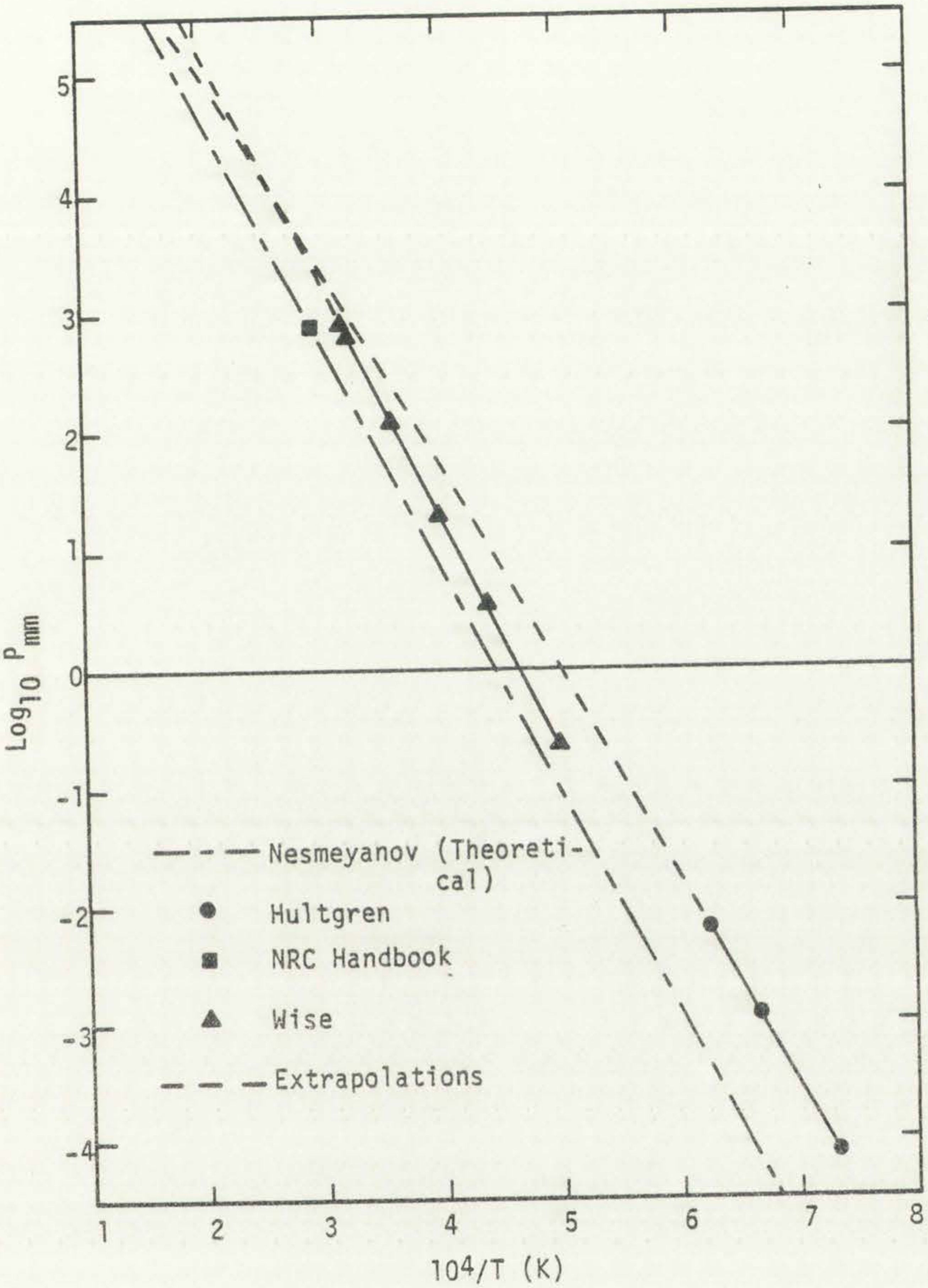

Figure L.3
Vapor pressure of Palladium.

D. Iron

The partial pressure data for iron is contained in Tables L.4a thru L.4c and Fig. L.4. Nesmeyanov's[1] curve is based on vapor pressures in the area of 10^{-4} - 10^{-5} mm Hg and is thus extrapolated well beyond its experimental limit. Hultgren's[2] curve is based principally on the experimental work of Morris, et al.[10] (1810 - 1889 K). The vapor pressure curve of Hornung[4] will be used due to its more appropriate experimental range (1809 - 3500 K).

TABLE L.4a

NESMEYANOV IRON PARTIAL PRESSURE DATA

T (K)	$\frac{10^4}{T}$	Log P_{mm}	P_{mm}
1453	6.882	-4.0	10^{-4}
1566	6.386	-3.0	10^{-3}
1698	5.889	-2.0	10^{-2}
1859	5.379	-1.0	10^{-1}
2063	4.847	0.0	1.0
2318	4.314	1.0	10.0
2649	3.775	2.0	100.0
3045	3.284	2.88	760.0

$$\text{Log } P_{mm} = -25.93396 - \frac{14124.5}{T} + .00113331T + 10.59505 \text{ Log } T$$

TABLE L.4b
HULTGREN IRON PARTIAL PRESSURE DATA

T (K)	$\frac{10^4}{T}$	Log P_{mm}	P_{atm}
1387	7.21	-5.12	10^{-8}
1485	6.73	-4.12	10^{-7}
1599	6.25	-3.12	10^{-6}
1732	5.77	-2.12	10^{-5}
1895	5.28	-1.12	10^{-4}

$$\text{Log } P_{mm} = 9.181 - \frac{19835}{T} \quad (1300 - 1889 \text{ K})$$

TABLE L.4c
HORNUNG IRON PARTIAL PRESSURE DATA

T (K)	$\frac{10^4}{T}$	$\ell n P_{atm}$	P_{atm}	Log P_{mm}
1800	5.556	-10.42	2.98×10^{-5}	-1.644
2000	5.0	-7.98	3.408×10^{-4}	- .587
2500	4.0	-3.60	.0273	1.32
3000	3.33	- .679	.507	2.59
3500	2.86	1.408	4.09	3.49

$$\ell n P_{atm} = 13.932 - \frac{4.693\ T_c}{T} \quad (1809 - 3500 \text{ K})$$

where

T_c = 9340 K (critical temperature).

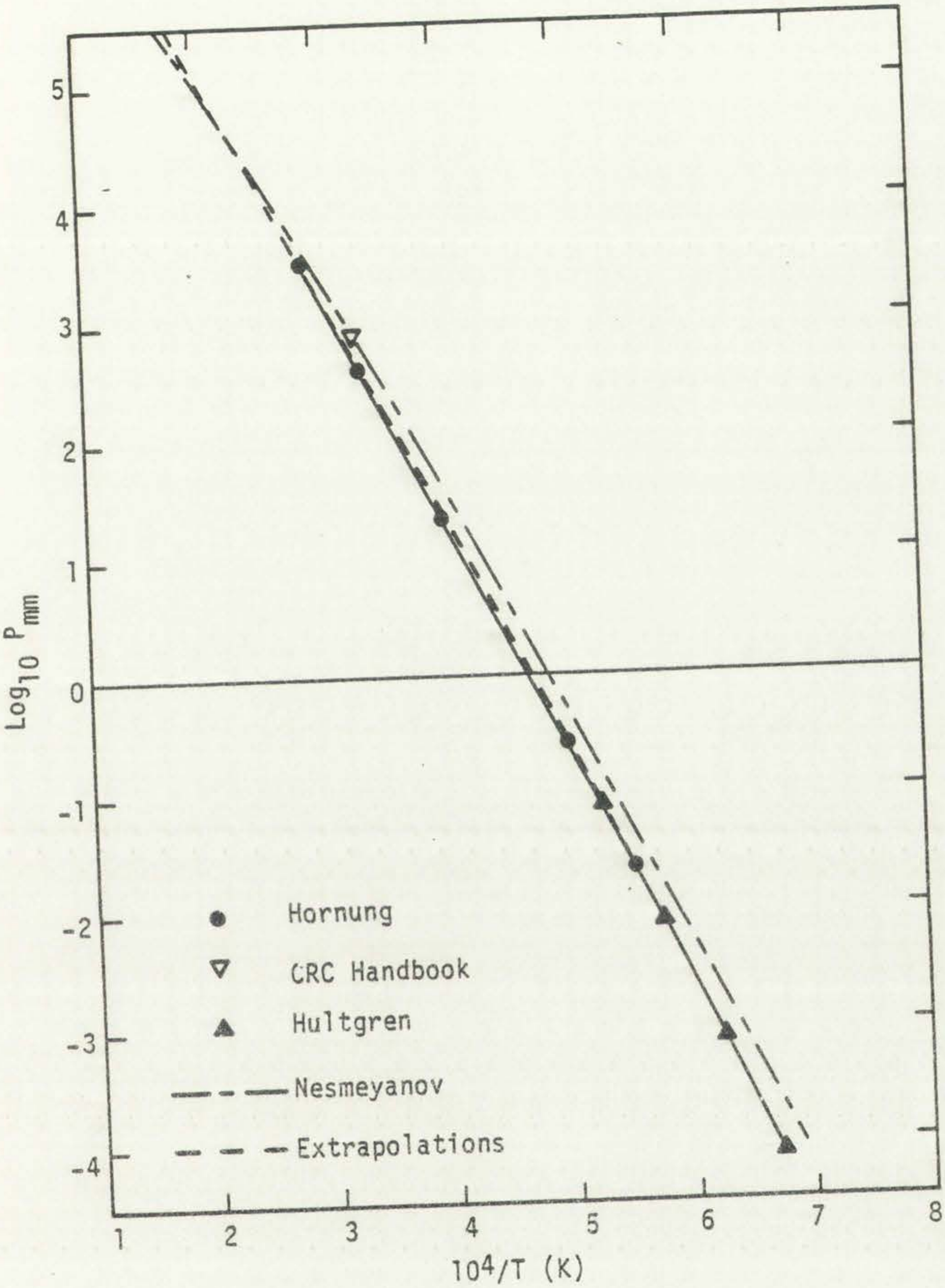

Figure L.4
Vapor pressure of iron.

From CRC[3] Handbook

Boiling Point = 3033 K

thus

$$\frac{10^4}{T} = 3.297, \log (760 \text{ mm}) = 2.88.$$

E. Tellurium

Figure L.5 and Tables L.5a and L.5b contain the work of various investigators on the saturation pressure of tellurium. Nesmeyanov[1] considers his upper end of reliability to be 1100 K. Baker[11] however, experimentally determined the vapor pressure in the range 981-1680 K. It should be noted that tellurium, in the vapor phase, exists as predominantly $Te_2(g)$ at least up until 1200 K. By observing the linear extrapolation of Baker's lower vapor pressure data, it appears that $Te_2(g)$ is dominant into the 1800 K range, or at least the disassociation occurs linearly. Stull and Sinke[12] list thermodynamic properties of $Te_2(g)$ to 3000 K. Baker's curve will be used unless more suitable data is found.

TABLE L.5a

NESMEYANOV TELLURIUM PARTIAL PRESSURE DATA

T (K)	$\frac{10^4}{T}$	Log P_{mm}	P_{mm}
1000	10.0	1.638	43.49
1250	8.0	2.7765	597.78
800	12.5	.1552	1.43

For Σ Te, i.e., Te(g) + Te_2(g)

$$\text{Log } P_{mm} = -32.44504 - \frac{4036.949}{T} - .00413735\ T + 14.08592 \text{ Log } T$$

(500 - 1100 K)

TABLE L.5b

BAKER TELLURIUM PARTIAL PRESSURE DATA

T(K)	$\frac{10^4}{T}$	P_{atm}	Log P_{mm}
981	10.19	.0434	1.518
1188	8.42	.494	2.574
1266	7.90	1.00	2.881
1323	7.56	1.58	3.079
1463	6.83	4.20	3.509
1580	6.33	8.16	3.792
1685	5.97	13.82	4.021
1780	5.62	21.00	4.203

$$\text{Log } P_{atm} = -\frac{6447}{T} - 1.0 \text{ Log } T + 8.1945 \ (981 - 1780 \text{ K}).$$

From CRC[3] handbook:

Boiling Point = 1263 K ,

thus

$$\frac{10^4}{T} = 7.92 \quad , \ \log (760 \text{ mm}) = 2.88 \quad .$$

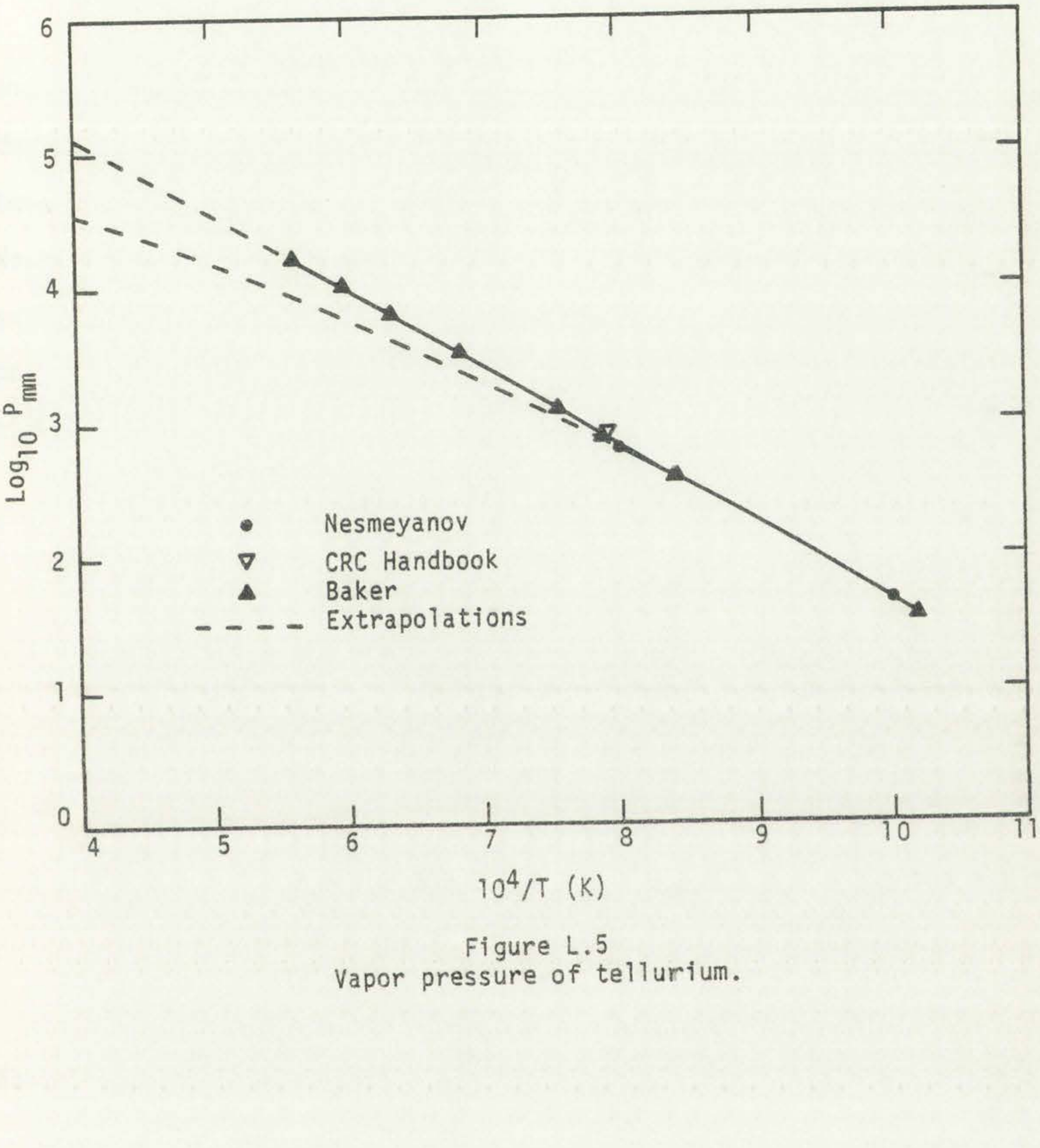

Figure L.5
Vapor pressure of tellurium.

F. Antimony

Gaseous Sb consists predominantly of polyatomic molecules, Sb_2 and Sb_4. It appears from Fig. L.6 that a shift in the temperature dependence of the average molecular weight occurs at the melting temperature. Hultgren's[2] work is based partially on the data of Nesmeyanov[1] and thus the close correlation of two curves. Further saturation data for Sb should be found, since the disassociation of the polyatomic molecules could alter the high temperature portion of the curve.

TABLE L.6a

NESMEYANOV ANTIMONY PARTIAL PRESSURE DATA

T(K)	$\frac{10^4}{T}$	Log P_{mm}	P_{mm}
800	12.50	-2.117	7.64×10^{-3}
900	11.11	- .759	1.74×10^{-1}
1000	10.0	- .106	7.83×10^{-1}
1200	8.33	.816	6.54
1500	6.67	1.83	67.8
1800	5.56	2.63	427.0
1898	5.27	2.88	760.0

For Σ Sb, i.e., Sb(g), Sb_2(g) and Sb_4(g).

TABLE L.6b

HULTGREN ANTIMONY PARTIAL PRESSURE DATA

T (K)	$\frac{10^4}{T}$	P_{atm}	Log P_{mm}
693	14.43	10^{-7}	-4.12
741	13.5	10^{-6}	-3.12
803	12.45	10^{-5}	-2.12
872	11.47	10^{-4}	-1.12
1007	9.93	10^{-3}	- .12
1225	8.16	10^{-2}	.881
1520	6.58	10^{-1}	1.88
1908	5.24	1.0	2.88

For Σ Sb

From CRC[3] handbook

Boiling Point = 2023 K

thus

$$\frac{10^4}{T} = 4.94, \log (760 \text{ mm}) = 2.88.$$

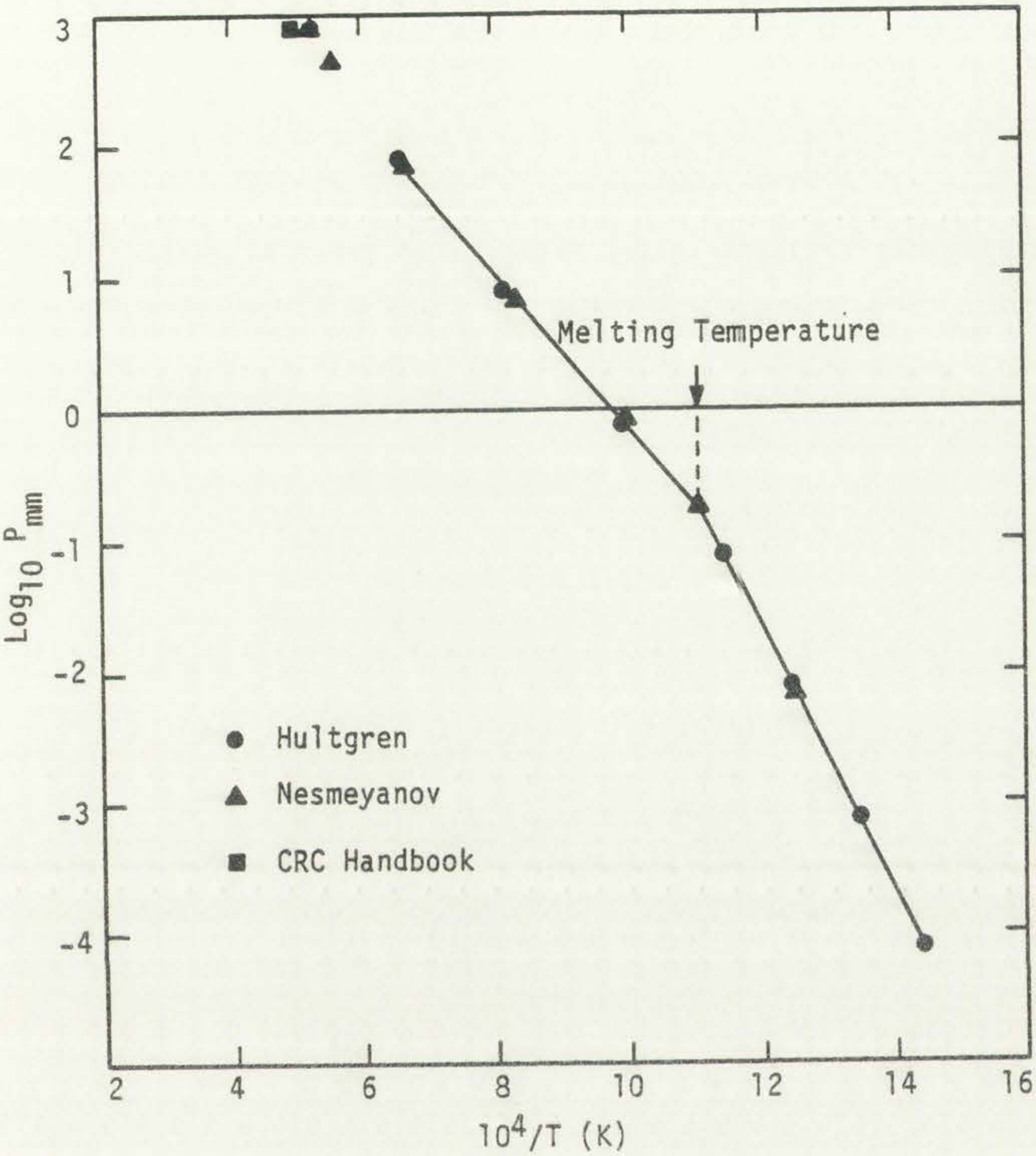

Figure L.6
Vapor pressure of Antimony.

G. Cesium

Nesmeyanov's[1] curve is based on reliable data determined at pressures less than 10 mm Hg. Thus in Fig. L.7, his curve is extrapolated well beyond the upper experimental limit. Stone's[13] curve is based on experimental points measured at higher temperatures than Hultgren[2] and will thus be assumed until better information is located. It should be noted in extrapolating the partial pressure Cs, that Cs(g) is made up of monatomic and diatomic molecules.

TABLE L.7a

NESMEYANOV CESIUM PARTIAL PRESSURE DATA

T (K)	$\frac{10^4}{T}$	Log P_{mm}	P_{mm}
800	12.5	2.162	145.37
959	10.428	2.882	761.32
1000	10.0	3.025	$1.0x10^3$
1250	8.0	3.656	$4.532x10^3$
1600	6.25	4.126	$1.336x10^4$
2000	5.00	4.367	$2.326x10^4$

$$\text{Log } P_{mm} = 8.22127 - \frac{4006.048}{T} - .0060194\ T - .19623 \text{ Log } T \text{ (Less 10 mm Hg)}$$

TABLE L.7b
HULTGREN CESIUM PARTIAL PRESSURE DATA

T (K)	$\frac{10^4}{T}$	P_{atm}	Log P_{mm}
800	12.5	.172	2.116
900	11.11	.551	2.662
955	10.47	.932	2.850
963	10.38	1.0	2.881
1000	10.0	1.32	3.001

$T \leq 1000$ K

TABLE L.7c
STONE CESIUM PARTIAL PRESSURE DATA

T (K)	$\frac{10^4}{T}$	P_{atm}	Log P_{mm}
943.33	10.601	1.0169	2.89
1558.611	6.416	33.53	4.406
1526.611	6.55	30.071	4.359
1020.8	9.796	1.9968	3.181
1148.28	8.709	5.00	3.580
1267.833	7.887	9.998	3.881
1411.556	7.084	10.346	4.167
920.78	10.86	.811	2.790

$$\text{Log } P_{atm} = 5.87303 - \frac{7040.7}{T} - .5329 \text{ Log } T\ (^{o}R)\ (920 - 1558\text{ K}) \quad .$$

From CRC[3] Handbook:

Boiling Point = 951.4 K

thus

$$\frac{10^4}{T} = 10.51, \log (760 \text{ mm}) = 2.88.$$

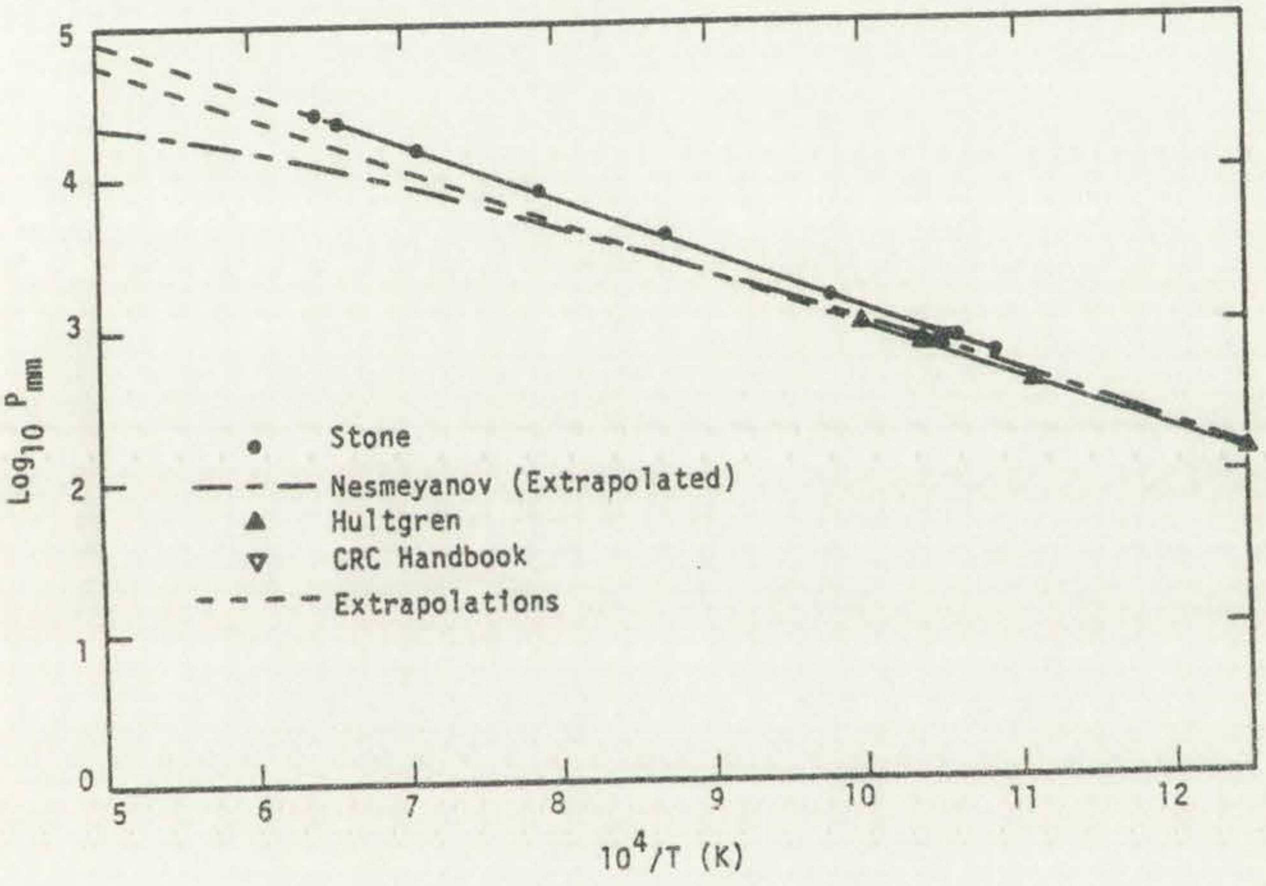

Figure L.7
Vapor pressure of Cesium.

REFERENCES

1. A. N. Nesmeyanov, Vapor Pressure of the Chemical Elements (Elsevier Publishing Company, 1963).

2. R. Hultgren, R. Orr, P. D. Anderson, K. K. Kelley, Selected Values of Thermodynamic Properties of Metals and Alloys (John Wiley and Sons, Inc., 1963).

3. R. C. Weast, CRC Handbook of Chemistry and Physics (The Chemical Rubber Company, 1972) 53rd edition.

4. K. Hornung, "Liquid Metal Coexistence Properties from Corresponding States and Third Law," Journal of Applied Physics, 46, No. 6 (1975).

5. A. H. Daane, F. H. Spedding, "Abstracts of Papers," 134th Meeting of the American Chemical Society, 255 (1958).

6. R. J. Ackermann, M. Kojima, E. G. Rauh, R. R. Walters, "The Thermodynamics of Vaporization of Cerium," Journal of Chemical Thermodynamics, 1, (1969) pp. 527-553.

7. E. M. Wise, Palladium Recovery, Properties, and Uses (Academic Press, 1968).

8. L. H. Dreger, J. L. Margrave, "Vapor Pressures of Platinium Metals. I. Palladium and Platinium," Journal of Physical Chemistry, 64 (1960) pp. 1323-1324.

9. R. F. Hampson and R. F. Walker, "The Vapor Pressure of Palladium," Journal of Research of the National Bureau of Standards - A. Physics and Chemistry, 66A, No. 2 (1962).

10. J. P. Morris, G. R. Zellans, S. L. Payne, R. L. Kipp, "Vapor Pressures of Liquid Iron and Liquid Nickel," U. S. Bur. Mines, Report Invest. No. 5364 (1957).

11. E. H. Baker, "The Boiling Point Relation for Tellurium at Elevated Pressures," Chemical Society London Journal (A) (1967).

12. D. R. Stull and G. C. Sinke, The Thermodynamic Properties of the Elements (American Chemical Society, 1956).

13. J. P. Stone, C. T. Ewing, J. R. Spann, E. W. Steinkuller, D. D. Williams, R. R. Miller, "High Temperature Vapor Pressures of Sodium, Potassium, and Cesium," Journal of Chemical and Engineering Data, 11, No. 3, (July 1966) pp. 315-320.

APPENDIX M

DERIVATION OF VAPOR PRESSURE EQUATION ASSUMING TEMPERATURE DEPENDENT LATENT HEAT OF VAPORIZATION

For compressible substance

$$dU = TdS - PdV \qquad (M\text{-}1)$$

where

U = internal energy,

T = temperature,

S = entropy,

P = pressure,

V = volume.

Using the Helmholtz function

$$A = U - TS$$

$$dA = dU - TdS - SdT \qquad (M\text{-}2)$$

Substitute Eq. (M-1) into Eq. (M-2)

$$dA = -PdV - SdT$$

$$-dA = PdV + SdT \qquad \text{(M-3)}$$

For $z = f(x,y)$

$$dz = \left.\frac{\partial z}{\partial x}\right|_y dx + \left.\frac{\partial z}{\partial y}\right|_x dy = Mdx + Ndy \quad ,$$

then

$$\left.\frac{\partial M}{\partial y}\right|_x = \left.\frac{\partial N}{\partial x}\right|_y \quad ,$$

thus from Eq. (M-3)

$$\left.\frac{\partial P}{\partial T}\right|_V = \left.\frac{\partial S}{\partial V}\right|_T \quad , \qquad \text{Maxwell relation} \quad . \qquad \text{(M-4)}$$

Consider the change of state from saturated liquid to saturated vapor of a pure substance. This occurs at constant temperature, and using saturated states, pressure and temperature are independent of volume. Thus Eq. (M-4) becomes

$$\frac{dP}{dT}_{sat} = \frac{S_g - S_f}{V_g - V_f} \quad , \qquad \text{(M-5)}$$

$$S_g - S_f = \frac{\Delta H}{T} \quad , \qquad \text{(M-6)}$$

where ΔH is the latent heat of sublimation or vaporization thus Eq. (M-5) becomes

$$\frac{dP}{dT} = \frac{\Delta H}{T\Delta V} \quad , \qquad \text{(M-7)}$$

where

ΔV = change in volume during transition from condensed to vapor phase.

Assume the volume of the condensed phase is small compared to the vapor phase. Using the Ideal Gas law, Eq. (M-7) becomes

$$\frac{dP}{dT} = \frac{P\Delta H}{RT^2} \quad ,$$

or

$$\frac{d\ell nP}{dT} = \frac{\Delta H}{RT^2} \quad . \qquad \text{(M-8)}$$

Now if one assumes a constant ΔH

integrating Eq. (M-8)

$$\ell n\ P = \frac{-\Delta H}{RT} + \text{constant} \quad ,$$

$$\text{Log } P = -\frac{\Delta H}{4.575T} + C = A + \frac{B}{T} \quad ,$$

which takes the straight line form.

Now assume ΔH is a function of temperature

$$\Delta H = \Delta H_o + aT + bT^2 + cT^3 + \text{--------} \quad . \qquad \text{(M-9)}$$

Substitute Eq. (M-9) into Eq. (M-8)

$$d\ell n\ P = \frac{\Delta H_o}{RT^2}\,dT + \frac{a}{R}\frac{dT}{T} + \frac{b}{R}\,dT + \frac{c}{R}\,TdT + \text{--------}\quad , \qquad \text{(M-10)}$$

integrate

$$\ell n\ P = -\frac{\Delta H_o}{RT} + \frac{a}{R}\,\ell nT + \frac{b}{R}\,T + \text{--------} + \text{constant}\quad , \qquad \text{(M-11)}$$

$$\text{Log } P = -\frac{\Delta H_o}{4.575T} + \frac{a}{1.987}\,\text{Log } T + \frac{b}{4.575}\,T + \text{---} + \text{constant}\ . \qquad \text{(M-12)}$$

Since $\ell n\ x = 2.3026$ Log x,

Eq. (M-12) has general form

$$\text{Log } P = A + \frac{B}{T} + cT + D\ \text{Log } T + \text{----}\quad , \qquad \text{(M-13)}$$

which is the general form used by Nesmeyanov.

Substituting (8-42) into Eq. (8-41)

$$\ln P = [illegible]$$

Integrate

$$\ln P = [illegible] + \text{constant} \quad (8-41)$$

$$\log P = [illegible] \quad (8-42)$$

Since ln x = 2.303 log x,

Eq. (8-42) has general form

$$\log P = A + \frac{B}{T} + CT + D \log T \quad (8-43)$$

which is the general form used by [illegible]

APPENDIX N
PROGRAM LISTING

```
      PROGRAM VAIL (INALL,TAPE9=INALL,OUT1,TAPE10=OUT1)
C     PROGRAM MAIN
      COMMON/BL1/QGEN(30),HG(30),R(20),K,DELTT,PI,IB,AEQ,QORIG(30)
      COMMON/BL2/DENFL,SHFL,CONFL,DENBO,SHBO,CONBO,DENCD,SHCD,CONCD,
     1DENNA,SHNA,CONNA,HCFLC,TMELT,HMELT,TVAP,HVAP,TEMAX
      COMMON/BL3/RADFL,THCLD,THBOND,HGT,DEC,THFLM,TEMPO,U,CDOUT,CDIN,
     1DHG,DR,HCOV,AREA,JM,IM,IMZ,JMZ,IA,TAVE,IPZ,HCFLOT,HCFLOB,
     2NPRINT,TPLEN,TSTOR(20,25),TSTOV(20,25)
      COMMON/BL5/TS(30,25),TSB(25,30,2),SGH(20,25),SVP(20,25),NCO
      COMMON/BL6/LJ,LT1,LT2,VLT,VLB,LT3,LBP,JC
      DIMENSION BS(15),DS(15),QYAVF(300),TTP2(300),E(15)
     1,COMP(15),PCRIT(15),TCRIT(15),ARK(15),BRK(15),CHI(15),DRINC(15)
C
C       THIS PROGRAM CALCS. VOL. EXPANSION DUE TO INCLUSION VOLITILIZA-
C         TION ASSUMING:
C      1)SEGRAGATION OF INCLUSION CONSTITUENTS.I.E. EACH COMPONENT
C      VAPORIZES WHEN ITS VAPOR PRESS. EXCEDES P-BULK WHEN IHOMO=0.
C     IF IHOMO=1,ASSUMES INCLUSIONS ARE SOLID SOLUTIONS. THUS
C     VAPORIZATION OCCURS WHEN SUM OF THE PARTIAL PRESSURES
C     EXCEEDS P-BULK(RAOULTS LAW).
C      2)INSTANT VAPORIZATION AND GROWTH AT TVAP.
  117 FORMAT(//,"****NODES IN FUEL ARE",I5,"THRU",I5)
  129 FORMAT(20X,I4,17X,F12.6,20X,F12.6)
  125 FORMAT(//,20X,"NODE",20X,"HEIGHT",20X,"Q GENERATION",//)
   83 FORMAT(3I10)
   85 FORMAT(3E20.7)
   87 FORMAT(2E20.7)
   89 FORMAT(//,"AXIAL NODES-I=",I5,"    FUEL NODES-I=",I5,"   NO.DELAY
     1GROUPS=",I5)
   91 FORMAT(/,"RAD.FUEL=",F12.6,"  THICK.CLD.=",F12.6,"  THICK,BOND=",
     1F12.6)
   93 FORMAT(/,"  HEIGHT FUEL=",F12.6,"  HEIGHT REF.+BLANK.=",F12.6,"
     1    EXTRAP. DIST.=",F12.6)
   95 FORMAT(/,"MAX.QGEN=",F12.6,"  QGEN IN REF.+BLANK.=",F12.6,"  PITCH
     1/DIA.=",F12.6)
   97 FORMAT(/,"INLET NA TEMP.=",F12.6,"    NA VEL.=",F12.6)
   99 FORMAT(/,"*** TIME STEP FOR FINITE DIFF. AND PTKEN=",F12.6)
   51 FORMAT(/,"MELT TEMP=",F12.6,"    HEAT OF FUSION=",F12.6)
   53 FORMAT(/,"VAP. TEMP=",F12.6,"    HEAT OF VAP.=",F12.6)
   54 FORMAT(/,"PROMPT NEUT. GEN. TIME=",E12.6,"    RAMP  INSERTION
     1 IN $/SEC.=",F12.6)
   55 FORMAT(//,"DENSITY",10X,"HEAT CAP.",10X,"THERM. COND. FOR FUEL.
     1CLAD,SODIUM,BOND")
   56 FORMAT(/,"LIMITING TIME=",F12.6,"    LIMITING TEMP=",F12.6)
   57 FORMAT(E12.6,5X,F12.6,7X,E12.6)
   59 FORMAT(//,10X,"BETA",15X,"LAMBDA")
   63 FORMAT(6X,E12.6,7X,F12.6)
  130 FORMAT(5X,"****** INPUT DATA IN CMS,SEC.,DEGREES K,CAL.",/)
  163 FORMAT(/,"TIME=",F7.5,"    P1=",E12.6,"    DT=",F7.5,"  D=",
     1F7.5,"    P1OUT=",E12.6)
  165 FORMAT(/,"REACTIVITY=",E12.6,"    P2=",E12.6,"    P3=",E12.6)
   71 FORMAT(8F10.3)
   72 FORMAT(2X,"TRANSFERRED VARIABLES",2X,"T=",F11.6,4X,"DT=",F11.6,4X,
     1"HOHEAT=",F15.8,4X,"TMAX",F11.6,3X,"PAVE ",E12.5)
   78 FORMAT(I5,2F12.4)
   80 FORMAT(3X,"HCOV=",E11.3,/)
   81 FORMAT(//,3X,"AXIAL NODE=",I3,3X,"HEIGHT=",F9.3,"CM",6X,"TEMP
     1 COOLANT=",F10.3)
   82 FORMAT(5(3X,F7.3,2X,F10.3),"  FUEL")
  143 FORMAT(//,8X,"***STEADY STATE TEMPERATURE DISTRIBUTION IN COOLANT
```

```
     1 AND FUEL PIN***",/)
 147 FORMAT(2(3X,F7.3,2X,F10.3),"     CLAD INNER AND OUTER TEMPS,")
 202 FORMAT(3X,"DELTT",F12.6,3X,"DT",F10.6,3X,"QZAV(CAL/CC SEC)",E12.5,
     13X,"QZAW(WATTS/CC)",E12.5)
 199 FORMAT(5(3X,"  R     ",2X,"  TEMP     "))
 144 FORMAT(////,3X,"***** TRANSIENT CALCULATION *****",//)
  21 FORMAT(I10)
  22 FORMAT(/,"PLENPRESS=",F10.5,"  RAD. INCL=",E12.6,"  NO.
     1 DENSITY OF INCL=",E12.6)
  24 FORMAT(/,"MATERIAL=",10X,"  MOLES/INCL")
  28 FORMAT(3X,I5,12X,E12.6)
  37 FORMAT(/,"ELEMENT",10X,"PCRIT",10X,"TCRIT")
  33 FORMAT(3X,I4,10X,E12.6,5X,E12.6)
  49 FORMAT(/,"NODE",15X,"CHI")
 301 FORMAT(/,10X,"***INCLUSION ASSUMED SEGREGATED***")
 304 FORMAT(/,10X,"***INCLUSION ASSUMED HOMOGENEOUS***")
C
C      UNITS INPUT ARE; CMS,SEC.,DEGREES K,CAL.
       READ(9,83) JM,IM,NP
       READ(9,83) IFLAG,IDATA,NPRINT
       READ(9,83) IHOMO
       READ(9,85) RADFL,THCLD,THBOND
       READ(9,85) HTFL,HTRB,ZEXT
       READ(9,85) PMAX,PMIN,PITCH
       READ(9,85) TEMPO,U,DELTT
C      DT MUST BE SMALL ENOUGH TO SATISFY THE CONVERGENCE CRITERION
C      OF THE FINITE DIFFERENCE HEAT TRANSFER EQUATIONS
       READ(9,85) DENFL,SHFL,CONFL
       READ(9,85) DENCD,SHCD,CONCD
       READ(9,85) DENNA,SHNA,CONNA
       READ(9,85) DENBD,SHBD,CONBD
       READ(9,85) PLNPRS,ROINC,DINC
       READ(9,85) (BS(J),J=1,NP,1)
       READ(9,85) (DS(J),J=1,NP,1)
       READ(9,87) TMELT,HMELT
       READ(9,87) TVAP,HVAP
       READ(9,87) PGT,RAMP
       READ(9,87) TIMAX,TEMAX
       IA=IM+1
       READ(9,85) (CHI(I),I=1,IA,1)
       READ(9,21) NUM
C      ORDER OF INCLUSION INPUT IS BA,CE,PD,FE,TE,SB,CS,MO,RU,RH,TC
       READ(9,85) (COMP(K),K=1,NUM,1)
       DO 39 K=1,NUM
       READ(9,87) PCRIT(K),TCRIT(K)
  39   CONTINUE
C      POWER DENSITY=600KW/LITER=144CAL/CM3.SEC
C      QGEN IS VOLUMETRIC HEAT GENERATION
       JMZ=JM+1
C
C       OUTPUT DATA
       IF(IDATA.LE.0) GO TO 40
       WRITE(10,130)
       WRITE(10,89) JM,IM,NP
       WRITE(10,91) RADFL,THCLD,THBOND
       WRITE(10,93) HTFL,HTRB,ZEXT
       WRITE(10,95) PMAX,PMIN,PITCH
       WRITE(10,97) TEMPO,U
       WRITE(10,99) DELTT
       WRITE(10,51) TMELT,HMELT
```

```
      WRITE(10,53) TVAP,HVAP
      WRITE(10,54) PGT,RAMP
      WRITE(10,56) TIMAX,TEMAX
      WRITE(10,55)
      WRITE(10,57) DENFL,SHFL,CONFL
      WRITE(10,57) DENCO,SHCO,CONCD
      WRITE(10,57) DENNA,SHNA,CONNA
      WRITE(10,57) DENBO,SHBD,CONBD
      WRITE(10,59)
      DO 61 J=1,NP,1
      WRITE(10,63) BS(J),DS(J)
   61 CONTINUE
      WRITE(10,22) PLNPRS,RDINC,DINC
      WRITE(10,24)
      IF(IHOMO.EQ.1) GO TO 300
      WRITE(10,301)
      GO TO 302
  300 WRITE(10,304)
  302 DO 26 K=1,NUM
      WRITE(10,28) K,COMP(K)
   26 CONTINUE
      WRITE(10,49)
      DO 47 I=1,IA,1
      WRITE(10,28) I,CHI(I)
   47 CONTINUE
      WRITE(10,37)
      DO 35 K=1,NUM,1
      WRITE(10,33) K,PCRIT(K),TCRIT(K)
   35 CONTINUE
   40 PI=3.14159
      TTEM=DELTT
C     SET INDEXES
C     K IS TIME INDEX FROM START OF TRANSIENT
      K=1
      KJ=2
      IMZ=IM + 3
      IPZ=IM+4
      IB=IM+2
      IA=IM+1
  200 CONTINUE
C
C     SET RADIAL NODES
      DR=(RADFL/FLOAT(IM))
      CDOUT=DEQ=RADFL + THBOND + THCLD
      CDIN=RADFL + THBOND
      AREA=(1./4.)*PI*CDOUT**2
      R(1)=0.0
      DO 201 I=2,IM,1
      R(I)=R(I-1) + DR
  201 CONTINUE
      R(IA)=RADFL
      R(IB)=CDIN
      R(IMZ)=CDOUT
C     FIND EQUIV. OUTER RADIUS OF NA FLOW FROM PITCH
      PITCM=PITCH*2.*R(IMZ)
      AEQ=2.*(.43301*PITCM**2-(PI*R(IMZ)**2)/2.)
      R(IPZ)=R(IM+4)=SQRT((AEQ/PI)+CDOUT*CDOUT)
C
C     SET AXIAL NODES
      DHG=(HTFL+2.*HTRB)/FLOAT(JM)
```

```
      HG(1)=0.0
      DO 111 J=2,JMZ,1
      JJ=J-1
      HG(J)=HG(JJ)+DHG
  111 CONTINUF
C     FIND NODES IN FUEL AND THOSE IN REFLEC.-BLANKET
      DO 113 J=1,JMZ,1
      IF(HG(J).LT.HTRB) GO TO 113
      IFUL1=J
      IFUL2=JMZ-(J-1)
      WRITE(10,117) IFUL1,IFUL2
      GO TO 43
  113 CONTINUE
C
C      CALC. REDLICH KWONG CONSTANTS
   43 RR=82.05
      DO 41 K=1,NUM,1
      IF(PCRIT(K).EQ.0.) GO TO 41
      ARK(K)=.4275*RR**2*TCRIT(K)**2.5/PCRIT(K)
      BRK(K)=.0866*RR*TCRIT(K)/PCRIT(K)
   41 CONTINUE
C
C     SET RADIAL INCLUSION NO. DENSITY DIST.
      DO 45 I=1,IA,1
      DRINC(I)=CHI(I)*(1.5955)*DINC
   45 CONTINUE
C
C      CALC. QGEN USING CHOPPED COSINE
      DO 121 J=1,JMZ,1
      QGEN(J)=PMIN
      QORIG(J)=QGEN(J)
  121 CONTINUE
      DO 123 J=IFUL1,IFUL2,1
      ZACT=HG(J)-HTRB
      QGEN(J)=PMAX*COS((ZACT+ZEXT)*PI/(HTFL+2.*ZEXT)-PI/2.)
      QORIG(J)=QGEN(J)
  123 CONTINUE
      WRITE(10,125)
      DO 127 J=1,JMZ,1
      WRITE(10,129) J,HG(J),QGEN(J)
  127 CONTINUE
C
C     CALC. S.S. TEMP. PROFILE
      WRITE(10,143)
      CALL SSTEMP
      WRITE(10,89) HCOV
      DO 203 J=1,JMZ,1
      WRITE(10,81) J,HG(J),TS(J,IPZ)
      WRITE(10,199)
      WRITE(10,92) (R(NL),TS(J,NL),NL=1,IA,1)
      WRITE(10,147) (R(NL),TS(J,NL),NL=IB,IMZ,1)
  203 CONTINUE
C
C     CALC. TRANSIENT TEMP. PROFILE
      WRITE(10,144)
C     SGM IS SIGNAL FOR MELTING, SET FLAGS
      DO 2 J=1,JMZ,1
      DO 2 I=1,IPZ,1
      SVP(I,J)=1
      SGM(I,J)=1
```

```
      TSTOR(I,J)=0.0
      TSTOV(I,J)=0.0
      TSB(I,J,1)=TS(J,I)
    2 CONTINUE
      NCO=0
      TIME=0.0
      P2=P3=1.0
      R2=0.0
      C0=1.0
      C1=C2=0.0
      DPM=.001
      P1=1.0
      B=0.0
      DO 161 I=1,NP,1
      B=B+BS(I)
      E(I)=BS(I)/DS(I)
  161 CONTINUE
      DO 3 I=1,300,1
      DELTT=TTEM
      NCO=NCO+1
      CALL POINT(P1,DELTT,C0,C1,C2,R2,E,DS,BS,B,PGT,NP,DPM,P2,P3,
     1RAMP,IFLAG,D,PLOUT)
C     DELTT= DELTA TIME FOR HEAT TRANSFER
C     AVE HEAT GENERATION TERM IN WATT  FOR COMPARE
      TIME=TIME+DELTT
      C0=P1
      C2=((P3-P1)-2.*(P2-P1))/(2.*D**2)
      C1=(-4.*P2+3.*P1+P3)/(2.*D)
      WRITE(10,163) TIME,P1,DELTT,D,PLOUT
      WRITE(10,165) R2,P2,P3
      IF(TIME.GE.TIMAX) STOP
      DO 149 J=1,JMZ,1
      QGEN(J)=QORIG(J)*P1
  149 CONTINUE
      IF(P1.GT.100.) NPRINT=1
      CALL TRANS
      IF(NCO.GT.0) GO TO 3
      CALL VAPOR(IA,IFUL1,IFUL2,SVP,SGM,PLNPRS,NUM,RDINC,COMP,
     1DINC,DR,DHG,PI,R,TSB,HG,JMZ,ARK,BRK,DRINC,IHOMO)
    3 CONTINUE
      K=1
      CALL EXIT
      END
C
C
      SUBROUTINE SSTEMP
      COMMON/BL1/QGEN(30),HG(30),R(20),K,DELTT,PI,IA,AEQ,QORIG(30)
      COMMON/BL2/DENFL,SHFL,CONFL,DENBD,SHBD,CONBD,DENCD,SHCD,CONCD,
     1DENNA,SHNA,CONNA,HCFLC,TMELT,HMELT,TVAP,HVAP,TFMAX
      COMMON/BL3/RADFL,THCLD,THBOND,HGT,DEQ,THFLM,TEMPO,U,CDOUT,CDIN,
     1DHG,DR,HCOV,AREA,JM,IM,IMZ,JMZ,IA,TAVE,IPZ,HCFLOT,HCFLOB,
     2NPRINT,TPLEN,TSTOR(20,25),TSTOV(20,25)
      COMMON/BL5/TS(30,25),TSB(25,30,2),SGM(20,25),SVP(20,25),NCO
C     HEAT TRANSFER COEFFICIENT FOR ANNULAR CHANNELS (PG 378.SENSONSKE)
      DE=4.*AEQ/(2.*PI*CDOUT)
      CIRCD=2.*PI*CDOUT
      PEC=((DE*U*DENNA*SHNA)/CONNA)
      RANNU=((R(IM+4)/R(IM+3))**0.30)
      HCOV=(CONNA/DE)*(2.80*RANNU)*(5.1 + (0.028*(PEC**0.80)))
C     FUEL-CLAD GAP THERMAL CONDUCTANCE(CAL/SEC CM2 C)  .45  USED BY MACFARLAND
```

```
      HCBOND=.45
      RSQ=(RADFL*RADFL)
      AF=PI*RSQ
      FLOW=U*DENNA*AEQ
      COFC=(AF/(FLOW*SHNA))
C     STEADY STATE TEMPERATURE DISTRIBUTION
      DO 2 J=1,JMZ,1
      IF(J .EQ. 1) GO TO 4
      GO TO 5
C     COOLANT TEMP.
    4 TS(J,IPZ)=TEMPO
      GO TO 6
    5 QAVE=((QGEN(J-1) + QGEN(J))/2.)
    8 TS(J,IPZ)=TS(J-1,IPZ) + (QAVE*COFC*DHG)
C     CLAD SURFACE
    6 TS(J,IMZ)=TS(J,IPZ) + ((QGEN(J)*AF)/(HCOV*CIRCD))
C     CLAD-BOND INTERFACE
      TS(J,IB)=TS(J,IMZ)+(((QGEN(J)*RSQ)/(2.*CONCD))*(ALOG(CDOUT/CDIN)))
C     BOND-FUEL INTERFACE
      TS(J,IA)=TS(J,IB)+(QGEN(J)*RADFL)/(2.*HCBOND)
C     TEMPERATURE DROP ACROSS FUEL
      DO 3 I=1,IM,1
      IQP=IA-I
      RAT=R(IQP)*R(IQP)
    3 TS(J,IQP)=TS(J,IA)+(QGEN(J)*(RSQ-RAT))/(4.*CONFL)
    2 CONTINUE
      TPLEN=TS(JMZ,IPZ)
      RETURN
      END
C
C
      SUBROUTINE TRANS
      COMMON/BL1/QGEN(30),HG(30),R(20),K,DELTT,PI,IB,AEQ,CORIG(30)
      COMMON/BL2/DENFL,SHFL,CONFL,DENBD,SHBD,CONBD,DENCD,SHCD,CONCD,
     1DENNA,SHNA,CONNA,HCFLC,TMELT,HMELT,TVAP,HVAP,TEMAX
      COMMON/BL3/RADFL,THCLD,THBOND,HGT,DEQ,THFLM,TEMPO,U,CDOUT,CDIN,
     1DHG,DR,HCOV,AREA,JM,IM,IMZ,JMZ,IA,TAVE,IPZ,HCFLOT,HCFLOB,
     2NPRINT,TPLEN,TSTOR(20,25),TSTOV(20,25)
      COMMON/BL5/TS(30,25),TSB(25,30,2),SGM(20,25),SVP(20,25),NCO
      COMMON/BL6/   LJ,LT1,LT2,VLT,VLB,LT3,LBP,JC
  107 FORMAT(3X,"TIME",F11.5,5X,"TLARGE",E12.5,5X,"J",I3)
  108 FORMAT(1X,I3,3X,5(F6.3,2X,E12.5,2X),/,7X,5(F6.3,2X,E12.5,2X),/,7X,
     15(F6.3,2X,E12.5,2X),/,7X,5(F6.3,2X,E1 .5,2X))
  120 FORMAT(3X,5(E13.4,5X))
  121 FORMAT(3X,"TIME",E11.4)
  122 FORMAT(3X,"HEAT TRANSFER STABILITY CM=",E10.4)
  123 FORMAT(3X,"WE NEED TO START RAYLEIGH EQ ---STOP")
  174 FORMAT(1X,"AX.NODE",5(2X,"R",7X,"TEMP.",7X))
   73 FORMAT(//,"****FUEL VAPORIZ. OCCURRING***STOPPED")
   75 FORMAT(//,"**MAX. TEMP. EXCEEDED AT NODE I=",
     1I5," J=",I5)
C     CONSTANTS PUT IN FOR LATENT HEAT OF MELTING      STEP 50
      K=1
C     HMELT/SHFL=APPROXMATELY 67/.08 = 838
      TMEQ=HMELT/SHFL
      TVEQ=HVAP/SHFL
      AA=R(IM)
      A=R(IA)
      BB=R(IB)
      C=R(IMZ)
```

```
      DD=R(IPZ)
      LA=10
      NA=100
      KA=1
C     LOG MEAN DISTANCE BETWEEN CLAD SURFACE AND OUTSIDE EDGE OF COOLANT
      RMN=((DD-C)/(ALOG(DD/C)))
      HCSTG=(.8)*((R(IM+4)/R(IM+3))**.3)*(5.1)*(CONNA/DEQ)
C     (PG 6-246,WASH-1106) 1760B/HR F2 F = .239CAL/CM2 SEC C
      HCBOND=.45
      DQ2=(DEQ*DEQ)
C     CONSTANTS FOR FUEL
      ALPHFL=(CONFL/(DENFL*SHFL))
      CM=((DR*DR)/(ALPHFL*DELTT))
C
C     CM IS STABILITY CRITERIA OF TRANSIENT HEAT TRANSFER EQS. CM>4
      WRITE(10,122) CM
   16 CONTINUE
      TIE=TIE + DELTT
C
C     CALC. COEF. NEEDED FOR TRANS. SOLUTION
      COEF1=DENFL*SHFL*(RADFL*DR-DR*DR/4.)
      COEF2=DENCD*SHCD*(CDIN*THCLD+THCLD*THCLD/4.)/2.
      COEF3=DENCD*SHCD*(CDOUT*THCLD-THCLD*THCLD/4.)/2.
      COEF4=DHG*DENNA*SHNA*AEQ
C
C     SOLUTION FOR OVERPOWER TRANSIENT,QGEN VARIABLE
      DO 60 J=1,JMZ,1
      QAVE=QGEN(J)
C     TRANSIENT SOLUTION AT R=0
      QGP=((QAVE*DELTT)/(SHFL*DENFL))
      TSB(1,J,K+1)=(TSB(1,J,K)*(1.-(4./CM)))+ (TSB(2,J,K)*(4./CM))
     1  + QGP
      IF(TSB(1,J,K+1) .GE. TMELT .AND. SGM(1,J) .LE. 2.) GO TO 22
      GO TO 24
   22 TSTOR(1,J)=TSTOR(1,J)+TSB(1,J,K+1)-TMELT
      IF(TSTOR(1,J).LT.TMEQ) GO TO 80
      TSB(1,J,K+1)=TMELT+TSTOR(1,J)-TMEQ
      SGM(1,J)=3.0
      GO TO 24
   80 TSB(1,J,K+1)=TMELT
   24 CONTINUE
      IF(TSB(1,J,K+1) .GE. TVAP .AND. SVP(1,J) .LE. 2.) GO TO 68
      GO TO 64
   68 TSTOV(1,J)=TSTOV(1,J)+TSB(1,J,K+1)-TVAP
      IF(TSTOV(1,J).LT.TVEQ) GO TO 81
      TSB(1,J,K+1)=TVAP+TSTOV(1,J)-TVEQ
      SVP(1,J)=3.0
      GO TO 64
   81 TSB(1,J,K+1)=TVAP
   64 CONTINUE
C     TRANSIENT SOLUTION ACROSS THE FUEL PIN
      DO 29 I=2,IM,1
      PMP=(1./CM)*(1.0+(DR/(2.*R(I))))
      PMM=(1./CM)*(1.0-(DR/(2.*R(I))))
      TSB(I,J,K+1)=(TSB(I-1,J,K)*PMM) + (TSB(I,J,K)*(1.-(2./CM)))
     1  + (TSB(I+1,J,K)*PMP)   + QGP
      IF(TSB(I,J,K+1) .GE. TMELT .AND. SGM(I,J) .LE. 2.) GO TO 28
      GO TO 27
   28 TSTOR(I,J)=TSTOR(I,J)+TSB(I,J,K+1)-TMELT
      IF(TSTOR(I,J).LT.TMEQ) GO TO 82
```

```
      TSB(I,J,K+1)=TMELT+TSTOR(I,J)-TMEQ
      SGM(I,J)=3.0
      GO TO 27
   82 TSB(I,J,K+1)=TMELT
   27 CONTINUE
      IF(TSB(I,J,K+1) .GE. TVAP .AND. SVP(I,J) .LE. 2.) GO TO 45
      GO TO 29
   45 TSTOV(I,J)=TSTOV(I,J)+TSB(I,J,K+1)-TVAP
      IF(TSTOV(I,J).LT.TVEQ) GO TO 83
      TSB(I,J,K+1)=TVAP+TSTOV(I,J)-TVEQ
      SVP(I,J)=3.0
      GO TO 29
   83 TSB(I,J,K+1)=TVAP
   29 CONTINUE
C     TRANSIENT SOLUTION AT FUEL-BOND INTERFACE
      TSB(IA,J,K+1)=TSB(IA,J,K)+(DELTT/COEF1)*(2.*CONFL*(RADFL-DR/2.)
     1*(TSB(IA-1,J,K)-TSB(IA,J,K))/DR-2.*HCBOND*RADFL
     1*(TSB(IA,J,K)-TSB(IB,J,K))+QAVE*(RADFL*DR-DR*DR/4.))
C     TRANSIENT SOLUTION AT BOND CLAD INTERFACE
      TSB(IB,J,K+1)=TSB(IB,J,K)+(DELTT/COEF2)*(HCBOND*RADFL
     1*(TSB(IA,J,K)-TSB(IB,J,K))-CONCD*(CDIN+THCLD/2.)
     1*(TSB(IB,J,K)-TSB(IMZ,J,K))/THCLD)
C     TRANSIENT SOLUTION AT CLAD-COOLANT INTERFACE
      TSB(IMZ,J,K+1)=TSB(IMZ,J,K)+(DELTT/COEF3)*(CONCD*(CDIN+THCLD
     1/2.)*(TSB(IB,J,K)-TSB(IMZ,J,K))/THCLD-CDOUT*HCOV*(
     1TSB(IMZ,J,K)-TSB(IPZ,J,K)))
C     TRANSIENT SOLUTION FOR FLOWING COOLANT
      IF(J.GT.1) GO TO 99
   90 TSB(IPZ,J,K+1)=TEMPO
      GO TO 97
   99 TSB(IPZ,J,K+1)=TSB(IPZ,J,K)+(TSB(IMZ,J,K)-TSB(IPZ,J,K))*
     12.*PI*CDOUT*DELTT*HCOV/(DENNA*SHNA*AEQ)+(TSB(IPZ,J-1,K)
     1-TSB(IPZ,J,K))*DELTT*U/DHG
   97 IF(NPRINT.GT.NCO) GO TO 60
      WRITE(10,121) TIE
      WRITE(10,174)
      WRITE(10,108) J,(R(IC),TSB(IC,J,K+1),IC=1,IPZ,1)
      IF(J.EQ.JMZ) NCO=0
   60 CONTINUE
C     RESET TEMPS FOR NEXT TIME STEP
      DO 66 J=1,JMZ,1
      DO 66 I=1,IPZ,1
      TSB(I,J,1)=TSB(I,J,2)
      IF(TSB(I,J,1).LT.TEMAX) GO TO 66
      WRITE(10,75) I,J
      CALL EXIT
   66 CONTINUE
      K=1
C
C
C     IF REGION TEMP ABOVE MELTING AND LATENT HEAT   GO TO RAYLEIGH EQ
      IPPA=IM+1
      DO 61 J=1,JMZ,1
      DO 61 I=1,IA,1
      IF(SGM(I,J) .GT. 2.) GO TO 62
      IF(SVP(I,J).GT.2) GO TO 71
   61 CONTINUE
      GO TO 63
   71 WRITE(10,73)
      GO TO 63
```

```
   62 WRITE(10,123)
   63 RETURN
      END
C
C
      SUBROUTINE POINT(P1,DT,C0,C1,C2,R2,E,DS,BS,B,PGT,NP,DPM,P2,P3
     1,RAMP,IFLAG,D,PLOUT)
      DIMENSION E(6),EL(6),DS(6),BS(6),AI(3,6),CI(6),BI(6)
      P1=1.0
      IF(DPM.EQ.0.0) RETURN
      DTEX=100.0
      IF(C2.NE.0.0) DTEX=-C1/2./C2
      IF(DTEX.GT.0.0) DT=AMIN1(DT,DTEX/3.)
   12 SD=0.0
      R1=R2+RAMP*DT*B
      DO 9 J=1,NP
      EL(J)=E(J)
      SD=SD+DS(J)*E(J)
    9 CONTINUE
      PL=P1=SD/(B-R1)
      PLOUT=PL
      IF(PL.LE.0.0) PL=P2**2/P3
      N=1
    1 D=T=DT/FLOAT(N)
      DO 3 J=1,NP
      X=DS(J)*D
      TERM=PGT/(2.*D)
      BI(J)=EXP(-X)
      CI(J)=1.-BI(J)
      IF(X.GT.0.1) GO TO 2
      AJ2=(1.-(1.-(1.-(1.-(1.-X/8.)*X/7.)*X/6.)*X/5.)*X/4.)/3.
      AJ1=(1.-X*AJ2)/2.
      AJ0=1.-X*AJ1
      GO TO 8
    2 AJ0=CI(J)/X
      AJ1=(1.-AJ0)/X
      AJ2=(1.-2.*AJ1)/X
    8 E(J)=EL(J)
      AI(1,J)=D*(AJ2+AJ1)/2.
      AI(2,J)=D*(-AJ2+AJ0)
      AI(3,J)=D*(AJ2-AJ1)/2.
    3 CONTINUE
      P2=C0
      P3=C0+(C1+C2*(-D))*(-D)
   10 DO 6 M=1,N
      R1=R2+RAMP*T*B
      SUM1=SUM2=0.0
      DO 4 J=1,NP
      SUM1=SUM1+DS(J)*(BS(J)*(P2*AI(2,J)+P3*AI(3,J))+E(J)*BI(J))
      SUM2=SUM2+DS(J)*BS(J)*AI(1,J)
    4 CONTINUE
      P1=(TERM*(4.*P2-P3)+SUM1)/(3.*TERM+B-R1-SUM2)
      IF(P1.LE.0.0) GO TO 7
      DO 5 J=1,NP
      E(J)=E(J)*BI(J)+(AI(1,J)*P1+AI(2,J)*P2+AI(3,J)*P3)*BS(J)
    5 CONTINUE
      T=T+D
      P4=P3
      P3=P2
      P2=P1
```

```
    6 CONTINUE
      IF(ABS((PL-P1)/(PL+P1)).LT.DPM) GO TO 30
      GO TO 7
   30 P2=P3
      P3=P4
      R2=R1
      RETURN
    7 PL=P1
      WRITE(10,14)
      IF(IFLAG.LE.0) GO TO 24
      WRITE(10,22) P1,P3,P4
   24 N=N*5
      IF(N.LT.125) GO TO 1
      WRITE(10,20) N
      WRITE(10,15)
      DT=DT/2.
      IF(DT.GT.1.E-6) GO TO 12
      WRITE(10,16)
   14 FORMAT(//,10X,"***NOTE D: TIME STEP, HAS CHANGED****")
   16 FORMAT(//,10X,"*** SEVERE PROB. IN POINT, NO CONVERG.**")
   15 FORMAT(//,10X,"*** NOTE DT CHANGED FOR CONVERG.**")
   20 FORMAT(" ***NOTE N.GE.125 BUT P1.GT.0.***",I4)
   22 FORMAT("TEST CONVERG. P1,P2,P3=",3E14.6)
      CALL EXIT
      END
C
C
      SUBROUTINE VAPOR(IA,IFUL1,IFUL2,SVP,SGM,PLNPRS,NUM,RDINC,COMP,
     1DINC,DR,DHG,PI,R,TSB,HG,JMZ,ARK,BRK,DRINC,IHOMO)
      DIMENSION PINC(20,25,15),SVP(20,25),SGM(20,25),COMP(15),R(20),
     1TSB(25,30,2),PP(20,25,15),VOL(15),IGRW(20,25),RADB(20,25)
     1,HG(30),CONT(15),CRK(5),VIG(15),ARK(15),BRK(15),ERK(8),X(8),
     1DRINC(15)
      CONV=1.0E-6
      PTOT=0.0
      TVOL=0.0
      TMOLE=0.0
C     GAS CONST. IN CM**3 ATM/K MOLE
      RR=82.05
      DO 125 K=1,NUM
      TMOLF=TMOLE+COMP(K)
      VOL(K)=0.0
  125 CONTINUE
      DO 123 I=1,IA
      DO 123 J=IFUL1,IFUL2
      IGRW(I,J)=1
      RADB(I,J)=RDINC
  123 CONTINUE
C       ASSUME SURFACE AREA PROP. TO MOLAR %
      DO 101 J=IFUL1,IFUL2
      DO 101 I=1,IA
      IF(I.GT.1) GO TO 115
      DVOL=PI*DHG*DR*DR/4.
      GO TO 117
  115 IF(I.LT.IA) GO TO 116
      DVOL=PI*DHG*(R(I)*DR-DR*DR/4.)
      GO TO 117
  116 DVOL=PI*DHG*2.*DR*R(I)
  117 IF(SVP(I,J).GT.1) GO TO 127
      PINC(I,J,1)=EXP(10.214-3.621*5200./TSB(I,J,1))
```

```
      PP(I,J,1)=PINC(I,J,1)*COMP(1)/TMOLE
      PINC(I,J,2)=10.**(5.50-21070./TSB(I,J,1))
      PP(I,J,2)=PINC(I,J,2)*COMP(2)/TMOLE
      PINC(I,J,3)=10.**(8.687-2.88-17494./TSB(I,J,1))
      PP(I,J,3)=PINC(I,J,3)*COMP(3)/TMOLE
      PINC(I,J,4)=EXP(13.932-4.693*9340./TSB(I,J,1))
      PP(I,J,4)=PINC(I,J,4)*COMP(4)/TMOLE
      PINC(I,J,5)=10.**(-6447./TSB(I,J,1)-ALOG10(TSB(I,J,1))+8.1945)
      PP(I,J,5)=PINC(I,J,5)*COMP(5)/TMOLE
      PINC(I,J,6)=10.**(5.896-2.88-5967.4/TSB(I,J,1))
      PP(I,J,6)=PINC(I,J,6)*COMP(6)/TMOLE
      PINC(I,J,7)=10.**(5.87303-7040.7/TSB(I,J,1)-.5329*ALOG10(1.8*TSB
     1(I,J,1)))
      PP(I,J,7)=PINC(I,J,7)*COMP(7)/TMOLE
      PINC(I,J,8)=10.**(7.1872-4284.)/TSB(I,J,1))
      PP(I,J,8)=PINC(I,J,8)*COMP(8)/TMOLE
      PINC(I,J,9)=10.**(-14.3373-29751.34/TSB(I,J,1)-.00054932
     1*TSB(I,J,1)+6.41032*ALOG10(TSB(I,J,1)))
      PP(I,J,9)=PINC(I,J,9)*COMP(9)/TMOLE
      PINC(I,J,10)=10.**(-267.2102+22487.72/TSB(I,J,1)-.00596694*
     1TSB(I,J,1)+79.2243*ALOG10(TSB(I,J,1)))
      PP(I,J,10)=PINC(I,J,10)*COMP(10)/TMOLE
      PINC(I,J,11)=10.**(5.8265-2.91176E4/TSB(I,J,1))
      PP(I,J,11)=PINC(I,J,11)*COMP(11)/TMOLE
      PINC(I,J,12)=10.**(6.43266-(3.0156E4)/TSB(I,J,1))
      PP(I,J,12)=PINC(I,J,12)*COMP(12)/TMOLE
      PINC(I,J,13)=10.**(4.488-7396.5/TSB(I,J,1))
      PP(I,J,13)=PINC(I,J,13)*COMP(13)/TMOLE
      PINC(I,J,14)=10.**(4.2162-(1.4061E4)/TSB(I,J,1))
      PP(I,J,14)=PINC(I,J,14)*COMP(14)/TMOLE
      IF(SGM(I,J).GT.1) GO TO 103
      SURF=.7
      GO TO 105
  103 SURF=.45
  105 PGR=PLNPRS+2.*SURF*9.869E-6/RADB(I,J)
      IF(IHOMO.EQ.1) GO TO 151
      DO 121 K=1,NUM
      IF(PINC(I,J,K).GT.PGR.AND.COMP(K).GT.0.0) GO TO 111
      VOL(K)=0.0
      GO TO 109
  111 IGRW(I,J)=3
C *****USING REDLICH KWONG EOS AND INSTANT GROWTH
C       CALC. COEFF. OF CUBIC EQ. OF REDLICH KWONG
      CRK(1)=PLNPRS
      CRK(2)=-RR*TSB(I,J,1)
      CRK(3)=ARK(K)/SQRT(TSB(I,J,1))-PLNPRS*BRK(K)**2
     1-RR*TSB(I,J,1)*BRK(K)
      CRK(4)=-ARK(K)*BRK(K)/SQRT(TSB(I,J,1))
      CALL CUBIC(CRK,ERK,CONV)
C   TO DETERMINE CORRECT ROOT, COMPARE TO IDEAL GAS SOLU.
      VIG(K)=RR*TSB(I,J,1)/PLNPRS
      DO 141 JJ=2,6,2
      IF(ERK(JJ).NE.0.0) GO TO 141
      JK=JJ-1
      X(JJ)=ABS(VIG(K)-ERK(JK))
      IF(JJ.GT.2) GO TO 143
      IROOT=1
      ROOT=X(2)
      GO TO 141
  143 IF(X(JJ).GT.ROOT) GO TO 141
```

```
      ROOT=X(JJ)
      IROOT=JJ-1
  141 CONTINUE
      VOL(K)=ERK(IROOT)*COMP(K)
      WRITE(10,113) I,J,K
  109 TVOL=TVOL+VOL(K)
      CONT(K)=100.*VOL(K)*DRINC(I)
  121 CONTINUE
      IF(IGRW(I,J).LE.1) GO TO 131
      SUMV=TVOL*DRINC(I)*DVOL
      VOLN=100.*SUMV/DVOL
      WRITE(10,137) (KK,CONT(KK),KK=1,NUM,1)
      WRITE(10,119) SUMV,TSB(I,J,1),VOLN
      SUMTV=SUMTV+SUMV
  131 TVOL=0.0
      GO TO 101
  127 WRITE(10,129) I,J
      GO TO 101
  151 PTOT=PP(I,J,1)
      DO 161 K=2,NUM
      PTOT=PTOT+PP(I,J,K)
  161 CONTINUE
      IF(I.EQ.10.AND.J.EQ.11) GO TO 171
      GO TO 173
  171 WRITE(10,175) PTOT,TSB(I,J,1)
  173 CONTINUE
      IF(PTOT.GT.PGR) GO TO 165
      TVOL=0.0
      GO TO 163
  165 IGROW(I,J)=3
C ****USING IDEAL GAS AND INSTANT GROWTH
      TVOL=TMOLE*RR*TSB(I,J,1)/PLNPRS
  163 SUMV=TVOL*DINC*DVOL
      VOLN=100.*SUMV/DVOL
      IF(IGROW(I,J).LE.1) GO TO 101
      WRITE(10,147) I,J
      WRITE(10,119) SUMV,TSB(I,J,1),VOLN
      SUMTV=SUMTV+SUMV
  101 CONTINUE
      PERC=100.*SUMTV/(PI*R(IA)*R(IA)*HG(JMZ))
      WRITE(10,133) SUMTV,PERC
      SUMTV=0.0
      PERC=0.0
  113 FORMAT("VAPORIZATION OCCURRING AT NODE I=",I4,"    J=",I4,"
     1  MATL VAPORIZING IS K=",I4)
  119 FORMAT("VOLUME INCREASE=",F12.6,"  TEMP=",E12.6,"  VOL% IN NODE="
     1,E12.6,//)
  129 FORMAT("FUEL VAPORIZATION OCCURRING AT NODE I=",I5,"  J=",I5)
  133 FORMAT(/,"TOTAL VOL FROM INCL=",E12.6,"    VOL%=",E12.6)
  137 FORMAT(3("  MATL=",I2,"  VOL% CONTR.=",E12.6))
  147 FORMAT("VAPORIZATION OCCURRING AT NODE I=",I4,"  J=",
     1I4,"    MATERIAL IS HOMOGEN. MIXTURE")
  175 FORMAT(/,"***SUM OF P.P.=",E12.6,"ATM. TEMP. IN
     1NODE I=10,J=11 IS ",E12.6)
      RETURN
      END
      SUBROUTINE CUBIC(C,E,DELT)
      DIMENSION CP(4),C(4),BN(3),P(3),ABSP(3),E(6)
      GUESS=0.0
      IFLAG1=0
```

```
      IFLAG2=0
      DINCR=.5
      COMP=2.**(-16)
      CP(1)=1.0
      CP(2)=C(2)/C(1)
      CP(3)=C(3)/C(1)
      CP(4)=C(4)/C(1)
      DO 50 I=1,6
      E(I)=0.0
   50 CONTINUE
  100 IF(IFLAG1.LT.5) GO TO 210
      IF(IFLAG2.GT.0) GO TO 110
  200 IFLAG1=0
      DINCR=8.0*DINCR
      GO TO 300
  110 IFLAG1=IFLAG1+1
  300 BN(1)=GUESS+DINCR
      BN(3)=GUESS
      BN(2)=GUESS-DINCR
      DO 330 I=1,3
      P(I)=((CP(1)*BN(I)+CP(2))*BN(I)+CP(3))*BN(I)+CP(4)
      ABSP(I)=ABS(P(I))
  330 CONTINUE
      GO TO 400
  350 DO 360 I=1,2
      II=I+1
      DIF=ABSP(I)-ABSP(II)
      ABDIF=ABS(DIF)
      IF(ABDIF.GT.DELT) GO TO 400
  360 CONTINUE
      GO TO 200
  400 IF(ABSP(3).LT.COMP) GO TO 500
  600 DO 660 I=1,2
      II=I
      IF(ABSP(I).LT.COMP) GO TO 610
  660 CONTINUE
      DO 670 I=1,2
      IF(ABSP(3).GT.ABSP(I)) GO TO 700
  670 CONTINUE
      DINCR=DINCR/2.0
      IF(COMP.GT.DINCR) GO TO 500
      IF(IFLAG2.GT.50) GO TO 500
      IFLAG2=IFLAG2+1
      GO TO 300
  700 IF(ABSP(1).LT.ABSP(2)) GO TO 780
      GUESS=BN(2)
      GO TO 100
  780 GUESS=BN(1)
      GO TO 100
  500 E(1)=GUESS
      GO TO 800
  610 E(1)=BN(II)
C     SYNYHETIC DIV. AND QUAD. SOLU.
  800 B2=CP(2)+E(1)
      B3=CP(3)+E(1)*B2
      DUM=B2**2-4.*B3
      IF(DUM.GT.0.) GO TO 810
      DUM=-DUM
      COMPL=(SQRT(DUM))/2.
      REAL=-B2/2.
      E(3)=REAL
      E(4)=COMPL
      E(5)=REAL
      E(6)=-COMPL
      GO TO 820
  810 REAL1=(-B2+SQRT(DUM))/2.0
      REAL2=(-B2-SQRT(DUM))/2.0
      E(3)=REAL1
      E(5)=REAL2
  820 RETURN
      END
```

APPENDIX O
DETERMINATION OF SURFACE TENSION

From Overbury:[1]

$$A = fN^{1/3} \left(\frac{M}{\rho}\right)^{2/3} \qquad (0\text{-}1)$$

where

A = area occupied by Avogadro's Number of atoms,

N = Avogadro's number,

M = atomic weight,

ρ = density,

f = structure factor, f = 1 simple cubic structure,

f = 1.09 for face centered cubic (fcc),

f = 1.12 for body centered cubic (bcc),

f = 1.14 for orthorhombic structure,

and

$$\sigma_{LM}(T) = A\,\sigma_L(T) \quad , \qquad (0\text{-}2)$$

where

σ_{LM} = molar surface Free Energy,

$$\sigma_{LM} = .15\ \Delta H_{vap} \qquad (0\text{-}3)$$

where

ΔH_{vap} = heat of vaporization.

Combining Eqs. (0-1), (0-2), and (0-3)

$$\sigma_L\ (T) = \frac{.15\ \Delta H_{vap}}{f\ N^{1/3}\ (\frac{M}{\rho})^{2/3}}\ . \qquad (0\text{-}4)$$

REFERENCE

1. S. H. Overbury, P. A. Bertrand, G. A. Somorjai, "The Surface Composition of Binary Systems Prediction of Surface Phase Diagrams of Solid Solutions," Chemical Reviews 75, No. 5 (October 1975).

VITA

Paul Sasa was born on November 27, 1945, in Brighton, Colorado. Upon graduating from Brighton High School in 1963, he went to the University of Colorado where he received his B.S. in Engineering Physics in 1968. After graduation, he worked one year for the Naval Missile Systems Engineering Station in Port Hueneme, California and then four years for the Bendix Corporation in Kansas City, Missouri. In 1973 he entered graduate school at the University of New Mexico and received his M.S. in Nuclear Engineering in 1974. In the summer of 1975, he was associated with Argonne National Laboratory in its Reactor Analysis and Safety Division. His Ph.D. research was conducted in the Fast Reactor Safety Division of the Los Alamos Scientific Laboratory in Los Alamos, New Mexico, and after graduation, he will join Rockwell International in Golden, Colorado. He has a wife, Janet.

VITA

Paul Sate was born on November 27, 1945, in Brighton, Colorado. Upon graduating from Brighton High School in 1963, he went to the University of Colorado where he received his B.S. in Engineering Physics in 1968. After graduation, he worked one year for the Naval Missile Systems Engineering Station in Port Hueneme, California and then four years for the Bendix Corporation in Kansas City, Missouri. In 1973 he entered graduate school at the University of New Mexico and received his M.S. in Nuclear Engineering in 1975. In the summer of 1975, he was associated with Argonne National Laboratory in its Reactor Analysis and Safety Division. His Ph.D. research was conducted in the Fast Reactor Safety Division of the Los Alamos Scientific Laboratory, Los Alamos, New Mexico, and after graduation, he will join Rockwell International in Golden, Colorado. He has a wife, Janet.